Nuclear Inst. and Methods in Physics Research, A 875 (2017) 10–15

Contents lists available at ScienceDirect

Nuclear Inst. and Methods in Physics Research, A

journal homepage: www.elsevier.com/locate/nima

An underground laboratory as a facility for studies of cosmic-ray solar modulation

N. Veselinović, A. Dragić *, M. Savić, D. Maletić, D. Joković, R. Banjanac, V. Udovičić

Institute of Physics, University of Belgrade, Pregrevica 118, 11080 Zemun, Serbia

ARTICLE INFO

Keywords:
Cosmic ray muons
Forbush decrease
Response function

ABSTRACT

The possibility of utilizing a shallow underground laboratory for the study of energy dependent solar modulation process is investigated. The laboratory is equipped with muon detectors at ground level and underground (25mwe), and with an underground asymmetric muon telescope to have a single site detection system sensitive to different median energies of primary cosmic-ray particles. The detector response functions to galactic cosmic rays are determined from Monte Carlo simulation of muon generation and propagation through the atmosphere and soil, based on CORSIKA and GEANT4 simulation packages. The present setup is suitable for studies of energy dependence of Forbush decreases and other transient or quasi-periodic cosmic-ray variations.

1. Introduction

Galactic cosmic rays (GCR) arriving at Earth after propagating through the heliosphere interact with nuclei in the atmosphere. These interactions of primary CRs lead to production of a cascade (shower) of secondary particles: hadrons, electrons, photons, muons, neutrinos. Ground based CR detectors are designed to detect some species of secondary cosmic radiation. Widely in use are neutron monitors [1,2], muon telescopes [3,4], various types of air shower arrays [5], γ-ray air Cherenkov detectors [6], air fluorescence detectors [7] etc.

The flux and energy spectra of GCR are modulated by the solar magnetic field, convected by the solar wind. Particularly affected are GCR at the low energy side of the spectrum (up to ~100 GeV). Therefore, secondary CRs generated in the atmosphere can be used for studying solar and heliospheric processes. Among the best known effects of the solar modulation are CR flux variations with 11 year period of the solar cycle, 22 year magnetic cycle, diurnal variation and Forbush decrease. The so called corotation with the solar magnetic field results in the flux variation with the 27-day period of solar rotation.

Modulation effects have been studied extensively by neutron monitors (NM) [8,9], sensitive up to several tens of GeV, depending on their geomagnetic location and atmospheric depth. Muon detectors at ground level are sensitive to primary particles of higher energies than NMs. Underground muon detectors correspond to even higher energy primaries. For this reason muon observations complement NM observations in studies of long-term CR variations, CR anisotropy and gradients or rigidity spectrum of Forbush decreases. However, muon observations suffer from difficulties to disentangle variations of atmospheric origin. While the effect of atmospheric pressure is similar to NMs and easy to account for, the temperature effect is more complicated. The entire temperature profile of the atmosphere is contributing, with different net temperature effect on muon flux at different atmospheric layers, as a result of interplay of positive and negative temperature effects. The positive temperature effect is a consequence of reduced atmospheric density with the temperature increase, resulting in less pion interactions and more decays into muons [10]. The negative temperature effect comes from the increased altitude of muon production at the periods of high temperature, with the longer muon path length and the higher decay probability before reaching the ground level [11]. Both effects are accounted for by the integral method of Dorman [12]. The negative temperature effect is dominant for low energy muons (detected at ground level) and the positive for high energy muons (detected deep underground). At shallow depth of several tens of meters of water equivalent both temperature effects contribute to the overall temperature effect. Several detector systems with different sensitivity to primaries at the same location have the advantage of sharing common atmospheric and geomagnetic conditions.

Belgrade CR station is equipped with muon detectors at ground level and at the depth of 25 m.w.e. Underground laboratory is reached only by muons exceeding energy threshold of 12 GeV. The existing detectors are recently amended by additional setup in an attempt to fully exploit laboratory's possibilities to study solar modulation at different

* Corresponding author.
E-mail address: dragic@ipb.ac.rs (A. Dragić).

http://dx.doi.org/10.1016/j.nima.2017.09.008
Received 31 May 2017; Received in revised form 30 August 2017; Accepted 3 September 2017
Available online 7 September 2017
0168-9002/

median rigidities. In the present paper the detector systems at the Belgrade CR station are described. Response functions of muon detectors to galactic cosmic rays are calculated. The detector system represents useful extension of modulation studies with neutron monitors to higher energies, as it is demonstrated in the case of a recent Forbush event.

2. Description of Belgrade CR station

The Belgrade cosmic-ray station, situated at the Low Background Laboratory for Nuclear Physics at Institute of Physics, is located at near-sea level at the altitude of 78 m a.s.l. Its geographic position is: latitude 44°51′N and longitude 20°23′E, with vertical cut-off rigidity 5.3 GV. It consists of the ground level lab (GLL) and the underground lab (UL) which has useful area of 45 m^2, dug at a depth of 12 m. The soil overburden consists of loess with an average density 2.0 ± 0.1 g/cm^3. Together with the 30 cm layer of reinforced concrete the laboratory depth is equivalent to 25 m.w.e. At this depth, practically only the muonic component of the atmospheric shower is present [13].

2.1. Old setup

The experimental setup [14] consists of two identical sets of detectors and read out electronics, one situated in the GLL and the other in the UL. Each setup utilizes a plastic scintillation detector with dimensions 100 cm × 100 cm × 5 cm equipped with 4 PMTs optically attached to beveled corners of a detector. Preamplifier output of two diagonally opposing PMTs are summed and fed to a digitizer input (CAEN FADC, type N1728B). FADC operates at 100 MHz frequency with 14 bit resolution. The events generating enough scintillation light to produce simultaneous signals in both inputs exceeding the given threshold are identified as muon events. The simulated total energy deposit spectrum is presented on the left panel of Fig. 1. After the appropriate threshold conditions are imposed on the signals from two diagonals, the spectrum is reduced to the one represented on the right panel of the same figure. Contribution from different CR components are indicated on both graphs and experimentally recorded spectrum is plotted as well.

Particle identification is verified by a two-step Monte Carlo simulation. In the first step development of CR showers in the atmosphere is traced, starting from the primary particles at the top of the atmosphere by CORSIKA simulation package. CORSIKA output contains information on generated particles (muons, electrons, photons, etc.) and their momenta at given observation level. More details on CORSIKA simulation will be given in Section 3. This output serves as an input for the second step in simulation, based on GEANT4. In the later step energy deposit by CR particles in the plastic scintillator detector are determined, together with the light collection at PMTs. Contributions from different CR components to recorded spectrum are also shown in Fig. 1.

According to the simulation, 87.5% of events in the coincident spectrum originate from muons. To account for the contribution from other particles to the experimental spectrum not all the events in the spectrum are counted when muon time series are constructed. Muon events are defined by setting the threshold corresponding to muon fraction of recorded spectrum. Threshold is set in terms of "constant fraction" of the spectrum maximum, which also reduces count rate fluctuations due to inevitable shifts of the spectrum during long-term measurements.

2.2. Upgrade of the detector system

Existing detectors enable monitoring of CR variations at two different median energies. An update is contemplated that would provide more differentiated response. Two ideas are considered. First one was to extend the sensitivity to higher energies with detection of multi-muon events underground. An array of horizontally oriented muon detectors ought to be placed in the UL. Simultaneous triggering of more than one detector is an indication of a multi-muon event. The idea was exploited in the EMMA underground array [15], located at the deeper underground laboratory in Pyhasalmi mine, Finland, with the intention to reach energies in the so called knee region. For a shallow underground laboratory, exceeding the energy region of solar modulation would open the possibility to study CR flux variations originating outside the heliosphere. Second idea is an asymmetric muon telescope separating muons with respect to zenith angle. Later idea is much less expensive to be put into practice.

Both ideas will be explained in detail and response function to GCR for existing and contemplated detectors calculated in the next section.

3. Calculation of response functions

Nature of variations of primary cosmic radiation can be deduced from the record of ground based cosmic ray detectors provided relation between the spectra of primary and secondary particles at surface level are known with sufficient accuracy. Relation can be expressed in terms of rigidity or kinetic energy.

Total detector count rate can be expressed as:

$$N(E_{th}, h, t) = \sum_i \int_{E_{th}}^{\infty} Y_i(E, h) \cdot J_i(E, t) dE \quad (1)$$

where E is primary particle energy, i is type of primary particle (we take into account protons and α particles), $J_i(E, t)$ is energy spectrum of primary particles, h is atmospheric depth and $Y_i(E, h)$ is the so called yield function. E_{th} is the threshold energy of primary particles. It depends on location (geomagnetic latitude and atmospheric altitude) and detector construction details. At a given location on Earth, only particles with rigidity above vertical rigidity cut-off contribute to the count rate. Also, detector construction often prevents detection of low energy particles. For instance, muon detectors are sometimes covered with a layer of lead. In present configuration our detectors are lead free.

Historically, yield functions were calculated empirically, often exploiting the latitude variations of neutron and muonic CR component [16–18]. With the advancement of computing power and modern transport simulation codes it became possible to calculate yield functions from the interaction processes in the atmosphere [19,20]. The yield function for muons is calculated as:

$$Y_i(E, h) = \int_{E_{th}}^{\infty} \int S_i(\theta, \phi) \cdot \Phi_{i,\mu}(E_i, h, E, \theta, \phi) dE d\Omega \quad (2)$$

where $S(\theta, \phi)$ is the effective detector area and integration is performed over upper hemisphere. $\Phi_{i,\mu}(E_i, h, E, \theta, \phi)$ is the differential muon flux per primary particle of the type i with the energy E_i.

Total differential response function:

$$W(E, h, t) = \sum_i Y_i(E, h) \cdot J_i(E, t) \quad (3)$$

when normalized to the total count rate gives the fraction of count rate originating from the primary particles with the energy in the infinitesimal interval around E. Integration of differential response function gives the cumulative response function.

The response functions of our CR detectors are calculated using Monte Carlo simulation of CR transport through the atmosphere with CORSIKA simulation package. Simulation was performed with protons and α-particles as primary particles. They make ~94% (79% + 14.7%) of all primaries [21]. Implemented hadron interaction models were FLUKA for energies below 80 GeV, and QGSJET II-04 for higher energies. If the old version of QGSJET is used, a small discontinuity in response function is noticed at the boundary energy between two models. Geomagnetic field corresponds to the location of Belgrade $B_x = 22.61$ μT, $B_z = 42.27$ μT. Power law form of differential energy spectrum of galactic cosmic rays $J_p(E) \sim E^{-2.7}$ is assumed. Energy range of primary particles is between 1 GeV and $2 \cdot 10^7$ GeV. Interval of zenith angles is $0° < \theta < 70°$. Low energy thresholds for secondary particles are: 150 MeV for hadrons and muons and 15 MeV for electrons

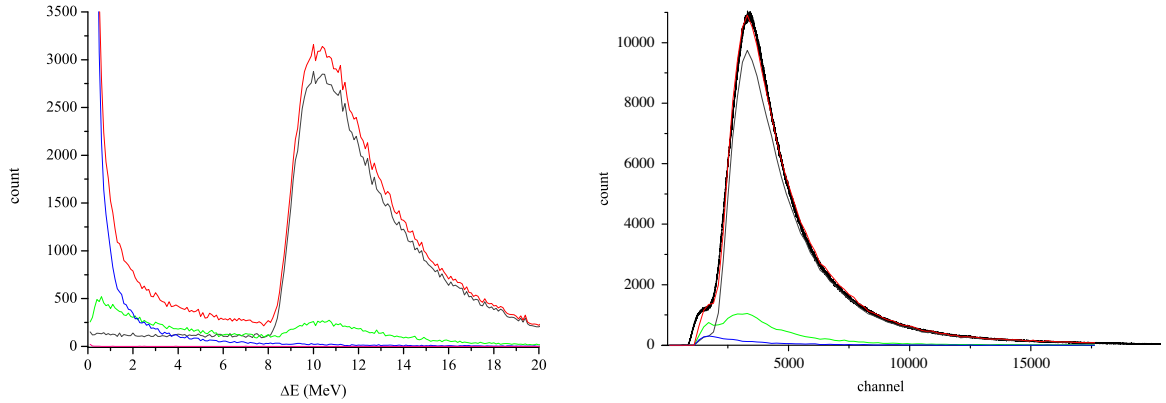

Fig. 1. Left — ΔE spectrum in the plastic scintillator detector, derived from GEANT simulation; right — the same, but for the events exceeding threshold on both diagonals. Contribution of different CR components to the total energy deposit in the detector: muons-gray line, photons-blue line, electrons-green line and sum of all contributions — red line. The black curve on the right panel is the experimental spectrum. (For interpretation of the references to color in this figure legend, the reader is referred to the web version of this article.)

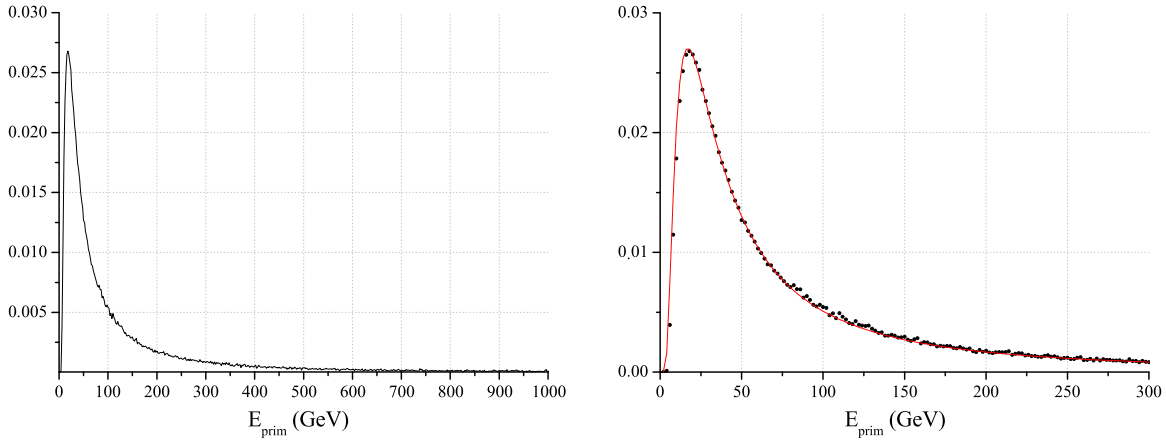

Fig. 2. Left: normalized total response function of ground level muon detector to galactic cosmic rays; right: same as left, fitted with Dorman function (red line). (For interpretation of the references to color in this figure legend, the reader is referred to the web version of this article.)

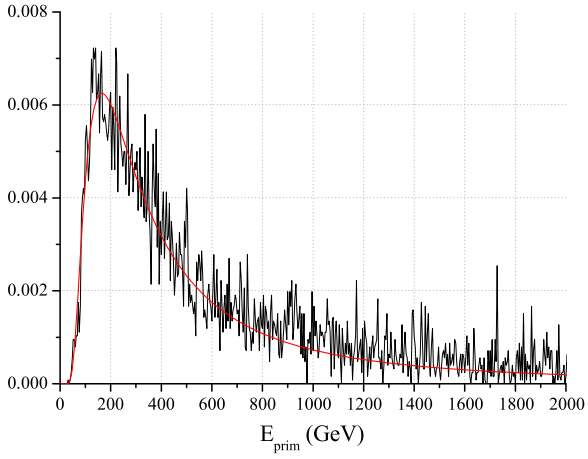

Fig. 3. Response function for multi-muon events in UL to galactic cosmic rays.

and photons. Selected atmospheric model is AT511 (Central European atmosphere for May 11 1993). Observational level is at 78m a.s.l.

For calculation of response functions for underground detectors, simulation of particle propagation through the soil overburden is performed using the code based on GEANT4 package. For precise calculation of energy loss, chemical composition of the soil needs to be known. The composition used in our work is taken from a geochemical study of neighboring loess sections of Batajnica and Stari Slankamen [22]. Most abundant constituents are quartz (SiO_2) 70%, alumina (Al_2O_3) 15% and quicklime (CaO) 10%, while others include Fe_2O_3, MgO, TiO_2, K_2O,.... Inaccuracy of our knowledge of the soil chemical composition should not strongly affect our results since, at relevant energies, dominant energy loss mechanism for muons is ionization which, according to Bethe–Bloch formula depends mostly on $\langle Z\rangle/\langle A\rangle$. Soil density profile is probed during laboratory construction. It varies slowly with depth and average density is found to be (2.0 ± 0.1) g/cm^3.

In the simulation, the effective area and angular acceptance of different modes of asymmetric muon telescope (single, coincident and anticoincident) are taken into account.

According to Dorman [12], response function can be parametrized as:

$$W(E) = \begin{cases} 0, & \text{if } E < E_{th}; \\ \dfrac{a \cdot k \cdot \exp(-aE^{-k})}{E^{(k+1)}(1 - aE_{th}^{-k})}, & \text{otherwise;} \end{cases} \tag{4}$$

with the high energy asymptotics: $W(E) \approx a \cdot k \cdot E^{-(k+1)}$.

3.1. Ground level

Calculated response function for ground level muon detector is presented on Fig. 2, together with fitted Dorman function (4).

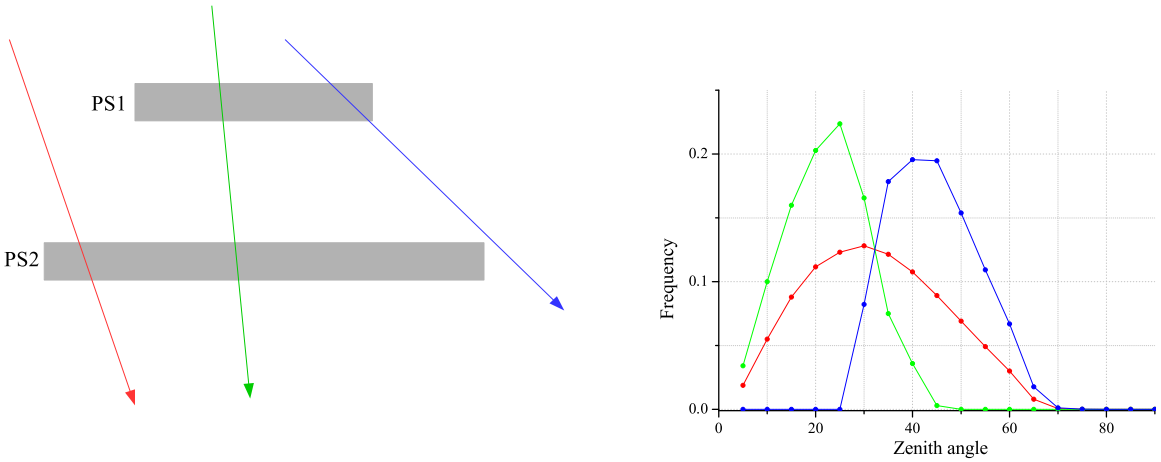

Fig. 4. Left: Schematic view of the asymmetric muon telescope; PS1 — plastic scintillator detector 1, PS2 — plastic scintillator detector 2. Right: angular distribution of detected muons in single mode (red), coincident mode (green) and anticoincident mode (blue), normalized to number of counts in each mode. (For interpretation of the references to color in this figure legend, the reader is referred to the web version of this article.)

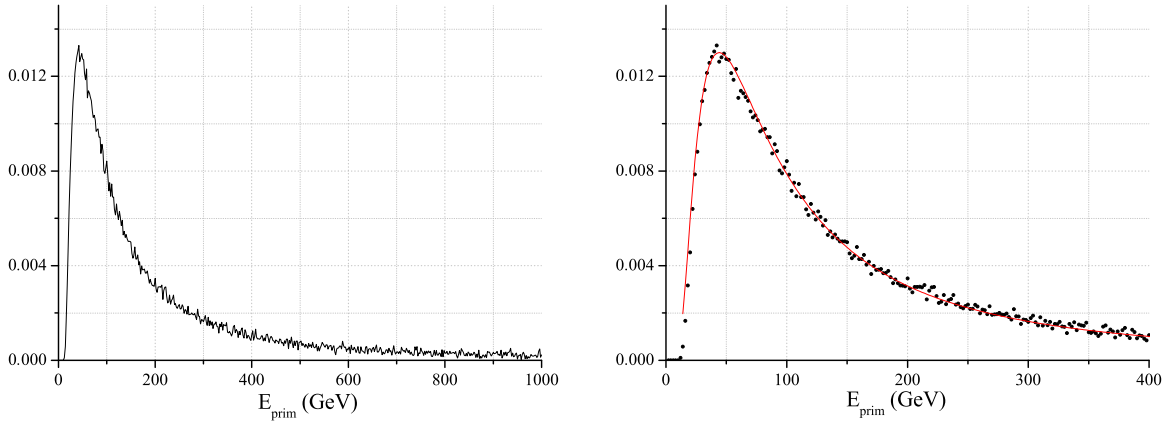

Fig. 5. Response function of single mode of ASYMUT in the UL to galactic cosmic rays. On the right panel the energy interval of interest is enlarged and Dorman function fit is plotted (red line). (For interpretation of the references to color in this figure legend, the reader is referred to the web version of this article.)

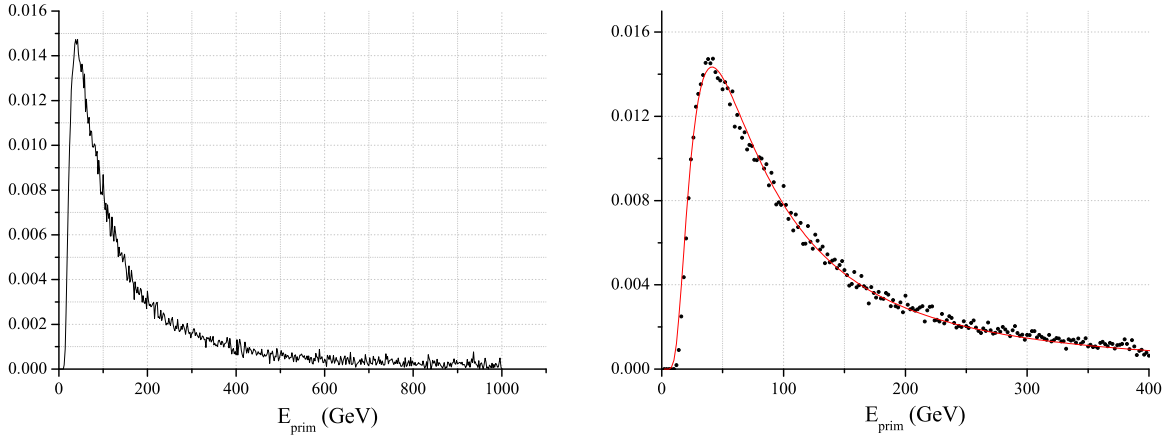

Fig. 6. Response function of coincident mode of asymmetric muon telescope in the UL to galactic cosmic rays. On the right panel the interesting energy interval is enlarged and Dorman function fit is plotted (red line). (For interpretation of the references to color in this figure legend, the reader is referred to the web version of this article.)

3.2. Underground

3.2.1. Multi-muon events

Count rate of multi-muon events underground turned out to be too low for the above mentioned array detector experiment to be feasible in our laboratory. To collect enough events for construction of the response function (Fig. 3), allowed muon separation is 200 m, fairly exceeding laboratory dimensions. Under these conditions calculated median energy is 270 GeV.

*3.2.2. **ASY**mmetric **MU**on **T**elescope (ASYMUT)*

Asymmetric muon telescope is an inexpensive detector, constructed from components already available in the laboratory. It consists of two plastic scintillators of unequal dimensions. The lower is identical to the

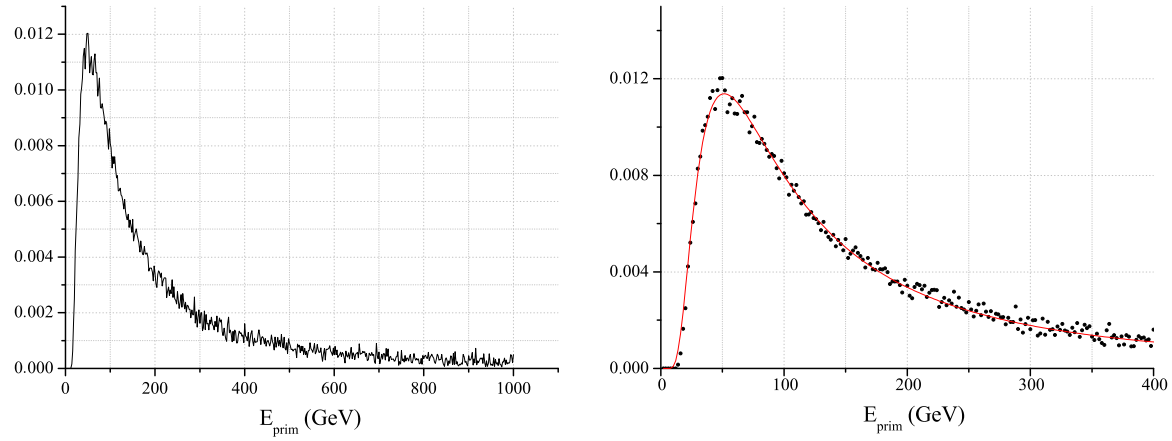

Fig. 7. Response function of anticoincident mode of asymmetric muon telescope in the UL to galactic cosmic rays. On the right panel the interesting energy interval is enlarged and Dorman function fit is plotted (red line). (For interpretation of the references to color in this figure legend, the reader is referred to the web version of this article.)

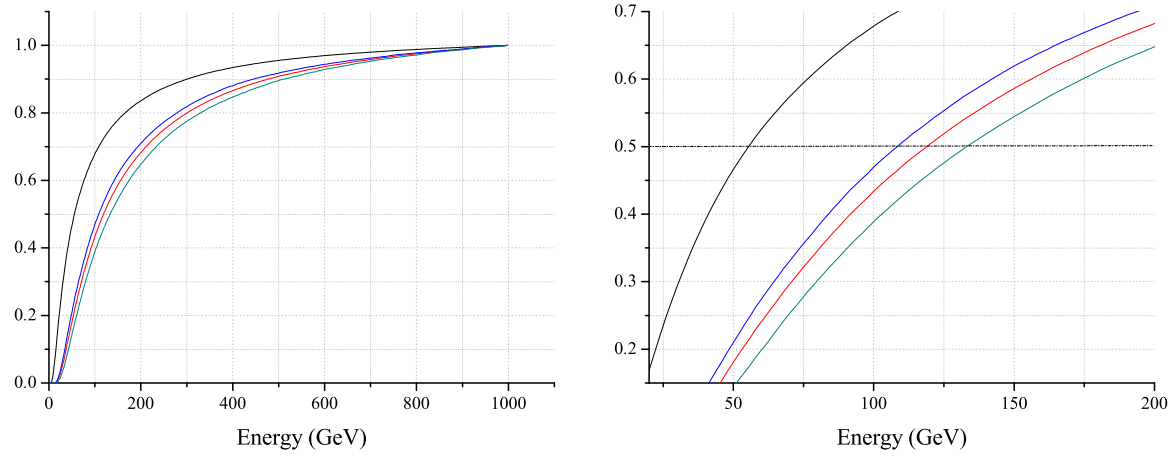

Fig. 8. Cumulative response function to galactic cosmic rays of different muon detectors in the Belgrade CR station: black curve — GLL; red curve — single UL; green curve — CC mode and blue curve — ANTI CC mode of asymmetric muon telescope. The 0.5 level corresponds to median energy. Cumulative response function with enlarged region around this level is shown in the right picture. (For interpretation of the references to color in this figure legend, the reader is referred to the web version of this article.)

one located in the GLL (100 ×100 ×5 cm) and upper one is 50 ×46 ×5 cm. Detectors are separated vertically by 78 cm, as depicted in Fig. 4, to have roughly the same count rate in the coincident and anticoincident mode. Lower detector in single mode operates in the same manner as the one in the GLL, with wide angular acceptance. The coincident mode is composed of the events registered in both upper and lower detector. In the anticoincident mode, muons passing through the upper but not the lower detector are counted. Therefore, the later mode favors inclined muon paths. Different angular distribution means different path length of muons registered in three modes of ASYMUT (right part of Fig. 4) and also different energy distribution of parental primary particles.

The response functions to GCR of three modes of ASYMUT are shown on Figs. 5–7 and respective cumulative response functions are shown on Fig. 8.

Important parameters describing shapes of response functions are summarized in Table 1. The most often used characteristics of a detector system is its median energy E_{med}. Primary particles with the energy below E_{med} give 50% contribution to detector count rate. The energy interval (($E_{0.05}$, $E_{0.95}$) is responsible for 90% of registered events. Fitted value of the parameter k from Dorman function (Eq. (4)) is also presented. The parameters $E_{0.05}$ and E_{med} are determined with 1 GeV accuracy, while the uncertainty of $E_{0.95}$ is much higher due to small number of very high energy events and is conservatively estimated as 10%.

Table 1
Sensitivity of Belgrade CR detectors (GLL — ground level; UL — underground based ASYMUT single mode; CC — ASYMUT coincident mode; ANTI — ASYMUT anticoincident mode) to GCR primary particles. Primaries with the energy below $E_{0.05}$ (and above $E_{0.95}$) contribute with 5% to the count rate of a corresponding detector. E_{med} is median energy, E_{th} threshold energy and k is Dorman parameter.

det	E_{th} (GeV)	$E_{0.05}$ (GeV)	E_{med} (GeV)	$E_{0.95}$ (GeV)	k
GLL	5	11	59	915	0.894(1)
UL	12	31	137	1811	0.971(4)
CC	12	27	121	1585	1.015(3)
ANTI	14	35	157	2031	0.992(4)

3.3. Conclusions

Usefulness of our setup for solar modulation studies is tested on the example of investigation of a Forbush decrease of 8 March 2012. In the first half of March 2012 several M and X class solar flares erupted from the active region 1429 on the Sun. The strongest were two X class flares that bursted on March 7. The first one is the X5.4 class flare (peaked at 00:24 UT) and the second one is the X1.3 class flare (peaked at 01:14 UT). The two flares were accompanied by two fast CMEs, one of which was Earth-directed [23]. Several magnetic storms were also registered on Earth, and a series of Forbush decreases is registered. The most pronounced one was registered on March 8. Characteristics of this event as recorded by various neutron monitors and our detectors are compared.

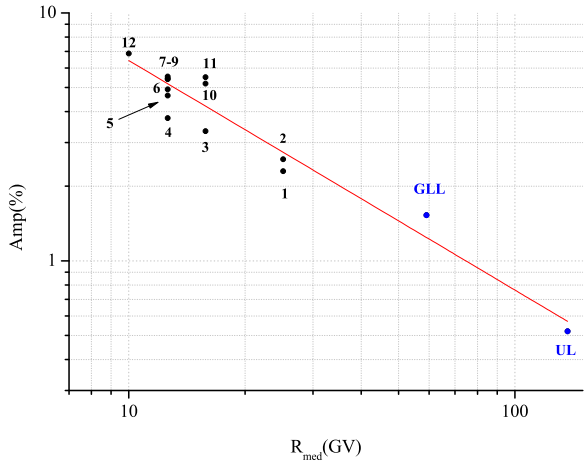

Fig. 9. Rigidity spectrum of FD from 12 March 2012. Black points represent the amplitude of the event as seen by twelve NMs: 1 — Athens, 2 — Mexico City; 3 — Almaty, 4 — Lomnicky stit; 5 — Moscow; 6 — Kiel; 7 — Yakutsk; 8 — Apatity; 9 — Inuvik; 10 — McMurdo; 11 — Thul; 12 — South Pole. Blue points are from Belgrade CR station: GLL — ground level and UL — underground. (For interpretation of the references to color in this figure legend, the reader is referred to the web version of this article.)

Amplitude of a Forbush decrease is one of its main characteristics. Dependence of FD amplitude on median rigidity (or energy) is expected to follow the power law: $\Delta N/N \sim R^{-\gamma}$ [12].

For investigation of rigidity spectrum of mentioned FD data from 12 NMs are combined with the data from our two detectors (GLL and UL) that were operational at the time of the event. Neutron monitor data in the period between 1 March 2012 and 1 April 2012 are taken from the NMDB database (www.nmdb.eu) [24]. The exponent of the rigidity spectrum of this FD γ is obtained by the least-square fitting of the data with the power function (Fig. 9) and found to be $\gamma = 0.92 \pm 0.18$. Presented analysis illustrates applicability of our setup for studies of consequences of CR solar modulation process in the energy region exceeding sensitivity of neutron monitors.

Acknowledgments

We are very grateful to late Prof. Ivan Aničin for his enthusiastic contributions, deep insights and valuable advice not just regarding work presented in this paper but also for being a real spiritus agens of our lab. We acknowledge the NMDB database (www.nmdb.eu), founded under the European Union's FP7 programme (contract no. 213007) for providing NM data. The present work was funded by the Ministry of Education, Science and Technological Development of the Republic of Serbia, under the Project No. 171002.

References

[1] J.A. Simpson, The cosmic ray nucleonic component: The invention and scientific uses of the neutron monitor, Cosmic Rays Earth (2000) 11–32.
[2] J.W. Bieber, Neutron monitoring: Past, present, future, in: Jonathan F.O. (Ed.) AIP Conference Proceedings, vol. 1516, No. 1, 2013.
[3] M.L. Duldig, Muon observations, in: Cosmic Rays and Earth, Springer, Netherlands, 2000, pp. 207–226.
[4] S. Cecchini, M. Spurio, Atmospheric muons: experimental aspects, Geosci. Instrum. Methods Data Syst. Discuss. 2 (2012) 603–641.
[5] K.-H. Kampert, A.A. Watson, Extensive air showers and ultra high-energy cosmic rays: a historical review, Eur. Phys. J. H 37 (3) (2012) 359–412.
[6] A. de Angelis, O. Mansutti, M. Persic, Very-high energy gamma astrophysics, Riv. Nuovo Cimento 31 (4) (2008) 187–246. http://dx.doi.org/10.1393/ncr/i2008-10032-2.
[7] F. Arqueros, J.R. Hörandel, B. Keilhauer, Air fluorescence relevant for cosmic-ray detection — review of pioneering measurements, Nucl. Instrum. Methods A 597 (2008) 23–31. http://dx.doi.org/10.1016/j.nima.2008.08.055.
[8] J.A. Lockwood, W.R. Webber, The 11 year solar modulation of cosmic rays as deduced from neutron monitor variations and direct measurements at low energies, J. Geophys. Res. 72 (23) (1967) 5977–5989.
[9] I.G. Usoskin, G.A. Bazilevskaya, G.A. Kovaltsov, Solar modulation parameter for cosmic rays since 1936 reconstructed from ground-based neutron monitors and ionization chambers, J. Geophys. Res. 116 (2011) A02104. http://dx.doi.org/10.1029/2010JA016105.
[10] A. Duperier, The meson intensity at the surface of the earth and the temperature at the production level, Proc. Phys. Soc. A 62 (11) (1949) 684.
[11] P.M. Blackett, On the instability of the barytron and the temperature effect of cosmic rays, Phys. Rev. 54 (11) (1938) 973.
[12] L. Dorman, Cosmic Rays in the Earth's Atmosphere and Underground, Springer Science + Business Media, LLC., New York, 2004.
[13] G. Hausser, Cosmic ray-induced background in ge-spectrometry, Nucl. Instrum. Methods B 83 (1–2) (1993) 223–228.
[14] A. Dragić, V. Udovičić, R. Banjanac, D. Joković, D. Maletić, N. Veselinović, M. Savić, J. Puzović, I.V. Aničin, The new setup in the Belgrade low-level and cosmic-ray laboratory, Nucl. Technol. Radiat. Prot. 26 (3) (2011) 181–192. http://dx.doi.org/10.2298/NTRP1101064N.
[15] T. Kalliokoski, L. Bezrukov, T. Enqvist, H. Fynbo, L. Inzhechik, P. Jones, J. Joutsenvaara, J. Karjalainen, P. Kuusiniemi, K. Loo, B. Lubsandorzhiev, V. Petkov, T. Rih, J. Sarkamo, M. Slupecki, W. Trzaska, A. Virkajrvi, Can EMMA solve the puzzle of the knee? Prog. Part. Nucl. Phys. 66 (2011) 468–472.
[16] W.H. Fonger, Cosmic radiation intensity-time variations and their origin. II. Energy dependence of 27-day variations, Phys. Rev. 91 (2) (1953) 351.
[17] E.E. Brown, Neutron yield functions for the nucleonic component of cosmic radiation, Il Nuovo Cimento (1955–1965) 6 (4) (1957) 956–962.
[18] L. Dorman, Cosmic Ray Variations, State Publishing House for Technical and Theoretical Literature, 1957.
[19] E.O. Fluckiger, et al., A parameterized neutron monitor yield function for space weather applications, in: Proceedings of the 30th International Cosmic Ray Conference, Mexico City, Mexico, vol. 1 (SH), 2008, pp. 289–292.
[20] M. Zazyan, A. Chilingarian, Calculations of the sensitivity of the particle detectors of ASEC and SEVAN networks to galactic and solar cosmic rays, Astropart. Phys. 32 (2009) 185–192.
[21] K. Nakamura, et al., 24. Cosmic rays, J. Phys. G 37 (2010) 075021.
[22] B. Buggle, B. Glaser, L. Zoller, U. Hambach, S. Markovic, I. Glaser, N. Gerasimenko, Geochemical characterization and origin of Southeastern and Eastern European loesses (Serbia, Romania, Ukraine), Quat. Sci. Rev. 27 (2008) 1058–1075.
[23] NASA Goddard Space Weather Research Center, Summary of the space weather event associated with the X5.4 and X1.3 flare on March 7.
[24] H. Mavromichalaki, et al., Applications and usage of the real-time Neutron Monitor Database, Adv. Space Res. 47 (12) (2011) 2210–2222.

MULTIYEAR INDOOR RADON VARIABILITY IN A FAMILY HOUSE – A CASE STUDY IN SERBIA

by

Vladimir I. UDOVIČIĆ [1*], ***Dimitrije M. MALETIĆ*** [1], ***Radomir M. BANJANAC*** [1], ***Dejan R. JOKOVIĆ*** [1], ***Aleksandar L. DRAGIĆ*** [1], ***Nikola B. VESELINOVIĆ*** [1], ***Jelena Z. ŽIVANOVIĆ*** [1], ***Mihailo R. SAVIĆ*** [1], ***and Sofija M. FORKAPIĆ*** [2]

[1]Institute of Physics, University of Belgrade, Belgrade, Serbia
[2] Department of Physics, Faculty of Science, University of Novi Sad, Novi Sad, Serbia

Scientific paper
http://doi.org/10.2298/NTRP1802174U

The indoor radon behavior has complex dynamics due to the influence of the large number of different parameters: the state of indoor atmosphere (temperature, pressure, and relative humidity), aerosol concentration, the exchange rate between indoor and outdoor air, construction materials, and living habits. As a result, indoor radon concentration shows variation, with the usual periodicity of one day and one year. It is well-known that seasonal variation of the radon concentration exists. It is particularly interesting to investigate indoor radon variation at the same measuring location and time period, each year, due to estimation of individual annual dose from radon exposure. The long-term indoor radon measurements, in a typical family house in Serbia, were performed. Measurements were taken during 2014, 2015, and 2016, in February and July, each year. The following measuring techniques were used: active and charcoal canisters methods. Analysis of the obtained results, using multivariate analysis methods, is presented.

Key words: radon variability, multivariate regression analysis, multi-seasonal radon measurements, indoor radon

INTRODUCTION

The research of the dynamics of radon in various environments, especially indoors, is of great importance in terms of protection against ionizing radiation and in designing of measures for its reduction. Published results and development of many models to describe the behavior of indoor radon, indicates the complexity of this research, especially with models for prediction of the variability of radon [1-3]. This is because the variability of radon depends on a large number of variables such as local geology, permeability of soil, building materials used for the buildings, the state of the indoor atmosphere (temperature, pressure and relative humidity), aerosol concentration, the exchange rate between indoor and outdoor air, construction materials, as well as the living habits of people. It is known that the indoor radon concentration variation has periodicity of one day and one year. It is also well-known that the seasonal variation of the radon concentration exists. This is why it is particularly interesting to investigate indoor radon variation at the same measuring location and time period, year after year, in order to estimate the individual annual dose from radon exposure. In that sense, we performed long-term indoor radon measurements in a typical family house in Serbia. Measurements were taken during the 2014, 2015, and 2016, in February and July, each year. We used the following measuring techniques: active and charcoal canisters methods. The detailed analysis of the obtained results using multivariate analysis (MVA) methods is presented in this paper.

First, MVA methods were tested on the radon variability studies in the Underground Low Background Laboratory in the Institute of Physics, Belgrade [4, 5]. Several climate variables: air temperature, pressure, and humidity were considered. Further advance was made by using all the publicly available climate variables monitored by nearby automatic meteorological station. In order to analyze the dependence of radon variation on multiple variables, multivariate analysis needs to be used. The goal was to find an appropriate method, out of the wide spectrum of multivariate analysis methods that are developed for the analysis of data from high-energy physics experiments, to analyze the measurements of variations of radon concentrations in indoor spaces. Previous

* Corresponding author; e-mail: udovicic@ipb.ac.rs

analysis were done using the maximum of 18 climate parameters and use and comparison of 8 different multivariate methods. In this paper the number of variables is reduced to the most important ones and new derived variables, like vapor pressure, simple modeled solar irradiance and simple modeled precipitation, which were introduced in the multivariate analysis.

INDOOR RADON MEASUREMENTS METHODS

Depending on the integrated measurement time, methods of measurement of the indoor radon concentrations may be divided into long-term and short-term ones. The device for the performed short-term radon measurements is SN1029 radon monitor (manufactured by the Sun Nuclear Corporation, NRSB approval-code 31822) with the following characteristics: the measurement range from 1 Bqm^{-3} to 99.99 $kBqm^{-3}$, accuracy equal to +25 %, sensitivity of 0.16 counts hour per Bqm^{-3}. The device consists of two diffused junction photodiodes as the radon detector which is furnished with sensors for temperature, barometric pressure, and relative humidity. The sampling time was set to 2 h. The method for Charcoal Canister used is: EERF Standard Operating Procedures for Radon-222 Measurement Using Charcoal Canisters [6], also used by major laboratories which conduct radon measurements in Serbia [7]. Exposure time of the charcoal canisters was 48 h. The connection between short term and long term measurements has attracted some interest previously [8].

The family house, selected for the measurements and analysis of variations of radon concentrations, is a typical house in Belgrade residential areas, with requirement of existence of cellar. House is built on limestone soil. Radon measurements were carried out in the living room of the family house, which is built of standard materials (brick, concrete, mortar) and isolated with styrofoam. During the period of measurements (winter-summer 2014, 2015, and 2016), the house was naturally ventilated and air conditioning was used in heating mode at the beginning of the measurement period. During the winter period measurements, the electrical heating was used in addition to air conditioning. Measured radon concentrations, room temperature (T_id), atmospheric pressure (P_id) and relative humidity (H_id) inside the house, were obtained using radon monitor. Values of meteorological variables, in the measurement period, were obtained from an automatic meteorological station, located near the house in which the measurement was performed. We used the following meteorological variables: external air temperature (T), also at height of 5cm, pressure (P) and humidity (H), solar irradiation, wind speed, precipitation, temperature of the soil at depths of 10 cm, 20 cm and 50 cm. The natural ventilation routine was not monitored. Since the ventilation is of crucial importance for the level of radon indoors [9], Multivariate regression analysis was used mainly for winter periods.

MULTIVARIATE REGRESSION ANALYSIS

In many fields of physics, especially in high-energy physics, there is the demand for detailed analyses of a large amount of data. For this purpose, the data analysis environment ROOT [10], is developed. ROOT is modular scientific software framework, which provides all the functionalities needed to deal with big data processing, statistical analysis, visualization and storage. A specific functionality gives the developed Toolkit for Multivariate Analysis (TMVA) [11]. The TMVA provides an environment for the processing, parallel evaluation and application of multivariate regression techniques.

TMVA is used to create, test and apply all available regression multivariate methods, implemented in ROOT, in order to find methods which are the most appropriate and yield maximum information on the dependence of indoor radon concentrations on the multitude of meteorological variables. Regression methods are used to find out which regression method can, if any, on the basis of input meteorological variables only, give an output that would satisfactorily close match the observed variations of radon concentrations. The output of usage of multivariate regression analysis methods has mapped functional behavior, which can be used to evaluate the measurements of radon concentrations using input meteorological variables only. All the methods make use of training events, for which the desired output is known and is used for training of Multivariate regression methods, and test events, which are used to test the MVA methods outputs.

RESULTS

Measurements were performed during February and July in 2014, 2015, and 2016 using radon monitor and charcoal canister measurements. The descriptive results are summarized in tab. 1. The measurements using radon monitor and charcoal canisters are in good agreement.

Previous work done by researchers from the Low Background Laboratory, Institute of Physics, Belgrade, using the MVA analysis in search of connections between radon concentration and meteorological variables, included only one period of measurement, February or July 2014 [4]. Now the MVA analysis is using all the measured data February/July 2014-2016. New variables introduced in MVA analysis are modeled solar irradiance, modeled precipitation and vapor

Table 1. Descriptive results of February and July 2014, 2015, and 2016 measurements, using radon monitor and charcoal canisters (only in February)

Results of measurements	2014		2015		2016	
	Feb.	July	Feb.	July	Feb.	July
Minimal radon activity using radon monitor [Bqm^{-3}]	15	0	28	0	12	3
Maximal radon activity using radon monitor [Bqm^{-3}]	1000	286	915	88	1013	262
Median radon activity using radon monitor [Bqm^{-3}]	418	25	524	22	412	28
Arithmetic mean of radon activity using radon monitor (standard deviation) [Bqm^{-3}]	402 (216)	40 (41)	508 (207)	27 (18)	423 (214)	39 (32)
Room temperature using radon monitor (standard deviation) [°C]	20.4 (0.8)	24.7 (0.9)	21.2 (0.6)	24.9 (0.8)	22.3 (0.6)	24.6 (0.8)
Relative humidity using radon monitor (standard deviation) [%]	67.4 (5.7)	67.8 (4.8)	68.2 (4.8)	51.5 (4.7)	64.0 (6.4)	58.9 (7.5)
Radon activity using charcoal canister (standard deviation) [Bqm^{-3}]	432 (10)	/	518 (6)	/	407 (5)	/

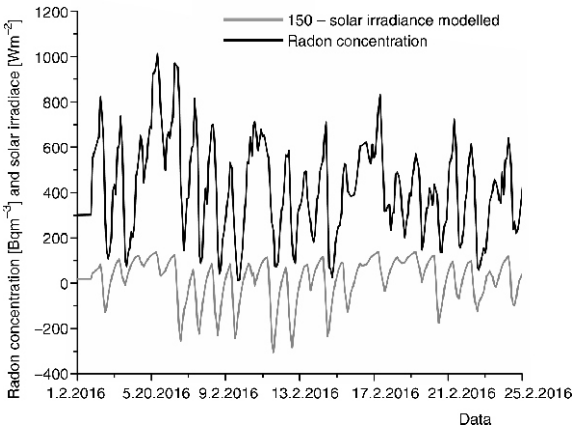

Figure 1. Modeled solar irradiance in comparison with measured radon concentration during February 2016

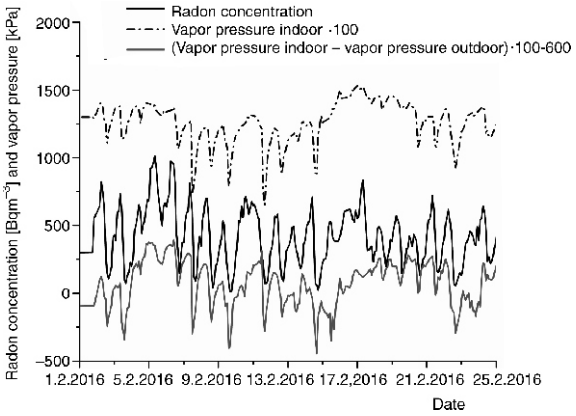

Figure 2. Vapor pressure in comparison with measured radon concentration during February 2016

pressure. In order to make use of intensity of solar irradiance during the whole day and night, the solar irradiance is modeled so that it includes 80 % of solar irradiance value from the previous measurement (previous hour) with addition of solar irradiance value for the actual hour of measurement (fig. 1). The value of 80 % is chosen so that the modeled solar irradiation has the best correlation with the radon measurements. Similar model of precipitation was used in this analysis. The next new variable is vapor pressure. The vapor pressure variable is calculated using the slope s(T), of the relationship between saturation vapor pressure and air temperature and is given by [12, 13], so that the vapor pressure equals relative humidity times saturation vapor pressure, fig. 2.

Before the start of training of Multivariate regression methods using TMVA toolkit in ROOT, the description of input meteorological variables is performed, mainly by looking into inter-correlations of input variables and their connections with the measured radon concentrations. The MVA is using all the measured data. Table 2 presents the meteorological variables and their module value of correlation with the measured radon concentrations (target), which is indicative in finding linear dependence of radon measurements and input variables. The second column in tab. 2 presents us with correlation ration values which indicate if there are some functional dependence (not only linear) between input variables and radon concentration, and the last column presents the mutual information which indicates if there is a non-functional dependence of input variables and radon measurements [11].

From tab. 2 it can be noticed that linear correlated values are not the only ones which can be used in MVA analysis, for example variable solar irradiance has high mutual information with the radon measurements.

In the data preparation for MVA training the whole dataset is consisting of many events. An event includes time of measurement, radon measurement and meteorological variables. The dataset is randomly split in two halves, one half of the events will be used for training of multivariate regression methods, and the other half of events for testing of methods, mainly to compare the measured and MVA evaluated values for radon concentration.

It turns out that the methods best suited for our purpose is the Boosted Decision Trees (BDT) method. This means that BDT gives the smallest difference be-

Table 2. Input variable rank and values for correlation, correlation ratio and mutual information, all with the measured radon concentrations (target) for February and July 2014-2016 measurements

Variable	Correlation with target		Correlation ratio		Mutual information	
	Rank	Value	Rank	Value	Rank	Value
Soil temperature depth 20 cm [°C]	1	0.87	1	0.60	13	1.48
Soil temperature depth 50 cm [°C]	2	0.86	2	0.57	14	1.31
Soil temperature depth 10 cm [°C]	3	0.82	3	0.54	9	1.84
Temperature outdoor [°C]	4	0.82	5	0.53	8	1.85
Vapor indoor – vapor od [mbar]	5	0.81	9	0.41	11	1.73
Temperature od – temperature id [°C]	6	0.80	4	0.53	6	1.92
Temperature height 5 cm [°C]	7	0.77	8	0.48	7	1.91
Vapor od [mbar]	8	0.76	10	0.41	5	1.92
Temperature id [°C]	9	0.75	7	0.49	17	1.16
Solar irradiance [Wm^{-2}]	10	0.61	6	0.50	2	2.23
Humidity indoor [%]	11	0.45	11	0.26	1	2.26
Humidity outdoor [%]	12	0.31	13	0.20	10	1.76
Air pressure outdoor [mbar]	13	0.27	17	0.07	12	1.55
Wind speed [ms^{-1}]	14	0.22	16	0.01	16	1.28
Air pressure indoor [mbar]	15	0.17	18	0.04	15	1.31
Humidity od – Humidity id [%]	16	0.10	14	0.19	4	2.11
Precipitation [Lm^{-2}]	17	0.01	15	0.19	18	1.13
Vapor indoor [mbar]	18	0.002	12	0.02	3	2.17

tween the measured radon concentration from test sample and the evaluation of value of radon concentration using input variables only. This can be seen in fig. 3, which shows the distribution of BDT and BDTG regression method outputs (evaluated values) in comparison with the measured radon concentration during February 2016.

Since TMVA has 12 different regression methods implemented, only some of those will give useful results when evaluating the radon concentration measurements. Table 4 summaries the results of MVA analysis. It shows the MVA methods RMS of difference of evaluated and measured radon concentration. Also, tab. 4 shows the mutual information of measured and MVA evaluated radon concentration. Besides

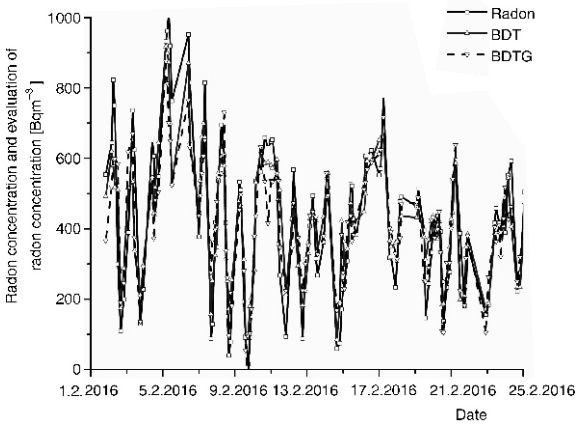

Figure 3. Comparison of MVA evaluated radon concentration and measured one from the test sample of events during February 2016

BDT, the Multi-Layer Perceptron (MLP) [10], an implementation of Artificial Neural Network multi variate method, also gives good results.

The MVA regression analysis results in mapped functional behavior and, as opposed to possible existence of theoretical modeling, which is independent of the number of measurements, MVA depends on the number of events. More events, the better mapped function we get as a result. In this sense, if the number of measurements is not great, multivariate analysis can be used only as help, to indicate which variables are more important to be used in theoretical modeling, for comparison of mapped and modeled functions, and modeled function test.

CONCLUSION

Indoor radon variation at one location in the same periods (February and July), was investigated for three years. Long-term indoor radon measurements show intense seasonal variation. The results obtained with different measuring methods are in good agreement. The radon behavior in the house is almost the same and shows good reproducibility year by year. The small variations in the year by year dynamics are originated mostly from the variations in meteorological variables during winter seasons and mostly due to ventilation habits during summer season. Ventilation habits were not monitored nor taken into account in MVA regression analysis. The preliminary results using multivariate analysis methods in TMVA are shown. Main output of Multivariate regression analy-

Table 3. Input variable correlation with the measured radon concentrations for February and July 2016

Correlation with target			
February 2016		July 2016	
Variable	Value	Variable	Value
Vapor id-vapor od [mbar]	0.58	Soil temperature depth 20 cm [°C]	0.46
Humidity id [%]	0.54	Soil temperature depth 50 cm [°C]	0.42
Vapor id [mbar]	0.52	Solar irradiance	0.32
Solar irradiance [Wm^{-2}]	0.48	Temperature id [°C]	0.30
Temperature od – temperature id [°C]	0.46	Soil temperature depth 10 cm [°C]	0.24
Temperature [°C]	0.44	Temperature od [°C]	0.21
Soil temperature depth 10 cm [°C]	0.43	Humidity od [%]	0.20
Soil temperature depth 20 cm [°C]	0.42	Humidity id [%]	0.19
Humidity [%]	0.38	Air pressure [mbar]	0.17
Temperature height 5 cm [°C]	0.32	Precipitation [Lm^{-2}]	0.17
Temperature id [°C]	0.29	Temperature od – temperature id [°C]	0.16
Air pressure od [mbar]	0.23	Air pressure_id [mbar]	0.16
Air pressure id [mbar]	0.21	Humidity od – humidity id [%]	0.14
Soil temperature depth 50 cm [°C]	0.20	Wind speed [ms^{-2}]	0.13
Precipitation [Lm^{-2}]	0.19	Temperature height 5 cm [°C]	0.12
Humidity od – humidity id [%]	0.15	Vapor id [mbar]	0.06
Vapor od [mbar]	0.08	Vapor od [mbar]	0.03
Wind speed [ms^{-1}]	0.05	Vapor id – vapor od [mbar]	0.02

Table 4. RMS of MVA method's evaluation error and mutual information; February/July 2014-2016

MVA method	RMS [Bqm^{-3}]	Mutual information
BDT	85.5	1.477
BDTG	92.1	1.614
MLP	101	1.401

sis is the initial version of *mapped* function of radon concentration dependence on multitude of meteorological variables. Simplification of MVA methods can be made by choosing only the most important input variables and exclude the other variables.

ACKNOWLEDGEMENTS

The authors acknowledge the financial support of the Ministry of Science, Technology and Development of Serbia within the projects: Nuclear Methods Investigations of Rare Processes and Cosmic Rays (grant number 171002) and Biosensing Technologies and Global System for Continuous Research and Integrated Management (grant number 43002).

AUTHORS' CONTRIBUTIONS

The idea for this paper came as a result of discussions of V. I. Udovičić, R. M. Banjanac, D. R. Joković, A. L. Dragić, and D. M. Maletić. Gathering climate data and MVA analysis was done by D. M. Maletić and V. I. Udovičić. Performed indoor radon measurements were done by V. I. Udovičić and S. M. Forkapić. Writing of the paper was done by D. M. Maletić and V. I. Udovičić. A. L. Dragić gave idea about using MVA methods in cosmic and radon measurements. N. B. Veselinović and M. R. Savić analyzed and validated climate data. J. Z. Živanović helped with MVA analysis. D. R. Joković helped with data analysis and paper technical preparation.

REFERENCES

[1] Collignan, B., *et al*., Development of a Methodology to Characterize Radon Entry in Dwellings, *Building and Environment, 57* (2012), Nov., pp. 176-183
[2] Li, F., Baixeras, C., The RAGENA Dynamic Model of Radon Generation, Entry and Accumulation Indoors, *Science of the Total Environment, 307* (2003), 1-3, pp. 55-69
[3] Jelle, B. P., *et al*., Development of a Model for Radon Concentration in Indoor Air, *Science of the Total Environment, 416* (2012), Jan., pp. 343-350
[4] Maletić, D., *et al*., Comparison of Multivariate Classification and Regression Methods for Indoor Radon Measurements, *Nucl Technol Radiat, 29* (2014), 1, pp. 17-23
[5] Udovičić, V., *et al*., Radon Problem in an Underground Low-Level Laboratory, *Radiation Measurements, 44* (2009), 9-10, pp. 1009-1012
[6] ***, EPA 520/5-87-005, Gray D.J, Windham S.T, United States Environmental Protection Agency, Montgomery, 1987
[7] Živanović, M. Z., *et al*., Radon Measurements with Charcoal Canisters, *Nucl Technol Radiat, 31* (2016), 1, pp. 65-72
[8] Stojanovska, Z., *et al*., Prediction of Long-Term Indoor Radon Concentrations Based on Short-Term Measurements, *Nucl Technol Radiat, 32* (2017), 1, pp. 77-84
[9] Nikolić, M. D., *et al*., Modelling Radiation Exposure in Homes from Siporex Blocks by Using Exhalation Rates of Radon, *Nucl Technol Radiat, 30* (2015), 4, pp. 301-305
[10] Brun, R., Rademakers, F., ROOT – An Object Oriented Data Analysis Framework, *Nucl. Inst. Meth. in Phys. Res., A 389* (1997), 1-2, pp. 81-86

[11] Hoecker, A., *et al*., TMVA – Toolkit for Multivariate Data Analysis, PoS ACAT 040, arXiv:physics/070 303, 2007
[12] Murray, F. W., On the Computation of Saturation Vapor Pressure, *J. Applied Meteorology, 6* (1967), 1, pp. 203-204
[13] Tetens, O., About Some Meteorological Aspects (in German), *Z. Geophys, 6* (1930), pp. 207-309

Received on October 6, 2018
Accepted on June 8, 2018

Владимир И. УДОВИЧИЋ, Димитрије М. МАЛЕТИЋ, Радомир М. БАЊАНАЦ, Дејан Р. ЈОКОВИЋ, Александар Л. ДРАГИЋ, Никола Б. ВЕСЕЛИНОВИЋ, Јелена З. ЖИВАНОВИЋ, Михаило Р. САВИЋ, Софија М. ФОРКАПИЋ

СТУДИЈА СЛУЧАЈА ВИШЕГОДИШЊЕ ВАРИЈАБИЛНОСТИ РАДОНА У ПОРОДИЧНОЈ КУЋИ У СРБИЈИ

Понашање радона у затвореном простору има сложену динамику због утицаја великог броја различитих параметара који утичу на његову варијабилност: метеоролошких (температура, притисак и релативна влажност), концентрације аеросола, брзине размене између унутрашњег и спољашњег ваздуха, грађевинских материјала и животних навика. Као резултат, концентрација радона у затвореним просторијама показује варијацију, уз стандардну периодичност од једног дана и једне године. Годишња варијабилност је добро позната сезонска варијација концентрације радона. Посебно је интересантно пратити вишегодишње варијације концентрације радона на истој мерној локацији и временском периоду, пре свега због процене индивидуалних годишњих доза од изложености радону. У типичној породичној кући у Србији извршена су дуготрајна мерења радона у дневном боравку. Мерења су рађена током 2014, 2015, и 2016. године, у фебруару и јулу, сваке године. Коришћене су следеће мерне технике: активна и метода коришћења угљених канистера. Добијени резултати анализирани су коришћењем мултиваријантне регресионе анализе.

Кључне речи: варијабилност радона, мултиваријантна регресиона анализа, радон у затвореним просторијама, вишегодишње мерење радона

Available online at www.sciencedirect.com

ScienceDirect

Advances in Space Research 63 (2019) 1483–1489

ADVANCES IN SPACE RESEARCH (a COSPAR publication)

www.elsevier.com/locate/asr

Rigidity dependence of Forbush decreases in the energy region exceeding the sensitivity of neutron monitors

M. Savić, N. Veselinović *, A. Dragić, D. Maletić, D. Joković, R. Banjanac, V. Udovičić

Institute of Physics, University of Belgrade, Pregrevica 118, 11080 Zemun, Serbia

Received 2 May 2018; received in revised form 14 September 2018; accepted 24 September 2018
Available online 28 September 2018

Abstract

Applicability of our present setup for solar modulation studies in a shallow underground laboratory is tested on four prominent examples of Forbush decrease during solar cycle 24. Forbush decreases are of interest in space weather application and study of energy-dependent solar modulation, and they have been studied extensively. The characteristics of these events, as recorded by various neutron monitors and our detectors, were compared, and rigidity spectrum was found. Linear regression was performed to find power indices that correspond to each event. As expected, a steeper spectrum during more intense extreme solar events with strong X-flares shows a greater modulation of galactic cosmic rays. Presented comparative analysis illustrates the applicability of our setup for studies of solar modulation in the energy region exceeding the sensitivity of neutron monitors.

Keywords: Forbush decrease; Muon CR station; Median rigidity

1. Introduction

Galactic cosmic rays (GCRs) traverse the heliosphere; this leads to variation in the cosmic ray (CR) flux due to solar activity. The influence of solar and heliospheric modulation is pronounced for primary CR particles with low rigidity or momentum over unit charge. CRs interact, upon arrival, with Earth's atmosphere causing electromagnetic and hadronic showers. A network of ground-based CR detectors, neutron monitors (NMs), and muon detectors, located at various locations around the globe, as well as airborne balloons and satellites, provide valuable data to study the effect of these modulations on the integrated CR flux with time. Energies of the primary particles in NMs are sensitive to the state of solar activity and reach up to 40 GeV. Muon detectors have a significant response from 10 GeV up to several hundred GeV for surface, and one order of magnitude greater for underground detectors, depending on the depth (Duldig, 2000). This energy interval allows muon detectors to monitor not only modulation effects on lower-energy CRs but also galactic effects on primary CRs with high energies where solar modulation is negligible. Because of the sensitivity to different energies of the primary particle flux, observations of muon detectors complement those of NMs in studies of long-term CR variations, CR anisotropy, and gradients or rigidity spectrum of Forbush decreases (FDs).

FDs (Forbush, 1954) represent decreases of the observed GCR intensity under the influence of coronal mass ejections (CMEs) and interplanetary counterparts of coronal mass ejections (ICMEs) and/or high-speed streams of solar wind (HSS) from the coronal holes (Belov, 2008). FDs belong to two types depending on the drivers: non-recurrent and recurrent decreases. This work addresses several non-recurrent FDs.

These sporadic FDs are caused by ICMEs. As the matter with its magnetic field moves through the solar system,

* Corresponding author.
E-mail address: veselinovic@ipb.ac.rs (N. Veselinović).

https://doi.org/10.1016/j.asr.2018.09.034
0273-1177/

it suppresses the CR intensity. FDs of this kind have an asymmetric profile, and the intensity of GCRs has a sudden onset and recovers gradually. Sometimes an early phase of FD prior to the dip (precursor of FD) shows an increase in CR intensity. These precursors of FDs are caused by GCR acceleration at the front of the advancing disturbance on the outer boundary of the ICME, as the primary CR particles are being reflected from the approaching shock (Papailiou et al., 2013). The FD profile depends on the area, velocity, and intensity of CME magnetic field produced in extreme events that originate at the Sun (Chauhan et al., 2008).

Data from observed modulation of GCR intensity contain information regarding the transport of GCRs through the interplanetary environment. GCR transport parameters are connected with the interplanetary magnetic field (IMF) in the heliosphere. It is empirically established that the radial diffusion coefficient is proportional to the rigidity of CR (Ahluwalia, 2005). In this article, we present an analysis of the amplitude of FD during four events, which were recorded by plastic scintillator muon detectors, located at the Belgrade muon station, as well as by a network of NMs.

2. Belgrade CR station

The Low-Background Laboratory for Nuclear Physics (LBLNP) is a part of the Institute of Physics, University of Belgrade. It is composed of two separate laboratory facilities, ground-level laboratory (GLL) and underground laboratory (UL), dug into a cliff. The overburden of the UL is approximately 12 m of loess soil, which is equivalent to 25 m of water (m.w.e). Laboratory is dedicated to measurements of low radiation activities and studies of muon and electromagnetic components of CRs at ground and shallow underground levels. The geographic position of the laboratory is at 75 m a.s.l., at 44°51′N latitude and 20°23′E longitude; geomagnetic vertical rigidity cutoff is 5.3 GV at the surface. The equipment was upgraded in 2008, and now, it consists of two identical sets of detectors and accompanying data processing electronics: one is situated in GLL and the other in UL. Detectors are a pair of plastic scintillator detectors, with dimensions of 100 cm × 100 cm × 5 cm and four PMTs that are directly coupled to the corners. Signals from two opposite PMTs on a single detector are summed, and the coincidence of the two diagonals is found. Fig. 1 presents the coincident sum spectra of two diagonals of large scintillator detectors.

Summing over diagonals suppresses the acquisition of electromagnetic component of the secondary CR shower and collects mainly the muon component of secondary CRs. A well-defined peak in the energy spectra corresponds to a muon energy loss of ~11 MeV. The average muon flux measured in the laboratory is 137(6) muons/m^{2}s for GLL and 45(2) muons/m^{2}s for UL. For more detailed description, see Dragić et al. (2011). Integral of this distribution, without low energy part, is used to form time series of this

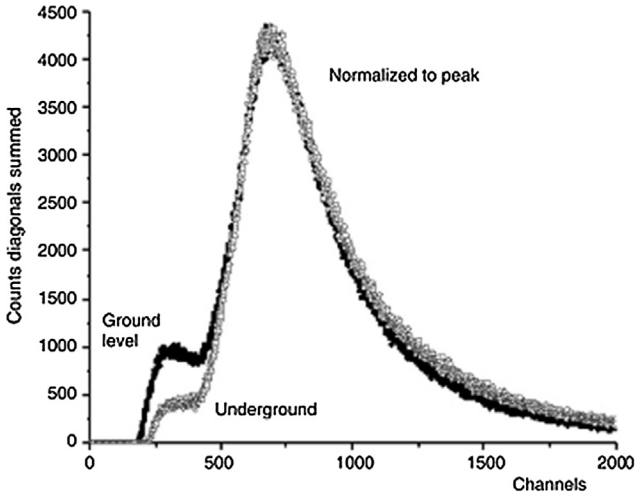

Fig. 1. The coincident spectra of two diagonals of large plastic detectors in UL and GLL normalized for comparison.

CR muons spectrum integrated over different time intervals. This time series is then corrected for efficiency, atmospheric pressure, and temperature (Savić et al., 2015).

The CR flux measured at the ground level varies because of changes in atmospheric conditions. Effects of the atmospheric pressure can be easily accounted for, similar like for NMs, but the temperature effect is somewhat more difficult to treat. The difficulties arise from the interplay of positive and negative temperature effects. With temperature increase, the atmospheric density decreases; hence, less pions interact and more muons are created from decay. The result is a positive effect of more muons at the ground level. On the other hand, the altitude of muon production level is high due to the expansion of the atmosphere when the temperature is high, muon path length is long, and decay probability of muons is high before they reach the ground level. Negative effect is dominant for low-energy muons (mostly detected in GLL) and positive for high-energy muons. A proper treatment of the temperature effect requires knowledge of the entire temperature profile of the atmosphere. This meteorological variation must be corrected to study CR variations originating outside the atmosphere.

For ground (and underground)-based CR detectors, the response function, i.e., the relation between particles of GCR spectra at the top of the atmosphere and recorded secondary particles at the surface level, should be accurately known. The total detector count rate can be expressed as follows (Caballero-Lopez and Moraal, 2012):

$$N(R_0,h,t) = \sum_i \int_{R_0}^{\infty} (S_i|(R,h) j_i(R,t))dR = \int_{R_0}^{\infty} W(R,h,t)dR \quad (1)$$

where $N(R_0,h,t)$ is the detector counting rate, R_0 is the geomagnetic cutoff rigidity, h is the atmospheric depth, and t represents time. $S_i(R,h)$ represents the detector yield

function for primary particles of type i and $j_i(R,t)$ represents the primary particle rigidity spectrum of type i at time t. The total response function $W(R,h,t)$ is the sum of $S_i(R,h)$ and $j_i(R,t)$. The maximum value of this function is in the range of 4–7 GV at sea level, depending on the solar modulation epoch at time t (Clem and Dorman, 2000). One of the methods to find this response function is to use the numerical simulation of propagation of CRs through the atmosphere. CORSIKA simulation package (Heck et al., 1998) was to simulate CR transport through the atmosphere and GEANT4 (Agostinelli et al., 2003) to simulate the propagation of secondary CRs through overburden and response of the detectors to find the relationship between the count rate at our site and the flux of primary particles on top of the atmosphere.

The excellent agreement of the simulated and measured flux (Fig. 2) allows us to establish that the cutoff energy for primary CR protons for showers detected in GLL is caused by its geomagnetic rigidity, and the median energy is ~60 GeV. For UL, the cutoff energy due to earth overburden is 12 GeV, and the median energy is ~120 GeV. These values give us opportunity to study solar modulation at energies exceeding energies detected with a NM. Observation of the solar activity and related magnetic disturbances in the heliosphere that create transient CR intensity variation at several different energies can provide an energy-dependent description of these phenomena.

3. Data analysis

The new setup in the LBLNP, presented by Dragić et al. (2011) coincides with the start of the 24th solar cycle, thus allowing us to observe the increase and decrease in solar activity and the effect of solar modulation at energies higher than ones studied using NMs.

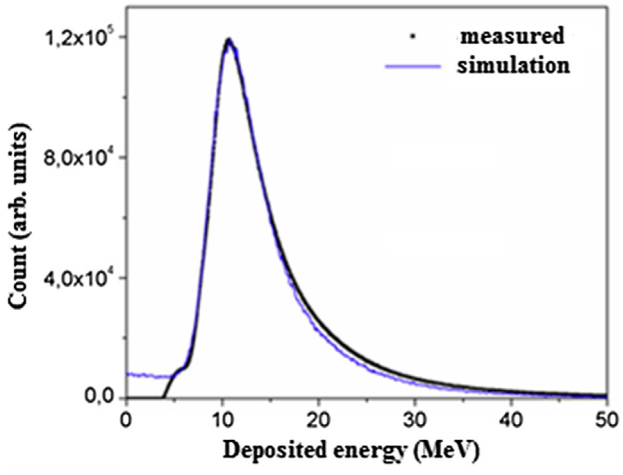

Fig. 2. Simulated (blue line) and measured spectra (black line) for muon detectors in UL. (For interpretation of the references to colour in this figure legend, the reader is referred to the web version of this article.)

Muon time series was searched for days where the average muon flux was significantly lower than the background level. The background level is determined from the moving averages of hourly count rates 10 days before the event. These decreases in the count rate, in GLL and UL, are then compared with space weather events of solar cycle 24. Data collected in UG and GLL are compared with four NM stations from the neutron monitor database [http://www.nmdb.eu/]. Three of these NMs (Athens, Rome, and Jungfraujoch) have cutoff rigidity and geographic proximity similar to the Belgrade CR station.

A high correlation is found between the count rates measured by the NMs in the LBLNP in March 2012 (Table 1), but for GLL and UL, as the cutoff energy of the primary flux increases, the correlation slightly decreases.

3.1. Selected Forbush decreases

The Belgrade CR station has detected, both in GLL and UL, several significant structures connected to some extreme solar effects. Several, more prominent, Forbush decreases occurred in March 2012, September 2014, June 2015, and most recently in September 2017.

The FD that occurred on March 8, 2012 was recorded at the Belgrade CR station as well as at other stations (Fig. 3). This FD was separated into two following two CMEs. These CMEs produced an intense disturbance in the interplanetary space and caused a severe geomagnetic storm when the shockwave reached Earth on March 8, 2012. During this event, a very complex combination of modulation occurs (Lingri et al., 2016). Two CMEs from the same active region as the September 10 (X1.6) flare produced FD on September 12, 2014. There was a relatively fast partial halo CME and a larger and rapidly moving halo CME trailing behind the first one on September 10. These two gave rise to the FD that was first detected by NMs on September 12, 2014. This FD was not a classical two-step FD as expected, probably due to the interaction of slower and faster CMEs. The FD profile (Fig. 3) showed a small second step several hours after the first, similar to the FD that occurred in February 2011 (Papaioannou et al., 2013). In June 2015, a large activity occurred in the Sun from powerful AR 2371 that produced several CMEs from the Sun. These CMEs induced a complex modulation of GCRs that led to an FD occurrence on June 22, 2015 with an unusual structure (Samara et al., 2018).

A sudden burst of activity from the Sun early in September 2017, after a prolonged period of low solar activity, produced several flares, including the largest solar flare seen from Earth since 2006, an X9.3 flare. This activity produced several Earth-directed CMEs. Throughout this time, Earth experienced a series of geomagnetic storms, which started promptly after the first CME. This unusual activity produced an FD, which was recorded with detectors in terms of ground level enhancement (GLE) on Earth and Mars (Guo et al., 2018).

Table 1
Correlation matrix of the linear correlation coefficient (in%) for recorded hourly flux at the Belgrade CR station with its temperature- and pressure-corrected underground and ground-level detectors (UL_tpc and GLL_tpc), only pressure-corrected detectors (UL_pc, GLL_pc), and raw data detectors (UL_raw and GLL_raw) and recordings at Rome, Oulu, Jungfraujoch (Jung.) and Athens NMs for March 2012.

UL_tpc	75	81	80	81	76	73	78	86	97	100
UL_pc	77	83	83	83	73	78	72	84	100	97
UL_raw	57	71	70	74	94	49	51	100	84	86
GLL_tpc	86	86	84	83	59	90	100	51	72	78
GLL_pc	90	92	90	89	56	100	90	49	78	73
GLL_raw	63	79	78	81	100	56	59	94	73	76
Oulu	90	98	98	100	81	89	83	74	83	81
Jung.	91	98	100	98	78	92	84	70	83	80
Rome	91	100	98	98	79	92	86	71	83	81
Athens	100	91	91	90	63	90	86	57	77	75
	Athens	Rome	Jung.	Oulu	GLL_raw	GLL_pc	GLL_tpc	UL_raw	UL_pc	UL_tpc

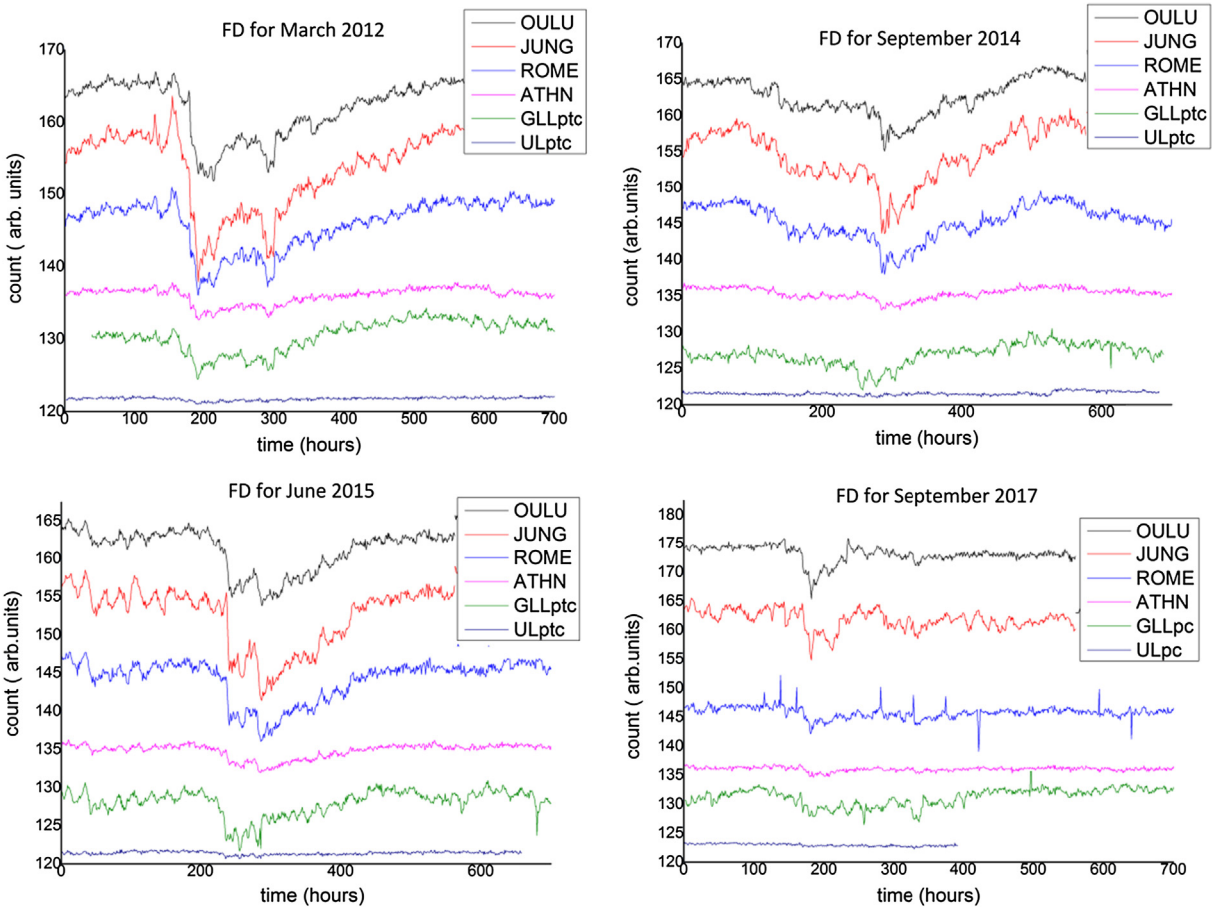

Fig. 3. Comparison of hourly time series over a one month period for pressure- and temperature-corrected count rates of the Belgrade muon monitor station (GLL_{ptc} and UL_{ptc}) and NMs at Athens (ATHN), Rome (ROME), Jungfraujoch (JUNG), and Oulu (OULU) for extreme solar events in March 2012, September 2014, and June 2015. Count rates are shifted for comparison. For extreme solar event in September 2017, for GLL and UL, the count rate is pressure-corrected only.

4. FD and median rigidity

For each event, we study the energy dependence of FD amplitude. The energy dependence of FD amplitude is expected to follow the power law: $\Delta N/N \sim R^{-\gamma}$ (Cane, 2000). To obtain reliable values of amplitudes, we defined amplitude as a relative decrease in the hourly count rate of the minimum compared with the average of seven days'

Table 2
Median and cutoff rigidity for several stations.

Stations	Median rigidity R_m (GV)	Min. rigidity R_0 (GV)
Athens	25.1	8.53
Mexico	25.1	8.28
Almaty	15.8	6.69
Lomnicky stit	12.6	3.84
Moscow	15.8	2.43
Kiel	15.8	2.36
Yakutsk	12.6	1.65
Apatity	12.6	0.65
Inuvik	12.6	0.3
Mc Murdo	12.6	0.3
Thule	12.6	0,3
South Pole	10	0.1
UL	122	12.3
GLL	63	5.3

count rate before FDs (not including possible precursory increases). Such a long base period was used because of the higher activity of the Sun prior to registrated FDs and sensitivity of the muon detectors.

Amplitudes are determined for two of our detectors and for 12 NMs. To investigate the rigidity spectrum of

Table 3
Power indices of the median rigidity dependence of the dip of the FD. Power indices are obtained for NMs only, NMs and the Belgrade muon station, and Belgrade station only.

γ	NM only	NM + Belgrade	Belgrade station only
March 2012	0.82 ± 0.08	0.78 ± 0.03	0.715
Sept. 2014	0.79 ± 0.16	0.67 ± 0.06	0.744
June 2015	0.57 ± 0.05	0.58 ± 0.02	0.764
Sept. 2017	1.27 ± 0.16	0.86 ± 0.07	0.739

mentioned FDs, the median rigidity R_m is defined. R_m is the rigidity of the response of the detector to GCR spectrum where 50% of the detector counting rate lies below R_m (Ahluwalia and Fikani, 2007). For this study, we used a list of R_m for 12 NM stations given by Minamino et al. (2014). For an NM, the median rigidity can be computed from the detector response function derived from surveys for particulate station, usually around the minima of solar activity; this is because the intensity of lowest rigidity GCRs is maximum at that time.

For the Belgrade muon station, R_m was found using the response function acquired by the Monte Carlo method of

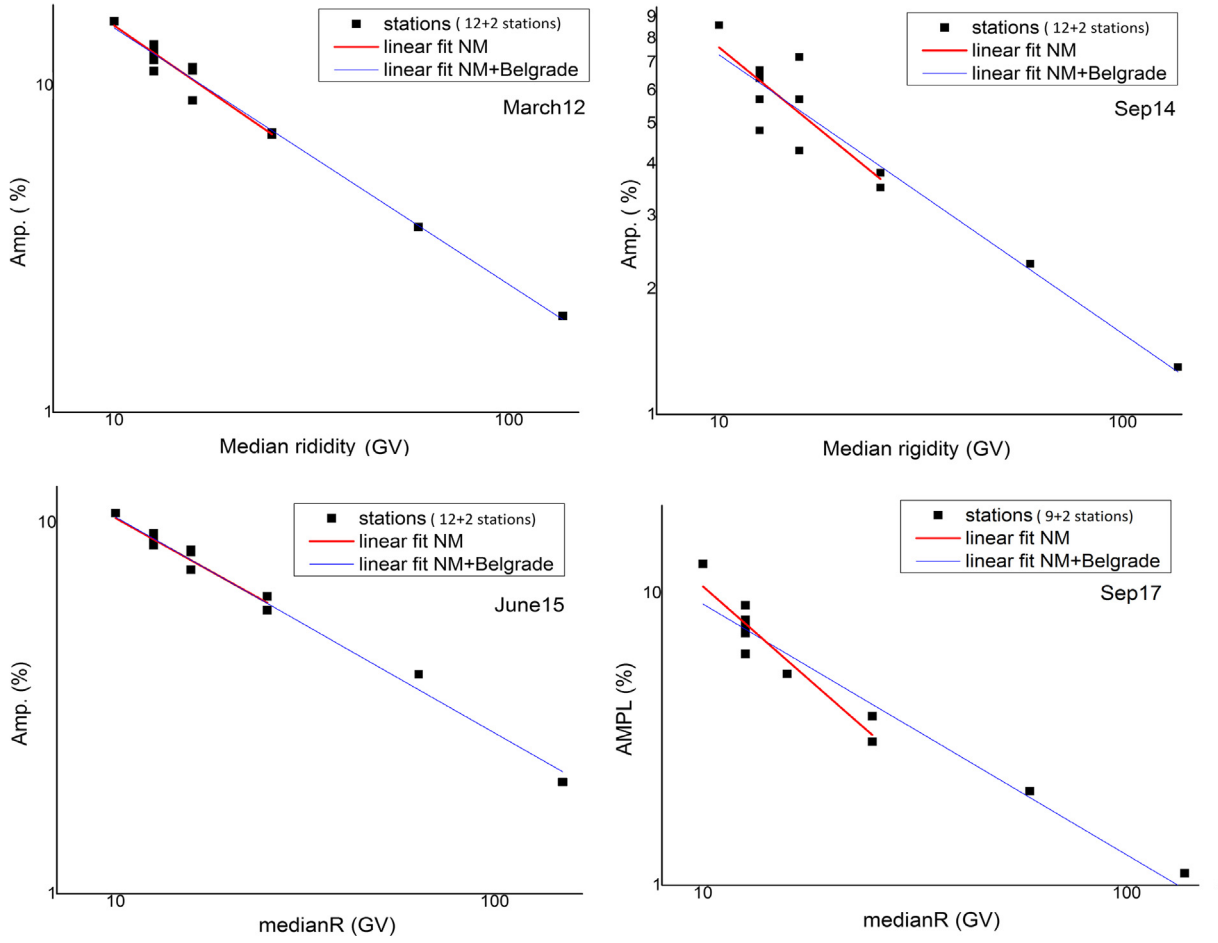

Fig. 4. Rigidity spectrum of FD from March 8, 2012, September 12, 2014, June 22, 2015, and September 8, 2017. Points represent the amplitude of the event as seen by NMs and the Belgrade CR station.

CR transport. Approximate values of R_m for the detectors used in this study are provided in Table 2.

For every selected event, a scatter plot is drawn (Fig. 4). All plots show, plotted in log-log scale, a clear median rigidity dependence of the amplitude of FD decrease.

Linear regression was performed to find power indices corresponding to each event. Power indices are given in Table 3.

Higher power indices can be due to more complex variations in GCRs. This more complex variation is a result of a series of CMEs during this event that leads to large compound ICME structure with multiple shocks and transient flow (Zhao and Zhang, 2016). Results obtained from the power law are generally consistent with those obtained in previous studies (Ahluwalia and Fikani, 2007, Lingri et al., 2016, Klyueva et al., 2017) conducted for NMs only.

A more significant difference observed for indices during the 2017 event was because we used only pressure-corrected data for the muon flux recorded at the Belgrade station. For all other events and data, we performed both pressure and temperature correction. Without temperature corrections, variation in the count rate in muon detectors is higher and it can affect the results.

We expect that when the newly improved, internally developed technique for temperature correction of the CR flux is implemented, the amplitude of the FD measured at the Belgrade muon station will be more consistent with other events and measurements. More data points on the graphs are needed to understand indices better, particularly in an energy region between NM and our laboratory. Similar work (Braun et al., 2009) discussed the extension up to 15 and 33 GeV, but there are no data available for FDs during cycle 24 and cannot be incorporated into this work. As for other operating muon telescopes, there is an agreement between the data obtained at our stations data and the URAGAN data for FD in June 2015 (Barbashina et al., 2016), but we have no data on other FDs and/or median energies of other stations. Our new experimental setup described elsewhere (Veselinović et al. 2017) will provide two additional median energies (121 and 157 GeV) to monitor variations in the CR flux.

5. Conclusion

The Belgrade CR station, with both ground level and underground setups, monitors the effect of solar modulation on the CR flux since 2008. Extreme solar events, like Forbush decreases, were detected during solar cycle 24 at the site, suggesting that these phenomena can be studied at energies higher than typical ones detected with NMs. GLL and UL data, as well as data from several NM stations, were used to analyze four intense FDs. The magnitude of FDs is energy (rigidity) dependent and follows the power law. Data used to find the rigidity dependence of these transient solar modulation of GCR were obtained over much higher range of rigidities than region NMs are sensitive in, thus allowing more extensive studies of CR solar modulation processes.

Acknowledgements

We acknowledge the NMDB (www.nmdb.eu), founded under the European Union's FP7 programme (contract no. 213007), for providing data. We acknowledge individual monitors for following the information given on the respective station information page. *Athens NM data were kindly provided by the Physics Department of the National and Kapodistrian University of Athens. Jungfraujoch NM data were kindly provided by the Physikalisches Institut, University of Bern, Switzerland.* Oulu NM *data were kindly provided by* http://cosmicrays.oulu.fi and Sodankyla Geophysical Observatory. Rome NM data were kindly provided by SVIRCO NM, supported by INAF/IAPS-UNIRoma3 COLLABORATION. We thank the anonymous referees for useful advices.

The present work was funded by the Ministry of Education, Science and Technological Development of the Republic of Serbia, under Project No. 171002.

References

Agostinelli, S., et al., GEANT4—A Simulation Toolkit, 2003. Nuclear Instruments and Methods in Physics Research Section A 506, pp. 250–303. https://doi.org/10.1016/S0168-9002(03)01368-8.

Ahluwalia, H.S., 2005. Cycle 20 solar wind modulation of galactic cosmic rays: understanding the challenge. J. Geophys. Res. 110, A10106. https://doi.org/10.1029/2005JA011106.

Ahluwalia, H.S., Fikani, M.M., 2007. Cosmic ray detector response to transient solar modulation: Forbush decreases. J. Geophys. Res. 112 (A8), A08105. https://doi.org/10.1029/2006JA011958.

Barbashina, N.S., Ampilogov, N.V., Astapov, I.I., Borog, V.V., Dmitrieva, A.N., Petrukhin, A.A., Sitko, O.A., Shutenko, V.V., Yakovleva, E.I., 2016. Characteristics of the Forbush decrease of 22 June 2015 measured by means of the muon hodoscope URAGAN. J. Phys.: Conf. Ser. 675 (3). https://doi.org/10.1088/1742-6596/675/3/032038, article id. 032038.

Belov, A.V., 2008. Forbush effects and their connection with solar, interplanetary and geomagnetic phenomena. In: Proceedings of the International Astronomical Union 4.S257, pp. 439–450. https://doi.org/10.1017/S1743921309029676.

Braun, I., Engler, J., Hörandela, J.R., Milke, J., 2009. Forbush decreases and solar events seen in the 10–20 GeV energy range by the Karlsruhe Muon Telescope. Adv. Space Res. 43 (4), 480–488. https://doi.org/10.1016/j.asr.2008.07.012.

Caballero-Lopez, R.A., Moraal, H., 2012. Cosmic-ray yield and response functions in the atmosphere. J. Geophys. Res. Space Phys. 117 (A12), 7461–7469. https://doi.org/10.1029/2012JA017794.

Cane, H.V., 2000. Coronal mass ejections and Forbush decreases. Space Sci. Rev. 93 (1–2), 55–77. https://doi.org/10.1023/1026532125747.

Chauhan, M.L., Jain Manjula, S.K., Shrivastava, S.K., 2008. Study of two major Forbush decrease events of 2005. In: Proceedings of the 30th International Cosmic Ray Conference, Mexico City, vol. 1 (SH), pp. 307–310. https://doi.org/10.7529/ICRC2011/V10/0097.

Clem, J.M., Dorman, L.I., 2000. Neutron monitor response functions, cosmic rays and earth. Space Sci. Rev. 93 (1/2), 335–359. https://doi.org/10.1023/A:1026515722112.

Dragić, A., Udovičić, V., Banjanac, R., Joković, D., Maletić, D., Veselinović, N., Savić, M., Puzović, J., Aničin, I.V., 2011. The new setup in the Belgrade low-level and cosmic-ray laboratory. Nucl.

Technol. Radiat. Protect. 26 (3), 181–192. https://doi.org/10.2298/NTRP1101064N.

Duldig, M.L., 2000. Muon observations. In: Bieber, J.W., Eroshenko, E., Evenson, P., Flückiger, E.O., Kallenbach, R. (Eds.), Cosmic Rays and Earth. Space Sciences Series of ISSI. Springer, Dordrecht, pp. 207–226. https://doi.org/10.1007/978-94-017-1187-6_1.

Forbush, S.E., 1954. World-wide cosmic ray variations, 1937–1952. J. Geophys. Res. 59 (4), 525–542. https://doi.org/10.1029/JZ059i004p00525.

Guo, J., Dumbović, M., Wimmer-Schweingruber, R.F., Temmer, M., Lohf, H., Wang, Y., Veronig, A., Hassler, D.M., Leila, M., Mays, L. M., Zeitlin, C., Ehresmann, B., Witasse, O., Freiherr von Forstner, J. L., Heber, B., Holmström, M., Posner, A., 2018. Modeling the evolution and propagation of the 2017 September 9th and 10th CMEs and SEPs arriving at Mars constrained by remote-sensing and in-situ measurement. Also Available at: arXiv preprint arXiv:1803.00461.

Heck, D., Knapp, J., Capdevielle, J.N., Schatz, G., Thouw, T., 1998. CORSIKA: a Monte Carlo code to simulate extensive air showers. Forschungszentrum Karlsruhe GmbH, p. V +90, TIB Hannover, D-30167 Hannover.

Klyueva, A.I., Belov, A.V., Eroshenko, E.A., 2017. Specific features of the rigidity spectrum of Forbush effects. Geomag. Aeron. 57 (2), 177–189. https://doi.org/10.1134/S0016793217020050.

Lingri, D., Mavromichalaki, H., Belov, A., Eroshenko, E., Yanke, V., Abunin, A., Abunina, M., 2016. Solar activity parameters and associated Forbush decreases during the minimum between cycles 23 and 24 and the ascending phase of cycle 24. Sol. Phys. 291 (3), 1025–1041. https://doi.org/10.1007/s11207-016-0863-8.

Minamino, Mohanty, Morishita, et al. for the GRAPES-3 Collaboration, 2014. Rigidity Dependence of Forbush Decreases, Poster #654. In: Proceedings of the 33rd International Cosmic Ray Conference, Rio de Janeiro, Brazil, pp. 3612–3615.

Papailiou, M., Mavromichalaki, H., Abunina, M., Belov, A., Eroshenko, E., Yanke, V., Kryakunova, O., 2013. Forbush decreases associated with western solar sources and geomagnetic storms: a study on precursors. Sol. Phys. 283 (2), 557–563. https://doi.org/10.1007/s11207-013-0231-x.

Papaioannou, A., Belov, A.A., Mavromichalaki, H., Eroshenko, E., Yanke, V., Asvestari, E., Abunin, A., Abunina, M., 2013. The first Forbush decrease of solar cycle 24. J. Phys. Conf. Ser. 409 (1). https://doi.org/10.1088/1742-6596/409/1/012202.

Samara, E., Smponias, I.A., Lytrosyngounis, I., Lingri, D., Mavromichalaki, H., Sgouropoulos, C., 2018. Unusual cosmic ray variations during the Forbush decreases of June 2015. Sol. Phys. 293 (67). https://doi.org/10.1007/S11207-018-1290-9.

Savić, M., Maletić, D., Joković, D., Veselinović, N., Banjanac, R., Udovičić, V., Dragić, V., 2015. Pressure and temperature effect corrections of atmospheric muon data in the Belgrade cosmic-ray station. J. Phys. Conf. Ser. 632 (1). https://doi.org/10.1088/1742-6596/632/1/012059, article id. 012059.

Veselinović, N., Dragić, A., Savić, M., Maletić, D., Joković, D., Banjanac, R., Udovičić, V., 2017. An underground laboratory as a facility for studies of cosmic-ray solar modulation. Nucl. Instrum. Meth. A875, 10–15. https://doi.org/10.1016/j.nima.2017.09.008.

Zhao, L.-L., Zhang, H., 2016. Transient galactic cosmic-ray modulation during solar cycle 24: a comparative study of two prominent forbush decrease events. Astrophys. J. 827 (1). https://doi.org/10.3847/0004-637X.

Astroparticle Physics 109 (2019) 1–11

Contents lists available at ScienceDirect

Astroparticle Physics

journal homepage: www.elsevier.com/locate/astropartphys

A novel method for atmospheric correction of cosmic-ray data based on principal component analysis

M. Savić, A. Dragić*, D. Maletić, N. Veselinović, R. Banjanac, D. Joković, V. Udovičić

Institute of Physics, University of Belgrade, Pregrevica 118, Zemun 11080, Serbia

ARTICLE INFO

Article history:
Received 23 August 2018
Revised 8 December 2018
Accepted 29 January 2019
Available online 29 January 2019

Keywords:
Cosmic rays
Muons
Atmospheric corrections
Principal component analysis

ABSTRACT

A new method for atmospheric correction of cosmic ray data is designed. It's fully empirical, based on the principal component analysis. The method requires knowledge of the pressure and the temperature profile of the atmosphere. It's applicable to all muon detectors. The method is tested on muon data from two detectors in Belgrade cosmic ray station, one located on the ground level and the other at the depth of 25 mwe. Correction reduces variance by 64.5% in ground level detector data and 38.1% in underground data. At the same time, the amplitude of the annual variation is reduced by 86.0% at ground level and 54.9% underground. With the same data sets the presented method performs better than the integral correction method.

1. Introduction

Count rates of ground based or underground cosmic-ray (CR) muon detectors are affected by atmospheric parameters (air pressure and temperature at different heights). The proper description of atmospheric effects is necessary for understanding primary CR variations, originating outside of the atmosphere.

Early studies in CR temporal variations [1,2] revealed the existence of a variation caused by the change of air pressure, the so called "barometric effect". With the increase in pressure the atmosphere represents thicker absorber, resulting in reduced number of muons reaching the ground level. Therefore, muon flux is expected to be anti-correlated with atmospheric pressure.

Observed negative correlation between muon flux and atmospheric temperature, the so called "negative temperature effect", has been explained by Blackett [3] to be a consequence of muon decay. During warm periods the atmosphere is expanded and the main layer of muon production (~100 mb) is higher, resulting in longer muon path and lower surviving probability to the ground level. Low energy muons are more affected, while the flux of high energy muons, capable of penetrating great depth, does not suffer. At deep underground experiments another type of temperature effect, "positive temperature effect" is pronounced [4]. Development of nuclear emulsions capable of detecting energetic charged particles lead to discovery of charged pions in CRs and $\pi - \mu$ decay [5–7]. The positive temperature effect is interpreted as a consequence of latter process [8,9]. Pions created in the interactions of primary CR particles with the atmospheric nuclei can decay into muons or interact with air nuclei. Higher temperature in the production layer means lower air density and consequently, lower interaction probability and higher muon production.

In most cases linear regression is sufficient to account for the barometric effect. The temperature effects are treated by empirical and theoretical methods. In addition to the barometric coefficient β, **the method of effective level of generation** [8] introduces two empirical parameters: α_H to encounter for muon intensity variations δI_μ correlated with the change of the height of generation level δH (negative effect) and α_T for the changes of the temperature of this level (positive temperature effect).

$$\delta I_\mu = \beta \delta p + \alpha_H \delta H + \alpha_T \delta T \tag{1}$$

Duperier method has been successfully used in many studies for the atmospheric corrections of muon data ([10–15] etc.).

It's been argued [16,17] that for correct temperature correction of muon detectors count rate the vertical temperature profile of the entire atmosphere needs to be known. In the so called **integral method** the muon intensity variations caused by the temperature are described by the equation:

$$\frac{\delta I_\mu}{I_\mu} = \int_0^{h_0} W_T(h)\delta T(h)dh \tag{2}$$

where $\delta T(h)$ is the variation of temperature at isobaric level h with respect to the referent value and $W_T(h)$ is the temperature coefficient density. The coefficients are calculated theoretically and the best known calculations are given in references [18,19].

* Corresponding author.
E-mail address: dragic@ipb.ac.rs (A. Dragić).

https://doi.org/10.1016/j.astropartphys.2019.01.006
0927-6505/

The **mass-average temperature method** [20] is a variant of the integral method, based on the assumption of small changes of the temperature coefficient density $W_T(h)$ with the atmospheric depth h allowing its average value $\overline{W}_T$ to be put in front of the integral in the Eq. (2) and on determination of the mass-averaged temperature T_m:

$$\frac{\delta I_\mu}{I_\mu} = \overline{W}_T(h)\int_0^{h_0}\delta T(h)dh = \overline{W}_T(h)\cdot\delta T_m \tag{3}$$

The method was used in numerous studies ([21–23] to name a few).

Another form of the integral method is **the effective temperature method** [24]. By introducing the temperature coefficient α_T:

$$\alpha_T = \int_0^{h_0} W_T(h)dh$$

the Eq. (2) can be normalized as:

$$\frac{\delta I_\mu}{I_\mu} = \int_0^{h_0} W_T(h)dh\cdot\frac{\int_0^{h_0} W_T(h)\delta T(h)dh}{\int_0^{h_0} W_T(h)dh} = \alpha_T\cdot\delta T_{eff} \tag{4}$$

where the effective temperature T_{eff} is defined as:

$$T_{eff} = \frac{\int_0^{h_0} W_T(h)T(h)dh}{\int_0^{h_0} W_T(h)dh}$$

The latter method is popular with the underground muon telescopes [25,26].

Different methods of atmospheric correction might be compared on the basis of several criteria. One is requirement of the lowest variance of corrected data. Since the most prominent temperature effect on CR time series is seasonal variation, another criterion is the smallest residual amplitude of seasonal variation after correction is applied. The latter does not take into account possible genuine seasonal variation of non-atmospheric origin.

Early studies comparing Dupierier's empirical and Dorman's theoretical methods ([27] and references therein) found similar accuracy of two methods, with essentially the same corrections at sea level, but with the integral method overestimating the temperature effect.

A more recent study [28] compared different methods of atmospheric correction for data from Nagoya and Tibet supertelescopes, as well as Yakutsk, Moscow and Novosibirsk telescopes. They found the mass-averaged temperature method to practically coincide with the integral method. On the other hand, the effective level of generation method for Nagoya shows discrepancy from the integral method in winter time, being able to eliminate only 50% of the temperature effect. Even with the integral method in the case of Tibet muon telescope the removal of temperature effect is achieved with the density of temperature coefficients 3 times higher than calculated ones. The precise origin of disagreement is unknown.

The method of the effective level of generation takes care of key physical causes of the temperature effect. However, it does not make optimal use of the temperature data. Also, the assumption of a single level of main muon production is a simplification. Detailed CORSIKA simulation of the shower development in the atmosphere reveals the actual distribution of the muon generation heights (see Fig. 1).

Different implementations of the integral method exist, employing different approximations, choice of parameters, models of the atmosphere, whether kaon contribution is taken into account, leading to differences in calculated density temperature coefficients (see for instance discussion in [29]). As already mentioned, on the case of Tibet telescope [28] theoretical calculations do not fully correspond to the local experimental conditions and the origin of disagreement is difficult to trace.

The effective temperature method lacks universality, since it works best with the data from deep underground detectors.

Here we propose a new method for atmospheric corrections. It's fully empirical, makes use of the available temperature data through entire atmosphere and it's applicable to arbitrary detector irrespective to energy sensitivity and is simple to implement. The method is based on the principal component analysis, thus reducing dimensionality of the problem, exploiting correlations between atmospheric variables and ensuring mutual independence of correction parameters. The price is loss of clear physical interpretation of these parameters, since the pressure and the temperature at different levels are treated on equal footing.

2. Method description

2.1. Meteorological data

Set of variables that enter principal component decomposition consists of atmospheric temperature profile for the given location as well as locally measured atmospheric pressure. Meteorological balloon soundings for Belgrade are not done frequently enough to be used for suggested analysis. As a consequence, modeled temperatures were used instead. However, there were enough balloon sounding data for testing consistency of the modeled temperatures.

There are several weather and global climate numerical models available today. Here, Global Forecast System [30] data was used. GFS is a weather forecast model, developed by National Centers for Environmental Prediction [31], which is able to predict large number of atmospheric and land-soil parameters. Apart from forecast data, GFS also provides retrospective data produced taking into account most recent measurements by a world wide array of meteorological stations. Retrospective data are produced four times a day at 00:00, 06:00, 12:00 and 18:00 UTC. Data with finer temporal resolution are obtained by cubic spline interpolation. Temperatures for the following 25 isobaric levels (in mb) were used for initial analysis: 10, 20, 30, 50, 70, 100, 150, 200, 250, 300, 350, 400, 450, 500, 550, 600, 650, 700, 750, 800, 850, 900, 925, 975, 1000. Horizontal spatial resolution for modeled data is 0.5 degrees, so coordinates closest to the experiment location (latitude 44.86, longitude 20.39), were selected with this precision. Before any further analysis was done, GFS modeled temperature profiles were compared to local meteorological balloon soundings for Belgrade, where balloon data was available. Fig. 2 shows profile of differences between modeled and measured values for different isobaric levels. Disagreement was found between measured and modeled temperature at the lowest level. As a result, it was decided not to use temperature data for isobaric level of 1000 mb in further analysis. Ground temperature data measured by local meteorological stations was used for lowest layer instead. Similar problem with the GFS data was reported before by [28] who found 5° C deviation in the summer time near ground level at Yakutsk location.

Atmospheric pressure and ground level temperature from the Republic Hydro-meteorological Service of Serbia was used to compose unique local pressure and temperature time series.

2.2. Cosmic-ray data

The analysis is performed on data from Belgrade muon detectors. The Belgrade cosmic-ray station, together with the present detector arrangement is described in details elsewhere [32]. Two muon detectors are located in the laboratory, one at the ground level and the other at the depth of 25 mwe. Data are recorded on the event-by event basis and can be integrated into the time series with the arbitrary time resolution. For most purposes hourly data are used. Muon detectors are sensitive to primary cosmic rays

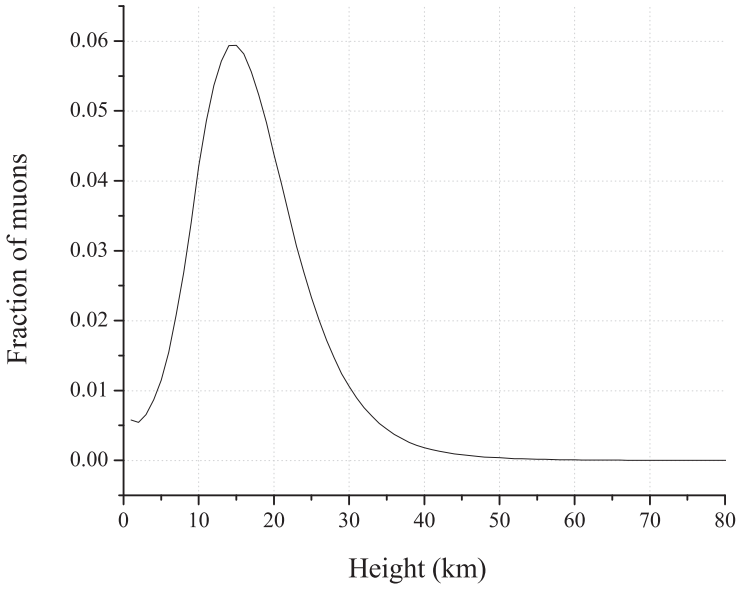

Fig. 1. Distribution of muon generation at different heights in the atmosphere, according to CORSIKA simulation.

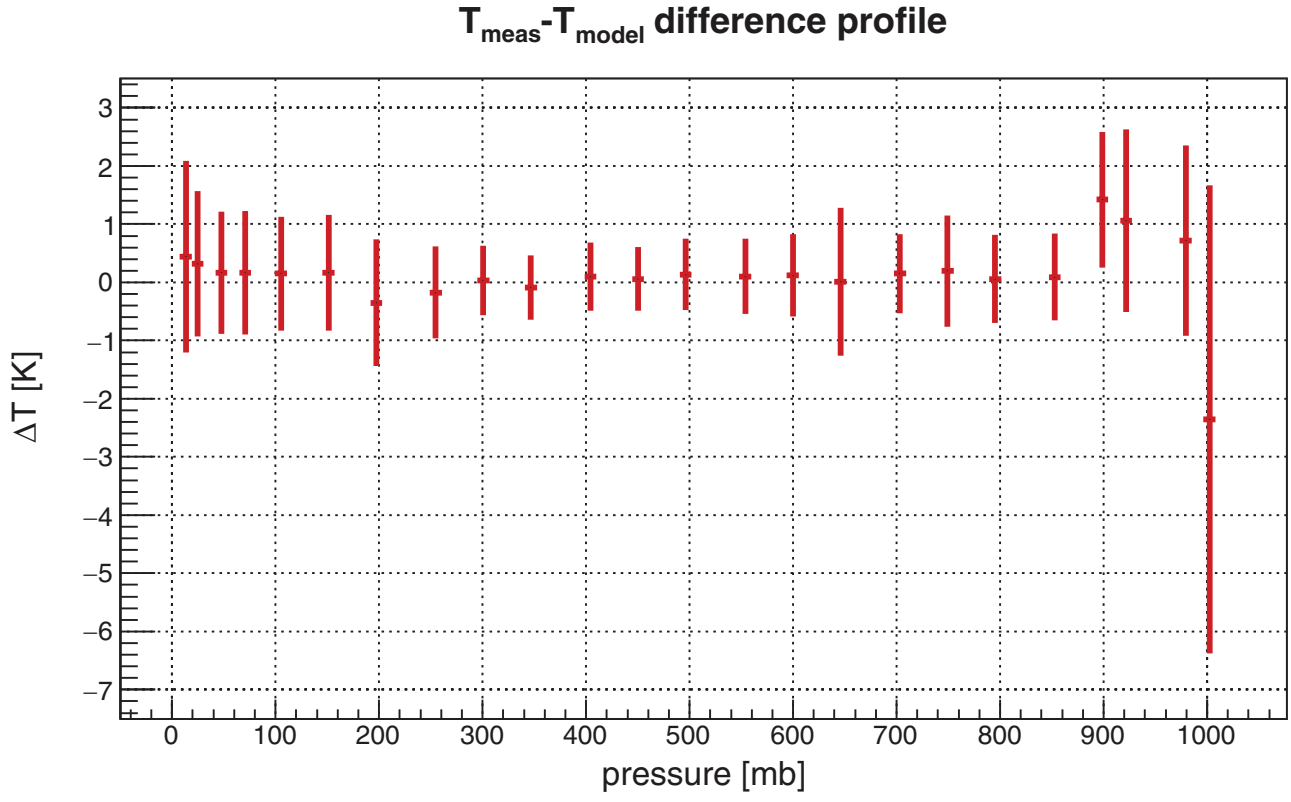

Fig. 2. Distribution of differences between measured temperatures and modeled by GFS.

of 59 GeV median energy in the case of ground level detector and 137 GeV for underground detector.

2.3. Principal component decomposition

Principal component analysis is a convenient and widely used data reduction method when dealing with strongly correlated data. It transforms the original set of variables into a set of uncorrelated variables (called principal components (PC)). The principal components are ordered according to decreasing variance. In our case, there are 26 input variables: 24 modeled temperatures (isobaric level 1000 mb temperature excluded), locally measured ground level temperature and local atmospheric pressure. Initial variables were centered and normalized before

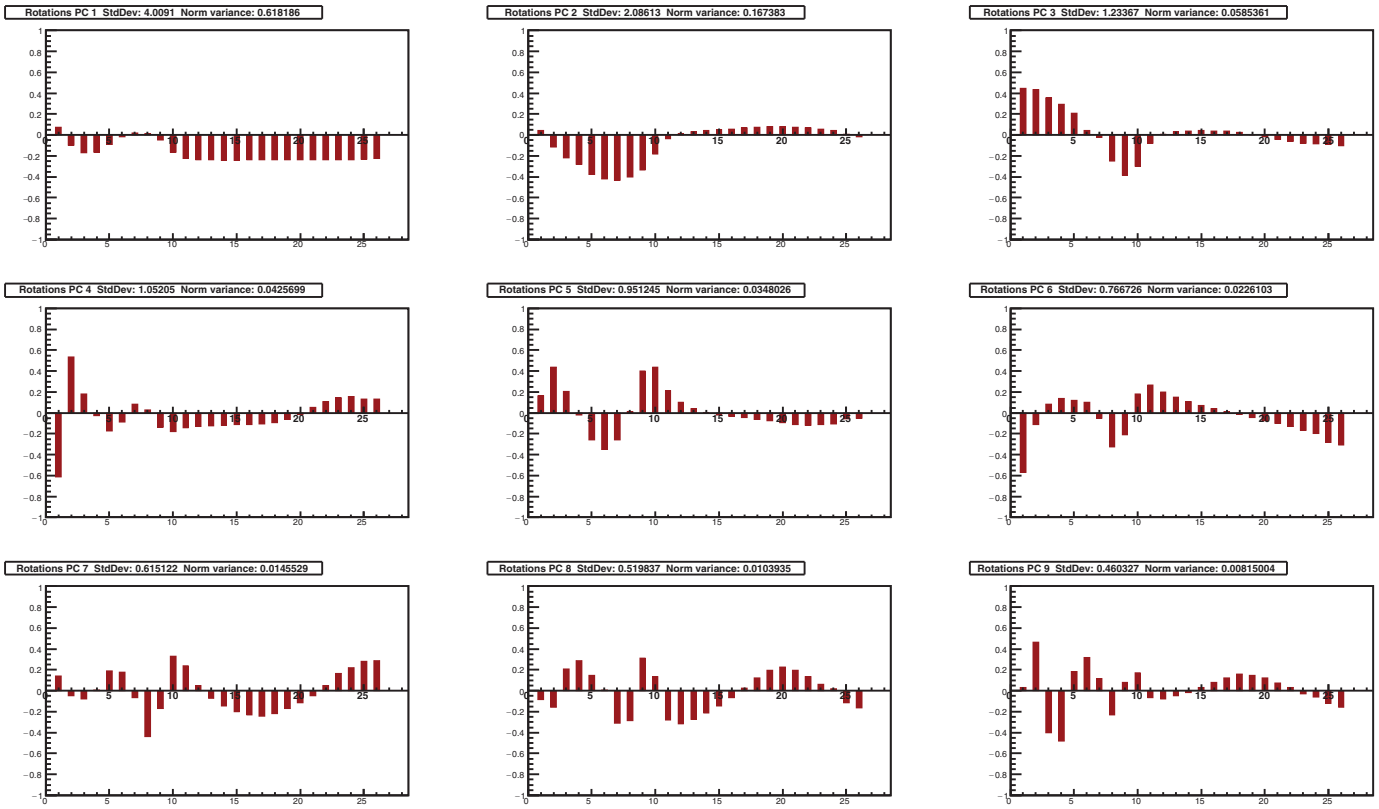

Fig. 3. Composition of nine principal components with largest variance (in decreasing order). Input variables are displayed on *X*-axis: 1 being pressure, 2 temperature of 10 mb isobaric level, 26 being local ground level temperature. *Y*-axis represents rotations.

decomposition. After decomposition, a new set of 26 principal components was obtained. Decomposition should not be regarded as universal, but it should be redone for every location and period under study.

One year was selected as a suitable time period for the analysis, in order to reduce possible seasonal bias, due to atmospheric temperature annual variation. Additional criteria were quality and consistency of muon data. Taking this into account, final time interval selected for analysis was from 01.06.2010 to 31.05.2011.

Fig. 3 shows composition plots for the first nine principal components, that account for 98% of total variance. *X*-axis represents input atmospheric variables, first being atmospheric pressure, followed by 10 mb layer temperature, last being ground level local temperature. *Y*-axis represents decomposition rotations for a given principal component. Interesting features observed on these plots are that first two principal components depend almost exclusively on temperature. The first one is mostly combination of temperatures in the troposphere (isobaric levels 250–1000 mb) with almost equal weights. The second eigenvector accounts for significant variance of temperatures in higher atmospheric levels (10–250 mb), with the strongest contribution centered in the tropopause. Components 3 to 6 have mixed p-T composition. The correlation of atmospheric pressure and temperature at different heights is not surprising. The diurnal and semi-diurnal oscillations of pressure are attributed to the warming of the upper atmosphere by the Sun [33]. This correlation makes it impossible to define a single barometric parameter in PCA based method of atmospheric corrections. It's worth mentioning that Dorman [34] recognizes three different barometric effects: absorption, decay and generation effect. It also indicates that empirical methods with separated pressure and temperature corrections might lead to overcorrection.

The values of the eigenvectors for these first nine components are also given in Table 1.

Fig. 4 shows plot of proportion of variance as well as plot of cumulative variance for obtained principal components. Corresponding numerical values are given in Table 2.

Usually, only a first few principal components (containing high fraction of total variance) are of practical interest. There are various different methods and rules for choosing how many PCs to retain in the analysis, none completely free of subjectivity (see for example a thorough discussion in [35]). A rule based on cumulative percentage of total variation usually recommends to retain PCs responsible for 70–90% of total variation. When one or two components are dominant, higher value (95%) is appropriate. In our case it would mean keeping first 6 PCs. According to Kaisser's rule only PCs with the eigenvalue $\lambda > 1$ should be retained. Jolliffe [35] suggested 0.7 as correct level, exceeded by six of our PCs. Another rule proposes to retain components with the eigenvalue above mean, a condition satisfied by first seven of our PCs. Another popular model is broken stick, but in application to our problem is too restrictive, leading to only two relevant PCs. The scree graph or log-eigenvalue diagram don't provide clean cut with our set of PCs.

To test the meaningfulness of potentially relevant PCs, the time series from PC data are constructed and tested whether they are distinguishable from white noise. The procedure is often done when principal component analysis is applied to atmospheric physics problems [36]. The time series with hourly resolution for the first three PCs are plotted on Fig. 5.

Table 1
Definition of first nine principal components.

Variables	Principal components								
	PC1	PC2	PC3	PC4	PC5	PC6	PC7	PC8	PC9
p	0.07699	0.04117	0.44694	−0.61285	0.16301	−0.57121	0.14028	−0.08106	0.03443
T(10)	−0.0947	−0.11603	0.43488	0.5344	0.43741	−0.11036	−0.04499	−0.15825	0.46469
T(20)	−0.16947	−0.21766	0.35754	0.18029	0.20527	0.08546	−0.07719	0.20635	−0.40309
T(30)	−0.16476	−0.27825	0.29593	−0.02505	−0.02204	0.14134	0.00634	0.28574	−0.47812
T(50)	−0.09124	−0.37682	0.20969	−0.17322	−0.25798	0.12084	0.19349	0.14645	0.18493
T(70)	−0.01483	−0.42304	0.04507	−0.08651	−0.3472	0.09965	0.18155	0.01024	0.31886
T(100)	0.02192	−0.43132	−0.02451	0.08228	−0.25692	−0.04937	−0.06464	−0.3103	0.1183
T(150)	0.01487	−0.40127	−0.24673	0.03037	0.012	−0.32566	−0.43658	−0.28393	−0.23316
T(200)	−0.04737	−0.33404	−0.38636	−0.13563	0.40141	−0.2069	−0.16852	0.31181	0.07995
T(250)	−0.16218	−0.17984	−0.29739	−0.18123	0.43708	0.18013	0.32866	0.13662	0.17389
T(300)	−0.22473	−0.03266	−0.07561	−0.14073	0.21179	0.26504	0.23807	−0.27931	−0.06785
T(350)	−0.2369	0.01439	0.00488	−0.12991	0.0998	0.1988	0.05306	−0.31612	−0.0771
T(400)	−0.23956	0.03362	0.02958	−0.12159	0.04075	0.14932	−0.06959	−0.27189	−0.04852
T(450)	−0.24028	0.04271	0.0402	−0.11503	0.00384	0.10744	−0.14772	−0.21165	−0.01823
T(500)	−0.24005	0.04935	0.0428	−0.11304	−0.02187	0.07218	−0.19893	−0.14512	0.03068
T(550)	−0.23958	0.05695	0.03965	−0.11295	−0.03254	0.0388	−0.23263	−0.06843	0.08056
T(600)	−0.23881	0.06549	0.03681	−0.10649	−0.04369	0.01102	−0.24562	0.02401	0.12499
T(650)	−0.23854	0.07279	0.0236	−0.09184	−0.06132	−0.01542	−0.21788	0.12597	0.15977
T(700)	−0.23835	0.0801	0.00429	−0.06052	−0.07601	−0.04668	−0.16785	0.19559	0.14932
T(750)	−0.23842	0.08071	−0.01837	−0.01332	−0.09245	−0.07308	−0.11295	0.22563	0.12401
T(800)	−0.23814	0.07557	−0.03907	0.05036	−0.10989	−0.09943	−0.04696	0.19596	0.07735
T(850)	−0.23701	0.0675	−0.06202	0.1081	−0.11988	−0.12745	0.04989	0.13672	0.0304
T(900)	−0.23535	0.05462	−0.07977	0.14776	−0.11454	−0.16955	0.16551	0.06204	−0.02952
T(925)	−0.23414	0.04606	−0.08313	0.15641	−0.10257	−0.19925	0.21877	0.01715	−0.05804
T(975)	−0.23108	0.00789	−0.08827	0.13022	−0.05888	−0.28046	0.284	−0.11523	−0.12249
T(1000)	−0.22494	−0.01582	−0.10092	0.13401	−0.04977	−0.30749	0.28553	−0.16516	−0.15908

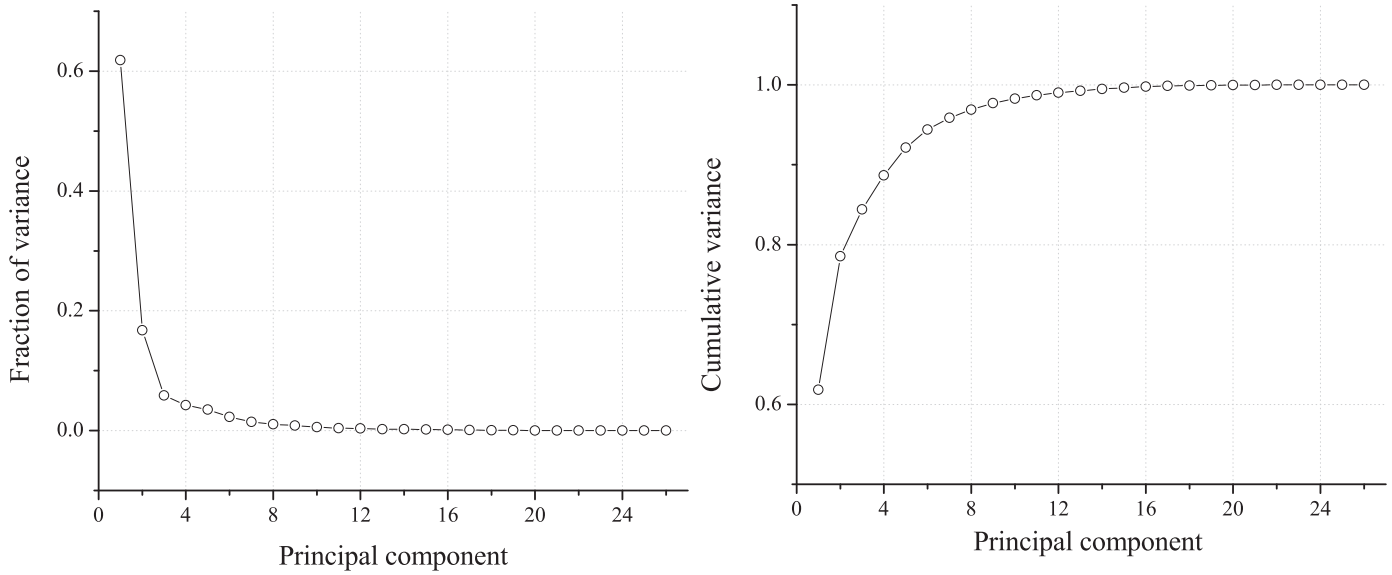

Fig. 4. Proportion of variance (left) and cumulative proportion of variance (right) for all 26 principal components.

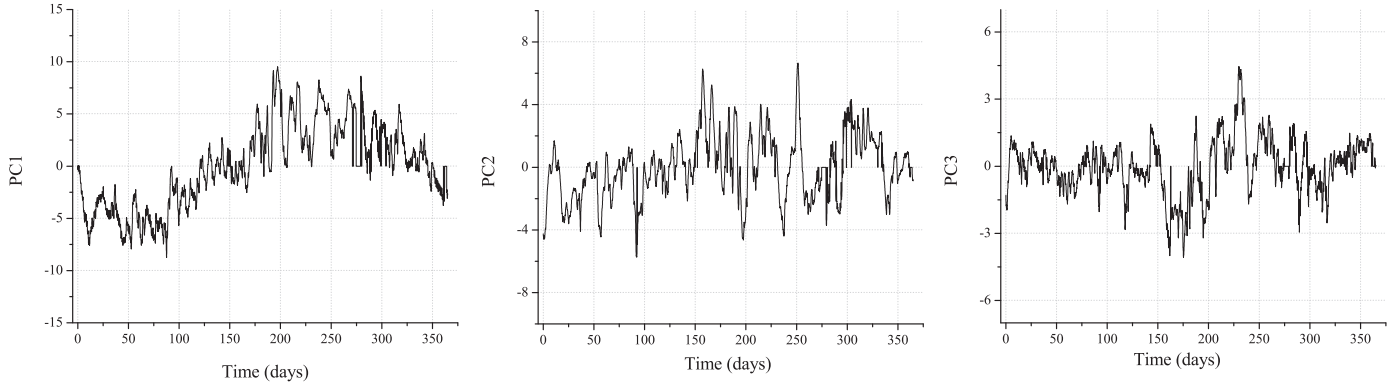

Fig. 5. Time series of the first 3 PCs.

Table 2
Variance (individual and cumulative) for all 26 PCs.

Principal component	Eigenvalue	Percentage of variance	Cumulative variance (%)
1	4.0091	0.618186	0.618186
2	2.08613	0.167383	0.785569
3	1.23367	0.0585361	0.844105
4	1.05205	0.0425699	0.886675
5	0.951245	0.0348026	0.921478
6	0.766726	0.0226103	0.944088
7	0.615122	0.0145529	0.958641
8	0.519837	0.0103935	0.969034
9	0.460327	0.00815004	0.977184
10	0.382006	0.00561263	0.982797
11	0.32832	0.00414592	0.986943
12	0.294489	0.00333553	0.990278
13	0.247876	0.00236317	0.992642
14	0.239462	0.00220546	0.994847
15	0.206157	0.00163465	0.996482
16	0.184453	0.00130857	0.99779
17	0.144657	8.04834E−4	0.998595
18	0.119676	5.5086E−4	0.999146
19	0.0938189	3.38538E−4	0.999485
20	0.0739496	2.10328E−4	0.999695
21	0.0586253	1.32189E−4	0.999827
22	0.0414996	6.62391E−5	0.999893
23	0.0338811	4.41511E−5	0.999937
24	0.0281359	3.04472E−5	0.999968
25	0.0219102	1.84637E−5	0.999986
26	0.0188263	1.36319E−5	1

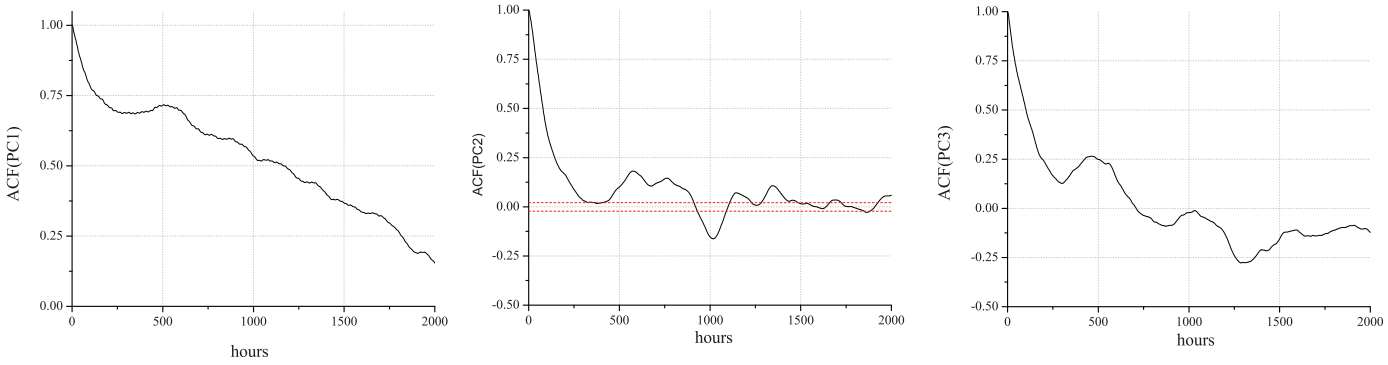

Fig. 6. Autocorrelation function of the first 3 PCs. Time lag is given in hours. In the case of PC2, 95% significance level is indicated by dashed red line. (For interpretation of the references to color in this figure legend, the reader is referred to the web version of this article.)

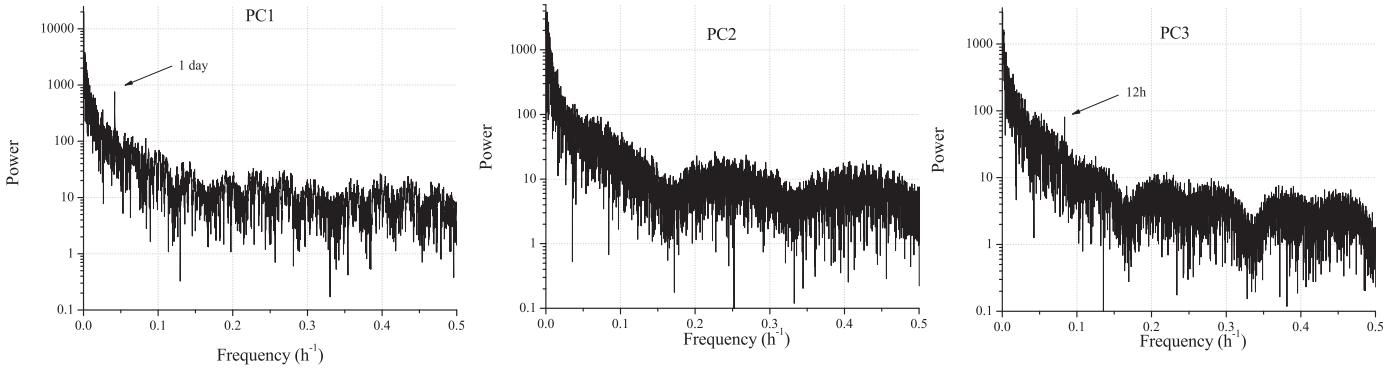

Fig. 7. Spectral analysis of time series of the first 3 PCs.

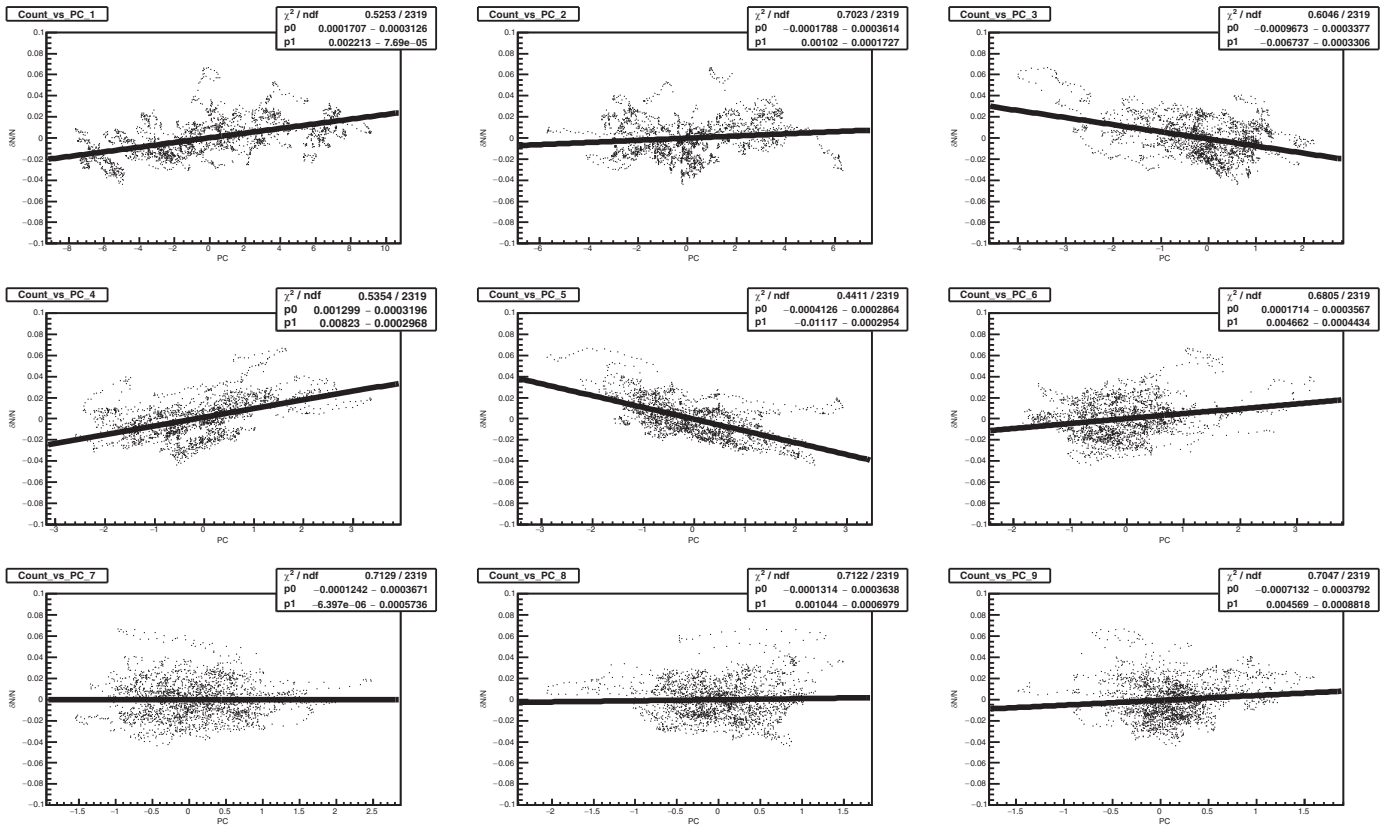

Fig. 8. Muon count dependence on principal components for the first nine principal components (GLL).

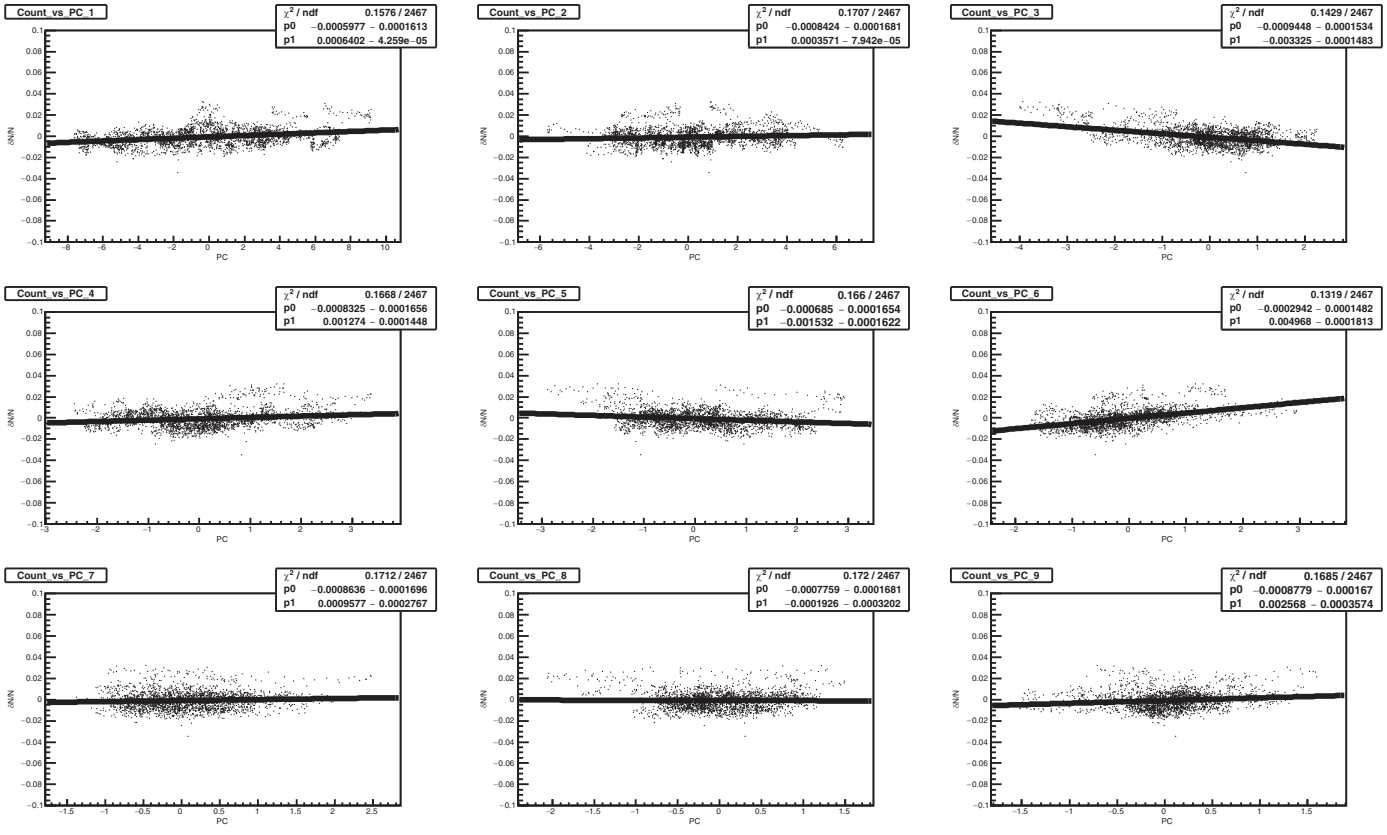

Fig. 9. Muon count dependence on principal components for the first nine principal components (UL).

The subsequent temperature and pressure measurements are highly correlated, as evident from autocorrelation function plot for selected PCs (Fig. 6).

The spectral analysis of the PC time series reveals, for PCs with the strong pressure component, semi-diurnal periodicity in addition to diurnal (Fig. 7).

Since our purpose is the regression of muon data with principal components, selecting the components with significantly high variance is not the main issue. It is more important to identify PCs with high correlation with CR data. Components with relatively low variance, can have high predictive power.

2.4. Correlation of principal components with CR muon count rate and correction of muon data

Scatter plot of muon count rate vs. PCs, together with the linear fit for the first nine principal components are shown on Fig. 8 (GLL) and Fig. 9 (UL). In the analysis hourly summed muon counts and principal component values for the respective hour were used. To minimize the effect of geomagnetic disturbances, only data for International Quiet Days were taken into account. The International Quiet Days are the days with minimum geomagnetic activity for each month. The selection of quiet days is deduced from K_p index. In our analysis 5 quietest days for each month are considered. The values of correlation coefficients are listed in Table 3.

Principal components PC1, PC3, PC4, PC5 and PC6 have been identified as ones with significant contribution to the muon flux variation. Interestingly enough, the PC2, responsible for 16.7% variance of the meteorological data has very little effect on muon flux, at neither ground nor underground level. Ground level muon flux variation is more affected by the first principal component, depending chiefly on the temperature in the troposphere. The finding agrees with usual negative temperature effect. The other PCs are difficult to compare with traditional correction parameters. Yet, the effect of PC3, that is composed more from upper atmosphere temperatures and hence could be loosely associated with positive temperature effect, is more pronounced for the underground muon flux. Fourth and fifth principal components with strong pressure contribution affect more ground level muon flux. On the other hand, PC6, also the one with high pressure component, has more pronounced influence on underground muon flux.

Gradients obtained from the fits for the significant principal components 1, 3, 4, 5 and 6 were then used to calculate the PCA corrected muon count according to the formula:

$$N_{\mu}^{(corr)} = N_{\mu} - < N_{\mu} > \sum_{i} k_i PC_i, \quad i = 1, 3, 4, 5, 6 \tag{5}$$

where $N_{\mu}^{(corr)}$ corr is the corrected muon count, N_{μ} is the raw muon count, $< N_{\mu} >$ is the mean count for the whole period, k_i are the gradients and PC_i are the corresponding principal components. Resulting corrected muon count time series are plotted on Figs. 10 (GLL) and 11 (UL) along with raw and pressure only corrected time series. Pressure corrected time series are produced for reference. Barometric coefficient was determined by applying linear regression to the same data set used for PCA. Data was previously corrected for temperature effect using integral method, as in Ref. [37]. Pressure corrected and PCA corrected time series are fitted with sine function with annual period in order to illustrate how PCA correction affects yearly variation induced by temperature effect.

PCA based atmospheric corrections remove 64.5% of total variance in GLL time series and 38.1% in UL time series. Pressure corrected CR time series exhibit annual variation, a consequence of

Table 3
Correlation coefficients between principal components and muon count rate in the ground level laboratory (GLL) and underground laboratory (UL).

PC	1	2	3	4	5	6	7	8	9	10	11	12	13	14	15	16	17	18	19	20	21	22	23	24	25	26
GLL	0.43	0.01	−0.37	0.48	−0.55	0.30	−0.01	0.03	−0.01	0.06	0.00	−0.04	0.00	0.01	0.02	−0.01	0.00	−0.01	−0.01	0.03	−0.03	0.00	0.02	−0.01	0.04	0.02
UL	0.26	0.02	−0.48	0.21	−0.19	0.52	0.02	0.04	0.07	0.04	0.01	−0.04	−0.07	0.06	−0.02	−0.05	0.04	0.04	−0.02	0.00	0.00	0.01	0.00	−0.03	0.01	0.01

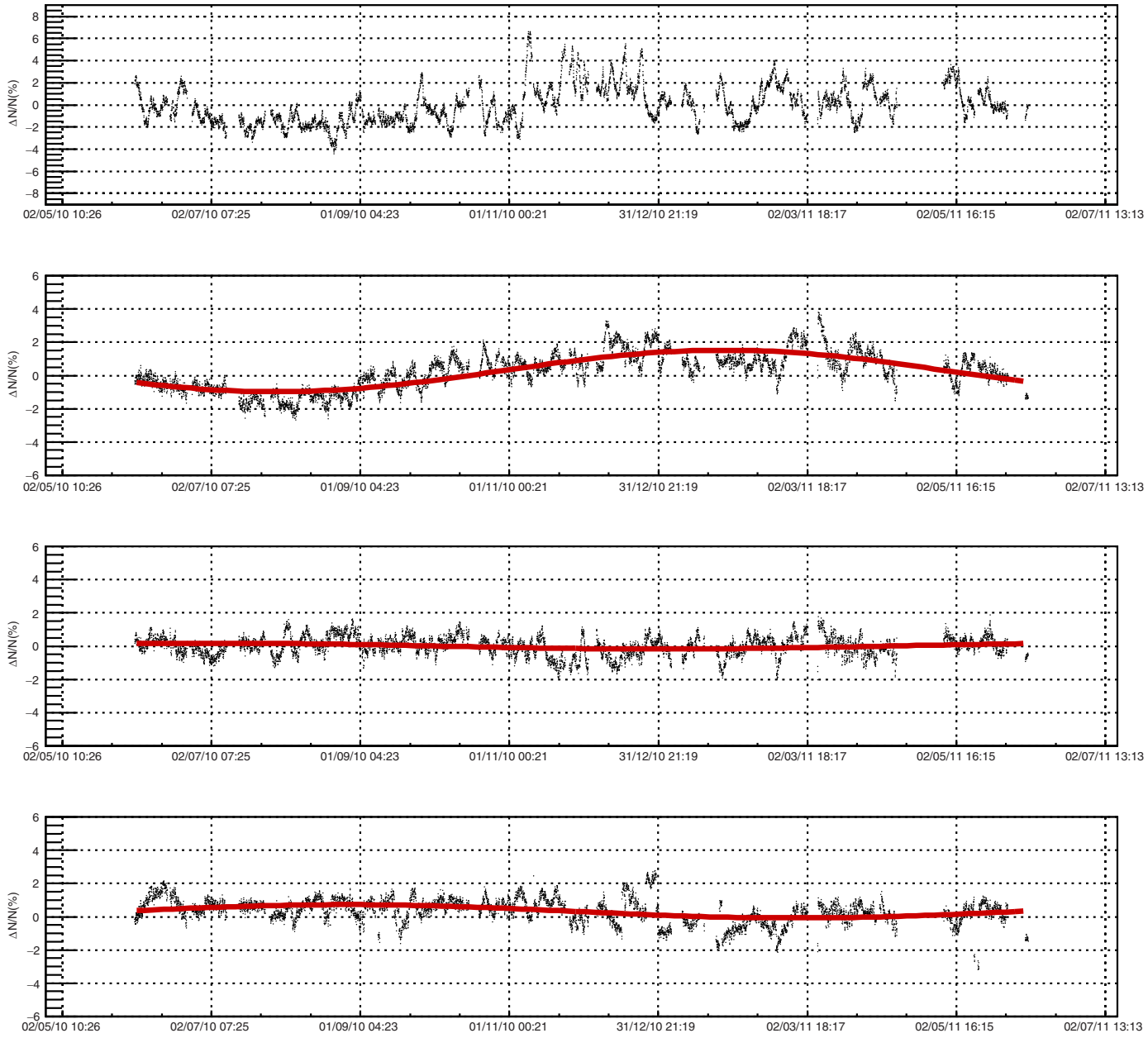

Fig. 10. Raw (upper panel), pressure corrected (middle panel), pressure+temperature corrected with PCA method (3rd panel from the top) and pressure+temperature corrected with integral method (lower panel) normalized muon count rate for GLL. The sine function with one year period is fitted to the data.

the temperature effect. The performance of the temperature correction may be tested by comparing the amplitude of the annual variation before and after correction. With presented method the amplitude of the annual variation is reduced by 86% (54.9%) in the case of GLL (UL) with respect to the pressure only corrected time series.

To further test the new method, the atmospheric correction of GLL data are performed by the integral method. The correction resulted in 56.25% of variance reduction and 68.1% of reduction of the amplitude of the annual wave. At least in the case of our CR data set the new method performs somewhat better than the integral method.

3. Conclusion

The principal component analysis is successfully used to construct a new empirical method for the atmospheric corrections of CR muon data. The method is equally applicable to all muon detectors, irrespective to location: ground level, shallow or deep underground. It requires knowledge of the atmospheric pressure and temperatures along the entire atmosphere, which is nowadays available in databases such as GFS. The method is suitable for the near real-time correction, with the delay defined by the availability of the atmospheric data (one day in the case of present GFS data). When applied to Belgrade muon data from two detectors

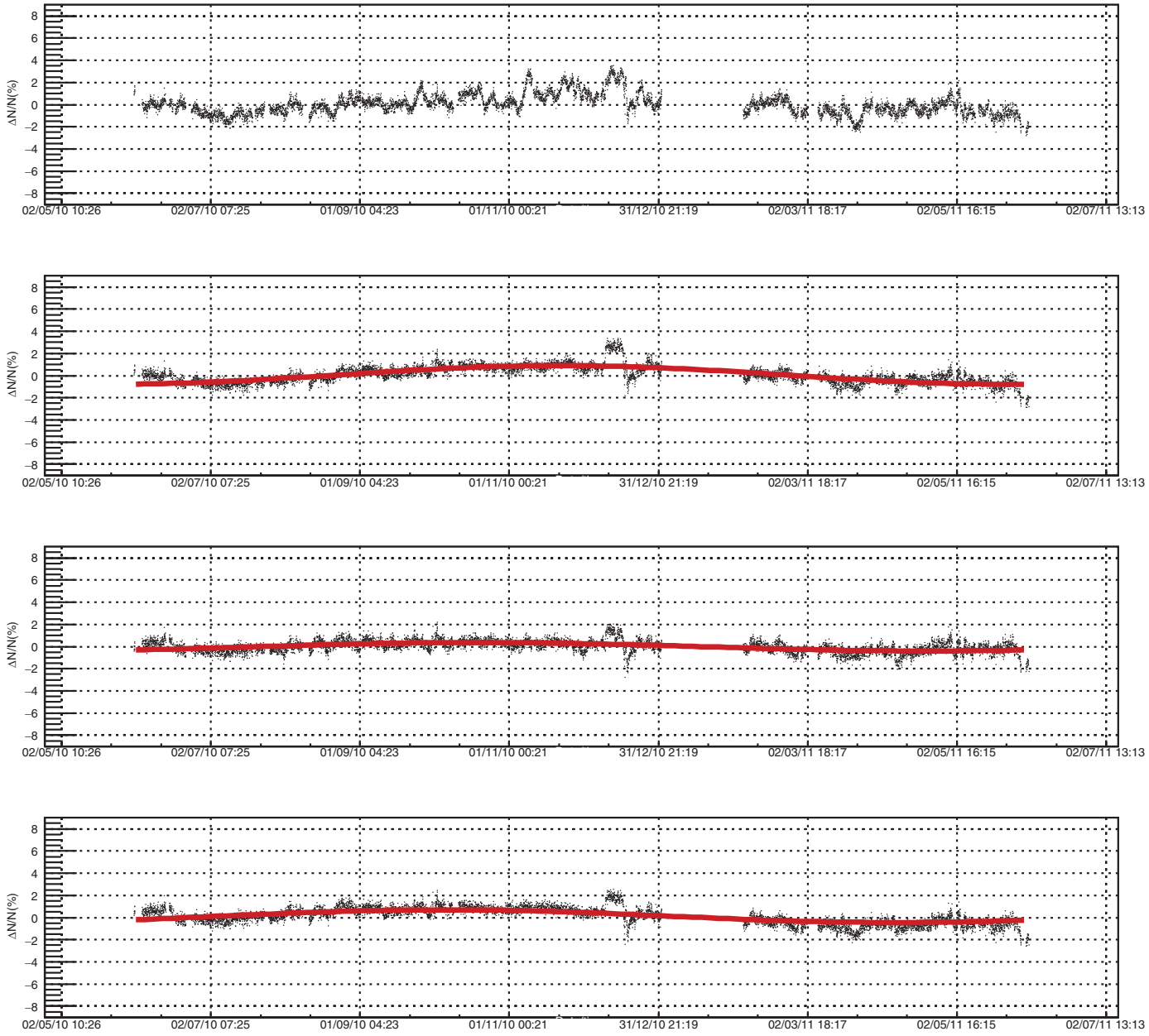

Fig. 11. Raw (upper panel), pressure corrected (middle panel), pressure+temperature corrected with PCA method (3rd panel from the top) and pressure+temperature corrected with integral method (lower panel) normalized muon count rate for UL. The sine function with one year period is fitted to the data.

(ground level and at 25 mwe), the method requires correction to five parameters, determined from linear regression. With the same CR dataset, the present method yields results superior to the integral method in terms of variance reduction and reduction of the annual variation. The new method is also suitable for temperature corrections of the neutron monitor data, which is seldom done in practice.

Acknowledgments

The authors are deeply grateful to Dr. Viktor Yanke for the encouragement and useful advice. The present work was funded by the Ministry of Education, Science and Technological Development of the Republic of Serbia, under the Project no. 171002.

References

[1] L. Myssowsky, L. Tuwim, Unregelmäßige intensitätsschwankungen der höhenstrahlung in geringer seehöhe, Zeitsch. Phys. 39 (2–3) (1926) 146–150.
[2] E. Steinke, Über schwankungen und barometereffekt der kosmischen ultrastrahlung im meeresniveau, Zeitsch. Phys. 64 (1–2) (1930) 48–63.
[3] P.M. Blackett, On the instability of the barytron and the temperature effect of cosmic rays, Phys. Rev. 54 (11) (1938) 973.
[4] M. Forro, Temperature effect of cosmic radiation at 1000-m water equivalent depth, Phys. Rev. 72 (9) (1947) 868.
[5] C.M.G. Lattes, G.P. Occhialini, C.F. Powell, Observations on the tracks of slow mesons in photographic emulsions, Nature 160 (4067) (1947) 486.
[6] C.M.G. Lattes, H. Muirhead, G.P. Occhialini, C.F. Powell, Processes involving charged mesons, Nature 159 (4047) (1947) 694.
[7] G. Occhialini, C. Powell, Nuclear disintegrations produced by slow charged particles of small mass, Nature 159 (4032) (1947) 186.
[8] A. Duperier, The meson intensity at the surface of the earth and the temperature at the production level, Proc. Phys. Soc. Lond. Sect. A 62 (11) (1949) 684.
[9] A. Duperier, Temperature of the upper atmosphere and meson production, Nature 167 (4243) (1951) 312.

[10] C. Baker, D. Hall, J. Humble, M. Duldig, Atmospheric correction analysis for the Mawson muon telescopes, in: International Cosmic Ray Conference, 3, 1993, p. 753.
[11] A. Maghrabi, M. Almutayri, Atmospheric effect on cosmic ray muons at high cut-off rigidity station, Adv. Astron. 2016 (2016).
[12] C.R. Braga, A. Dal Lago, T. Kuwabara, N.J. Schuch, K. Munakata, Temperature effect correction for the cosmic ray muon data observed at the Brazilian Southern Space Observatory in São Martinho da Serra, J. Phys. 409 (2013) 012138 IOP Publishing..
[13] G.C. Castagnoli, M. Dodero, Temperature effect of the muon component underground and pion attenuation length, Il Nuovo Cimento B (1965–1970) 51 (2) (1967) 525–534.
[14] A. Fenton, R. Jacklyn, R. Taylor, Cosmic ray observations at 42 m we underground at hobart, tasmania, Il Nuovo Cimento (1955–1965) 22 (2) (1961) 285–295.
[15] M. Zazyan, M. Ganeva, M. Berkova, V. Yanke, R. Hippler, Atmospheric effect corrections of mustang data, J. Space Weather Space Clim. 5 (2015) A6.
[16] L. Dorman, The temperature effect of the hard component of cosmic rays, Doklady Akad. Nauk SSSR 95 (1954).
[17] E. Feinberg, On the nature of cosmic ray barometric and temperature effects, DAN SSSR 53 (5) (1946) 421–424.
[18] L.I. Dorman, Cosmic ray variations, Technical Report, Foreign Technology Div Wright-Patterson AFB OHIO, 1957.
[19] K. Maeda, M. Wada, Atmospheric temperature effect upon the cosmic-ray intensity at sea level, J. Sci. Res. Inst. 48 (1954).
[20] V. Dvornikov, Y.Y. Krest'yannikov, A. Sergeev, Determination of the variation of average-mass temperature of the atmosphere by data of cosmic ray intensity, Geomag. Aeron. 16 (1976) 923–925.
[21] V. Yanchukovsky, G.Y. Filimonov, R. Hisamov, Atmospheric variations in muon intensity for different zenith angles, Bull. Russ. Acad. Sci. 71 (7) (2007) 1038–1040.
[22] R. De Mendonça, C. Braga, E. Echer, A. Dal Lago, K. Munakata, T. Kuwabara, M. Kozai, C. Kato, M. Rockenbach, N. Schuch, et al., The temperature effect in secondary cosmic rays (muons) observed at the ground: analysis of the Global MUON Detector Network data, Astrophys. J. 830 (2) (2016) 88.
[23] A. Dmitrieva, I. Astapov, A. Kovylyaeva, D. Pankova, Temperature effect correction for muon flux at the earth surface: estimation of the accuracy of different methods, J. Phys. 409 (2013) 012130. IOP Publishing.
[24] P.H. Barrett, L.M. Bollinger, G. Cocconi, Y. Eisenberg, K. Greisen, Interpretation of cosmic-ray measurements far underground, Rev. Mod. Phys. 24 (3) (1952) 133.
[25] S. Tilav, P. Desiati, T. Kuwabara, D. Rocco, F. Rothmaier, M. Simmons, H. Wissing, et al., Atmospheric variations as observed by IceCube, arXiv:1001.0776 (2010).
[26] P. Adamson, C. Andreopoulos, K. Arms, R. Armstrong, D. Auty, D. Ayres, C. Backhouse, J. Barnett, G. Barr, W. Barrett, et al., Observation of muon intensity variations by season with the Minos far detector, Phys. Rev. D 81 (1) (2010) 012001.
[27] H. Carmichael, M. Bercovitch, J.F. Steljes, Introduction of meteorological corrections into meson monitor data, Tellus 19 (1) (1967) 143–160, doi:10.1111/j.2153-3490.1967.tb01468.x.
[28] M.D. Berkova, A.V. Belov, E.A. Eroshenko, V.G. Yanke, Temperature effect of the muon component and practical questions for considering it in real time, Bull. Russ. Acad. Sci. 75 (6) (2011) 820–824, doi:10.3103/S1062873811060086.
[29] A. Dmitrieva, R. Kokoulin, A. Petrukhin, D. Timashkov, Corrections for temperature effect for ground-based muon hodoscopes, Astropart. Phys. 34 (6) (2011) 401–411, doi:10.1016/j.astropartphys.2010.10.013.
[30] Global forecast system (GFS), https://www.ncdc.noaa.gov/data-access/modeldata/model-datasets/global-forcast-system-gfs.
[31] National centers for environmental prediction (NCEP), http://www.ncep.noaa.gov/.
[32] A. Dragić, V. Udovičić, R. Banjanac, D. Joković, D. Maletić, N. Veselinović, M. Savić, J. Puzović, I.V. Aničin, The new setup in the Belgrade low-level and cosmic-ray laboratory, Nucl. Technol. Radiat. Protect. 26 (3) (2011) 181–192.
[33] B. Haurwitz, The diurnal surface-pressure oscillation, Arch. Meteorol. Geophys. Bioklimatol. Ser. A 14 (4) (1965) 361–379, doi:10.1007/BF02253483.
[34] L.I. Dorman, Cosmic Rays in the Earth's Atmosphere and Underground, Springer Netherlands, 2004, doi:10.1007/978-1-4020-2113-8.
[35] I. Jolliffe, Principal Component Analysis, Springer-Verlag, 2002, doi:10.1007/b98835.
[36] R.W. Preisendorfer, D.M. Curtis, Principal component analysis in meteorology and oceanography, Elsevier, Amsterdam, 1988.
[37] M. Savić, D. Maletić, D. Joković, N. Veselinović, R. Banjanac, V. Udovičić, A. Dragić, Pressure and temperature effect corrections of atmospheric muon data in the belgrade cosmic-ray station, J. Phys. Conf. Ser. 632 (1) (2015) 012059.

NUKLEONIKA 2020;65(2):121–125
doi: 10.2478/nuka-2020-0019

ORIGINAL PAPER

Radon variability due to floor level in two typical residential buildings in Serbia

Vladimir Udovicic, Nikola Veselinovic, Dimitrije Maletic, Radomir Banjanac, Aleksandar Dragic, Dejan Jokovic, Mihailo Savic, David Knezevic, Maja Eremic Savkovic

Abstract. It is well known that one of the factors that influence the indoor radon variability is the floor level of the buildings. Considering the fact that the main source of indoor radon is radon in soil gas, it is expected that the radon concentration decreases at higher floors. Thus at higher floors the dominant source of radon is originating from building materials, and in some cases there may be deviations from the generally established regularity. In such sense, we chose one freestanding single-family house with loft and other 16-floor high-rise residential building for this study. The indoor radon measurements were performed by two methods: passive and active. We used passive devices based on track-etched detectors: Radtrak^2 Radonova. For the short-term indoor radon measurements, we used two active devices: SN1029 and SN1030 (manufactured by Sun Nuclear Corporation). The first device was fixed in the living room at the ground level and the second was moved through the floors of the residential building. Every measuring cycle at the specified floor lasted seven days with the sampling time of 2 h. The results show two different indoor radon behaviours regarding radon variability due to floor level. In the single-family house with loft we registered intense difference between radon concentration in the ground level and loft, while in the high-rise residential building the radon level was almost the same at all floors, and hence we may conclude that radon originated mainly from building materials.

Keywords: Radon variability • Time series

V. Udovicic✉, N. Veselinovic, D. Maletic, R. Banjanac, A. Dragic, D. Jokovic, M. Savic, D. Knezevic
Institute of Physics Belgrade
University of Belgrade
Pregrevica 118 St., 11080 Belgrade, Serbia
E-mail: udovicic@ipb.ac.rs

M. Eremic Savkovic
Serbian Radiation and Nuclear Safety and Security Directorate
Masarikova 5 St., 11000 Belgrade, Serbia

Received: 30 November 2019
Accepted: 17 January 2020

Introduction

Radon sources in the buildings are primarily from soil, building materials and water. Considering the nature of the occurrence and all the sources, the concentration of radon is higher in the ground-floor rooms compared with that in the higher floors of the dwellings in apartments. In the literature one can find a lot of papers dealing with the influence of various factors, including the floor levels, on the radon concentration and variability. In one group of the articles, investigation of the indoor radon concentration distribution due to floor levels of the buildings is the part of the data analysis which was drawn from the national or regional radon surveys [1–6] and others are dedicated to these specific studies [7–11]. In the case of the big buildings with a several number of floors a deviation from the general regularity can be observed, since the dominant source of indoor radon at higher floors is building materials. On the other hand, the radon variability due to floor level, especially in big cities with a much higher number of high-rise buildings and population density compared with rural environments, may have an impact on the assessments of the effective dose from radon exposure at the national level. Usually, the indoor radon map represents the arithmetic mean value of indoor radon concentration on the ground floor, and thus it is not

representative of the radon exposure to all citizens since most people do not live on the ground floor. So, it is necessary to convert indoor radon map to a dose map. One of the examples is presented as a plan to develop models that allow correction from ground-floor dwellings to the real situation, accounting data from the national buildings database [12]. In Serbia, national typology of residential buildings is based on the results from the monography "National typology of residential buildings of Serbia" by a group of authors from the Faculty of Architecture [13]. There are six types of the residential buildings in Serbia: two for family housing – freestanding single-family house and single-family house in a row and four types for multifamily housing – freestanding residential building and residential building (lamella) (apartment block with repeated multiple lamellar cores and separate entrances), residential building in a row, and high-rise residential building. Distribution of buildings by type at the national level shows that 97% of all residential buildings are family housing. Also, for all defined types of buildings, number of floors ranges from one to eight above the ground level. Freestanding family houses are mostly ground floor (37%) or ground floor with loft in use (26%), while there is a very low representation of houses that have more than two floors (5%), with average floor level of family buildings of 1.4 [13]. In such sense, we chose one freestanding single-family house with loft with well-known radon characteristics [14] and one 16-floor high-rise residential building for this study.

Materials and methods

Two housing units were selected, one from the family housing group and one high-rise residential building from the collective housing group. The family house has a characteristic construction style in which the house has been built for several years with constant upgrading, which can potentially be a source of radon entry into such houses. The house has a basement and is made of standard materials (brick block, concrete, plaster). Finally, insulation was made using 5-cm thick styrofoam. Long-term measurements of radon concentrations have been carried out in this house by various methods, and several scientific papers have been published so far [14–16].

From the group of residential buildings for collective housing, we chose high-rise building in New Belgrade. It was built in the 1960s as block type. The soliter has a basement, while on the ground floor there are outlets and business premises. The apartments are located in the first floor upward. The soliter has 16 floors. One of the important parameters in the selection of building in municipality New Belgrade is the fact that this municipality is the most populated in Serbia.

The long-term radon measurements were performed with passive device Radtrak² Radonova based on CR-39 track detector. The detectors were exposed for three months from March to June. In the high-rise building, passive radon detectors were deployed at some of the floors in one or several apartments. Time series of measured radon concentrations in the studied residential buildings were obtained using two active devices: SN1029 with the following characteristics declared by the manufacturer – the measurement ranging from 1 Bq·m^{-3} to 99.99 kBq·m^{-3}, accuracy equal to ±25%, sensitivity of 0.16 counts/h/Bq·m^{-3} and SN1030 with the following characteristics – the measurement ranging from 1 Bq·m^{-3} to 99.99 kBq·m^{-3}, accuracy equal to ±20%, sensitivity of 0.4 counts/h/Bq·m^{-3}. SN1029 device were calibrated at the accredited metrological Lab (SUJCHBO Kamenna, Czech Republic) in 2015 and model SN1030 were calibrated by the manufacturer in 2017. The both instruments participated in 2018 NRPI Intercomparisons of radon gas continuous monitors and also, SN1029 device participated in 2015 NRPI Intercomparisons of radon gas measurement devices at SURO v.v.i. Institute, Prague, Czech Republic within the IAEA Technical Cooperation Projects RER 9153 and RER 9127, with excellent results. These are measuring devices of simple construction and practical application. It is a counter with the addition of a sensor for measuring meteorological parameters. The operator can adjust the time sequences from 0.5 h to 24 h. One measurement cycle can take 1000 h or a total of 720 time sequences (the number of successive measurements, i.e. points in a time series). The devices were set to operate in a 2-h time sequence. One was fixed in the downstairs living room and the other was fixed in repositioning floors in apartment buildings. Each measurement cycle on a given floor lasted seven days.

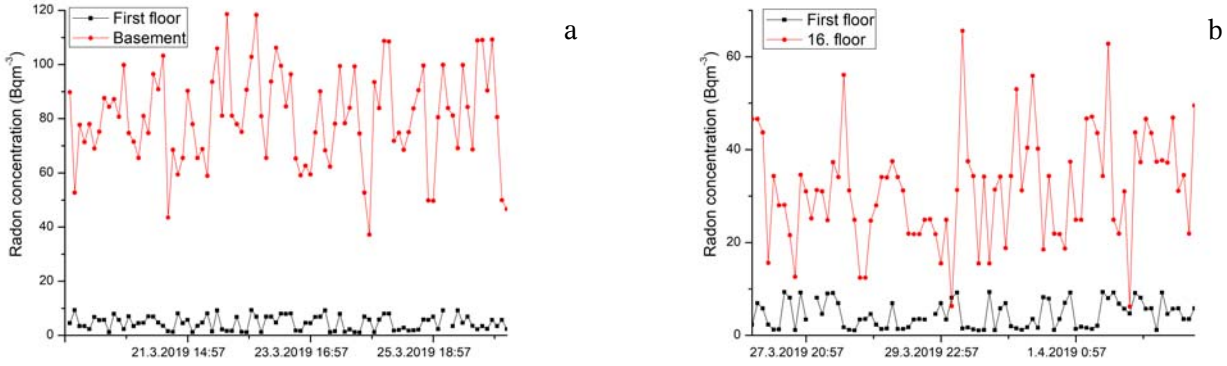

Fig. 1. The time series of the radon concentrations at the first floor vs. basement (a) and 16th floor (b) in the big residential building.

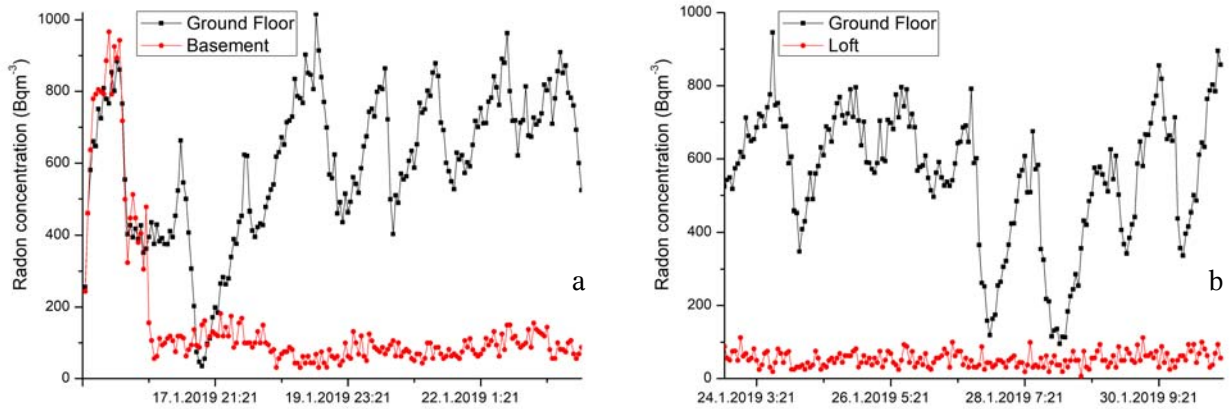

Fig. 2. The time series of the radon concentrations at the first floor vs. basement (a) and loft (b) in the single-family house.

Table 1. Results of indoor radon measurements in the high-rise residential building using passive (Radtrak[2] Radonova) and active radon devices

Floor level	Radon concentration/ Passive device (Radtrak[2]) [Bq·m^{-3}]	Average radon concentration per floor level (Radtrak[2]) [Bq·m^{-3}]	Arithmetic mean (standard deviation) radon concentration over measuring cycle [Bq·m^{-3}]
Basement	52 ± 10 69 ± 12 38 ± 10 55 ± 10	53.5	81(17)
1	<10 14 ± 8	14	5(3)
2	17 ± 8	17	24(9)
3			25(10)
4	21 ± 8 20 ± 8	20.5	26(11)
5	11 ± 8 27 ± 10	19	
6	22 ± 8 12 ± 8 17 ± 8	17	
7	23 ± 8	23	25(10)
8	22 ± 8	22	
9	15 ± 8 16 ± 8 22 ± 8	17.7	24(10)
10	20 ± 8 15 ± 8	17.5	
11	16 ± 8	16	
12	<10	<10	
14	20 ± 8 17 ± 8	18.5	29(9)
15	15 ± 8 16 ± 8	15.5	
16	31 ± 8	31	32(12)
Overall mean	24	21.6	30

Results and discussions

Figure 1 shows the illustrative examples that show radon time series from high-rise building, and Fig. 2 originates from the observed single-family house.

The arithmetic mean radon concentrations obtained from long- and short-term measurements are shown in Tables 1 and 2 for high-rise building and single-family house with loft, respectively.

In the family house, it is possible to notice marked variations in radon concentration with 1-day periodicity. Also interesting is the ratio of radon concentration on the ground floor to the basement of the house, which is the opposite of the usual situation in houses with a basement. This inverse behaviour can be explained by the fact that the basement does not cover the whole ground floor but a smaller part of it. The rest of the ground floor is covered by a concrete slab as a substrate, but cracks and poor joint with the walls are potential sources of elevated radon. Also, the differences in the results between two methods, passive and active devices, are due to the fact that presented radon values are measured in different seasons. With high-rise residential building, the situation is the opposite and it can be considered from the first floor that the dominant source of radon is the building material. There may even be a slight increase in the mean radon concentration on the higher floors. Also, the results show very low radon level on the first floor (well below the outdoor values) in the apartment. In such sense, we performed test intercomparison radon measurements for two active devices SN1029 and SN1030 in well-defined and controlled radon atmosphere (radon concentration below 30 Bq·m^{-3}) in the Underground Low-background Laboratory in the Institute of Physics Belgrade [17, 18]. Additional testing includes the same place and time of the measurements but different sampling time set to 1, 2, 4, 8 and 12 h. The results are shown in Table 3.

In the above performed measurements, both devices show significant differences in the low-level radon range, which may originate from individual instruments characteristics presented in the "Materials and methods" section.

Table 2. Results of indoor radon measurements in the single-family house with loft using passive (Radtrak² Radonova) and active radon devices

Floor level	Radon concentration/Passive device (Radtrak²) [Bq·m⁻³]	Arithmetic mean (standard deviation) radon concentration over measuring cycle [Bq·m⁻³]
Basement		160(202)
Ground level	330 ± 50	579(194)
Loft	18 ± 8	53(21)

Table 3. Test intercomparison indoor radon measurements with active radon devices SN1029 and SN1030

	Arithmetic mean (standard deviation) radon concentration over measuring cycle [Bq·m⁻³]				
Sampling time [h]	1	2	4	8	12
SN1029	28(12)	28(11)	27(7)	23(6)	32(14)
SN1030	12(6)	14(7)	10(3)	12(5)	14(6)

Conclusions

The results show that the radon behaviour in two different residential buildings is diametrically opposite. In the single-family house with loft we registered intense difference between radon concentration in the ground level and loft, while in the high-rise residential building the radon level was almost the same at all floors and hence we may conclude that radon originated mainly from building materials. However, the results from the high-rise building can be predicted on the basis of work of a group of authors who have determined the internal exposure from construction material used in Serbia which originates from the exhalation of radon and thoron [19] and the study presented in this article [10]. We can expect similar results in any other multistorey buildings in Serbia. In the future work, we will focus on the additional radon measurements in the typical residential buildings from other types of houses.

Acknowledgments. The authors acknowledge funding provided by the Institute of Physics Belgrade through the grant by the Ministry of Education, Science and Technological Development of the Republic of Serbia.

ORCID

V. Udovicic http://orcid.org/0000-0002-7839-1537

References

1. Bochicchio, F., Campos-Venuti, G., Piermattei, S., Nuccetelli, C., Risica, S., Tommasino, L., Torri, G., Magnoni, M., Agnesod, G., Sgorbati, G., Bonomi, M., Minach, L., Trotti, F., Malisan, M. R., Maggiolo, S., Gaidolfi, L., Giannardi, C., Rongoni, A., Lombardi, M., Cherubini, G., D'Ostilio, S., Cristofaro, C., Pugliese, M., Martucci, V., Crispino, A., Cuzzocrea, P., Sansone Santamaria, A., & Cappai, M. (2005). Annual average and seasonal variations of residential radon concentration for all the Italian Regions. *Radiat. Meas*., *40*, 686–694.
2. Friedmann, H. (2005). Final results of the Austrian Radon Project. *Health Phys*., *89*(4), 339–348.
3. Du, L., Prasauskas, T., Leivo, V., Turunen, M., Pekkonen, M., Kiviste, M., Aaltonen, A., Martuzevicius, D., & Haverinen-Shaughnessy, U. (2015). Assessment of indoor environmental quality in existing multifamily buildings in North-East Europe. *Environ. Int*., *79*, 74–84.
4. Cucoş (Dinu), A., Cosma, C., Dicu, T., Begy, R., Moldovan, M., Papp, B., Niță, D., Burghele, B., & Sainz, C. (2012). Thorough investigations on indoor radon in Băița radon-prone area (Romania). *Sci. Total Environ*., *431*, 78–83.
5. Yarmoshenko, I., Vasilyev, A., Malinovsky, G., Bossew, P., Žunić, Z. S., Onischenko, A., & Zhukovsky, M. (2016). Variance of indoor radon concentration: Major influencing factors. *Sci. Total Environ*., *541*, 155–160.
6. Kropat, G., Bochud, F., Jaboyedoff, M., Laedermann, J. P., Murith, C., Palacios, M., & Baechler, S. (2014). Major influencing factors of indoor radon concentrations in Switzerland. *J. Environ. Radioact*., *129*, 7–22.
7. Borgoni, R., De Francesco, D., De Bartolo, D., & Tzavidis, N. (2014). Hierarchical modeling of indoor radon concentration: how much do geology and building factors matter? *J. Environ. Radioact*., *138*, 227–237.
8. Xie, D., Liao, M., & Kearfott, K. J. (2015). Influence of environmental factors on indoor radon concentration levels in the basement and ground floor of a building – A case study. *Radiat. Meas*., *82*, 52–58.
9. Man, C. K., & Yeung, H. S. (1999). Modeling and measuring the indoor radon concentrations in high-rise buildings in Hong Kong. *Appl. Radiat. Isot*., *50*, 1131–1135.
10. Vukotić, P., Zekić, R., Antović, N. M., & Andjelić, T. (2019). Radon concentrations in multi-story buildings in Montenegro. *Nucl. Technol. Radiat. Prot*., *34*, 165–174.
11. Lorenzo-González, M., Ruano-Ravina, A., Peón, J., Piñeiro, M., & Barros-Dios, J. M. (2017). Residential radon in Galicia: a cross-sectional study in a radon-prone area. *J. Radiol. Prot*., *37*(3), 728–741.
12. Elío, J., Cinelli, G., Bossew, P., Gutiérrez-Villanueva, J. L., Tollefsen, T., De Cort, M., Nogarotto, A., & Braga, R. (2019). The first version of the Pan-European Indoor Radon Map. *Nat. Hazards Earth Syst. Sci.*, *19*, 2451–2464.
13. Jovanović Popović, M., Ignjatović, D., Radivojević, A., Rajčić, A., Ćuković Ignjatović, N., Đukanović, Lj., & Nedić, M. (2013). *National typology of residential*

buildings in Serbia. Belgrade: Faculty of Architecture University of Belgrade.
14. Udovičić, V., Maletić, D., Banjanac, R., Joković, D., Dragić, A., Veselinović, N., Živanović, J., Savić, M., & Forkapić, S. (2018). Multiyear indoor radon variability in a family house–A case study in Serbia. *Nucl. Technol. Radiat. Prot*., *33*(2), 174–179.
15. Maletić, D., Udovičić, V., Banjanac, R., Joković, D., Dragić, A., Veselinović, N., & Filipović, J. (2014). Comparison of multivariate classification and regression methods for indoor radon measurements. *Nucl. Technol. Radiat. Prot*., *29*, 17–23.
16. Filipović, J., Maletić, D., Udovičić, V., Banjanac, R., Joković, D., Savić, M., & Veselinović, N. (2016). The use of multivariate analysis of the radon variability in the underground laboratory and indoor environment. *Nukleonika*, *61*(3), 357–360. DOI: 10.1515/nuka-2016-0059.
17. Udovičić, V., Aničin, I., Joković, D., Dragić, A., Banjanac, R., Grabež, B., & Veselinović, N. (2011). Radon time-series analysis in the Underground Low-level Laboratory in Belgrade, Serbia. *Radiat. Prot. Dosim*., *145*(2/3), 155–158.
18. Udovičić, V., Filipović, J., Dragić, A., Banjanac, R., Joković, D., Maletić, D., Grabež, B., & Veselinović, N. (2014). Daily and seasonal radon variability in the underground low-background laboratory in Belgrade, Serbia. *Radiat. Prot. Dosim*., *160*(1/3), 62–64.
19. Ujić, P., Čeliković, I., Kandić, A., Vukanac, I., Đurašević, M., Dragosavac, D., & Žunić, Z. S. (2010). Internal exposure from building materials exhaling ^{222}Rn and ^{220}Rn as compared to external exposure due to their natural radioactivity content. *Appl. Radiat. Isot*., *68,* 201–206.

Eur. Phys. J. D (2021) 75:173
https://doi.org/10.1140/epjd/s10053-021-00172-x

THE EUROPEAN PHYSICAL JOURNAL D

Regular Article - Plasma Physics

Correlation analysis of solar energetic particles and secondary cosmic ray flux

Nikola Veselinović[a], Mihailo Savić, Aleksandar Dragić, Dimitrije Maletić, Radomir Banjanac, Dejan Joković, David Knežević, and Vladimir Udovičić

Institute of Physics Belgrade, University of Belgrade, Pregrevica 118, Belgrade 11080, Serbia

Received 31 January 2021 / Accepted 5 May 2021 / Published online 8 June 2021

Abstract. Galactic cosmic rays entering heliosphere are modulated by interplanetary magnetic field which is carried away from the Sun by the solar wind. Cosmic rays are additionally modulated by coronal mass ejections and shock waves, which can produce Forbush decrease, a transient decrease in the observed galactic cosmic ray intensity. Measurements of magnetic field and plasma parameters in near-Earth space detect regularly coronal mass ejections, so it is important to understand the correlation between near-Earth particles fluxes associated with these coronal mass ejections and Forbush decreases. By combining in situ measurements of solar energetic particles with ground-based observations by the Belgrade muon detector, we analysed the dynamics of the variation of galactic cosmic rays. Correlation between variations of the flux of the cosmic rays and average in situ particle fluxes was investigated during Forbush decreases. Correlation exhibited dependence on the energy of solar wind particles, but also on cut-off rigidities of cosmic rays detected on the ground. The goal of cross-correlation analysis is to help in better understanding of how coronal mass ejections affect space weather as well as the effects they have on primary cosmic ray variations as detected by ground-based cosmic ray detectors.

1 Introduction

Space weather has been widely used as a term to define impact of the Sun, heliosphere and geomagnetic field on our biosphere and our technological systems. Understanding space weather is a matter of both scientific interest and practical importance as its impact could potentially be hazardous to our civilisation. Cosmic ray (CR) observations can also be used to study space weather. Primary (or galactic) CRs are high-energy nuclei (mainly protons) that originate from outside of our solar system. Their flux and energy range is covering several tens of orders of magnitude (flux from 10^{-28} up to 10^{4} $(\mathrm{m}^2\ \mathrm{sr\ sec\ eV/nucleon})^{-1}$ and energy range up to 10^{21} eV [10]). As charged particles, CRs are sensitive to magnetic field, so often it is more convenient to use geomagnetic rigidity instead of energy to characterise primary CRs. Geomagnetic rigidity is defined as $R = B\rho = pq$, where B is the magnetic field, ρ is the gyroradius of the particle due to this field, p is the particle momentum and q is its charge [14]. As they traverse interplanetary space, galactic CRs interact with heliospheric magnetic field. The heliosphere is the region of space around the Sun dominated by the solar wind and the interplanetary magnetic field (IMF). The solar wind is a stream of supersonic plasma blowing outward from the Sun. IMF represents solar magnetic field carried by highly conducting solar wind plasma. Interaction of CRs with this large-scale field modulates CRs flux intensity measured on Earth, which is nested deep inside the heliosphere. Interaction with the heliosphere causes gradient and curvature drift motion of CRs and scattering by the magnetic irregularities embedded in the solar wind [19]. Variations in the solar magnetic field directly affect the heliosphere, most prominent being the solar cycle variation with a period of about 11 years. Solar cycle affects activity of the Sun which is visible in varying number of sunspots, solar flares (SFs) and coronal mass ejections (CMEs). Coronal mass ejection is an extreme solar activity event, followed by significant release of charged particles and accompanying magnetic field from solar corona. Intensity of measured CRs flux anticorrelates with the activity of the Sun, with lower intensity during maximum of the solar cycle and higher intensity during minimum of solar activity.

One of the transient phenomena of this interaction is the Forbush decrease (FD), which represents a rapid depression in CR flux. It is usually characterised by a sudden decrease reaching minimum within one day, followed by a subsequent gradual recovery phase, which

Supplementary information The online version of this article (https://doi.org/10.1140/epjd/s10053-021-00172-x) contains supplementary information, which is available to authorized users.

[a] e-mail: veselinovic@ipb.ac.rs (corresponding author)

can last for several days. Typical causes of FD are transient interplanetary events related to interplanetary coronal mass ejections (ICMEs). If the speed of the ICME is greater than fast magnetosonic wave speed in the solar wind reference frame, ambient solar wind plasma will be compressed. The shock can be formed, which is driven ahead of ICME and can cause enhancement of IMF. FD can also be formed due to corotating interaction regions between different solar wind streams with different speed [2]. In this paper, we will only focus on ICME induced FDs, of which we will study four cases.

Correlation between parameters characterising FDs (like magnitude of the decrease, duration, one-step or two-step FDs, etc.) and solar wind parameters has been studied for some time. There is reasonable evidence for correlation between FD magnitude and amplitude of magnetic field enhancement B, velocity of CME, maximum solar wind velocities and other parameters as shown in [7,22]. Also, profile of FDs is modelled and compared with CME magnetic structure, starting from the simple force-free flux rope with circular cross section, but it can deviate from this ideal concept. FD magnitude is explained with cumulative effect of diffusion of CRs through the turbulent sheath region [3,11]. FD is also energy dependent, where amplitude of decrease is typically around several percent. Higher-rigidity CRs only weakly interact with magnetic disturbances, so no significant change of the flux can be expected for CRs with rigidity of several dozen GV [9]. In order to detect FD at any location, larger statistics are needed for CRs of lower energy. CRs also interact with geomagnetic field which imposes the minimal rigidity CRs must have in order to reach Earth's surface. This geomagnetic cut-off rigidity depends on geomagnetic latitude. It is smaller at the poles and increases with latitude, with some exceptions due to deviation of Earth's magnetic field from the magnetic dipole model (i.e., South Atlantic anomaly [4]).

Primary CRs arriving at Earth interact with atoms and molecules in Earth's atmosphere. CRs with energy above 300−400 MeV/nucleon generate showers of secondary particles. These secondary CRs consist of electrons and photons (electromagnetic component) and harder, in terms of energy, nuclear component of the cascade. Nuclear component, at the bottom of the atmosphere, is composed mainly of muons, protons, neutrons and neutrinos. Secondary CRs can be observed with detectors in the atmosphere (balloon probes), on the ground or even underground. High-energy muons can penetrate deep underground and can be an important component of the background in experiments requiring high sensitivity (dark matter search, proton decay, etc.).

There is a well-known correlation between parameters of solar wind plasma and CR flux, and the goal of this paper is to extend the study of FDs, specifically its magnitude and time evolution, to wider range of parameters of the heliosphere measured routinely with satellites. We concentrate our study on previously scarcely used parameters of the solar wind, particularly flux of charged particles of different energies. These particles are the source of inhomogeneity in the IMF, so the goal is to try and find distinguishing characteristics of FDs, like magnitude of decrease and FD profile that can be related to the satellite proton flux data, and examine their potential correlation with other space weather parameters. This additional information can be useful in finding explicit connection between parameters of solar wind and CR flux and can lead to better understanding of these complex processes.

2 CR data

In order to provide higher count rate, detector on Earth has to be omnidirectional and to detect integral flux over different range of energies. For the last seventy years secondary CRs are measured using standard ground-based neutron monitors (NMs) [6]. There is a worldwide network of NMs (http://www01.nmdb.eu/) that measures flux of secondary CRs originated from primary CRs with rigidity range approximately between 1 GV and 20 GV. Every node of the worldwide network of ground stations has its unique cut-off rigidity depending on its geomagnetic coordinates and height. The other type of widely used ground-based CR detectors are muon monitors. Muon monitors are sensitive to primary CRs of higher rigidity and complement NMs measurements [26]. Worldwide network of these muon stations is still rudimentary, but it can provide insight into flux variation of primary CRs with energies higher than CRs detected by NMs. Since both NMs and muon detectors are energy-integrating detectors and use entire atmosphere above it as a moderator, it is not trivial to relate count rate of these detectors to the flux or energy spectrum of primary CRs at the top of the atmosphere. One needs to know the response of a detector to a unit flux of CRs with the given energy, the so-called detector yield function. Yield functions can be calculated either theoretically, using a numerical simulation of the nucleonic cascade caused by energetic cosmic rays in the Earth's atmosphere, e.g., [8], or semi-empirically, for example based on a latitudinal survey [16].

As flux of secondary cosmic rays is also sensitive to varying properties of the atmosphere through which these CRs propagate, it is necessary to conduct flux correction of the measured flux for atmospheric parameters, where atmospheric pressure correction is the most important. In addition to atmospheric pressure, CR muons are sensitive to temperature variations in the atmosphere, starting from the top of the atmosphere all the way to the ground level. There are several procedures for corrections of these effects which are regularly used. Most commonly used are the integral method and the method of effective level of generation, but some novel techniques have also been introduced in recent years [25]. Correction for these atmospheric parameters is necessary in order to increase detector sensitivity to

Table 1 Properties of primary CR flux related to muons detected at Belgrade CR station

Detector	Muon flux $1/(m^2s)$	$E_{0.05}$ (GeV)	E_{med} (GeV)	$E_{0.95}$ (GeV)	Cut-off rigidity (GV)
GLL	137(6)	11	59(2)	915	5.3
UL	45(2)	31	137(5)	1811	12

variations of primary CRs flux and more precisely study the influence of solar modulation on galactic CRs.

Belgrade CR station started collecting data with the current experimental set-up in 2009. The station consists of two separate detector units: one placed on ground level (GLL) and the other in shallow underground (UL), both utilising the same experimental set-up. Such configuration provides opportunity to monitor muon fluxes in two different energy ranges with all other external parameters (such as atmospheric parameters, geomagnetic location and experimental set-up) being the same. Underground part of the station detects muons originated from primary CRs with higher energy because of the layer of soil overburden (13 m of loess) which absorbs lower-energy muons. Details of the detector systems at the Belgrade CRs station as well as calculated response functions are presented in [29]. The station is situated at the Laboratory for Nuclear Physics at the Institute of Physics Belgrade, Serbia. The altitude of the station is 78 m above sea level. Its geographic coordinates are: 44°51′ N and 20°23′ E, with geomagnetic latitude of 39°32′ N. Sensitivity of Belgrade CR detectors to galactic CRs is given in Table 1, where primary CRs with the energy below $E_{0.05}$ (and above $E_{0.95}$) contribute with 5% to the count rate of the corresponding detector, and E_{med} is median energy based on simulation. In preparation for the analysis, detected muon count rates are corrected for efficiency, as well as for barometric and atmospheric temperature effects. Temperature effect correction is done using integral method [24].

3 Satellite data

In recent years, satellites provide new direct measurements of primary CRs flux in the heliosphere and the geomagnetic field. Also, detectors mounted on spacecraft allow us to probe even further, as Voyager recently crossed heliospheric boundary and for the first time galactic CRs flux was measured outside the heliosphere. The problem with such measurements is limitation to the size of the detectors, due to constraints of the construction of the satellites. In order to have valid statistics and good resolution, only low-energy particle flux can be measured. These low-energy particles are sensitive to geomagnetic field, which can introduce additional perturbation. Also, measurements of low-energy CRs can be masked by the increased flux of low-energy solar energetic particles (SEPs) in the MeV energy range. FDs detected by ground-based detectors are measured in energy range several orders of magnitude higher than the energy range available to satellites measurements. (NMs detect flux that originate from $\sim$ 10 GeV, single muon detectors higher than that up to $\sim$ 100 GeV, while solar weather satellite measurements range up to several 100 MeV.) SEP occurrence is sporadic and depends on which part of the solar cycle we are in, so long-term studies with stable data quality are necessary if we are to study solar modulation of CRs. Such long-term measurements have been performed with various spacecrafts during the last four decades. Data measured on different interplanetary locations are then used for modelling of the heliosphere, which is important for understanding and forecasting space weather. This is a relatively new and dynamic field that is still expanding. More in situ measurements that can be catalogued [17] and compared with data from ground based stations will improve our understanding of near space environment.

In this paper, we use proton data from ERNE (Energetic and Relativistic Nuclei and Electron experiment) detector at the SOHO (Solar and Heliospheric Observatory) (https://omniweb.gsfc.nasa.gov/ftpbrowser/flux_spectr_m.html), which has been performing measurements in Lagrangian point L1 for the last quarter of a century described in [13] and references therein. Experiments that collects in situ particles data are ERNE and COSTEP (Comprehensive SupraThermal and Energetic Particle analyser), where data are combined to meet requirements of the mission. ERNE detector provides proton flux data in relatively large energy range (1.6 to 131 MeV) separated in several energy channels (1.3−1.6, 1.6−2.0, 2.0−2.5, 2.5−3.2, 3.2−4.0, 4.0−5.0, 5.0−6.4, 6.4−8.0, 8.0−10, 10−13, 13−16, 16−20, 20−25, 25−32, 32−40, 40−50, 50−64, 64−80, 80−100, 100−130 MeV) . Measurements are taken with two different detectors: LED (low-energy detector) covers lower-energy and HED (high-energy detector) which covers higher-energy channels [28]. Satellites, including SOHO, also measure in situ parameters of the space environment and gather data about magnetic field, solar wind and concentration and flux of various types of particles on the location. Satellite data relevant to heliospheric studies are, among other places, available at GSFC/Space Physics Data Facility, in the form of low- and high-resolution OMNI data (https://spdf.gsfc.nasa.gov/pub/data/omni/low_res_omni/). In this study, we used the low-resolution OMNI data that contain hourly data for the solar wind magnetic field and plasma parameters, energetic proton fluxes, and geomagnetic and solar activity indices for different regions in proximity to Earth [12].

4 Four prominent FD events during rising phase of solar cycle 24

Previous (24th) solar cycle started in December 2008 and ended in November 2019 (as available from Sunspot Index and Long-term Solar Observations database http://www.sidc.be/silso/node/167). It had an unusually weak maximum, with smoothed maximum international sunspot number of 116. For comparison, in cycles 22 and 23 this number was 214 and 180, respectively (as available from Sunspot Index and Long-term Solar Observations database http://sidc.be/silso/home). Same period was also characterised by smaller number of FDs, especially ones with larger amplitudes.

There were fifteen strong FDs (with magnitude of decrease larger than 5% for particles with 10 GV rigidity) recorded in the rising phase of solar cycle 24, however in this study we will limit our analysis to four events detected by the Belgrade Cosmic Ray Station (http://www.cosmic.ipb.ac.rs/). Other prominent FDs that occurred in this period have not being detected by either GLL or UL detector due to discontinuity of operation, so they have been omitted from this study. All four events followed ejections from an active region on the Sun, accompanied by a solar flare with interplanetary shock wave and sudden storm commencing (SSC), and disturbance in the geomagnetic field. All of these FDs were seen by the NM detector network as well.

First significant FD of solar cycle 24 was recorded on 18 February 2011 and has been caused by a CME heading directly towards Earth [20]. It has been detected by most ground stations around the world. Its morphology is influenced by the interaction of two CMEs, first slower and the second faster (with respective speeds of 390 km/s and 1020 km/s), that occurred a day apart [27]. Geomagnetic activity has been relatively weak due to orientation of the magnetic field of the ejecta [21].

Second event was observed on 7 March 2012. It included an X-class flare (X5.4), that occurred in NOAA AR 11429 with an intense halo CME, followed by several smaller flares and another partial CME. It caused one of the strongest FDs of the last solar cycle. Observed solar activity was also related to the intense geomagnetic storm that followed [15].

A strong SF (X1.6) was detected by several spacecrafts during 10 September 2014, originating from active region NOAA AR 2158. Based on the SOHO coronagraph images, this flare was associated with a CME that was aimed towards Earth, where it arrived on September 12. This activity resulted in a major geomagnetic storm, one of the strongest in 2014.

In the second half of June 2015, solar activity was very intense, since a number of CMEs and flares were produced from the powerful AR 12371, which dominated solar activity during that period [23]. The impact of these CMEs on the Earth's magnetosphere resulted in a moderate to severe G4-class geomagnetic storm that occurred on the summer solstice. The result was a very interesting and unusual modulation galactic CRs flux, which appeared as a series of FDs.

For the study of FD events and their relationship with IMF and geomagnetic disturbances, researchers from IZMIRAN (Pushkov Institute of Terrestrial Magnetism, Ionosphere and Radio Wave Propagation, Russian Academy of Sciences) created an FD database (http://spaceweather.izmiran.ru/eng/dbs.html) which contains various FD parameters, as well as their relationship with heliospheric and geomagnetic parameters covering several solar cycles [1]. Properties of the four selected FDs, taken from the IZMIRAN database, are given in Table 2.

5 Data analysis

In order to establish the usability of SOHO SEP flux data in the study of CR variations, we will first analyse how muon count rate time series compare with some of the IMF parameters more commonly used in the analysis of solar activity-induced CR variations. To this end, we compare hourly muon count rates (measured by Belgrade muon station and corrected for atmospheric effects) with time series for selected parameters from OMNI database. To give more weight to this qualitative analysis, we concentrate only on periods of extreme solar activity, in particular periods of the occurrence of four FD events described in Sect. 4. We then examine the relationship between measured muon count rates and the SOHO/ERNE SEP flux data and analyse any discerning features in comparison with the ones observed in OMNI data time series. The period selected for this analysis is approximately one solar rotation of 27 days. All probes at L1 are about an hour upstream of the magnetosphere so all their data are interspersed with data from spacecraft close to Earth (e.g., IMP 8). In order to compute hourly averages "at Earth" this time shift has to be taken into account (https://omniweb.gsfc.nasa.gov/html/ow_data.html).

Next, we investigate the short-term correlation between SEP flux and muon count rate data during time periods of four selected FDs. Muon time series for this procedure were selected for times where average muon flux was significantly lower than the background level. Background level was determined from moving averages for hourly count rates 10 days before the event. We then perform correlative analysis between SOHO SEP flux data and muon count rates for a period of one year (from 01.06.2010 to 31.05.2011), in order to establish the long-term relationship. For further insight, we also look into the correlation between these variables during the periods of reduced geomagnetic activity (International Quiet Days) and increased geomagnetic activity (International Disturbed Days).

Finally, we look in greater detail into SOHO SEP flux time series. In order to perform more quantitative analysis, time-integrated flux is calculated for SEP data for different SOHO energy bins and for the duration of selected FD events. In order to provide a parameter for characterisation for different FD events, calculated integral flux is plotted as a function of proton energy and

Table 2 Selected FD and interplanetary disturbance parameters (taken from IZMIRAN database)

Parameter	FD 1	FD 2	FD 3	FD 4	Parameter comment
Date of FD	18.2.2011.	8.3.2012.	12.9.2014.	22.6.2015.	
Date of parent solar event	15.2.2011.	7.3.2012.	10.9.2014.	21.6.2015.	
AR number	1158	11429	2158	12371	NOAA active region
V_{meanC}	584	1198	906	1040	The average ICME velocity between the Sun and the Earth, calculated using the time of the beginning of the associated CME observations (in km/s)
V_{max}	691	737	730	742	Maximal hourly solar wind speed in the event (in km/s)
B_{max}	31	23.1	31.7	37.7	Maximal hourly IMF strength in the event (in nT)
B_{zmin}	– 5.5	– 16.1	– 9.5	– 26.3	Minimal hourly Bz component of the IMF in the event (in nT)
R_{bulk}	72.25	146.2	131.35	171.25	An estimate of the maximum proton rigidity (in GV) that can be reflected by the total magnetic field, integrated from the event onset to the FD minimum
Magn	5.2	11.7	8.5	8.4	FD magnitude for particles with 10 GV rigidity, calculated as maximal range CRs density variations in the event, obtained by GSM from NM network data (in %)
MagnM	4.7	13.1	6.9	10.4	FD magnitude for particles with 10 GV rigidity, corrected on magnetospheric effect with Dst-index (in %)
TminM	7	20	9	11	Time from the FD onset to minimum, calculated from the data corrected for magnetospheric effect
Kp_{max}	5	8	6.33	8.33	Maximal Kp-index in the event
Ap_{max}	48	207	94	236	Maximal 3-hour Ap-index in the event
Dst_{min}	– 30	– 143	– 75	– 204	Minimal Dst-index in the event (in nT)
Flare class	X2.2	X5.4	X1.6	M2.6	Associated X-ray flare data
SSN	85	97	126	56	Number of sunspot at the FD onset day

fitted with a power function. Dependence of magnitude for selected FDs on the exponents obtained from fitted distributions is then analysed.

6 Results and discussion

Comparison between time series of selected IMF parameters from OMNI database and muon count rate time series during the periods of four selected FD events is shown in Fig. 1. Observed anticorrelation between muon count rates and proton flux and temperature, as well as with the overall IMF magnetic field and detected plasma speed, is in agreement with previously stated evidence in the literature [30].

Similar comparison between muon count rate time series and selected channels of SOHO/ERNE proton flux data for the same time intervals is shown in Fig.

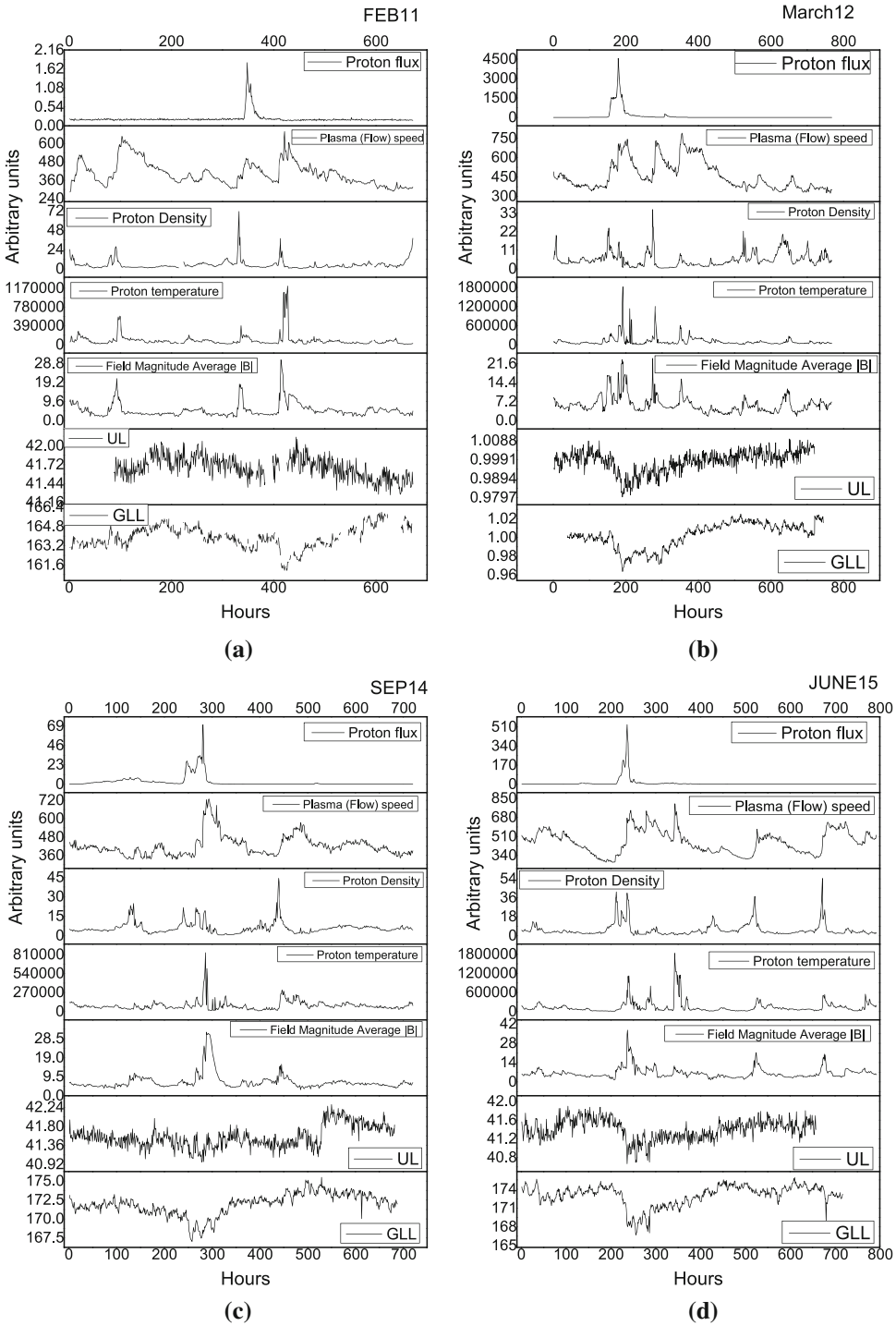

Fig. 1 Time series for particle and plasma parameters (taken from OMNI database) in the time interval of approximately one month around the occurrence of four selected FD events: **a** February 2011 (start of time interval on 1 February), **b** March 2012 (start of time interval on 1 March), **c** September 2014 (start of time interval on 1 September) and **d** June 2015 (start of time interval on 13 June)

2. For the sake of clarity, we chose three energy channels (1.6−2 MeV, 16−20 MeV, 100−130 MeV), approximately one order of magnitude apart, where first channel is measured with LED and the other two with HED detector on SOHO/ERNE instrument. In case of the February 2011 event, there is an observable time lag (≈55 h) between the increase of measured proton flux at low-energy channels (1.6−2 MeV and 16−20 MeV energy channels) and the beginning of FD recorded at ground station. This time lag is also present between

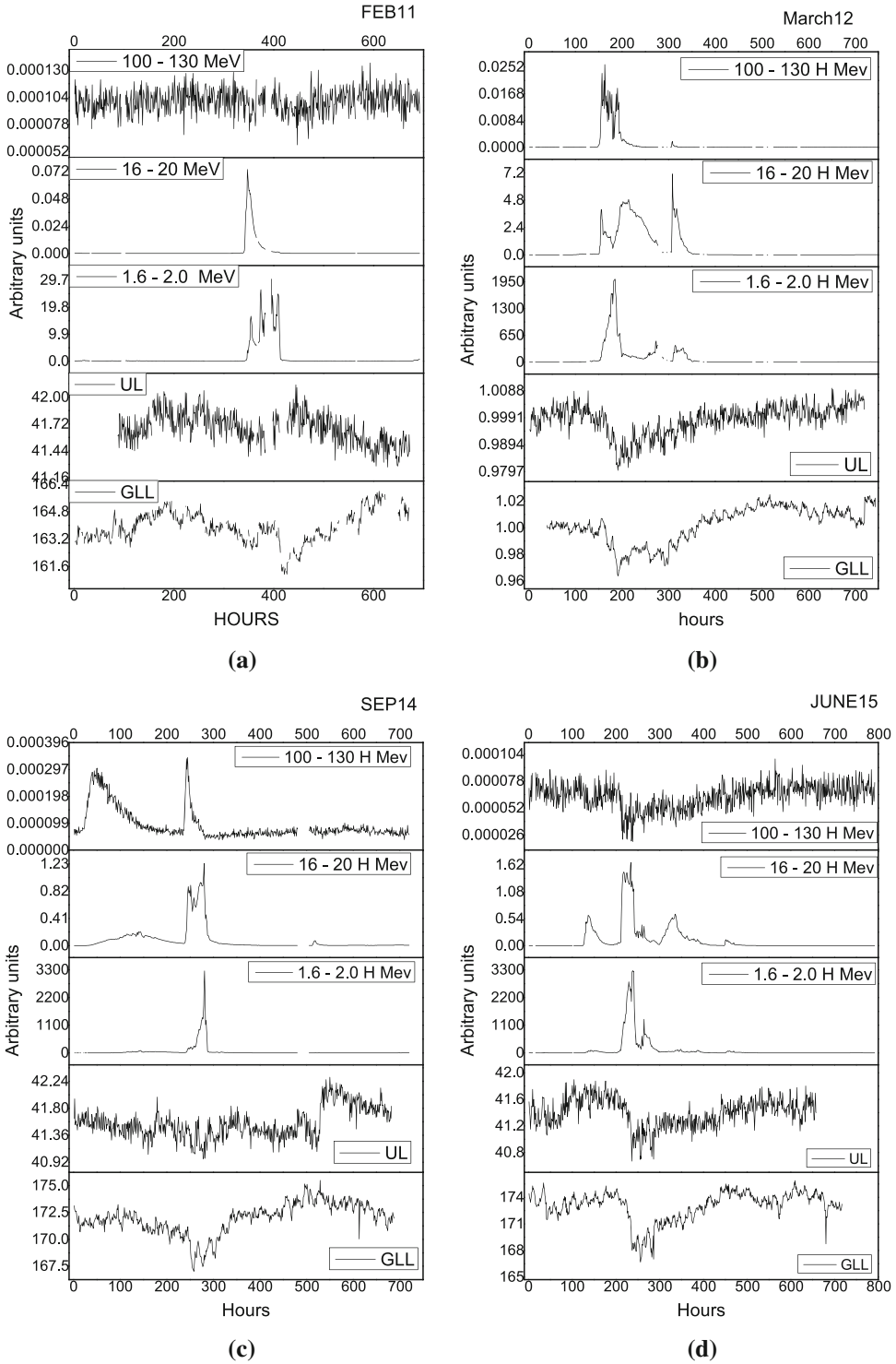

Fig. 2 Hourly time series for different proton channels from SOHO/ERNE and two muon detectors at Belgrade CR station, in the time interval of approximately one month around the occurrence of four selected FD events: **a**)February (start of time interval on 1 February) 2011, **b** March 2012 (start of time interval on 1 March), **c** September 2014 (start of time interval on 1 September) and **d** June 2015 (start of time interval on 13 June)

OMNI proton flux data and ground station measurements for this FD alone. FD is a complex modulation of CR flux that depends on a lot of parameters, like magnitude of magnetic field and its components, speed of solar wind and CMEs (with CME average speed ≈ 490 km/s), most of which are listed in Table 2. Parameter values for all four ICMEs are mostly comparable, but one difference that stands out is the discrep-

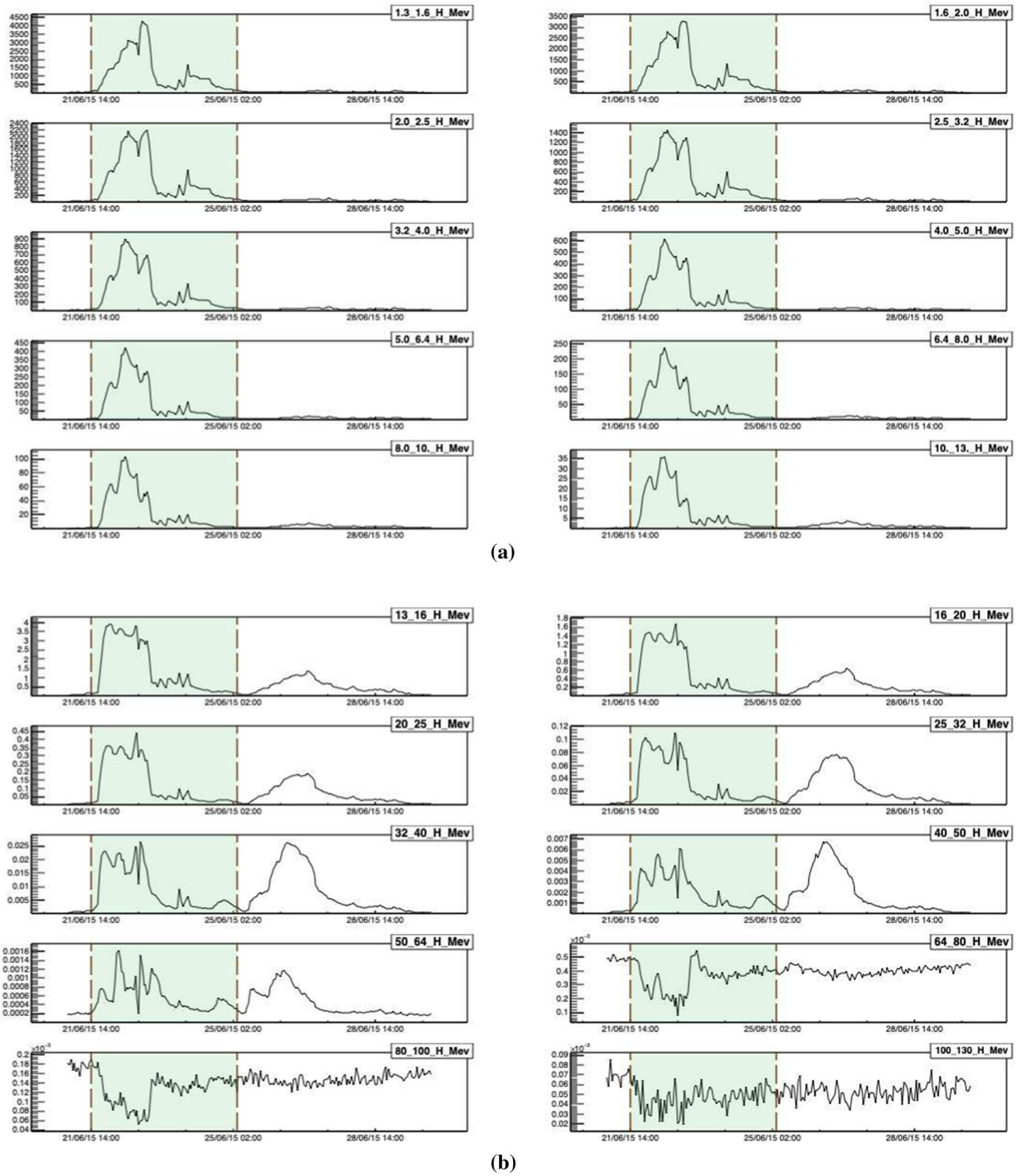

Fig. 3 Differential SEP fluxes during extreme solar event in June 2015, measured by SOHO/ERNE proton channels. Vertical dashed lines indicate the time for the start and the end of interval used to calculate the integral flux

ancy in average CME velocity (584 km/s from Table 2.) for the FD of February 2011, which can possibly explain the observed time lag for this particular FD.

Based on the observed time lag and other coincident features, we can establish good agreement between SOHO low-energy channel data and OMNI data time series. As for high-energy channels, SEP time series in 100−130 MeV energy range for February 2011 and June 2015 events appear to correlate with muon count rate measurements on the ground. One possible explanation

Table 3 Statistical correlation between Belgrade CR station and SOHO/ERNE measurements during the periods of four selected FD events

FD	Energy range (MeV)	GLL		UL	
		Pearson coefficient	P value	Pearson coefficient	P value
FEB 11	1.6–2.0 H	– 0.10877	0.01	– 0.05285	0.2
	16–20 H	– 0.18384	2×10^{-5}	– 0.10732	0.01
	100–130 H	0.24204	$< 10^{-6}$	– 0.13212	0.02
MAR 12	1.6–2.0 H	– 0.48477	$< 10^{-6}$	– 0.43994	$< 10^{-6}$
	16–20 H	– 0.72033	$< 10^{-6}$	– 0.68221	$< 10^{-6}$
	100–130 H	– 0.29172	$< 10^{-6}$	– 0.27822	$< 10^{-6}$
SEP 14	1.6–2.0 H	– 0.2839	$< 10^{-6}$	– 0.48052	$< 10^{-6}$
	16–20 H	– 0.37814	$< 10^{-6}$	– 0.63735	$< 10^{-6}$
	100–130 H	– 0.04951	0.007	– 0.10466	0.2
JUN 15	1.6–2.0 H	– 0.3921	$< 10^{-6}$	– 0.27531	$< 10^{-6}$
	16–20 H	– 0.31229	$< 10^{-6}$	– 0.17113	$< 10^{-6}$
	100–130 H	0.48588	$< 10^{-6}$	0.39296	$< 10^{-6}$

could be that in addition to SEP these energy channels are also populated by very low-energy CRs.

We can further investigate this assumption by looking more closely into SOHO SEP flux time series for one of the two weaker FD events. We have selected June 2015 event, as time series for higher-energy channels appear to be slightly more informative. Figure 3 shows proton flux series for all energy channels measured by SOHO/ERNE detector. From these plots, it is apparent that proton fluxes for energies larger than 64 MeV exhibit different dynamic relative to fluxes of lower energies, and seem to be in anticorrelation with them. This indeed supports the assumption these channels are populated by low-energy CR.

Another way we can illustrate this observation more quantitatively is by performing correlative analysis. Firstly, we will look into short-term correlations between proton flux and muon count rate time series during four selected FD evens. Correlation between respective time series was found using Pearson correlation coefficient. For significance two-tailed test is used. Correlation coefficient and its significance level between ground station and in situ measurement from SOHO/ERNE instrument is given in Table 3.

Due to higher energy of the primary CRs detected in UL, the correlation between SEPs and measured flux in UL is smaller than correlation between SEPs and flux measured in GLL. The greatest anticorrelation (i.e., between GLL and UL data and 16−20 MeV protons ≈ -0.7) is observed for the strongest ICME (and corresponding FD) of March 2012, and this anticorrelation is observed in all energy channels. However, for lower-intensity events of June 2015 and February 2011, correlations between detected CR flux in GLL and highest energy channel (100−130 MeV) are mostly positive. These observations further confirm the assumption about high-energy channels being populated by low-energy CR, which is especially evident in case of low-intensity FD events.

Table 4 Pearson correlation coefficient for the correlation between CR flux detected at Belgrade CR station (GLL detector) and flux of protons of different energies detected with SOHO/ERNE detector, for the period of one year (from June 2010 May 2011)

	GLL	
	Pearson coefficient	P value
H 1.3–1.6 MeV	– 0.02	0.13
H 1.6–2.0 MeV	– 0.02	0.16
H 2.0–2.5 MeV	– 0.02	0.20
H 2.5–3.2 MeV	– 0.01	0.27
H 3.2–4.0 MeV	– 0.01	0.36
H 4.0–5.0 MeV	– 0.01	0.57
H 5.0–6.4 MeV	< 0.01	0.75
H 6.4–8.0 MeV	< 0.01	1.00
H 8.0–10 MeV	< 0.01	0.78
H 10–13 MeV	0.01	0.57
H 13–16 MeV	0.01	0.41
H 16–20 MeV	0.01	0.31
H 20–25 MeV	0.01	0.26
H 25–32 MeV	0.01	0.24
H 32–40 MeV	0.01	0.27
H 40–50 MeV	0.01	0.46
H 50–64 MeV	< 0.01	0.80
H 64–80 MeV	0.05	< 0.01
H 80–100 MeV	0.12	< 0.01
H 100–130 MeV	0.07	< 0.01

Similar results, with even greater correlation between the entire time profile for flux measured with NMs and solar wind speed and magnetic field during ICME, are reported for stronger FDs during solar cycle 23 [5].

Next, we will analyse long-term correlations between SOHO proton flux and measured muon count rates. Pearson coefficients for this correlation over a period of one year (from June 2010 May 2011), when activity of the Sun was low at the commencement of the 11-years cycle, are presented in Table 4. Here we see very

Table 5 Pearson correlation coefficient for the correlation between CR flux detected at Belgrade CR station (GLL detector) and flux of protons of different energies detected with SOHO/ERNE detector, during international geomagnetically quiet and disturbed days for the period of one year (from June 2010 May 2011)

	GLL Quiet days		GLL Disturbed days	
	Pearson coefficient	P value	Pearson coefficient	P value
H 1.3–1.6 MeV	0.01	0.61	− 0.05	0.13
H 1.6–2.0 MeV	0.01	0.80	− 0.05	0.14
H 2.0–2.5 MeV	0.02	0.30	− 0.05	0.13
H 2.5–3.2 MeV	0.03	0.11	− 0.05	0.12
H 3.2–4.0 MeV	0.04	0.04	− 0.05	0.10
H 4.0–5.0 MeV	0.05	0.02	− 0.06	0.08
H 5.0–6.4 MeV	0.05	0.01	− 0.06	0.07
H 6.4–8.0 MeV	0.06	0.01	− 0.06	0.06
H 8.0–10 MeV	0.06	0.01	− 0.06	0.06
H 10–13 MeV	0.06	0.01	− 0.06	0.07
H 13–16 MeV	0.06	< 0.01	− 0.06	0.08
H 16–20 MeV	0.06	< 0.01	− 0.05	0.10
H 20–25 MeV	0.06	< 0.01	− 0.05	0.12
H 25–32 MeV	0.06	< 0.01	− 0.05	0.15
H 32–40 MeV	0.06	< 0.01	− 0.04	0.20
H 40–50 MeV	0.06	< 0.01	− 0.02	0.57
H 50–64 MeV	0.07	< 0.01	0.07	0.03
H 64–80 MeV	0.25	< 0.01	0.08	0.02
H 80–100 MeV	0.38	< 0.01	0.11	< 0.01
H 100–130 MeV	0.15	< 0.01	0.09	0.01

little correlation between CR and proton fluxes in all but the highest energy channels (above 64 MeV).

Table 5 shows the same correlation analysis if only data for 10 geomagnetically quietest or 5 geomagnetically most disturbed days of each month (http://isgi.unistra.fr/events_qdays.php) are used. The fact that we observe a significant increase of positive correlation coefficients in the case of geomagnetically quiet days, further corroborates the assumption about the mixed nature of particles that populate higher-energy channels. Consequentially, care should be taken how data from these channels are treated in analysis.

To provide further quantitative support for the use of SOHO SEP flux measurements in the analysis of FD events, we will calculate integral proton flux in all energy channels for the four selected FDs. Integration intervals are selected to include the period of increased proton flux that corresponds to a particular FD, but not to extend the interval to include potential follow-up structures that cannot be associated with the event. One such selection for all energy channels, for June 2015 event, is indicated by dashed lines in Fig. 3. In Fig. 4, we show thusly calculated integral flux as a function of particle energy (where lower boundary values from SOHO SEP energy bins are taken), using both linear and log scale for clarity.

One feature that can be noticed from plots in Fig. 4 is that integral flux drops off is more steeply in February 2011 than for others studied FDs, where a change in the trend between high-energy and low-energy range can be observed. FD that occurred in March 2012 was the longest and the most intensive of the four. Steepness of the integral flux for this FD shows relatively more populated proton channels with higher energies compared to weaker FD. This is in agreement with strongest modulation of CRs flux during this FD. There is a discontinuity in the integral flux between proton energy channel 13−16 MeV and 16−20 MeV due to different acquisition method from different instruments, and possibly because of degradation of the detectors on board the spacecraft [13] and saturation of the instrument due to high intensity of solar protons [18].

One simple way to characterise relative abundance of SEP particles of different energies for a given event would be to fit described integral flux distribution with a power function, where (in a simple approximation) larger exponent would indicate greater relative abundance of lower-energy particles, while smaller exponent would point to greater relative abundance of higher-energy particles. Distributions were fitted with a power function given by the formula $I(E) = a * E^b$ (where I is the integral flux and E is particle energy), resulting fits represented by red lines in Fig. 4, while values for the exponents of power function fits are represented in Table 6.

If SOHO protons flux measurements are to be proved useful in the analysis of FD events, SEP flux characteristics should correlate with some of the FD and interplanetary disturbance parameters. To test this, we have analysed dependence of different FD parameters on the exponent of the integral proton flux power distribution (labelled b in the formula in previous paragraph). We have found some correlation for most tested parameters, most striking being one between the magnitude

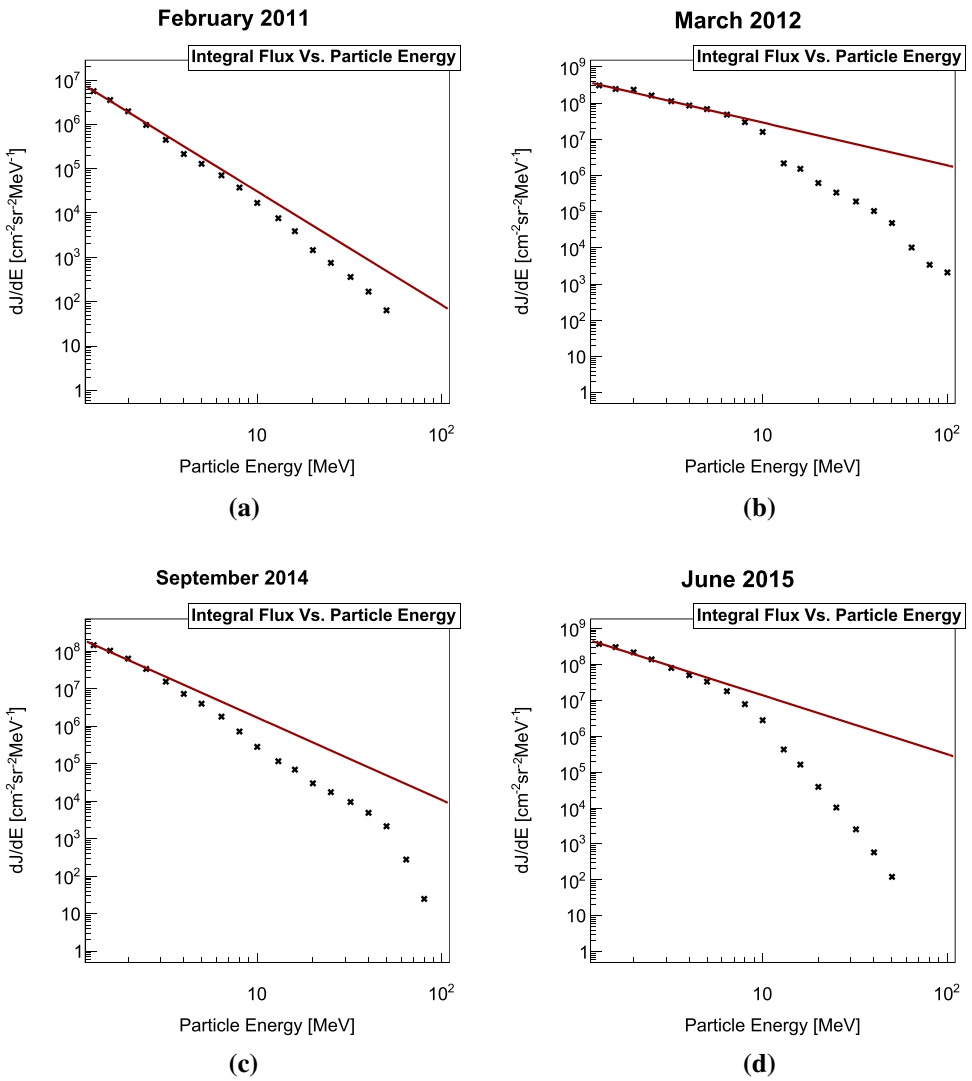

Fig. 4 Time-integrated flux of differential SEP fluxes during the four selected FD events: **a** February 2011, **b** March 2012, **c** September 2014 and **d** June 2015, in linear and logarithmic scale. Power function fits are represented by red lines

Table 6 Exponent values of power function fits of integral proton flux distributions

FD	Power function exponent values
FEB 2011	– 2.56
MAR 2012	– 1.18
SEP 2014	– 2.20
JUN 2015	– 1.64

of FD for particles with 10 GV rigidity (corrected for magnetospheric effect) and the exponent of the integral flux. This dependence (strictly for illustrative purposes fitted with linear fit) is shown in Fig. 5.

Observed strong dependence is potentially a very good indicator that SOHO SEP flux measurements can be a valid source of data to be used in the analysis of interplanetary disturbances and their interaction with cosmic rays.

7 Conclusions

Analysing strong aperiodic variations of cosmic ray flux, such as Forbush decreases, allows us to study violent processes that occur on the Sun, and corresponding perturbations in the heliosphere, using Earth-based detectors. In addition to cosmic ray flux and magnetic field data commonly used to study such events, we have extended analysis to include proton flux measurements, obtained using spacecraft mounted detectors. Based on the analysis of four selected Forbush decrease events, we have found SOHO/ERNE proton flux measurements to be consistent with solar plasma parameters, as well as with observations by the ground-based muon detectors.

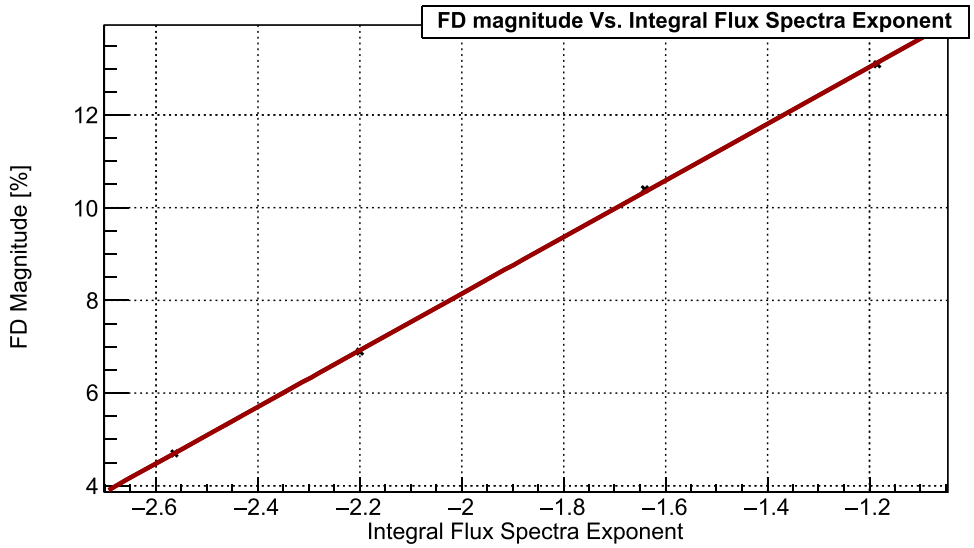

Fig. 5 Dependence of FD magnitude, corrected for magnetospheric effect with Dst-index for particles with 10 GV rigidity, on the power exponent of the integral SEP flux, four selected FD events: **a** February 2011, **b** March 2012, **c** September 2014 and **d** June 2015. Linear fit (for illustrative purposes) is indicated by the red line

We have concluded that during Forbush decrease events lower-proton-energy channels are dominated by SEP particles, while in higher-energy channels there is a contribution of low-energy cosmic rays, especially apparent during less intense events. We have found a clear correlation between Forbush decrease magnitude (corrected for magnetospheric effect with Dst-index for particles with 10 GV rigidity) and power exponent of the integral flux of SOHO/ERNE measurements. This result gives grounds to further pursue the analysis of heliospheric proton flux data, as it may yield additional valuable information. Such information can potentially help us to classify and study in greater detail the dynamics of interaction of cosmic rays in the heliosphere.

Acknowledgements The authors acknowledge funding provided by the Institute of Physics Belgrade, through the grant by the Ministry of Education, Science and Technological Development of the Republic of Serbia. We also acknowledge use of NASA/GSFC's Space Physics Data Facility's OMNIWeb (or CDAWeb or ftp) service and OMNI data as well as team behind SOHO, which is a project of international collaboration between ESA and NASA. We would also like to thank the referees for constructive and useful advice.

Data Availability Statement "This manuscript has data included as electronic supplementary material".

References

1. A.A. Abunin, M.A. Abunina, A.V. Belov, S.P. Gaidash, E.A. Eroshenko, I.I. Pryamushkina, L.A. Trefilova, E.I. Gamza, J. Phys. Conf. Ser. **1181**, 012062 (2019). https://doi.org/10.1088/1742-6596/1181/1/012062
2. K.P. Arunbabu, H.M. Antia, S.R. Dugad, S.K. Gupta, Y. Hayashi, S. Kawakami, P.K. Mohanty, T. Nonaka, A. Oshima, P. Subramanian, A and A **555**, A139 (2013). https://doi.org/10.1051/0004-6361/201220830
3. K.P. Arunbabu, H.M. Antia, S.R. Dugad, S.K. Gupta, Y. Hayashi, S. Kawakami, P.K. Mohanty, A. Oshima, P. Subramanian, A and A **580**, A41 (2015). https://doi.org/10.1051/0004-6361/201425115
4. C.R.A. Augusto, V. Kopenkin, C.E. Navia, K.H. Tsui, H. Shigueoka, A.C. Fauth, E. Kemp, E.J.T. Manganote, M.A. Leigui de Oliveira, P. Miranda, R. Ticona, A. Velarde, ApJ **759**, 143 (2012). https://doi.org/10.1088/0004-637X/759/2/143
5. A. Bhaskar, G. Vichare, K.P. Arunbabu et al., Astrophys. Space Sci. **361**, 242 (2016). https://doi.org/10.1007/s10509-016-2827-8
6. V. Belov, SpaceSci. Rev. **93**(1), 79–105 (2000). https://doi.org/10.1023/A:1026584109817
7. H.V. Cane, Space Sci. Rev. **93**, 55–77 (2000). https://doi.org/10.1023/A:1026532125747
8. J.M. Clem, L.I. Dorman, Space Sci. Rev. **93**, 335–359 (2000). https://doi.org/10.1023/A:1026508915269
9. E.S. Comedi, A.S. Elias, B.S. Zossi, S. Bruno, JASTP **211**, 105475 (2020). https://doi.org/10.1016/j.jastp.2020.105475
10. M. Duldig, Science **314**(5798), 429–430 (2006). https://doi.org/10.1126/science.1134046
11. M. Dumbović, B. Vršnak, J. Guo et al., Sol. Phys. **295**, 104 (2020). https://doi.org/10.1007/s11207-020-01671-7
12. J.H. King, N.E. Papitashvili, J. Geophys. Res. **110**, A02104 (2005). https://doi.org/10.1029/2004JA010649
13. P. Kühl, B. Heber, R. Gómez-Herrero, O. Malandraki, A. Posner, H. Sierks, J. Space Weather Space Clim. (2020). https://doi.org/10.1051/swsc/2020056
14. S.Y. Lee, *Accelerator Physics*, 2nd edn. (World Scientific, Singapore, 2004)

15. M. Livada, H. Mavromichalaki, C. Plainaki, Astrophys. Space Sci. **363**, 8 (2018). https://doi.org/10.1007/s10509-017-3230-9
16. R.A. Caballero-Lopez, H. Moraal, JGR Space Phys. **117**, A12 (2012). https://doi.org/10.1029/2012JA017794
17. R. Miteva, S.W. Samwel, M.V. Costa-Duarte, JASTP (2018). https://doi.org/10.1016/j.jastp.2017.05.003
18. R. Miteva, D. Danov, in *Proceedings of the tenth Workshop 'Solar Influences on the Magnetosphere, Ionosphere and Atmosphere', Primorsko, Bulgaria*, ed. by K. Georgieva, B. Kirov, D. Danov, 2018. https://doi.org/10.31401/WS.2018.proc
19. H. Moraal, Space Sci. Rev. **176**, 299–319 (2013). https://doi.org/10.1007/s11214-011-9819-3
20. S.Y. Oh, Y. Yi, A Sol. Phys. **280**, 197–204 (2012). https://doi.org/10.1007/s11207-012-0053-2
21. A. Papaioannou, A. Belov, H. Mavromichalaki et al., J. Phys. Conf. Ser. **409**, 012202 (2013). https://doi.org/10.1088/1742-6596/409/1/012202
22. A. Papaioannou, M. Belov, E. Abunina, A. Eroshenko, A. Abunin, S. Anastasiadis, Patsourakos, H. Mavromichalaki, ApJ **890**, 101 (2020). https://doi.org/10.3847/1538-4357/ab6bd1
23. E. Samara, A. Smponias, I. Lytrosyngounis et al., Sol. Phys. **293**, 67 (2018). https://doi.org/10.1007/s11207-018-1290-9
24. M. Savic, A. Dragic, N. Veselinovic et al., *XXV ECRS 2016 Proceedings—eConf C16-09-04.3*, e-Print: 1701.00164 [physics.ins-det], arXiv:1701.00164v1
25. M. Savić, A. Dragić, D. Maletić et al., Astropart. Phys. (2019). https://doi.org/10.1016/j.astropartphys.2019.01.006
26. M. Savić, N. Veselinović, A. Dragić et al., ASR **63**, 4 (2019). https://doi.org/10.1016/j.asr.2018.09.034. ISSN 0273-1177
27. M. Temmer, A.M. Veronig, V. Peinhart, B. Vršnak, ApJ **785**, 85 (2014). https://doi.org/10.1088/0004-637X/785/2/85
28. J. Torsti, E. Valtonen, M. Lumme et al., Sol. Phys. **162**, 505–531 (1995). https://doi.org/10.1007/BF00733438
29. N. Veselinović, A. Dragić, M. Savić, D. Maletić, D. Joković, R. Banjanac, V. Udovičić, NIM A **875**, 1 (2017). https://doi.org/10.1016/j.nima.2017.09.008. ISSN 0168-9002
30. L.-L. Zhao, H. Zhang, ApJ **827**, 13 (2016). https://doi.org/10.3847/0004-637X

Space Weather

RESEARCH ARTICLE
10.1029/2020SW002712

Modeling Meteorological Effects on Cosmic Ray Muons Utilizing Multivariate Analysis

M. Savić[1], D. Maletić[1], A. Dragić[1], N. Veselinović[1], D. Joković[1], R. Banjanac[1], V. Udovičić[1], and D. Knežević[1]

[1]Institute of Physics Belgrade, University of Belgrade, Belgrade, Serbia

Key Points:

- Correction of meteorological effects on muon component of secondary cosmic rays significantly extends the usability of muon monitors
- A new method for modeling of meteorological effects utilizing multivariate analysis and machine learning techniques is presented
- Correction efficiency of the best performing algorithm is greater than for other commonly used methods

Correspondence to:
M. Savić,
msavic@ipb.ac.rs

Citation:
Savić, M., Maletić, D., Dragić, A., Veselinović, N., Joković, D., Banjanac, R., et al. (2021). Modeling meteorological effects on cosmic ray muons utilizing multivariate analysis. *Space Weather*, *19*, e2020SW002712. https://doi.org/10.1029/2020SW002712

Received 30 DEC 2020
Accepted 13 JUL 2021

Abstract Correction of meteorological effects on muon component of secondary cosmic rays significantly extends the usability of muon monitors. We propose a new data driven empirical method for correction of meteorological effects on muon component of secondary cosmic rays, based on multivariate analysis. Several multivariate algorithms implemented in Toolkit for Multivariate Data Analysis with ROOT framework are trained and then applied to correct muon count rate for barometric and temperature effects. The effect of corrections on periodic and aperiodic cosmic ray variations is analyzed and compared with integral correction method, as well as with neutron monitor data. The best results are achieved by the application of linear discriminant method, which increases sensitivity of our muon detector to cosmic ray variations beyond other commonly used methods.

Plain Language Summary Primary cosmic rays are energetic particles that arrive at Earth from space. On their journey toward Earth they are affected by the solar wind (a stream of charged particles emanating from the sun), which has information about various solar processes embedded in it. In top layers of the atmosphere primary cosmic rays interact with nuclei of air molecules and produce large number of secondary particles that propagate toward Earth's surface. These secondary particles preserve information about variations of primary cosmic rays, which allows for the study of solar processes using Earth based detectors. One type of secondary particles that can be detected on the ground are muons. However, muons are affected by the conditions in the atmosphere, which can disturb the information about variations of primary cosmic rays. That is why it is important to model these atmospheric effects on cosmic ray muons as well as possible so they can be corrected for. In this study, we present a new method for modeling and correction of atmospheric effects on cosmic ray muons, that is based on multivariate analysis utilizing machine learning algorithms. This method increases sensitivity of our muon detector to cosmic ray variations beyond other commonly used methods.

1. Introduction

Meteorological effects on muon component of secondary cosmic rays have been known and studied for almost a century. A number of meteorological parameters contribute to variation of muon flux in the atmosphere, but two are the most significant: atmospheric pressure and atmospheric temperature.

Aperiodic fluctuations of intensity, discovered in the very early cosmic ray measurements, were eventually attributed to the variation of atmospheric pressure by Myssowsky & Tuwim (1926) (associated effect dubbed *barometric*), while *temperature effect* has been discovered more than a decade later and has two components: *negative* (first quantitively described by Blackett, 1938) and *positive* (suggested by Forró, 1947). Barometric effect represents variation of muon flux due to variation of the mass of the absorber (air column) above the detector. Negative temperature effect is a consequence of dependence of effective height of muon generation level on the atmospheric temperature, resulting in longer muon path and increased probability of decay with higher temperature. Positive temperature effect has to do with positive correlation between atmospheric temperature and air density, decreasing the probability of nuclear interactions and increasing the probability of decay of muon-generating pions with the increase of temperature.

In order to study variations of primary cosmic rays (CR) using Earth based muon detectors, it is of the utmost importance to describe these meteorological effects as precisely as possible so they can be corrected for. A precise correction for meteorological effects significantly increases sensitivity of muon detectors to CR variations, making them a more usable counterpart to neutron monitors (the other widely used type of

ground based cosmic ray detectors), as muon detectors are normally responsive to higher energy primary cosmic rays. Additionally, muon monitors have a unique application in diagnostics of the atmosphere, allowing for prediction of atmospheric temperatures provided a good model of meteorological effects is available (Belov et al., 1987; Kohno et al., 1981).

Several empirical and theoretical models of meteorological effects have been proposed over the years, based on which corrections can be performed. Even though full set of meteorological effects is larger, in this analysis we will concentrate on the correction of temperature and barometric effect only, so results can be more easily compared to other methods.

Some of the most commonly used methods for temperature correction are: method of effective level of generation, introduced by Duperier (1949), integral method, developed by Feinberg (1946), Dorman (1954), and others (Maeda & Wada, 1954; Wada, 1962), method of mass-averaged temperature developed by Dvornikov et al. (1976), and method of effective temperature (mostly applicable to underground detectors) (Barrett et al., 1952).

Each of these methods have their own advantages, but in this study, we have decided to use the integral method as a reference against which to compare the results of our analysis. Main reason being is that it is derived from the theory of meteorological effects, which involves the most detailed analysis, as well as it being the least approximative. According to this approach, relative variation of muon count rate due to the temperature effect can be expressed as:

$$\left(\frac{\delta I}{I}\right)_{temp} = \int_0^{h_0} \alpha(h) \cdot \delta T(h) \cdot dh, \tag{1}$$

where α is temperature coefficient density function, δT is temperature variation and h_0 is atmospheric depth of the observation level expressed in g/cm^2. Temperature coefficient density function is calculated theoretically, while temperature variation is calculated relative to some reference temperature for the period, usually mean temperature. In practical application, integration in Equation 1 is substituted with a sum, taking into account some finite number of isobaric levels.

Analysis of barometric effect is also included in the theory of meteorological effects, but barometric coefficient is rarely calculated theoretically. Most commonly it is determined using linear regression, assuming linear dependence between atmospheric pressure and muon flux:

$$\left(\frac{\delta I}{I}\right)_{pres} = \beta \cdot \delta P, \tag{2}$$

where β is barometric coefficient, and δP represents atmospheric pressure variation.

Each of the mentioned methods is at least in some part approximative, so the idea behind this work is to introduce a new empirical method for correction of meteorological effects that would be data driven, assuming as little as possible upfront. Other advantages of such approach are that it does not depend on the design of the detector, location of the site or topology of the surrounding terrain (as these would ideally be factored in by the model), and that it can be applied in near-real time. Additionally, proposed method can be used in the analysis and potential correction of temperature effect of neutron component of cosmic rays, as part of detected neutrons can originate from cosmic ray muons captured in the nuclei of the shielding of a neutron monitor detector (Dorman, 2004). Finally, in principle it can easily be generalized to take wider set of meteorological parameters into account.

As the presented problem is multidimensional, involving a relatively large number of correlated variables, we have decided to employ multivariate analysis, relying on machine learning techniques. In some recent work (Morozova et al., 2017; Savic et al., 2019) decorrelation of atmospheric variables and numerical modeling has been successfully applied to the study of interaction of cosmic rays with Earth's atmosphere, so utilizing adaptive and flexible machine learning methods could possibly yield further improvement, potentially revealing additional dependencies and taking higher order effects into account. This approach involves application of a number of multivariate algorithms, more or less rooted in statistical machine learning, to our problem and comparing their consistency and effectiveness with selected reference results.

Large part of variations observed in continuous cosmic ray measurements can be attributed to different space weather phenomena, due to modulation of primary cosmic rays in the heliosphere. In terms of temporal properties, they can be classified as periodic or aperiodic. We will test how newly introduced methods for correction of meteorological effects affect the sensitivity for detection of both periodic as well as aperiodic variations of muon flux of nonterrestrial origin, and how it ultimately compares to the sensitivity of neutron monitors.

2. Data

For the analysis of meteorological effects both muon flux and meteorological data are needed. Muon flux was measured experimentally in the Low Background Laboratory at the Institute of Physics Belgrade, while meteorological data is a combination of modeled atmospheric temperature profiles, and atmospheric pressure and ground level temperature measured locally.

2.1. CR Muon Data

Low Background Laboratory (LBL) is located on the grounds of the Institute of Physics Belgrade. Geographical coordinates for the laboratory are 44°51′N and 20°23′E, with elevation of 75 m and geomagnetic cutoff rigidity of 5.3 GV. Detector system is comprised of a 100 × 100 × 5 cm plastic scintillator with accompanying read-out electronics. Median energy for the detector system is (59 ± 2) GeV (Veselinović et al., 2017), with muon flux of $(1.37 \pm 0.06) \times 10^{-2}$ per cm^2 s. Electron contamination determined for a previously used experimental setup was ∼24% (Dragić et al., 2008), and is assumed to be comparable for the current one (Joković, 2011). More detailed description of the laboratory and the experimental setup can be found elsewhere (Dragic et al., 2011). Native muon count rate data has time resolution of 5 min, but hour sums are also frequently used in analysis.

Continuous cosmic ray muon flux measurements have been ongoing in LBL since 2002, current setup being utilized since 2009. Data are available to public via an online interface on the Belgrade Cosmic Ray Station internet site (Low Background Laboratory for Nuclear Physics, 2020).

As with any long-term measurement, some shorter interruptions and inconsistencies are unavoidable, hence when choosing the interval to be used for the analysis we decided to use a one-year period from June 1, 2010 to May 31, 2011, where measurements had the most continuity and consistency. Additionally, using a one-year period should remove any potential bias, primarily due to annual temperature variation.

2.2. Meteorological Data

Meteorological parameters needed for the analysis come from two sources: Atmospheric temperature profile data are produced by an atmospheric numerical model, while atmospheric pressure and ground temperature data come from local measurements.

Meteorological balloon soundings above Belgrade done by Republic Hydro-meteorological Service of Serbia (RHMZ, 2020) are not frequent enough for the purposes of this analysis, so modeled data for atmospheric temperature profile are used instead. Several numerical atmospheric models can provide such data. In this work, we have chosen Global Forecast System (GFS) produced by National Centers for Environmental Prediction (GFS, 2020), which has been found to be in best agreement with ballon soundings done above Belgrade. Comparison was done where soundings data were available, as described in our previous study (Savic et al., 2019). GFS provides a large number of modeled atmospheric parameters among which are atmospheric temperatures for different isobaric levels. Modeled data sets are being produced four times per day (at hours 00:00, 06:00, 12:00, and 18:00). In addition, analysis data are also available, reprocessed *post festum* and taking into account real data measured by world network of meteorological services. In this analysis, we have been using such reprocessed atmospheric temperatures for the following isobaric levels: 10, 20, 30, 50, 70, 100, 150, 200, 250, 300, 350, 400, 450, 500, 550, 600, 650, 700, 750, 800, 850, 900, 925, and 975 mb. Data are available with spatial resolution of 0.5° of geographical longitude/latitude, so coordinates closest to the laboratory coordinates were chosen. Data were then interpolated with cubic spline, similar as in Berkova et al. (2012), and sampled in finer time resolution needed for the analysis.

Atmospheric pressure and ground temperature data are compiled from different meteorological stations in and around Belgrade, and then interpolated as described in more detail elsewhere (Savic et al., 2016). Finally, unique time series of combined modeled and measured meteorological data, with finest time resolution of 5 min, is assembled to be used in the analysis.

3. Methodology

The use of machine learning has seen an unprecedented expansion in the last decade. The main strength of such approach being that it does not assume any a priori model, but is data driven and thus able to potentially discover hidden dependencies. This is especially true when applied to large data sets with many correlated variables. In this study, we want to establish whether such approach would yield any improvements when applied to the problem of meteorological effect on cosmic ray muons.

To test this, we have decided to use toolkit for multivariate analysis (TMVA) package which provides a ROOT-integrated environment for application of multivariate classification and regression techniques (Hoecker et al., 2007). The package has been developed for the use in high-energy physics and contains implementation of a number of supervised learning algorithms, which utilize training and testing procedures on a sample data set to determine the mapping function. Mapping function maps the input parameters to output target value, trying to model the actual functional dependence ("target" function) as accurately as possible. The structure of the mapping function is algorithm specific, and can be a single global function or a set of local models. Trained algorithm is then applied to the full data set and provides either a signal/background separation (in case of classification) or prediction of target value (in case of regression).

For us, the later application is especially interesting. The idea is to train the mapping function, using meteorological parameters as input variables, and muon count rate as the regression target, and use trained function to produce the predicted target output for a larger data set. In principle, implementation of this procedure is specific for different analysis frameworks. TMVA provides template code for the training and application of multivariate methods, where optimal parameters obtained in the training/testing phase are stored in "weight" files to be used in the application phase. Thusly predicted muon count rate would ideally contain only variations related to meteorological effects, while the residual difference between modeled and measured muon count rate would contain variations of non-meteorological origin. We would apply this procedure for a number of algorithms implemented in TMVA, compare their performance and efficiency based on several criteria, and finally suggest the methods best suited for the modeling, and ultimately the correction, of meteorological effects.

Corrected muon count rate would be calculated according to the following equation:

$$N_{\mu}^{(corr)} = \Delta N_{\mu} + \langle N_{\mu} \rangle, \tag{3}$$

where

$$\Delta N_{\mu} = N_{\mu}^{(mod)} - N_{\mu} \tag{4}$$

is the difference between the modeled and measured muon count rate.

Not all machine learning methods are equally suited for all types of problems and selection of the optimal method for a particular application is rarely straightforward. The efficiency of different algorithms depends on a number of factors: Whether they are used for classification or regression, is correlation between parameters linear or nonlinear, what is the general complexity of the problem and required level of optimization, and so on. One can only assume the efficiency of any given algorithm upfront but there is no clear general rule which one will perform best in a particular situation. Often, several algorithms with specific strengths and weaknesses can be applied to the same problem and only through analysis of the final result the optimal one can be determined. For this reason, in our analysis we have decided to indiscriminately include the largest number of algorithm classes available in TMVA, and only after extensive parallel testing narrow the selection down to the optimal one.

We will briefly describe different classes of multivariate methods available in TMVA, as well as list specific algorithms that were chosen as representative for each class. First class are methods based on probability

density estimation (PDE) techniques, where actual probability density function is estimated based on the available data. Here we have selected to test two specific multidimensional implementations, somewhat similar in nature: PDE range-search (PDE-RS) and k-nearest neighbor (KNN) algorithms. Examples of use of this approach for multivariate regression are scarce, but the success with which PDERS was applied in classification problems in high-energy physics (Carli & Koblitz, 2003) motivated its use here. Second class are methods based on function discriminant analysis. These methods are widely used for dimensionality reduction and classification. Here, we selected the linear discriminant (LD) algorithm which shares some similarities in the approach with principal component analysis (PCA), in that it maps a space of potentially correlated input variables onto a smaller space of uncorrelated variables, but in addition to PCA it also maximizes the separation between output classes, making it a natural choice for application to our problem. Algorithms that employ higher order functions were also tested, but as could be expected performed more poorly. Application of artificial neural networks (ANN) to multivariate regression problems has seen expansion in recent years, where ANN methods often perform better than more straightforward regression techniques, especially if some degree of nonlinearity is present. Even though the dependence of cosmic ray muon flux on atmospheric temperatures is linear, we felt it is certainly worth investigating how ANN methods would perform when applied to this problem, and if any additional hidden dependence would be revealed. We have chosen to apply the MLP, as it is the fastest and most flexible available ANN algorithm in TMVA. Finally, method of boosted regression trees (BDT) employs a larger number (*forest*) of binary decision trees, which split the phase space of input variables based on a yes/no decision to a series of sequential cuts applied, so to predict a specific value of the output variable. They have been very successfully applied to classification problems in high-energy physics (Lalchand, 2020), but can also be used for multivariate regression with the similar rationale as for the ANN. We have selected two representative algorithms for testing: boosted decision tree (BDT) and gradient boosted decision tree (BDTG).

In this analysis, the procedure is applied to correction of barometric and temperature effect but it is easy to see how it can be extended to include more atmospheric variables, especially as such data is readily available from atmospheric numerical models.

3.1. Training Procedure

For the training/testing data subset we have selected data for the 10 geomagnetically quietest days of each month (list provided by GFZ German Research Center for Geosciences, GFZ Potsdam, 2020), as we expect variations due to meteorological effects to be more pronounced here. This subset was then further split into training and testing data set, where 70% of randomly selected data was used for training while remaining 30% was used for testing. Data time resolution used was 5 min as it gave us a larger statistics for training.

There is a number of settings that can be manipulated for each of the multivariate algorithms used. They vary from some basic parameters, to selection of different subalgorithms or various options that can be turned on or off. For each algorithm, we have selected the optimal set of parameters. The criterium for optimal performance was minimizing the average quadratic deviation of the modeled output versus the target value. Also, where allowed by the algorithm, input variables were decorrelated prior to further processing.

Table 1 shows the values of average quadratic deviation for the modeled output (modeled muon count rate) versus the target value (measured muon count rate) for different algorithms. First two columns refer to the training data subset while second two columns refer to the testing data subset. First and third column represent average quadratic deviation defined as $(\Sigma(f_{MVA} - f_{target})^2)^{1/2}$ (where f_{MVA} and f_{target} represent modeled and measured count rates, respectively), while second and fourth columns represent truncated average quadratic deviation which takes into account 90% of data with least deviation. As previously mentioned, the criterium for selection of optimal parameters for every algorithm is the minimal value of average quadratic deviation for the test data subset.

3.2. Algorithm Performance Analysis

All presented multivariate algorithms have no built in knowledge about the studied effect, so in addition to quantitative test mentioned in the section above, we introduce some qualitative analysis designed to estimate the integrity of modeled data. Prime concern here would be to test whether the suggested procedure

Table 1
Average Quadratic Deviation for Selected Multivariate Methods

Method	Training		Testing	
	Average deviation (counts/5 min)	Truncated deviation (counts/5 min)	Average deviation (counts/5 min)	Truncated average (counts/5 min)
PDERS	234	185	258	201
KNN	224	177	233	185
LD	286	225	284	223
MLP	228	180	234	186
BDT	219	182	237	188
BDTG	223	174	236	187

Abbreviations: BDT, boosted decision tree; BDTG, gradient boosted decision tree; KNN, k-nearest neighbor; LD, linear discriminant.

for the correction of barometric and temperature effect (PT correction) removes these meteorological effects only, while leaving all other features nonperturbed. To this end, we will analyze several distributions of modeled data, compare them with raw and reference PT corrected data (obtained using the integral method) and look for possible anomalous features.

First, we will look into structure of distributions of difference between modeled and measured muon count rate as a function of measured count. We want to make comparison between these distributions in the training phase (for the test data subset) and after the trained algorithm was applied to the full data set. We would expect these distributions to be consistent, and appearance of some new structures or strong trends would point to some perturbation in the application phase. We have selected two examples to illustrate the difference in consistency of application of trained algorithms—BDTG and PDERS, their distributions shown in Figure 1.

We can see that distributions for BDTG algorithm for test data subset (Figure 1a) and full data set (Figure 1b) are fairly similar, and any structures and trends in the test distributions are mostly well replicated in the full data set distributions (different statistics taken into account). This is the case for most applied algorithms except for PDERS, where some dependence of the count rate, negligible for the test data distribution (Figure 1c), exists for the full data set distribution (Figure 1d).

Another, more important feature, is that for some algorithms distributions we analyzed in the previous paragraph are not smooth, but rather display some structures. To get further insight into these structures, for all featured methods we plotted distributions of modeled muon count rate along with the distribution of raw count rate on the same graph, as shown in Figure 2.

In order to better understand shapes of distributions and any structures observed in plots in Figure 2, it would be helpful to compare them to equivalent plots for muon count rates corrected for pressure and temperature effects using a well-established reference method. However, before we take a look at these distributions, we will first briefly describe procedures used to obtain reference PT correction.

Temperature and barometric effect are typically corrected for independently, where one of several methods mentioned in Section 1 is used for temperature correction, and barometric coefficient for pressure correction is determined empirically. Integral method for correction of temperature effect is widely accepted as the most accurate one. It is based on the theory of meteorological effects and takes complete atmospheric temperature profile and relevant processes into account. Most thorough description of the theory of meteorological effects is given by Dorman (2004), where temperature coefficient density function $\alpha(h)$ in Equation 1 is given in its integral form. In order to be applied, this function is then calculated through integration, substituting parameters specific to the location of the experiment. Temperature coefficient density functions for the location of Low Background Laboratory for Nuclear Physics were calculated using Monte Carlo integration technique. In order to determine barometric coefficient, temperature corrected muon data were plotted as a function of atmospheric pressure (using entries for 10 geomagnetically quietest days

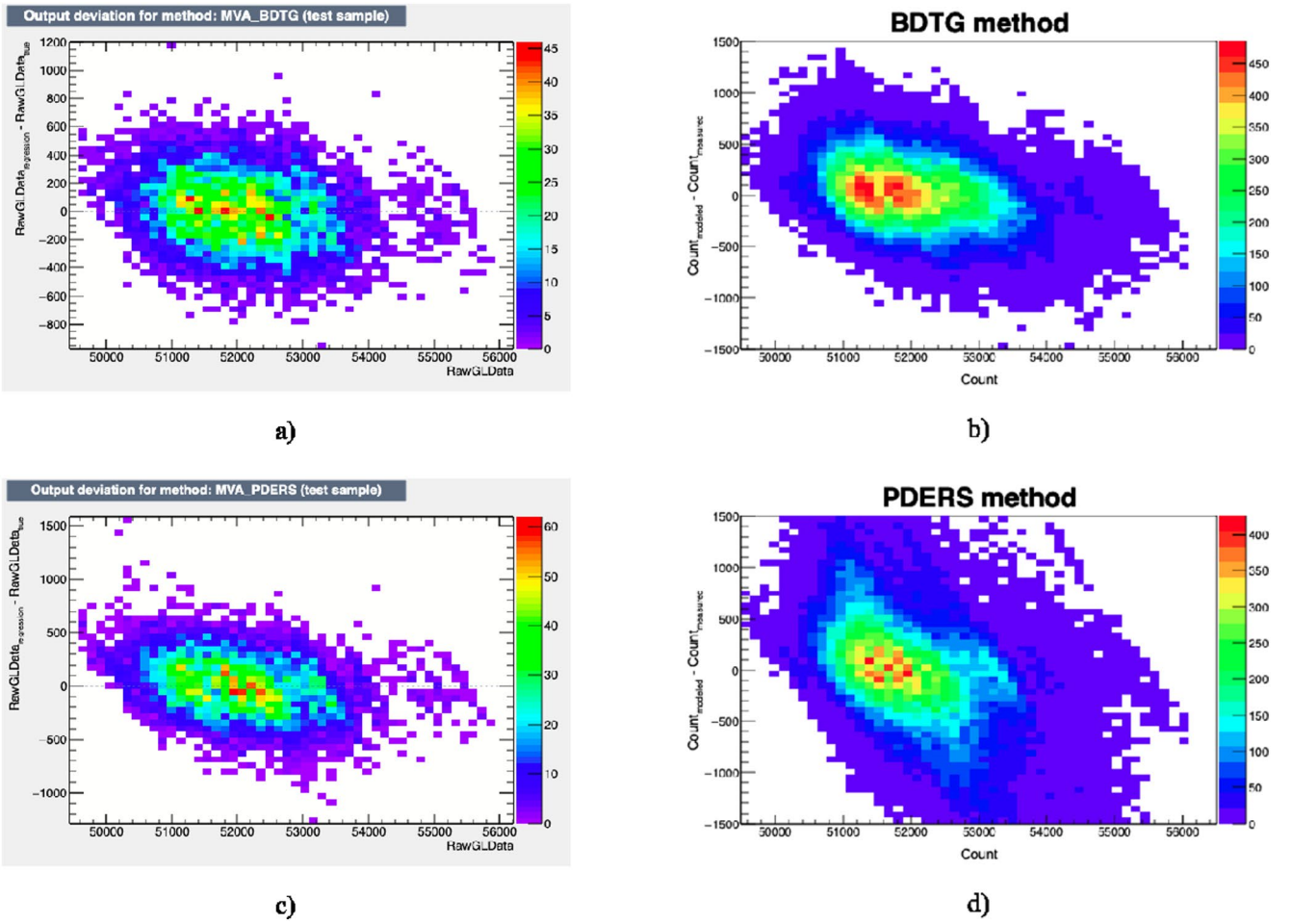

Figure 1. Distribution of difference between modeled (regression) and measured (true) muon count rate as a function of measured muon count rate for: (a) gradient Boosted decision tree (BDTG)—test data set, (b) BDTG—full data set, (c) PDERS—test data set, and (d) PDERS—full data set.

of each month only), coefficient determined via linear regression separately for each calendar year. Both procedures are presented in greater detail in our previous work (Savic et al., 2016).

Distributions equivalent to ones shown in Figures 1 and 2 were plotted for reference pressure and temperature corrected data, as shown in Figure 3. The analog for the modeled muon count rate is calculated from the variation due to pressure and temperature effects calculated based on the integral method. It is worth pointing out that distributions for reference PT corrected data are noticeably less smooth, which can be mostly attributed to lower statistics used as only hour summed data was available for this correction.

Based on these plots, we can conclude that we should not expect a significant deviation between raw and corrected data and that corresponding distributions should not have any characteristic structures. Most plots in Figure 2 are consistent with this expectation, however, some structures can be observed in KNN plots, and to a degree in BDT plots, while distribution plotted for PDERS algorithm does not have these structures but appears to somewhat deviate from raw data distribution.

Another insight into performance and consistency of different multivariate algorithms when applied to the modeling of meteorological parameters can be gathered by the way of spectral analysis of PT corrected data. Pressure and temperature corrected muon count rate was determined for all selected algorithms using modeled data, as described in Section 3. Since some gaps exist in our muon data, Lomb-Scargle algorithm was used to obtain the power spectra, as it is less sensitive to uneven data sampling (Press et al., 2007). Figure 4 shows power spectra for raw and muon count rates corrected for pressure and temperature effects using integral and two illustrative examples of multivariate methods. Full spectrum as well as selected interval

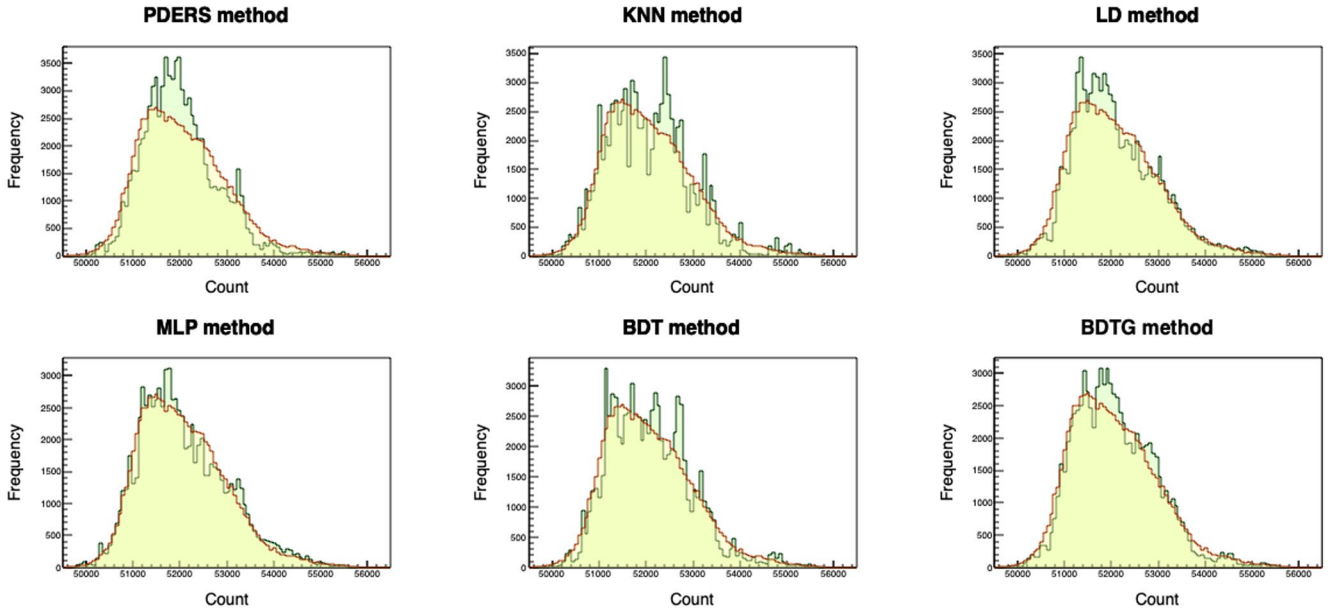

Figure 2. Comparison between distributions of raw (yellow) and muon count rate modeled by selected multivariate methods (green).

of frequencies around the periodicity of one day are shown, red dashed line indicating significance level of 0.01.

If integral method is again used as a reference, we can see that thus obtained PT correction does not remove daily variation, but rather makes it more pronounced. This should not come as a surprise, as only smaller part of the diurnal variation can be attributed to meteorological effects (Quenby & Thambyahpillai, 1960), while larger part is of nonmeteorological origin. Hence, removing variation due to atmospheric pressure would make daily variation more prominent. LD, and to a degree BDT/BDTG methods, have an effect on daily variation similar to the integral method, but for BDT method (bottom right in Figure 4) we observe emergence of some frequencies with significant power that cannot be associated with any known periodicity of cosmic rays, and probably have artificial origin. Such features are even more pronounced for the remaining multivariate algorithms, where in addition an over-reduction of power frequency corresponding to diurnal variation to can be observed. Over-reduction of daily variation coupled with introduction of artificial variations with significant powers points to possible inadequateness or overtraining of some of the multivariate methods.

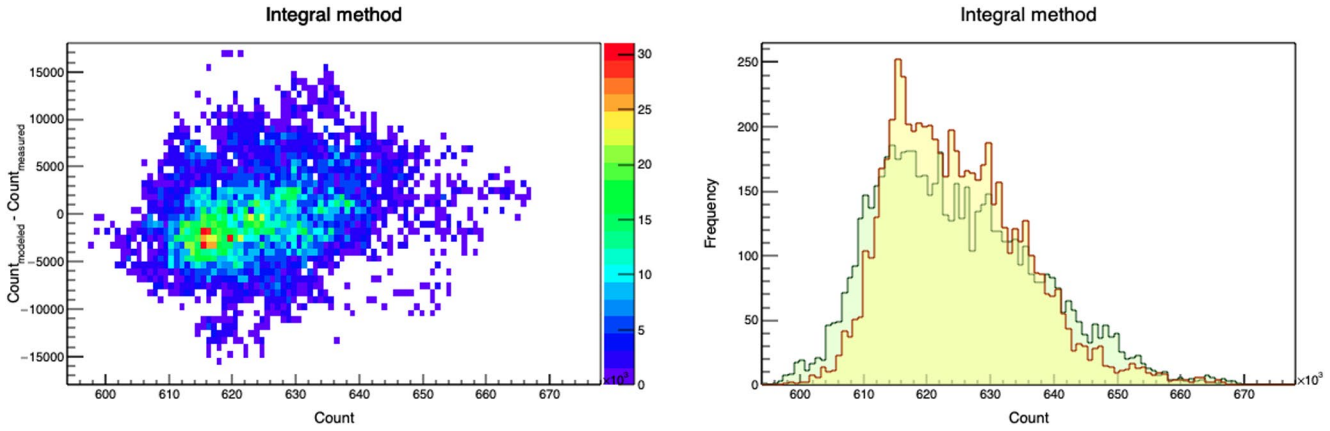

Figure 3. Distribution of difference between muon count rate calculated from the variation due to pressure and temperature effect using integral method and measured muon count rate as a function of measured muon count rate (left), and comparison between distributions of raw (yellow) and calculated muon count rate (green) shown on the right.

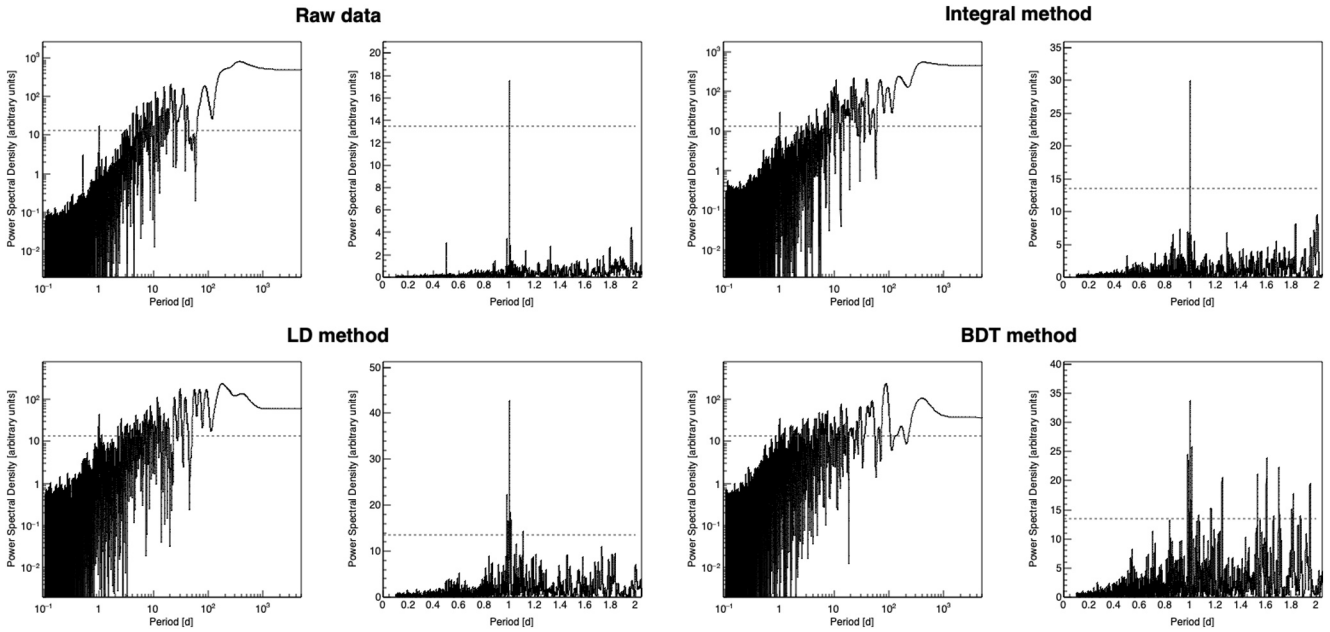

Figure 4. Power spectra for raw data (top left), PT corrected data using integral method (top right), and PT corrected data using selected multivariate methods (second row). For each method, both full spectrum and a range of frequencies around periodicity of one day are shown. Significance level of 0.01 is indicated by the red dashed line.

The effect on annual variation is difficult to determine based on the spectral analysis as period of only one year is analyzed, but we will introduce some quantitative tests in the next section that will help us with this estimate.

4. Results

We will use two criteria to estimate the efficiency of newly introduced methods for PT corrections. One will rely on the effectiveness with which the multivariate algorithms remove the annual variation and reduce variance, while the other will be based on the effect the correction has on detection sensitivity for aperiodic events, such as Forbush decreases (Forbush, 1937). In both cases, we will compare the results with the ones obtained by the integral method.

4.1. Effects of PT Correction on Periodic CR Variations

Significant part of the annual variation of cosmic ray muon flux can be attributed to the variation of atmospheric temperature (Hess, 1940). As mentioned before, the effectiveness with which this effect is corrected for will affect the detector sensitivity to variations of primary cosmic rays of non-atmospheric origin.

We will examine time series for pressure and temperature corrected data and compare them with raw and pressure corrected time series, especially taking note of how PT correction affects the annual variation. In order to estimate this effect, we fit the time series (except for raw data) with sine function with a period of one year. The amplitude of pressure corrected data determined from such fit will be used as an estimate of the annual muon flux variation, and serve as a reference against which to compare the effect of PT correction by different methods. In Figure 5 time series for raw, pressure corrected and pressure and temperature corrected data are shown. For the sake of simplicity, not all time series for data PT corrected using multivariate algorithms are shown, but rather only characteristic ones. Table 2 shows values for the annual variation amplitude for pressure and PT corrected time series, as well as possibly more informative reduction of annual variation calculated relative to the amplitude of the pressure corrected muon flux.

While, time series in Figure 5 for data PT corrected using integral, LD and BDTG methods do not seem to have some unexpected fluctuations, that is not the case for MLP method, where one can observe some

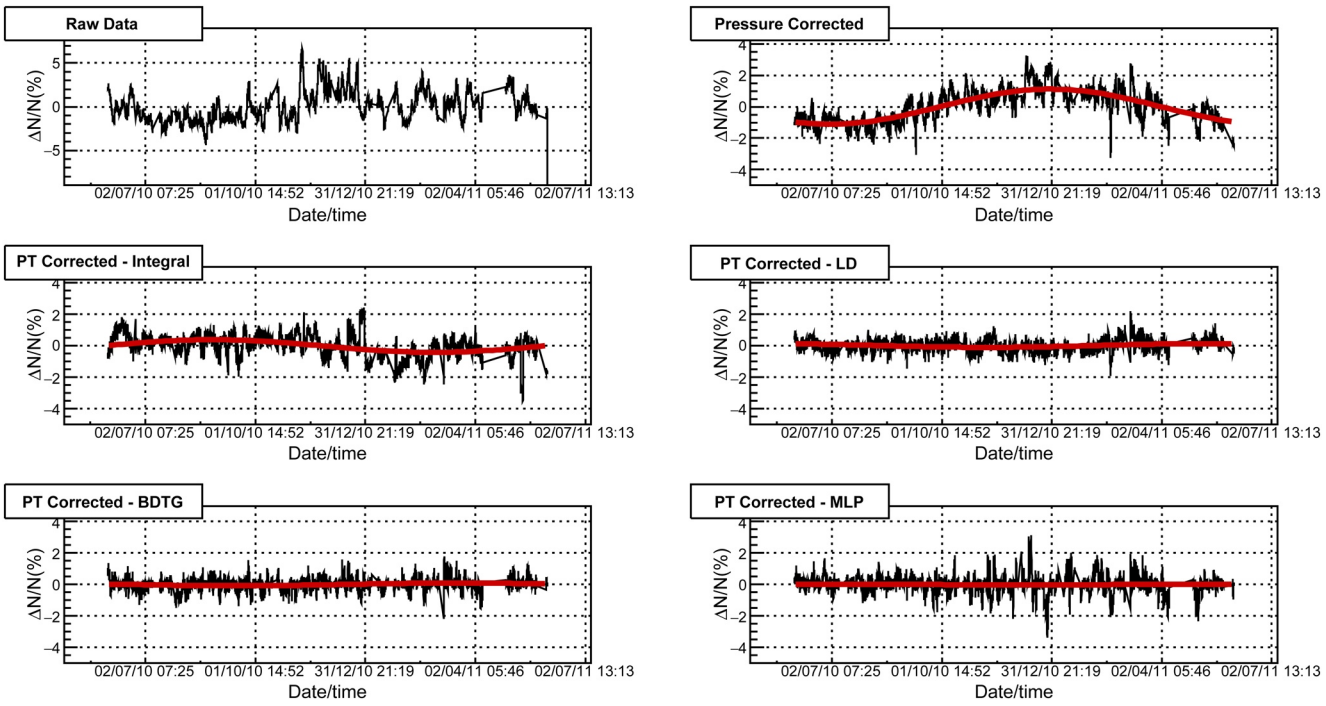

Figure 5. Muon count rate time series for the period from June 1, 2010 to May 31, 2011: raw data (top left), pressure corrected data (top right), PT corrected data using integral method (second row left) and data PT corrected using selected multivariate methods.

data that appears to deviate from the mean more significantly than what would be intuitively expected. For remaining multivariate algorithms this is even more the case. In order to try and quantify this visual comparison, we will analyze the effect corrections have on standard deviation of the data. If calculated relative to the mean muon flux for the whole period, standard deviation would be sensitive to the residual annual variation. To make standard deviation independent of the seasonal variation, we used a moving ten-day window to determine the mean value and then calculated the standard deviation relative to it.

Figure 6 shows distributions of relative variation of muon flux in respect to the moving window mean value for raw data and PT corrected data using integral, LD and MLP methods. It is based on these distributions that standard deviation was determined and results are presented in Table 3. Comparing standard deviations for PT corrected muon flux obtained by multivariate methods with the one obtained by the integral method, we can see that for LD, BDT, and BDTG algorithms they have comparable values. The difference is somewhat larger in the case of MLP, which is in accordance with features observed in Figure 6, while it is significantly larger for the remaining algorithms. This indicates that PT correction performed using KNN and PDERS (and possibly MLP) algorithms probably introduces some artificial features into PT corrected muon flux data.

Table 2
Amplitude and Reduction of the Amplitude of Annual Variation Relative to Pressure Corrected Data (P Corrected) for PT Corrected Data (Using Integral and Selected Multivariate Methods)

Method	Amplitude (%)	Relative reduction (% of P corrected)
P corrected	1.11 ± 0.09	/
Integral	0.40 ± 0.03	64 ± 6
PDERS	0.09 ± 0.02	92 ± 3
KNN	0.24 ± 0.04	79 ± 5
LD	0.11 ± 0.03	90 ± 4
MLP	0.03 ± 0.01	98 ± 2
BDT	0.12 ± 0.03	89 ± 4
BDTG	0.086 ± 0.009	92 ± 2

Abbreviations: BDT, boosted decision tree; BDTG, gradient boosted decision tree; KNN, k-nearest neighbor; LD, linear discriminant.

One way to evaluate the effectiveness of different algorithms in reduction of the seasonal variation even better, would be to compare the PT corrected muon data to pressure corrected time series for selected neutron monitor detectors. The reasoning is based on a well-known fact that meteorological effects on the neutron component of secondary cosmic rays are dominated by the barometric effect. Temperature effect does exist for the secondary cosmic ray neutrons, but whether calculated theoretically (Dorman, 2004) or determined experimentally (Kaminer et al., 1965), it is still an order of magnitude smaller than for the muon component and typically not corrected for in neutron monitor data. Based on this, we

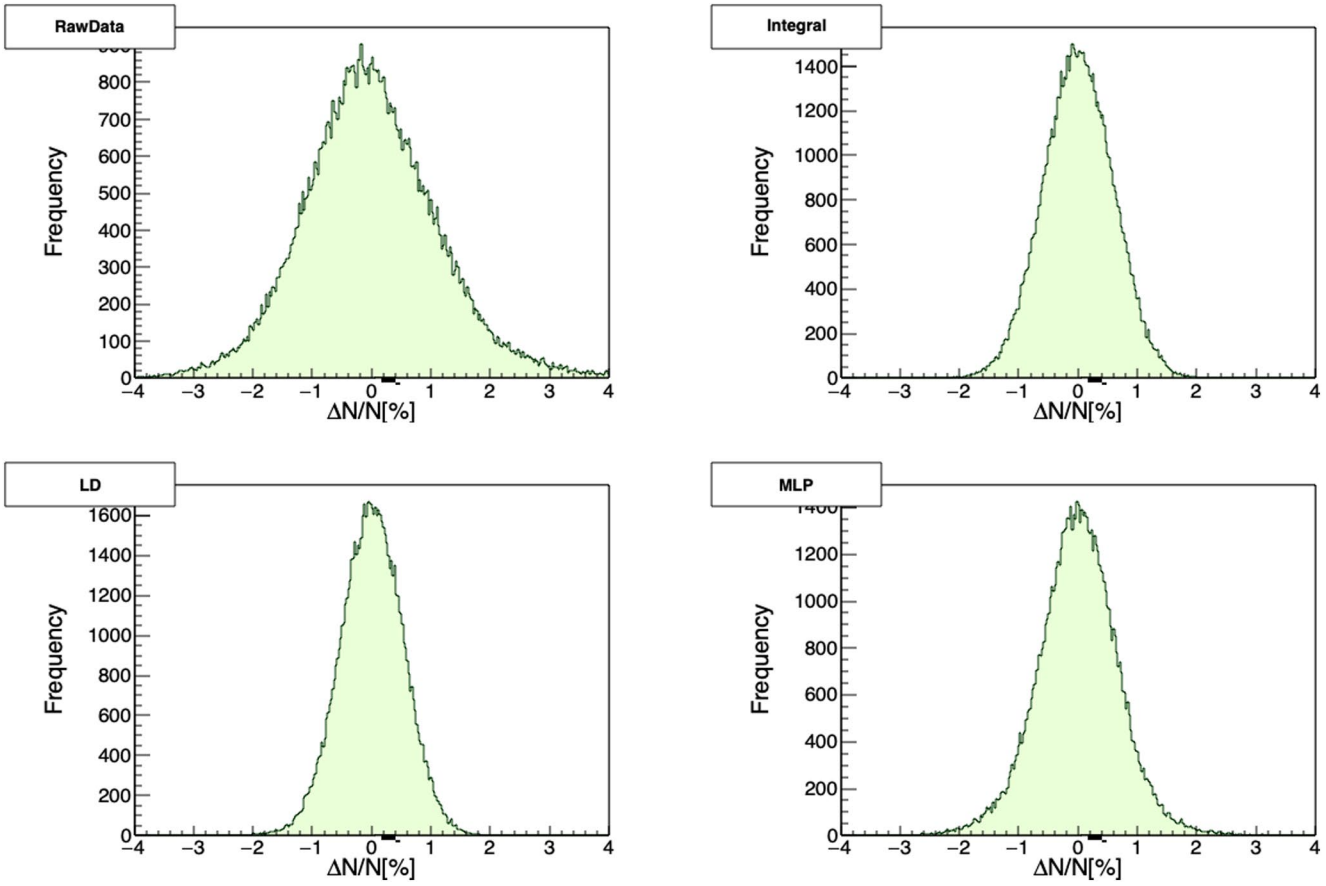

Figure 6. Relative variation of muon count rate calculated in respect to mean count in the ten-day moving window, for raw data (top left), PT corrected using integral method (top right), and data PT corrected using selected multivariate methods (second row).

believe pressure corrected neutron monitor data to be (in the first approximation) independent from meteorological effects, and hence a good reference for the evaluation of effectiveness of different methods for PT corrections of muon flux data.

For this comparison, we have chosen neutron monitors located in Athens and Rome, as they had the most consistent operation in the period we use for the analysis. Respective geomagnetic cutoff rigidities for these neutron monitors are 8.53 and 6.27 GV. Pressure and efficiency corrected relative neutron count rate was acquired via Neutron Monitor Database (NEST, 2020), presented for the said period in Figure 7. As for the muon flux data, relative neutron count rate time series were fitted with sinusoidal function, with a period of one year, to obtain the amplitude used as an estimate of the annual variation. Neutron monitors are more sensitive to lower energy secondaries than muon detectors so their time series can exhibit larger variations, which in turn can affect the fitting algorithm. However, in this case the fits seem to be dominantly affected by the relatively stable period between June and November 2010, hence we believe them to be a reliable estimate of the seasonal variation amplitude. Thus acquired annual variation amplitude for Rome neutron monitor is (0.29 ± 0.01)%, while for the Athens neutron monitor it is (0.17 ± 0.05)%.

Table 3
Standard Deviation of Relative Variation of Muon Count Rate for Raw and Data Corrected for Pressure and Temperature Effect (Using Integral and Selected Multivariate Methods)

Method	Raw	Integral	PDERS	KNN	LD	MLP	BDT	BDTG
Relative deviation (%)	1.117	0.592	0.990	0.785	0.533	0.687	0.607	0.551

Abbreviations: BDT, boosted decision tree; BDTG, gradient boosted decision tree; KNN, k-nearest neighbor; LD, linear discriminant.

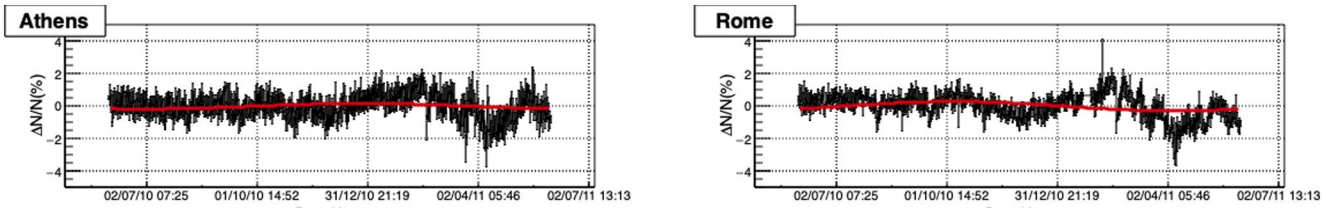

Figure 7. Relative neutron count rate time series for the period from June 1, 2010 to May 31, 2011 for Athens (left) and Rome (right) neutron monitors.

Comparing these values with the ones in Table 2, we see that methods KNN, LD, and BDT yield the most similar results. PDERS and MLP seem to underestimate the annual variation, while the integral method estimates a somewhat larger value.

Observed overall poor performance of KNN and PDERS algorithms could possibly be explained by the fact that these algorithms perform best when applied to problems involving strong nonlinear correlations, and are less efficient when dependencies between variables are dominantly linear (Hoecker et al., 2007). Additionally, these algorithms typically need a large training sample, so possibly statistics in our analysis was inadequate. However, artificial neural networks (such as MLP) should in principle be well suited for multivariate linear regression, and perform better than observed results suggest. Most likely, using minimization of the average quadratic deviation as a sole criterium for the selection of optimal parameters in the training phase may lead to overtraining (Montgomery et al., 2006), and additional qualitative criteria (i.e., ones introduced here) and more careful parameter control should also be used. BDT and BDTG algorithms performed reasonably well even though they are not optimized for treatment of linear multivariate problems, however, spectral analysis indicates a further improvement can be made. Additionally, all algorithms would probably benefit from a longer data interval of several years being used.

4.2. Effects of PT Correction on Aperiodic CR Variations

As mentioned before, apart from increasing sensitivity of muon detectors to periodic variations of primary cosmic rays, correcting raw muon flux data for meteorological parameters also affects detector sensitivity to aperiodic events which occur due to heliospheric modulation of primary cosmic rays. Here, we will analyze the effect PT correction, performed by application of different multivariate algorithms, has on detection of Forbush decrease events. We have chosen to concentrate on Forbush decreases as our muon detector is much less sensitive to other aperiodic events, such as ground level enhancements (GLE).

Forbush decrease (FD) events are typically characterized by their amplitude, so it could be a natural choice for a parameter to be used as a measure of detection sensitivity. However, another requirement for definition of sensitivity could be that detected signal significantly deviates from random fluctuations. That is, why we have decided to use the ratio of the amplitude to the standard deviation of muon flux, or relative amplitude, as an estimate of sensitivity to aperiodic events, rather than the actual amplitude. As we primarily focus on the magnitude of Forbush decreases, when we mention an FD event in the following text it mainly refers to the decrease phase and not the recovery phase.

To determine the amplitude, we have used a method proposed by Barbashina et al. (2009). The idea is to make the result independent from different trends leading up to, and following the actual FD. To do this, two intervals are defined: one i days before the onset of the FD, where i can have value (1,…,n) days, and the other p days after the end of the decrease, where p can have value (1,…,m) days. These intervals are then detrended using fit parameters obtained from linear regression. Mean count is determined for the detrended time series before the onset of FD for j days (where $j = 1,\ldots,i$), and for the detrended time series during recovery stage for q days (where $q = 1,\ldots,p$). Thus, in total we obtain $n!$ values for mean detrended count before the onset of FD, and $m!$ values for mean detrended count for the recovery stage. FD amplitude estimate is then calculated for each combination of "before" and "after" values according to the following formula:

$$A_{ij}^{pq} = \frac{\langle I_{before}^{(i,j)} \rangle - \langle I_{after}^{(p,q)} \rangle}{\langle I_{before}^{(i,j)} \rangle} \times 100\%, \tag{5}$$

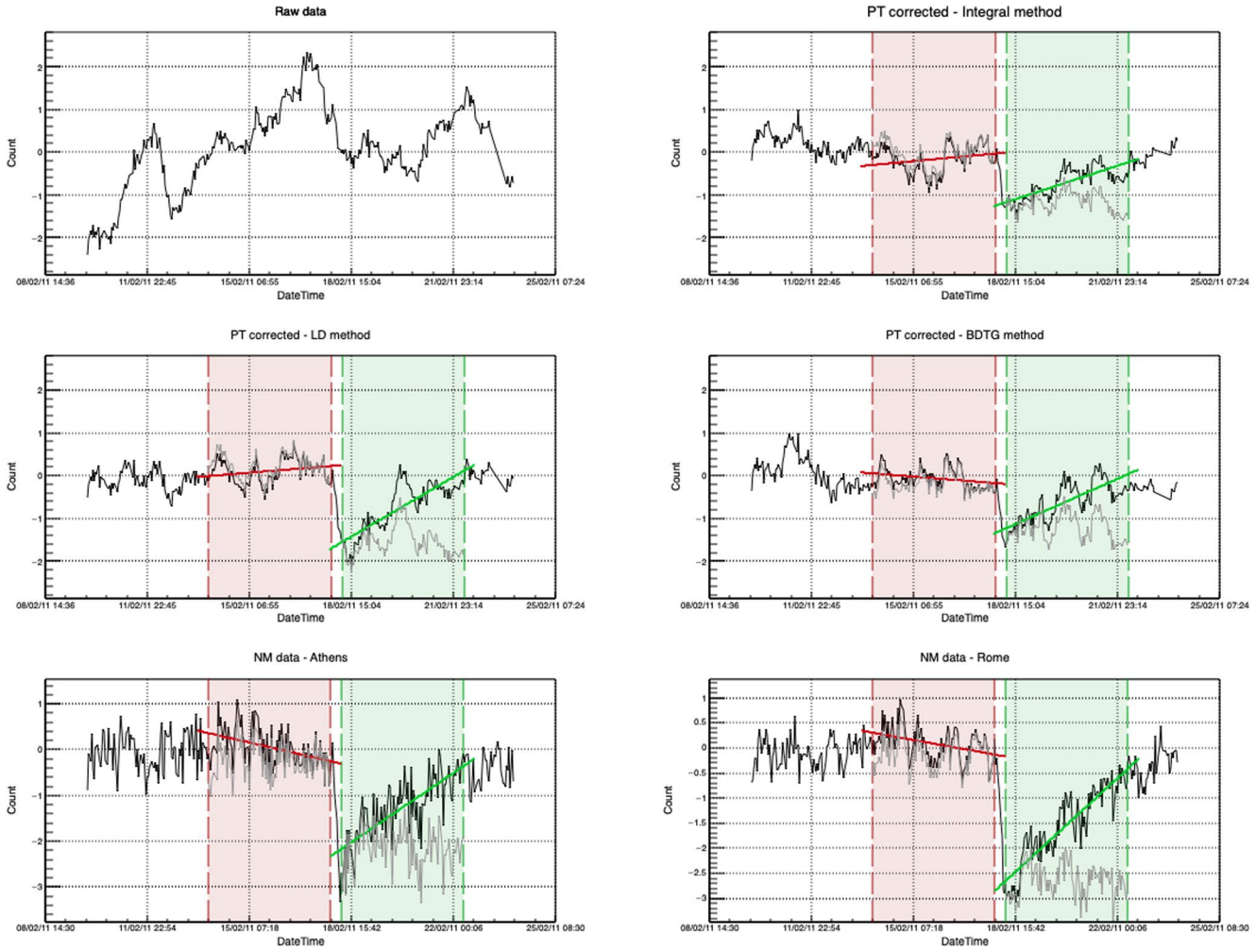

Figure 8. Time series for the interval around Forbush decrease of February 18, 2011: raw muon data (top left), PT corrected muon data using integral (top right), linear discriminant (center left) and gradient boosted decision tree (center right) methods, and neutron monitor data for Athens (bottom left) and Rome (bottom right) neutron monitors. Interval leading into (red) and following the Forbush decrease (FD) (green) are highlighted, as well as detrended intervals used to determine FD amplitude (gray).

where I_{before} and I_{after} are respective values for mean detrended count for intervals before the onset and after the end of the Forbush decrease. Finally, FD amplitude is calculated as the average of individual A_{ij}^{pq} values, rms deviation from the mean of the distribution used as an error estimate.

During the one-year period we used for the analysis there was a large number of Forbush events, but most of them had rather small amplitudes. We have analyzed several, however, here we will focus on the one with the largest magnitude as the results are most easily interpreted. The event is a Forbush decrease that occurred on February 18, 2011 in relation to X2.2 solar flare, and according to IZMIRAN space weather database (IZMIRAN, 2020) had 10 GV rigidity particle variation magnitude of 5.4. In Figure 8, we have shown plots that represent procedure described in the previous paragraph, applied to PT corrected datasets using integral method and selected multivariate algorithms. Procedure is also applied to pressure and efficiency corrected data for Athens and Rome neutron monitors, raw data also presented for reference. On the plots, interval leading to the onset of FD is indicated by red dashed lines, while recovery interval after the decrease is indicated by green dashed lines. We have chosen the lengths of both intervals to be four days ($n = m = 4$). Linear fits are represented by solid red and green lines, respectively, while detrended intervals are plotted using gray lines. Amplitudes and relative amplitudes calculated from the differences of means of detrended intervals are shown in Table 4.

Table 4
Amplitudes and Relative Amplitudes for the Forbush Decrease of February 18, 2011 for PT Corrected Muon Data and Selected Neutron Monitors

Method/NM monitor	Integral	LD	BDTG	Athens	Rome
FD amplitude (%)	1.38 ± 0.14	1.96 ± 0.18	1.10 ± 0.13	1.97 ± 0.15	2.68 ± 0.15
Relative FD amplitude	4.31 ± 0.44	7.09 ± 0.65	4.78 ± 0.56	5.30 ± 0.40	8.65 ± 0.48

Abbreviations: BDTG, gradient boosted decision tree; FD, Forbush decrease; LD, linear discriminant.

We see that relative amplitudes for this Forbush decrease, calculated based on data corrected for pressure and temperature using LD and BDTG algorithms, have sensitivity that is comparable or better than the sensitivity of integral method, even approaching the sensitivity of reference neutron monitors in the case of LD algorithm. However, when LD algorithm is concerned, such result can be at least in part explained by the fact that the calculated absolute FD amplitude is larger than expected for a muon detector. We would expect this value to be comparable to the value calculated based on the integral method. The reason for this discrepancy could be systematic, but also could be somewhat related to features of the studied FD event. Ideally, we should extend this analysis to more events, but selected time period was relatively calm in terms of solar activity, and February 2011 event was the only significant one with magnitude for 10 GV rigidity particles larger than five. Preliminary analysis done on Forbush decrease events of larger magnitude, that are outside the period used for analysis in this work, does show somewhat smaller effect for LD method, so that could be one of the focuses in the continuation of this work. We have excluded plots for the remaining multivariate algorithms as the results were either poorer (in the case of BDT and MLP) or inconsistent (in the case of PDERS and KNN).

5. Conclusions

We have selected a number of multivariate algorithms included in the TMVA package to apply for the correction of barometric and temperature effect on cosmic ray muons. Optimal parameters were determined for each algorithm based on the average quadratic deviation of modeled from measured data. Different distributions of modeled data for training phase and after the application of trained methods were compared to estimate the performance of selected algorithms. Pressure and temperature correction was done and spectral analysis performed to further test the algorithm consistency. The effect of the correction was analyzed for long-term (annual) and short-term (Forbush decrease) cosmic ray variations. In both cases, the efficiency of multivariate algorithms was compared to integral method and pressure corrected neutron monitor data.

Multidimensional probability density estimator algorithms (PDERS and KNN) appear not to be well suited for the modeling of pressure and temperature effect, most likely due to highly linear correlations between variables. MLP seems to have underperformed, while methods based on boosted decision trees (particularly BDTG) proved to be more successful, especially when effect on aperiodic variations was concerned. It should be expected that both MLP and BDT(G) methods can be improved if a longer period is used for analysis and parameters beyond average quadratic deviation of modeled data are used for algorithm optimization during training phase. Out of presented algorithms, LD proved to be the most consistent and effective in removing the pressure and temperature effects. In terms of the effect of PT correction on annual and aperiodic variations, this method matched or outperformed the integral method, while the effect it had on aperiodic effects was somewhat overestimative. This could give us grounds to assume at least part of the temperature effect is not taken into account by the integral method, and that there could be room for further improvement in modeling of meteorological effects beyond what theory currently provides.

Data Availability Statement

Raw muon count rate data set used in this study are publicly available online on the Belgrade Cosmic Ray Station site (http://www.cosmic.ipb.ac.rs/). Modeled atmospheric temperature data are available online on the NOAA GFS page (https://www.ncdc.noaa.gov/data-access/model-data/model-datasets/global-forcast-

system-gfs). Latest atmospheric pressure and ground temperature data are available online on the site of Republic Hydro-meteorological Service of Serbia (http://www.hidmet.gov.rs/). List of international geomagnetically quiet days can be downloaded from the GFZ site (https://www.gfz-potsdam.de/en/kp-index/). Neutron monitor data can be accessed online via NEST browser interface (http://www01.nmdb.eu/nest/).

Acknowledgments
The authors acknowledge funding provided by the Institute of Physics Belgrade, through the grant by the Ministry of Education, Science and Technological Development of the Republic of Serbia.

References

Barbashina, N., Dmitrieva, A., Kompaniets, K., Petrukhin, A., Timashkov, D., Shutenko, V., et al. (2009). Specific features of studying Forbush decreases in the muon flux. *Bulletin of the Russian Academy of Sciences: Physics*, *73*, 343–346. https://doi.org/10.3103/S1062873809030198

Barrett, P. H., Bollinger, L. M., Cocconi, G., Eisenberg, Y., & Greisen, K. (1952). Interpretation of cosmic-ray measurements far underground. *Reviews of Modern Physics*, *24*, 133–178. https://doi.org/10.1103/RevModPhys.24.133

Belov, A., Blokh, Y., Dorman, L., & Rogovaya, S. (1987). The temperature diagnostics of the atmosphere allowing for the temperature of the near-surface layer. *International Cosmic Ray Conference*, *4*, 263.

Berkova, M., Belov, A., Eroshenko, E., & Yanke, V. (2012). Temperature effect of muon component and practical questions of how to take into account in real time. *Astrophysics and Space Sciences Transactions*, *8*, 41–44. https://doi.org/10.5194/astra-8-41-2012

Blackett, P. M. S. (1938). On the instability of the Barytron and the temperature effect of cosmic rays. *Physical Review*, *54*, 973–974. https://doi.org/10.1103/PhysRev.54.973

Carli, T., & Koblitz, B. (2003). A multi-variate discrimination technique based on range-searching. *Nuclear Instruments and Methods in Physics Research Section A: Accelerators, Spectrometers, Detectors and Associated Equipment*, *501*, 576–588. https://doi.org/10.1016/S0168-9002(03)00376-0

Dorman, L. I. (1954). On the temperature effect of the hard component of cosmic rays. *Reports of Academy of Sciences of USSR (DAN SSSR)*, *95*, 49–52.

Dorman, L. I. (2004). *Cosmic rays in the Earth's atmosphere and underground*. Springer. Retrieved from https://books.google.rs/books?id=mKLv68WBu5kC

Dragić, A., Joković, D., Banjanac, R., Udovičić, V., Panić, B., Puzović, J., & Aničin, I. (2008). Measurement of cosmic ray muon flux in the Belgrade ground level and underground laboratories. *Nuclear Instruments and Methods in Physics Research Section A: Accelerators, Spectrometers, Detectors and Associated Equipment*, *591*(3), 470–475.

Dragic, A. L., Udovicic, V. I., Banjanac, R., Jokovic, D. R., Maletic, D. M., Veselinovic, N. B., et al. (2011). The new set-up in the Belgrade low-level and cosmic-ray laboratory. *Nuclear Technology & Radiation Protection*, *26*(3), 181–192. https://doi.org/10.2298/NTRP1103181D

Duperier, A. (1949). The meson intensity at the surface of the Earth and the temperature at the production level. *Proceedings of the Physical Society Section A*, *62*(11), 684–696. https://doi.org/10.1088/0370-1298/62/11/302

Dvornikov, V. M., Krestyannikov, Y. Y., & Sergeev, A. (1976). Determination of the mass-average temperature on the cosmic ray intensity data. *Geomagnetism and Aeronomy*, *16*, 923–925.

Feinberg, E. L. (1946). On the nature of cosmic ray barometric and temperature effects. *Reports of Academy of Sciences of USSR (DAN SSSR)*, *53*, 421–424. https://doi.org/10.1038/157421a0

Forbush, S. E. (1937). On the effects in cosmic-ray intensity observed during the recent magnetic storm. *Physical Review*, *51*, 1108–1109. https://doi.org/10.1103/PhysRev.51.1108.3

Forró, M. (1947). Temperature effect of cosmic radiation at 1000-m water equivalent depth. *Physical Review*, *72*, 868–869. https://doi.org/10.1103/PhysRev.72.868

GFS. (2020). Retrieved from https://www.ncdc.noaa.gov/data-access/model-data/model-datasets/global-forcast-system-gfs

GFZ Potsdam. (2020). Retrieved from https://www.gfz-potsdam.de/en/kp-index/

Hess, V. F. (1940). On the seasonal and the atmospheric temperature effect in cosmic radiation. *Physical Review*, *57*, 781–785. https://doi.org/10.1103/PhysRev.57.781

Hoecker, A., Speckmayer, P., Stelzer, J., Therhaag, J., von Toerne, E., Voss, H., & Zemla, A. (2007). *Tmva—Toolkit for multivariate data analysis*. Ithaca, NY: Cornell University.

IZMIRAN. (2020). Retrieved from http://spaceweather.izmiran.ru/eng/dbs.html

Joković, D. (2011). *Detekcija i spektroskopija miona iz kosmičkog zračenja plastičnim scintilacionim detektorima (Detection and spectroscopy of cosmic ray muons with plastic scintillation detectors) (Doctoral dissertation)*. Faculty of Physics, University of Belgrade. Retrieved from http://www.cosmic.ipb.ac.rs/documents/jokovic-thesis.pdf

Kaminer, N. S., Ilgatch, S. F., & Khadakhanova, T. S. (1965). Temperature effect of the cosmic ray neutron component. In *Proceedings of the 9th International Cosmic Ray Conference* (Vol. 1, p. 486).

Kohno, T., Imai, K., Inue, A., Kodama, M., & Wada, M. (1981). Estimation of the vertical profile of atmospheric temperature from cosmic-ray components. In *Proceedings of the 17th International Cosmic Ray Conference* (Vol. 10, p. 289).

Lalchand, V. (2020). Extracting more from boosted decision trees: A high energy physics case study. In *33rd Annual Conference on Neural Information Processing Systems* (Vol. 1).

Low Background Laboratory for Nuclear Physics. (2020). Retrieved from http://www.cosmic.ipb.ac.rs/

Maeda, K., & Wada, M. (1954). Atmospheric temperature effect upon the cosmic ray intensity at sea level. *Journal of the Scientific Research Institute*, *48*, 71–79.

Montgomery, D. C., Peck, E. A., & Vining, G. G. (2006). *Introduction to linear regression analysis* (4th ed.). Hoboken, NJ: Wiley & Sons.

Morozova, A. L., Blanco, J. J., & Ribeiro, P. (2017). Modes of temperature and pressure variability in midlatitude troposphere and lower stratosphere in relation to cosmic ray variations. *Space Weather*, *15*(5), 673–690. https://doi.org/10.1002/2016SW001582

Myssowsky, L., & Tuwim, L. (1926). Unregelmäßige intensitätsschwankungen der höhenstrahlung in geringer seehöhe. *Zeitschrift für Physik*, *39*, 146–150. https://doi.org/10.1007/BF01321981

NEST. (2020). Retrieved from http://www01.nmdb.eu/nest/

Press, W. H., Teukolsky, S. A., Vetterling, W. T., & Flannery, B. P. (2007). *Numerical recipes 3rd edition: The art of scientific computing* (3rd ed.). New York: Cambridge University Press.

Quenby, J. J., & Thambyahpillai, T. (1960). Atmospheric temperature effects on the solar daily variation of cosmic ray intensity. *The Philosophical Magazine: A Journal of Theoretical Experimental and Applied Physics*, *5*(54), 585–600. https://doi.org/10.1080/14786436008241210

RHMZ. (2020). Retrieved from http://www.hidmet.gov.rs/index-eng.php

Savic, M., Dragic, A., Veselinovic, N., Udovicic, V., Banjanac, R., Jokovic, D., & Maletic, D. (2016). Effect of pressure and temperature corrections on muon flux variability at ground level and underground. In *25th European cosmic ray Symposium*.

Savic, M. R., Dragic, A. L., Maletic, D. M., Veselinovic, N. B., Banjanac, R. M., Jokovic, D. R., & Udovicic, V. I. (2019). A novel method for atmospheric correction of cosmic-ray data based on principal component analysis. *Astroparticle Physics*, *109*, 1–11. https://doi.org/10.1016/j.astropartphys.2019.01.006

Veselinović, N., Dragić, A., Savić, M., Maletić, D., Joković, D., Banjanac, R., & Udovičić, V. (2017). An underground laboratory as a facility for studies of cosmic-ray solar modulation. *Nuclear Instruments and Methods in Physics Research Section A: Accelerators, Spectrometers, Detectors and Associated Equipment*, *875*, 10–15. https://doi.org/10.1016/j.nima.2017.09.008

Wada, M. (1962). Atmospheric effects on the cosmic-ray meson intensity. *Journal of the Physical Society of Japan Supplement*, *17*, 508. https://doi.org/10.1143/jpsj.17.1805

HDZZ CRPA

ZBORNIK PROCEEDINGS

RADOVA OF THE
JEDANAESTOG ELEVENTH
SIMPOZIJA SYMPOSIUM OF
HRVATSKOG THE CROATIAN
DRUŠTVA ZA RADIATION
ZAŠTITU OD PROTECTION
ZRAČENJA ASSOCIATION

Urednici / *Editors*

Vanja Radolić
Marina Poje Sovilj
Ines Krajcar Bronić

Zagreb
2017

AN OVERVIEW OF THE RADON RESEARCH IN THE INSTITUTE OF PHYSICS BELGRADE

Vladimir Udovičić, Dimitrije Maletić, Aleksandar Dragić, Radomir Banjanac, Dejan Joković, Mihailo Savić and Nikola Veselinović
Institute of Physics, University of Belgrade, Belgrade, Serbia
udovicic@ipb.ac.rs

INTRODUCTION

Radon studies in the Institute of Physics Belgrade last a few decades. The first project related to radon was searching for connection between radon variability in soil and water and seismic activity in Montenegro [1]. After that, in the Low-Background Laboratory for Nuclear Physics, Institute of Physics Belgrade, the new research topics of rare nuclear processes was in the scientific focus. There was the need to build up the laboratory space to accomplish this type of research. In the 1997, underground low-background laboratory was built in, with the aim of investigating the rare nuclear processes. In the laboratory of this type, the influence of radon on the natural background radioactivity is dominant and there is an imperative that radon levels must be as low as it possible, with minimal time variation. In that sense, continuous radon monitoring became the mandatory activity. This paper presents the results of many years of radon monitoring in the underground low-background laboratory in the Institute of Physics Belgrade.

Besides radon monitoring in the laboratory, we work on several research topics regarding radon: using multivariate classification and regression methods, as developed for data analysis in high-energy physics and implemented in the TMVA software package, to study connection of climate variables and variations of radon concentrations, modelling of the indoor radon behaviour and radon mapping. All these research activities are presented in this work in more details.

RADON MONITORING IN THE UNDERGROUND LOW-BACKGROUND LABORATORY

The Low-Background Laboratory for Nuclear Physics at the Institute of Physics in Belgrade is a shallow underground laboratory (Figure 1). The laboratory was built in the loamy loess cliff on the bank of the river Danube with the overburden of 12 m of soil. It has an active area of about 60 m^2.

The walls, the floor and the ceiling of the laboratory are built of reinforced concrete of 30 cm thickness. From the measurements of the absolute flux of cosmic-ray muons in the underground as well as in the ground level laboratory [2] it was estimated that the equivalent depth of the laboratory is about 25 m.w.e. (a shielding thickness of the overburden soil expressed as water equivalent thickness). Description of the laboratory is presented in more detail elsewhere [3].

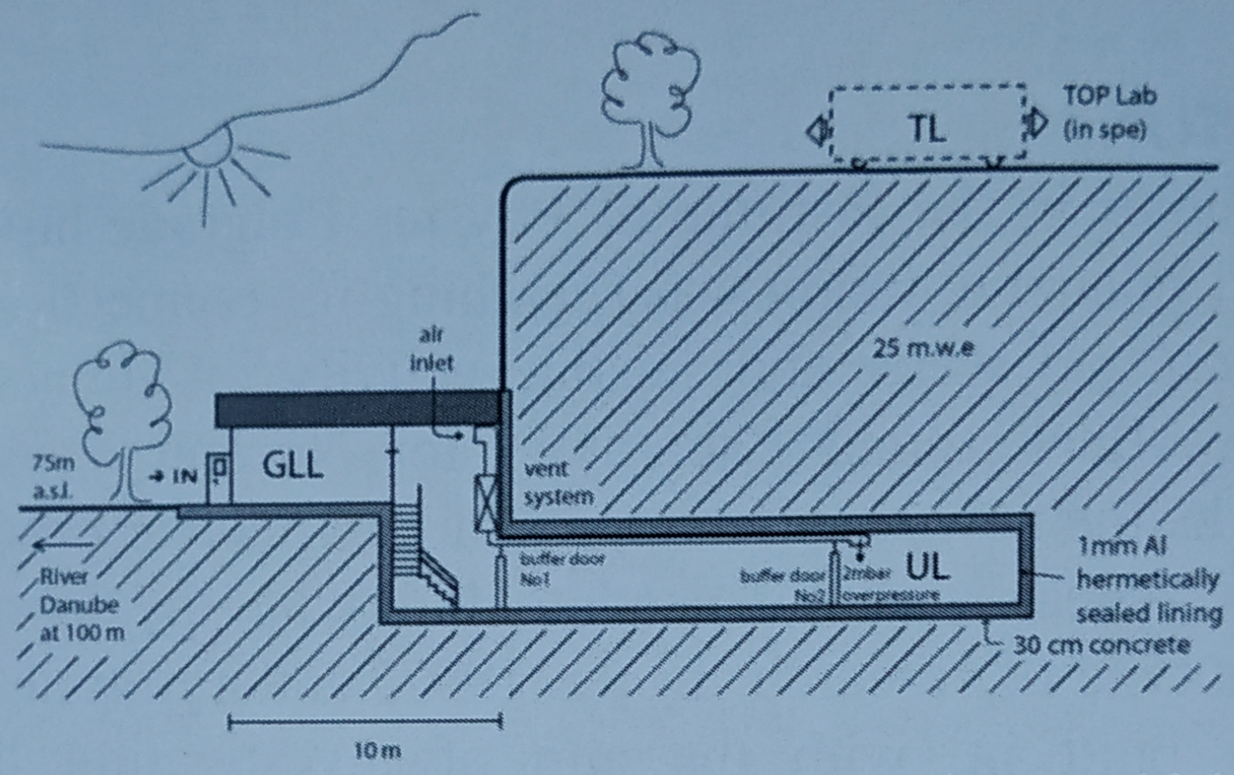

Figure 1. Cross-section of the underground low-background laboratory at the Institute of Physics Belgrade.

The system for the reduction of radon concentration in the laboratory consists of three stages. First, the active area of the laboratory is completely lined up with aluminium foil of 1 mm thickness, which is hermetically sealed with a silicon sealant to minimize the diffusion of radon from surrounding soil and concrete used for construction. The second one is the ventilation system. The laboratory is continuously ventilated with fresh air, filtered through one rough filter for dust elimination followed by the battery of coarse and fine charcoal active filters. The inlet of air is outside of the laboratory, at the height of 2.5 m above the ground. Finally, the parameters of the ventilation system are adjusted so as to result in an overpressure of about 2 mbar over the atmospheric pressure, which further prevents radon diffusion through eventual imperfections in the aluminium layer.

The device for the performed short-term radon measurements is SN1029 radon monitor (manufactured by the Sun Nuclear Corporation, NRSB approval code 31822) with the following characteristics: the measurement range from 1 Bq m^{-3} to 99.99 kBq m^{-3}, accuracy equal to ±25 %, sensitivity of 0.16 counts hour per Bq m^{-3}. With these characteristics, SN1029 radon monitor is defined as a high-sensitivity passive instrument

for the short-term radon measurements and it is an optimal solution for radon monitoring in the underground laboratory.

The radon data from radon monitor device SN1029 for the period of 3 years are spectrally analysed. The Lomb-Scargle periodogram analysis method has been used in spectral analysis of radon time series. The obtained periodogram show two periodicity, on the 1 day and 1 year [4]. Mean radon value is 13.8 Bq m^{-3} with standard deviation of 9.9 Bq m^{-3} over the 3 years of continuos measurements with daily and sesonal variability [5]. It has been shown that the radon behaviour in the underground low-level laboratory in Belgrade has the similar characteristics as in the other underground environment (caves, mines, boreholes and so on), because it has the same source and the places are completely surrounded with the soil.

MVA METHODS AND MODELLING OF THE INDOOR RADON BEHAVIOUR

The demand for detailed analyses of large amount of data in high-energy physics resulted in wide and intense development and usage of multivariate methods. Many of multivariate methods and algorithms for classification and regression are already integrated into the analysis frame work ROOT, more specifically, into the toolkit for multivariate analysis (TMVA). We use these multivariate methods to create, test and apply all available classifiers and regression methods implemented in the TMVA in order to find the method that would be the most appropriate and yield maximum information on the dependence of indoor radon concentrations on the multitude of climate variables. The first step is to calculate and rank the correlation coefficients between all the variables involved, what will help in setting up and testing the framework for running the various multivariate methods contained in the TMVA. Although these correlation rankings will later be superseded by method specific variable rankings, they are useful at the beginning of the analysis. The next step is to use and compare the multivariate methods in order to find out which one is best suited for classification (division) of radon concentrations into what would be considered acceptable and what would be considered increased concentration in indoor spaces. Main aim is to find out which method can, if any, on the basis of input climate variables only, give an output that would satisfactorily close match the observed variations of radon concentrations. Towards this aim, this work were tested in a many specific cases (underground low-background laboratory and other indoor environment) to

comprise the multitude of possible representative situations that occur in real life.

The test of multivariate methods, implemented in the TMVA software package, applied to the analysis of the radon concentration variations connection with climate variables in different indoor spaces demonstrated the potential usefulness of these methods. It appears that the method can be used with sufficient accuracy (around 15 %) for prediction of the radon concentrations. All the obtained results were published in several research articles [6-8].

RADON MAPPING IN SERBIA

In the last three years, we were involved in the establishing national radon action plan (RAP) and performed first national indoor radon survey as a leading institution in the technical support of the project. The responsibility for the establishment and implementation of RAP is on national regulatory body: Serbian Radiation Protection and Nuclear Safety Agency (SRPNA). As a first step in RAP, it was the national indoor radon survey in Serbia performed during 2015-2016. The project was supported by IAEA through the national project: SRB9003 - Enhancing the Regulatory Infrastructure and Legislative System, with two components:

- Expert mission on „National Radon Trial Survey and Raising Awareness of Key Stakeholders„ held in SRPNA, Belgrade, 2 - 4 February 2015.
- Equipment: Leasing of 6000 track-etched indoor radon detectors; the distribution of detectors across the Serbian territory was the responsibility of SRPNA.

Also, during the realization of the national programme for indoor radon measurements, Institute of Physics Belgrade and other research institutions involved in the project together with the SRPNA, performed good communication strategy (first basic information leaflet on radon to accompany the measurement explaining the purpose of the measurement, internet site, public relation, public education...) which led to high survey efficiency (about 90 %), together with very hard field work. In total 6000 detectors have been distributed during October 2015 and exposed in houses and apartments for six months (till April 2016). Afterwards, the detectors were collected and sent to an authorized laboratory (Landauer Nordic AB) to be processed and consequently, we got data for the first national indoor radon survey. The preliminary results and radon map was presented at the 8th Conference of Protection against Radon at Home and at Work, 12 - 14 September 2016, Prague, Czech Republic [9].

Acknowledgements

The authors acknowledge the financial support of the Ministry of Education, Science and Technology Development of Serbia within the projects: 171002 - Nuclear Methods Investigations of Rare Processes and Cosmic Rays and 43002 - Biosensing Technologies and Global System for Continuous Research and Integrated Management.

REFERENCES

[1] Antanasijević R, Milošević I. Correlation between the concentration of 222-Rn at the Earth's surface and in waters with seismic activities. Nucl. Tracks Radiat. Meas. 1990;17:79.

[2] Dragić A, Joković D, Banjanac R, Udovičić V, Panić B, Puzović J, Aničin I. Measurement of cosmic ray muon flux in the Belgrade ground level and underground laboratories. Nucl. Instr. Meth. Phys. Res. 2008;A591:470–475.

[3] Dragić A, Udovičić V, Banjanac R, Joković D, Maletić D, Veselinović N, Savić M, Puzović J, Aničin I. The new set-up in the Belgrade low-level and cosmic-ray laboratory. Nucl. Technol. Radiat. Protect. 2011; 26(3):181–192.

[4] Udovičić V, Aničin I, Joković D, Dragić A, Banjanac R, Grabež B, Veselinović N. Radon time-series analysis in the underground low-level laboratory in Belgrade, Serbia. Radiat. Prot. Dosim. 2011;145:155–158.

[5] Udovičić V, Filipović J, Dragić A, Banjanac R, Joković D, Maletić D, Grabež B, Veselinović N. Daily and seasonal radon variability in the underground low-background laboratory in Belgrade, Serbia. Radiat. Prot. Dosim. 2014;160(1-3):62-64.

[6] Maletić D, Udovičić V, Banjanac R, Joković D, Dragić A, Veselinović N, Filipović J. Comparison of multivariate classification and regression methods for the indoor radon measurements. Nucl. Technol. Radiat. Prot. 2014; 29(1): 17–23.

[7] Maletić D, Udovičić V, Banjanac R, Joković D, Dragić A, Veselinović N, Filipović J. Correlative and multivariate analysis of increased radon concentration in underground laboratory. Radiat. Prot. Dosim. 2014;162:148-151.

[8] Filipović J, Maletić D, Udovičić V, Banjanac R, Joković D, Savić M, Veselinović N. The use of multivariate analysis of the radon variability in the underground laboratory and indoor environment. Nukleonika 2016; 61(3):357-360.

[9] Udovičić V, Maletić D, Eremić Savković M, Pantelić G, Ujić P, Čeliković I, Forkapić S, Nikezić D, Marković V, Arsić V, Ilić J, Nilsson P. Preliminary results of the first national indoor radon survey in Serbia. In: Book of Abstracts of 8th Conference of Protection against Radon at Home and at Work, September 12-14, 2016; Prague, Czech Republic.

AN OVERVIEW OF THE RADON RESEARCH IN THE INSTITUTE OF PHYSICS BELGRADE

Vladimir Udovičić, Dimitrije Maletić, Aleksandar Dragić, Radomir Banjanac, Dejan Joković, Mihailo Savić and Nikola Veselinović
Institute of Physics, University of Belgrade, Belgrade, Serbia
udovicic@ipb.ac.rs

Institute of Physics Belgrade has a long tradition in the radon research. In the 1997, underground low-background laboratory was built in, with the aim of investigating the rare nuclear processes. The experiments and routine measurements in the underground low-background laboratory require low levels of radon concentration with minimum temporal variations. From the beginning, continuous monitoring of radon concentration is being carried out. Radon monitoring in the underground laboratory is done with the passive and active devices. Besides radon monitoring in the laboratory, we work on several research topics regarding radon: using multivariate classification and regression methods, as developed for data analysis in high-energy physics and implemented in the TMVA software package, to study connection of climate variables and variations of radon concentrations, modelling of the indoor radon behaviour and radon mapping. In the last three years, we were involved in the establishing national radon action plan and performed first national indoor radon survey as a leading institution in the technical support of the project. In this work, all these radon activities are described in details.

TEERAS 2017

III EAST EUROPEAN RADON SYMPOSIUM

15 - 19 MAY
PARK HOTEL MOSKVA
SOFIA

Book of Abstracts

P2

Correlative, multivariate and periodicity analysis of the variations of low radon concentrations in an shallow underground laboratory

Dimitrije Maletic1, Vladimir Udovicic1, Radomir Banjanac1, Dejan Jokovic1, Mihailo Savic1, Nikola Veselinovic1, Jelena Zivanovic1, Aleksandar Dragic1*
Institute of Physics, University of Belgrade

The results of correlative, multivariate and periodicity analysis of the variation of low radon concentrations in shallow underground laboratory, in the Institute of Physics Belgrade, is presented and discussed. Correlative and periodicity analysis results show possible connection of environmental variables with radon concentration. Multivariate classification and regression methods are used to study the connection of climate variables and the variation of radon concentrations. Resulting 'mapped' functional behaviour of radon concentrations on input variables can be used as a good tool for further study of radon concentration connection with independent variables or group of strongly correlated variables. The result presented in this paper suggest the usefulness of multivariate method analysis as a helping tool for prediction of radon concentrations and a tool for checking the model of radon concentration in shallow underground laboratory and underground spaces with ventilation.

P3

Development of protocol for radon measurements in multi-storey buildings in Russia

Aleksey Vasilyev, Georgy Malinovsky, Alexandra Onishchenko*
Institute of Industrial Ecology, Ekaterinburg, Russia

Radon is one of the most important indoor pollutant, which is the second cause of lung cancer next to smoking. To investigate the relationship between radon and lung cancer it is necessary to assess indoor radon concentration. Multi-storey block buildings represent the main type of dwellings in urban cities of Russia. Despite the existing radon measurements protocols being reasonable for single-family houses, short-term measurements in multi-storey buildings are still an open question (number of measurements, number of floors to study, etc.) Radon concentrations on different floors in multi-storey building are unpredictable even if we know the radon entry and dilution rates.Main physical quantities, affecting indoor radon concentrations in multi-storey energy-efficient buildings in Ekaterinburg, Russia, were studied and related multi-cham-

The Henryk Niewodniczanski
Institute of Nuclear Physics
Polish Academy of Sciences
Radzikowskiego 152, 31-342 Kraków, Poland
www.ifj.edu.pl/badania/publikacje
Kraków, May 2019

BOOK of ABSTRACTS
3rd International Conference
"Radon in the Environment 2019"
27-31 May 2019, Kraków, Poland

A29

RADON VARIABILITY DUE TO FLOOR LEVEL IN THE TWO TYPICAL RESIDENTIAL BUILDINGS IN SERBIA

Vladimir Udovičić [1], Nikola Veselinovic[1], Dimitrije Maletic[1], Radomir Banjanac[1], Aleksandar Dragic[1], Dejan Jokovic[1], Mihailo Savic[1], David Knezevic[1], Maja Eremic Savkovic[2]

[1] *Institute of Physics Belgrade, University of Belgrade, Belgrade, Serbia*

[2] *Serbian Radiation and Nuclear Safety and Security Directorate, Belgrade, Serbia*

E-mail: udovicic@ipb.ac.rs

It is well known that one of the factors that influences the indoor radon variability is the floor level of the buildings. Considering the fact that the main source of indoor radon is radon in soil gas, it is expected that the radon concentration decreases at higher floors. Thus, at higher floors the dominant source of radon is originating from building materials and in some cases there may be deviations from the generally established regularity. On the other hand, the radon variability due to floor level, especially in big cities with a much higher number of high-rise buildings and population density compared with rural environments, may have an impact on the assessments of collective dose from radon.

According to the national typology [1], there are six types of residential buildings in Serbia; two for family housing: Freestanding single-family house and single-family house in a row, and four for multi-family housing: Freestanding residential building, residential building - lamela (apartment block with repeated multiple – lamellar – cores and separate entrances), residential building in a row and high-rise residential building. Distribution of buildings by type at national level shows that 97.23% of all residential buildings are family housing. Also, for all defined types of buildings number of floors ranges from one to eight above the ground level. Freestanding family houses are mostly ground floor (37%) or ground floor with loft in use (26%), while there is a very low representation of houses that have more than two floors (5%), with average height of family buildings of 1.4. In that sense, we chose one freestanding single-family house with loft with well-known radon characteristics [2] and one sixteenth floor high-rise residential building for this study.

The indoor radon measurements are performed with two active devices. One was fixed in the living room at the ground level and the second one was moved through the floors of the residential building. Every measuring cycle at the specified floor lasted seven days with the sampling time of the two hours. In this work, the analysis of the obtained results is shown in details.

Ref.

[1] Jovanović Popović M., Ignjatović D., Radivojević A., Rajčić A., Ćuković Ignjatović N., Đukanović Lj. & Nedić M. (2013), National Typology of Residential Buildings in Serbia, Faculty of Architecture University of Belgrade, Belgrade (2013), ISBN 978-86-7924-102-3.

[2] Udovičić V., Maletić D., Banjanac R., Joković D., Dragić A., Veselinović N., Živanović J., Savić M., Forkapić S. Multiyear Indoor Radon Variability in a Family House – a Case Study in Serbia, Nuclear Technology and Radiation Protection Vol. XXXIII, No. 2 (2018), pp. 174-179.

ДРУШТВО ЗА ЗАШТИТУ ОД ЗРАЧЕЊА
СРБИЈЕ И ЦРНЕ ГОРЕ

ЗБОРНИК РАДОВА

XXIX СИМПОЗИЈУМ ДЗЗСЦГ
Сребрно језеро
27- 29. септембар 2017. године

Београд
2017. године

STUDIJA SLUČAJA SEZONSKE VARIJACIJE KONCENTRACIJE RADONA U PORODIČNOJ KUĆI U SRBIJI

Vladimir UDOVIČIĆ[1], Dimitrije MALETIĆ[1], Aleksandar DRAGIĆ[1], Radomir BANJANAC[1], Dejan JOKOVIĆ[1] i Sofija FORKAPIĆ[2]

1) Univerzitet u Beogradu, Institut za fiziku u Beogradu, Beograd, Srbija, udovicic@ipb.ac.rs

2) Univerzitet u Novom Sadu, PMF Novi Sad, Novi Sad, Srbija, sofija@df.uns.ac.rs

SADRŽAJ

Usled uticaja velikog broja parametara, ponašanje radona u zatvorenim prostorijama ima složenu dinamiku. Na osnovu merenja koncentracije radona, izdvajaju se dve periodičnosti, dnevna i sezonska. U ovom radu su prikazani rezultati merenja koncentracije radona u jednoj tipičnoj porodičnoj kući u Srbiji, u toku tri sukcesivne godine u februaru i julu svake godine. Korišćene su sledeće tehnike merenja radona: aktivna i metoda ugljenih kanistara. Takođe su prikazani rezultati ovih interkomparativnih merenja.

1. UVOD

Istraživanje dinamike radona i primena mera za njegovo smanjenje u različitim sredinama, naročito u zatvorenim prostorijama, ima veliki značaj u smislu zaštite od jonizujućih zračenja. Objavljeni rezultati i razvoj mnogih modela kojima se opisuje ponašanje radona ukazuju na složenost ovog istraživanja, posebno sa modelima za predviđanje varijabilnosti radona [1-3]. To je zato što varijabilnost radona zavisi od velikog broja faktora kao što su geologija, propustljivost zemljišta, građevinski materijali koji se koriste za izgradnju kuća i zgrada, stanje unutrašnje atmosfere (temperatura, pritisak i relativna vlažnost), koncentracija aerosola, brzina razmene između unutrašnjeg i spoljašnjeg vazduha, kao i životnih navika ljudi. Poznato je da varijabilnost koncentracije radona ima dve glavne periodičnosti i to od jednog dana i jedne godine. Takođe je poznato da postoji sezonska varijacija koncentracije radona. To je razlog zašto je posebno zanimljivo istražiti varijaciju radona na istom mernom mestu, iz godine u godinu, zbog procene individualne godišnje doze od izlaganja radonu. U tom smislu, pratili smo dugoročne varijacije koncentracije radona u jednoj tipičnoj porodičnoj kući u Srbiji. Merenja su obavljena tokom 2014., 2015. i 2016. godine, u februaru i julu, svake godine. Koristili smo sledeće merne tehnike: aktivna i metoda korišćenja ugljenih kanistara. Detaljna analiza dobijenih rezultata je prikazana u ovom radu.

2. METODE MERENJA RADONA

Vremenske serije merenih koncentracija radona, temperature i relativne vlažnosti u ispitivanoj kući dobijene su pomoću uređaja SN1029 (proizvođača Sun Nuclear Corporation). To je merni uređaj jednostavne konstrukcije i primene u praksi. U suštini, radi se o brojaču sa dodatkom senzora za merenje meteoroloških parametara. Nedostatak uređaja je nemogućnost merenja koncentracije radona u zemljištu i vodi. Operater može podesiti vremenske sekvence od 0,5 sati do 24 sati. Jedan ciklus merenja može trajati 1000 sati ili ukupno 720 vremenskih sekvenci (broj sukcesivnih merenja, odnosno tačaka u vremenskoj seriji). Uređaj je bio podešen da radi u vremenskoj sekvenci od 2 sata.

Simultano su mereni temperatura, vazdušni pritisak i vlažnost. U saradnji sa kolegama iz Laboratorije za ispitivanje radioaktivnosti uzoraka i doze jonizujućeg i nejonizujućeg zračenja, PMF, Novi Sad urađena su interkomparativna merenja, korišćenjem standardne skrining metode za merenje koncentracije radona pomoću adsorpcije na aktivnom uglju prema US EPA protokolu 520/5-87-005 [4], tokom februara 2014., 2015. i 2016. godine. Porodična kuća izabrana za merenja i analize varijacije radona je tipična kuća u Beogradu (slika 1).

Slika 1. Porodična kuća u kojoj su vršena merenja

Karakterističan je stil gradnje u kome se kuća gradi više godina uz konstantno dograđivanje i nadogradnju, što potencijalno može biti izvor ulaska radona u takve kuće. Kuća ima podrum i izgrađena je od standardnih materijala (cigla-blok, beton, malter). Na kraju je urađena i izolacija korišćenjem stiropora debljine 5 cm. Merenja radona su izvršena u dnevnoj sobi porodične kuće. Tokom perioda merenja (zima-leto 2014, 2015. i 2016), kuća je prirodno ventilirana i korišćen je klima uređaj u oba režima, grejanja i hlađenja. Tokom zimskog perioda merenja pored klima uređaja, korišćena je termoakumulaciona peć i uljani radijatori. Izmerene koncentracije radona, sobna temperatura (T) i relativna vlažnost unutar kuće su dobijeni korišćenjem radon monitora.

3. REZULTATI

Merenja su obavljena tokom februara i jula 2014., 2015. i 2016. koristeći radon monitor i metode pomoću adsorpcije na aktivnom uglju. Rezultati su prikazani u tabeli 1. Uočena je izrazita sezonska varijacija radona, pri čemu je koncentracija radona u zimskom periodu za red veličine veća nego u letnjem periodu. Rezultati merenja radona pomoću dve različite metode su u dobroj saglasnosti.

Tabela 1. Rezultati merenja radona, temperature i vlažnosti vazduha tokom februara i jula 2014., 2015. i 2016.

	2014.		2015.		2016.	
	Februar	**Juli**	**Februar**	**Juli**	**Februar**	**Juli**
Minimum [Bqm^{-3}]	15	0	28	0	12	3
Maximum [Bqm^{-3}]	1000	286	915	88	1013	262
Mediana [Bqm^{-3}]	418	25	524	22	412	28
AM(SD) [Bqm^{-3}]	402(216)	40(41)	508(207)	27(18)	423(214)	39(32)
Temperatura [^oC]	20,4(0,8)	24,7(0,9)	21,2(0,6)	24,9(0,8)	22,3(0,6)	24,6(0,8)
Vlažnost [%]	67,4(5,7)	67,8(4,8)	68,2(4,8)	51,5(4,7)	64,0(6,4)	58,9(7,5)
Ugljeni kanister [Bqm^{-3}]	432(10)	/	518(6)	/	407(5)	/

4. ZAKLJUČAK

U ovom radu, praćena je varijabilnost radona u dnevnoj sobi jedne porodične kuće u Beogradu tokom dva izabrana meseca u godini (februar i juli), i to tri godine za redom, 2014., 2015. i 2016. Rezultati pokazuju izrazitu sezonsku varijaciju, s tim što nivoi radona za iste mesece u godini pokazuju relativnu reproducibilnost. Male varijacije su uslovljene, pre svega varijacijama meteo parametara. Takođe, interkomparativna merenja radona dvema različitim metodama pokazuju dobru saglasnost.

5. ZAHVALNICA

Ovaj rad je realizovan uz podršku Ministarstva prosvete, nauke i tehnološkog razvoja Republike Srbije u okviru projekta pod brojem III43002.

6. LITERATURA

[1] D. Maletić, V. Udovičić, R. Banjanac, D. Joković, A. Dragić, N. Veselinović, J. Filipović. Comparison of multivariate classification and regression methods for indoor radon measurements. *Nuclear Technology and Radiation Protection* 29, 2014, 17-23.

[2] D. Maletić, V. Udovičić, R. Banjanac, D. Joković, A. Dragić, N. Veselinović, J. Filipović. Correlative and multivariate analysis of increased radon concentration in underground laboratory. *Radiation Protection Dosimetry* 162 (1-2), 2014, 148-151.

[3] J. Filipović, D. Maletić, V. Udovičić, R. Banjanac, D. Joković, M. Savić, N. Veselinović. The use of multivariate analysis of the radon variability in the underground laboratory and indoor environment. *Nukleonika* 61(3), 2016, 357-360.

[4] EPA 520/5-87-005, Gray D.J, Windham S.T, United States Environmental Protection Agency, Montgomery, 1987.

CASE STUDY OF THE INDOOR RADON SEASONAL VARIABILITY IN THE FAMILY HOUSE IN SERBIA

Vladimir UDOVIČIĆ[1], Dimitrije MALETIĆ[1], Aleksandar DRAGIĆ[1], Radomir BANJANAC[1], Dejan JOKOVIĆ[1] i Sofija FORKAPIĆ[2]

1) University of Belgrade, Institute of Physics Belgrade, Belgrade, Serbia, udovicic@ipb.ac.rs

2) University of Novi Sad, PMF Novi Sad, Novi Sad, Serbia, sofija@df.uns.ac.rs

ABSTRACT

Due to the impact of a large number of parameters, the behavior of radon indoors has complex dynamics. Radon time-series analysis, based on the short-term indoor radon measurements performed worldwide, shows two main periodicity: daily and seasonal. This paper presents the results of the indoor radon measurements in a typical family house in Serbia, during three successive years in February and July each year. The following techniques were used for radon measurements: active and charcoal canister methods. It also presents the results of these intercomparison measurements.

KORIŠĆENJE MULTIVARIJANTNE ANALIZE ZA PREDVIĐANJE GEOGENOG RADONSKOG POTENCIJALA

Sofija FORKAPIĆ[1], Dimitrije MALETIĆ[2], Jovica VASIN[3], Kristina BIKIT[1], Dušan MRĐA[1], Ištvan BIKIT[1], Vladimir UDOVIČIĆ[2], Radomir BANJANAC[2]

1) Univerzitet u Novom Sadu, Prirodno-matematički fakultet, Novi Sad, Srbija, sofija@df.uns.ac.rs

2) Univerzitet u Beograd, Institut za fiziku, Beograd, Srbija, maletic@ipb.ac.rs

3) Univerzitet u Novom Sadu, Institut za ratarstvo i povrtarstvo, Novi Sad, Srbija, jovica.vasin@ifvcns.ns.ac.rs

SADRŽAJ

Geogeni radonski potencijal koji izdvaja radon u podzemnim slojevima kao dominantan uzrok akumulacije radona u zatvorenim prostorijama i koji je nezavisan od ljudskog uticaja i vremenski konstantan u geološkim okvirima predstavlja glavni alat za iznalaženje radonom ugroženih područja. U nedostatku podataka za permeabilnost zemljišta za radon i malog broja merenja radona u zemljištu, upotrebljena je multivarijantna analiza velikog broja raspoloživih geohemijskih podataka, merenja radioaktivnosti zemljišta i koncentracija aktivnosti radona u zatvorenim prostorijama datih lokacija na području Vojvodine. Nekoliko uporedivih metoda iz ROOT okvira za analize softverskog paketa TMVA je korišćeno za analizu zavisnosti koncentracije radona u zatvorenom od mnoštva ulaznih varijabli. BDTG kao najpodobnija metoda je pokazala da su varijable sa najvećim uticajem na koncentraciju radona u zatvorenim prostorijama pored sadržaja ukupnog azota, koncentracije aktivnosti radionuklida u zemljištu na profilu dubine od 30 cm i sadržaj humusa i gline. Dobijeni rezultati pokazuju dobro slaganje sa nedavnim ispitivanjem emanacije radona iz zemljišta na području grada Novog Sada.

1. UVOD

Poznato je da radon i njegovi kratkoživeći potomci daju najveći doprinos efektivnoj dozi koju stanovništvo primi od jonizujućuh zračenja [1]. Nedavna epidemiološka istraživanja pokazala su da rizik od radona postoji i pri koncentracijama za koje se ranije smatralo da su zanemarive. U svim evropskim zemljama se sprovode mapiranja radona, a rezultati se sumiraju u publikaciji zajedničkog istraživačkog centra Europske komisije (JRC EC) koji koordinira projekt izrade evropskog atlasa prirodne radioaktivnosti. Naime, sve države članice EU (uključujući i zemlje kandidate za članstvo) prema direktivi EU [2] moraju propisati referentne nivoe radona u boravišnim i radnim prostorijama i identifikovati područja sa visokim radonskim potencijalom. Postoje dva koncepta u definiciji radonskog potencijala: prema broju objekata sa koncentracijama radona iznad referentnog nivoa – indoor radon potential IRP i prema lokalnim geofizičkim parametrima kao što su koncentracija radona u zemljištu i permeabilnost zemljišta (geogeni radonski potencijal GRP). Na koncentraciju radona u boravišnim i radnim prostorijama utiče mnogo faktora koji se mogu podeliti na privremene koji zavise od antropogenog uticaja ili trenutnih uslova (kao što su životne navike, način gradnje, građevinski materijal, meteorološi uslovi) i trajne koje zavise od geofizičkih parametara (kao što su raspored stena u tlu, sadržaj uranijuma i radijuma u zemljištu i stenama, permeabilnost zemljišta za radon, granulacija i hemijske

karakteristike zemljišta). Radon dominanto potiče od povišene koncentracije radijuma i uranijuma u stenama koje se nalaze duboko ispod tla i zbog toga što je radon inertan gas lako napušta mesto formiranja i difunduje kroz debele slojeve zemljišta usled gradijenta u koncentraciji i pritisku.

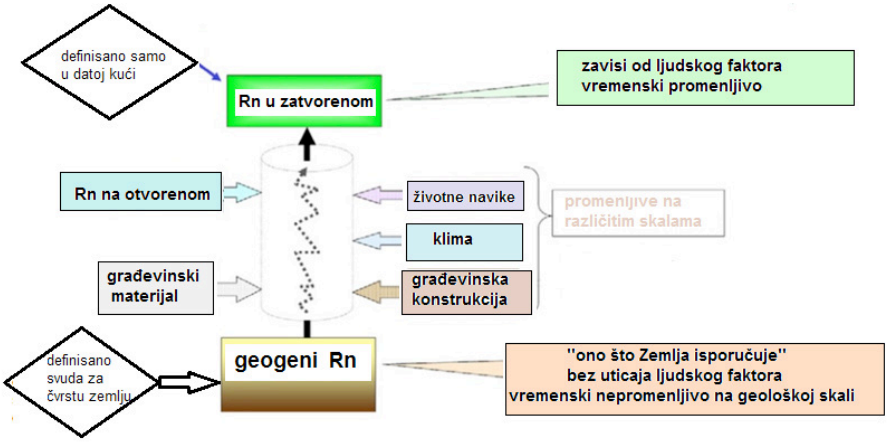

Slika 1. Kompleksni uticaji na radon u zatvorenim prostorijama i geogeni radonski potencijal [4]

Geogeni radonski potencijal (GRP) određenog područja se može odrediti na osnovu koncentracije radona u zemljištu i permeabilnosti zemljišta na osnovu sledeće empirijske formule [5]:

$$GRP = \frac{C}{-log_{10}k - 10} \quad (1)$$

gde je C koncentracija radona [Bq/m^3] u zemljištu i k permeabilnost zemljišta [m^2].Ovako određeni geogeni radonski potencijal se upoređuje sa kartama geomorfoloških jedinica datog područja, kartama koncentracije uranijuma i radijuma u zemljištu i pedološkim kartama u cilju identifikacije radonom ugroženih područja.U nedostatku merenja koncentracije radona u zemljištu, kao i zbog nemogućnosti da se meri permeabilnost zemljišta za radon, naši prvi pokušaji da se proceni GRP na osnovu postojećih baza podataka su bili da se detaljno analiziraju korelacije između dostupnih geohemijskih podataka i merenja koncentracije radona u zatvorenim prostorijama kako bi se predvidela radonom ugrožena područja i validovale geogene prognoze. U tu svrhu primenjeni su multivarijantnimetodi, razvijeni u CERN-u za analizu velikog broja događaja u eksperimentalnoj fizici visokih energija, kako bi se ispitale sve moguće korelacije između velikog broja sistematskih ispitivanja koncentracija radona u zatvorenom na području Vojvodine u periodu od 2002-2005. godine koje je sprovela Laboratorija za ispitivanje radioaktivnosti uzoraka i doze jonizujućeg i nejonizujućeg zračenja, PMF-a u Novom Sadu. [6]. Za vojvođansko zemljište postoji bogata sistematika merenja radioaktivnosti i geohemijskih karakteristika nastala upravo u tom periodu (2001-2010) u saradnji laboratorije u Novom Sadu sa Institutom za ratarstvo i povrtarstvo iz Novog Sada. Izbor lokaliteta za poređenje vrednosti je bio po kriterijumima zastupljenosti površina podpojedinim geomorfološkim celinama [7] i pojedinim tipovima zemljišta [8-9].

Institut za fiziku u Beogradu je primenio sve dostupne regresione metode implementirane u TMVA (Toolkit for Multivariate analysis) [10] da bi odredio i rangirao korelacione koeficijente u cilju iznalaženja najpogodnijeg metoda koji će dati najbolje korelacije

koncentracija radona od mnoštva ulaznih parametara. Da bi ova multivarijantna klasifikacija bila moguća set ulaznih događaja je morao biti podeljen na one koji odgovaraju signalu (povišene koncentracije radona) i one koje odgovaraju fonu (ispod granice od 120 Bq/m^3 koja daje najbolje razdvajanje rezultata) (slika 3). Metoda multivarijantne regresije, međutim, ne zahteva ovakvo preliminarno razdvajanje podataka i zbog toga je opštijeg karaktera.

2. METODOLOGIJA UZORKOVANJA I MERENJA

Merenje koncentracije radona u zatvorenim prostorijama je sprovedeno metodom trag detektora tipa CR39 koji su u zatvorenoj difuzionoj komori bili izlagani na oko 3000 lokacija u Vojvodini u prizemnim prostorijama u trajanju od 90 dana u zimskim mesecima: decembar, januar i februar u periodu od 2002-2005.Nagrizanje i očitavanje tragova je izvršeno kod proizvođača opreme Radosys Company, Mađarska. Za ovu studiju izračunate su srednje vrednosti koncentracija radona za mesta u neposrednoj blizini lokaliteta uzorkovanja zemljišta.Tipovi zemljišta kojim pripadaju ispitivani uzorci su: černozem, humoglej, fluvisol, pseudoglej, solonjec, kambisol, solončak i arenosol, po IUSS klasifikaciji [9].Sa svake odabrane lokacije uzeto je 10 mikro uzoraka zemljišta sa površine od 10 x 10 m, a zatim napravljen jedan kompozitni uzorak mešanjem. Za ispitivanje radioaktivnosti uzorci zemljišta su uzeti sa dve dubine: iz površinskog sloja (0–10 cm) i sa dubine do 30 cm agrohemijskom sondom. Hemijske analize zemljišta su izvršene samo na uzorcima sa dubine od 30 cm.Uzorci zemljišta su sušeni na 105^oC do konstantne mase, usitnjeni, homogenizovani i mereniu cilindričnim posudama na kapi detektora. Koncentracije aktivnosti radionuklida gama emitera u zemljištu određene su metodom niskofonske gama spektrometrije na dva HPGe detektora visoke rezolucije u pasivnoj zaštiti. Za prikupljane i analizu gama spektara korišćen je softver Genie 2000. pH-vrednost određena je u suspenziji zemljišta sa vodom (10 g: 25 cm^3) i suspenziji zemljišta sa kalijum hloridom, potenciometrijski, pH metar PHM62 standard-Radiometar Copenhagen. Sadržaj humusa određen je metodom Tjurin-a; ukupan sadržaj azota po Kjldahlu na sistemu za digestiju i titraciju Tacator; lakopristupačni fosfor i lakopristupačni kalijum (ekstrakcijom sa amonijum laktatom) - AL metodom. Za određivanje mehaničkog sastava zemljišta korišćene su metode: frakcionisanje pomoću serije sita i pipet metoda. U cilju ostvarivanja peptizacije mehaničkih elemenata uzorci zemljišta se tretiraju natrijum-pirofosfatom. Na osnovu veličine čestica prema IUSS klasifikaciji mogu se odrediti sledeće frakcije: krupan pesak (0,2–2 mm), sitan pesak (0,02–0,2 mm), fini prah (0,002-0,02 mm) i glina (<0,002 mm) [9].

3. REZULTATI I DISKUSIJA

U tabeli 1. prikazani su linearni korelacioni koeficijenti koji nam ukazuju na veličinu korelacije između ulaznih veličina i koncentracije radona. Može se uočiti da radon najbolje korelira sa radionuklidima na dubini od 30 cm.

Za primenu multivarijantnih metoda, ispitivani uzorak mora da ima značajnu statistiku. Pošto to nije bilo zadovoljeno, veštački se povećao uzorak dupliranjem svih vrednosti, ali uz modifikaciju množenjem inicijalnih vrednosti ulaznih parametara i koncentracija radona sa 1+slučajne Gausove vrednosti sa sigma 1/10.

Tabela 1. Korelacioni koeficijenti između radona i ulaznih parametara

Redni br.	Parametar	Korelacioni koeficijenat
1	Elevation	+0,11
2	pH	0
3	$CaCO_3$	-0,03
4	Humus	+0,15
5	Ukupan N	+0,13
6	P_2O_5	-0,01
7	K_2O	+0,01
8	Krupan pesak	-0,08
9	Sitan pesak	-0,19
10	Prah	+0,16
11	Glina	+0,17
12	Ra-226 30cm	+0,27
13	U-238 30cm	+0,17
14	Th-232 30cm	+0,22
15	K-40 30cm	+0,10
16	U-238 površina	-0,17
17	Ra-226 površina	+0,04
18	Th-232 površina	0
19	K-40 površina	+0,02
20	Cs-137 površina	-0,17

Ulazni parametri (karakteristike zemljišta i sadržaj radionuklida na površini i na dubini od 30 cm) su korišćeni za testiranje i evaluaciju 12 multivarijantnih metoda koje postoje u okviru TMVA. Najbolji metod je onaj koji zadržava maksimalnu vrednost odbacivanja fona pri najvećoj efikasnosti signala (slika 2). Na osnovu takvog kriterijuma kao metoda koja najefikasnije klasifikuje ulazne događaje, odabrana je metoda BDT (Boosted Decision Trees method). Ovo se može ilustrovati na slici 3. koja prikazuje raspodelu izlaznih veličina BDT klasifikacione metode za ulazne signale i fonske događaje. Drugi najbolji izbor je primena ANN Multilayer Perceptrons metode (MLP).

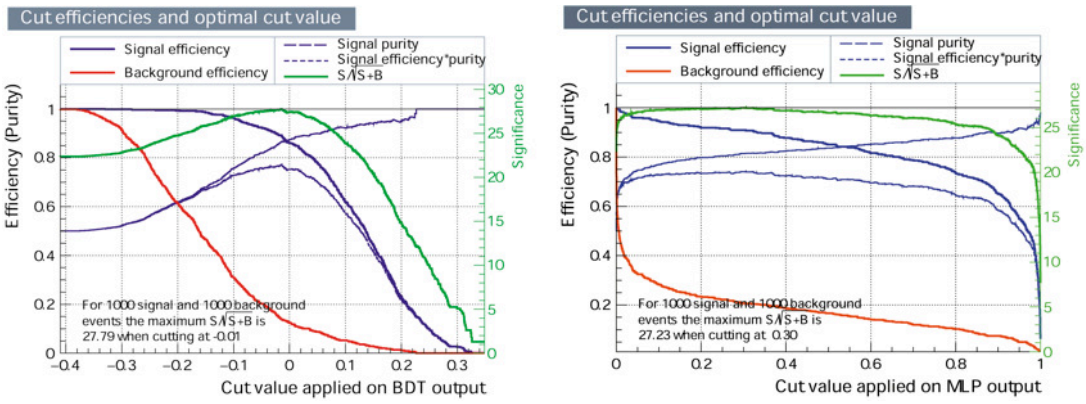

Slika 2. Efikasnost odsecanja i optimalna vrednost odsecanja za BDT (levo) i MLP (desno) multivarijantnih metoda za radonske koncentracije

Tabela 2. Rezultati evaluacije metoda rangirani po najboljoj efikasnosti signali i čistoći površine. @B je deo fonskih događaja koji su klasifikovani kao događaji signala

MVA metoda	Efikasnost signala prema efikasnosti fona (greška):				podela	značaj
	@B=0,01	@B=0,10	@B=0,30	ROC-integ		
BDT	0,212(16)	0,814(16)	0,959(08)	0,932	0,609	1,614
BDTG	0,243(17)	0,767(17)	0,966(07)	0,927	0,611	1,676
MLPBNN	0,224(17	0,754(17)	0,957(08)	0,922	0,600	1,579
MLP	0,228(17)	0,728(18)	0,955(08)	0,919	0,577	1,540
SVM	0,211(16)	0,797(16)	0,938(09)	0,918	0,587	1,611
RuleFit	0,162(15)	0,671(19)	0,906(12)	0,891	0,482	1,263
LikelihoodPCA	0,000(00)	0,491(20)	0,845(14)	0,843	0,404	1,099
LD	0,047(08)	0,348(19)	0,744(18)	0,789	0,271	0,806
Likelihood	0,031(07)	0,328(19)	0,674(19)	0,764	0,208	0,589
FDA_GA	0,031(07)	0,147(14)	0,363(19)	0,611	0,093	0,353

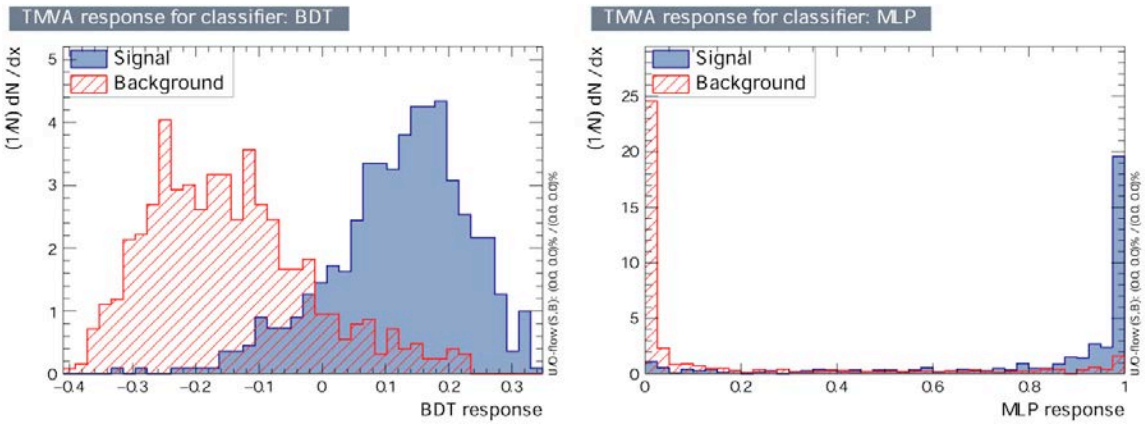

Slika 3. Raspodela izlaznih vrednosti BDT i ANN MLP klasifikacionih metoda za ulazni signal i fonske događaje

Rangiranje BDTG ulaznih varijabli (tabela 3) je izvedena brojanjem koliko često se varijable koriste pri donošenju odluka u svakom čvorištu stabla, pri čemu je ova vrednost otežana brojem podela i brojem događaja u čvoru. Kao što se vidi iz tabele 3, pored ukupnog azota, najvažnije varijable za koncentracije radona u zatvorenim prostorijama su koncentracije radionuklida na 30cm dubine.

Najbolji regresioni metodi koji daju izlazne veličine najpribližnije stvarnim vrednostima koncentracije radona su ponovo BDT, a kao druga MLP, isto kao i u slučaju multivarijantnog klasifikatora. Slika 4 prikazuje distribuciju koncentracija radona i izlaznih veličina iz MPL evaluacije koncentracija radona na osnovu svih ulaznih parametara.

Da bi procenili kvalitet korišćenog metoda poređene su razlike između izlaznih vrednosti iz MLP multivarijantne regresione metode i vrednosti merenih koncentracija radona (slika 5). Slika ukazuje na dobru moć predviđanja varijacija koncentracija radona na

osnovu celokupnog seta ulaznih parametara pomoću multivarijantnih regresionih metoda.

Tabela 3. Ulazni parametri poređani po značaju za BDTG MVA metodu za radon

BDTG rang	Paremetar	Značaj varijable x 10^{-2}
1	Ukupan N	6,490
2	U-238 30cm	6,425
3	K-40 30cm	6,040
4	Th-232 30cm	5,495
5	Humus	5,490
6	K_2O	5,406
7	glina	5,360
8	U-238 površina	5,218
9	Sitan pesak	5,116
10	$CaCO_3$	5,081
11	P_2O_5	5,003
12	Cs-137 površina	4,715
13	Ra-226 30cm	4,656
14	Nadmorska visina	4,595
15	K-40 površina	4,509
16	pH	4,435
17	Ra-226 površina	4,188
18	Prah	4,082
19	Th-232 surface	4,026
20	Krupan pesak	3,671

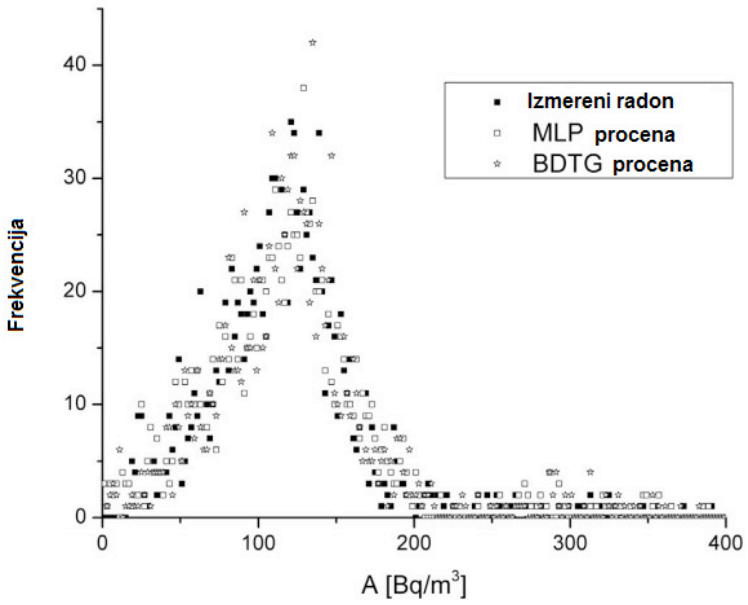

Slika 4. Raspodela merenih koncentracija radona i izlaznih podataka iz MLP multivarijantnog regresionog metoda za koncentracije radona

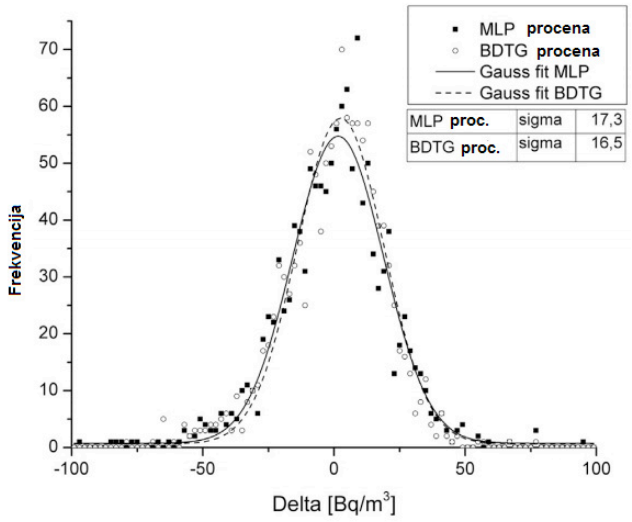

Slika 5. Raspodela razlika izlaznih veličina iz MLP metoda i merenih radonskih koncentracija

4. ZAKLJUČAK

U ovom radu detaljno je opisana mogućnost primene multivarijantne analize za procenu radonskog potencijala. Odabrana je najadekvatnija metoda za analizu radonskih merenja među velikim brojem multivarijantnih metoda, koje su razvijene za analizu podataka u fizici visokih energija i implementirane u TMVA softverski paket. Evaluacijom i rangiranjem dobijenih rezultata na osnovu efikasnosti i čistoće signala izdvojene su dve metode koje daju najbolje rezultate u analizama: BDT i MLP koja se bazira na veštačkoj neuralnoj mreži (ANN). Rezultati dalje multivarijantne analize daju uvid u zavisnost koncentracije radona od koncentracija ostalih radionuklida u zemljištu i geohemijskih karakteristika zemljišta. BDTG multivarijantni metod pokazuje da su varijable od najvećeg značaja za koncentracije radona u zatvorenom: koncentracije radionuklida u dubljim slojevima zemljišta, ali takođei sadržaji humusa i gline u zemljištu (tabela 3). Dodatno, multivarijantni regresioni metodi daju dobru aproksimaciju koncentracije radona korišćenjem celokupnog seta ulaznih parametara. Sve to potvrđuje da su radiogeohemijski podaci korisni za generisanje mapa radonom ugroženih područja. Potvrđena je pretpostavka da tip zemljišta koji sadrži najveći procenat gline i humusa u najvećoj meri adsorbuje i zadržava radon u zemljištu i doprinosi povišenim koncentracijama radona u zatvorenom, odnosno radonskom potencijalu. Ovaj zaključak se može primeniti za odabir lokacija za buduća merenja permeabilnosti zemljišta kada se nabavi neophodna oprema. Dobijena najbolja korelacije koncentracija radona sa sadržajem ukupnog azota u zemljištu predstavlja interesantan rezultat koji će biti dalje proučavan u narednim studijama proučavanja emanacije radona iz zemljišta.

5. ZAHVALNICA

Autori se zahvaljuju na finansijskog podršci Pokrajinskom sekretarijatu za zaštitu životne sredine i održivog razvoja i Ministarstvu prosvete, nauke i tehnološkog razvoja u okviru projekata OI171002 i III43002.

6. LITERATURA

[1] UNSCEAR, 2008, Ionizing Radiation: Sources and Effects, UNSCEAR 2008 REPORT, VOLUME II, United Nations, New York (2008)

[2] WHO, 2009 Handbook on Indoor Radon – a Public Health Perspective

[3] Council Directive 2013/59/EURATOM of 5 December 2013 laying down basic safety standards for protection against the dangers arising from exposure to ionising radiation, and repealing Directives 89/618/Euratom, 90/641/Euratom, 96/29/Euratom, 97/43/Euratom and 2003/122/Euratom, Article 74 Indoor exposure to radon

[4] V. Gruber et al., The European map of geogenic radon potential, *Journal of Radiological Protection* 33 (2013) 51-60

[5] Neznal M, Neznal M, Matolin M, Barnet i and Miksova J 2004 The New Method for Assessing the Radon Risk of Building Sites (*Czech Geological Survey Special Papers vol 16)* (Prague: Czech Geological Survey)

[6] Forkapić, S., et al., 2007. Indoor radon in rural dwellings of the south-Pannonian region. *Radiat. Prot. Dosim*.123 , pp. 378-383

[7] Košćal, M., Menković, Lj., Knežević, M., Mijatović, M., (2005): Geomorfološka karta Vojvodine sa tumačem. Geozavod – Gemini, Beograd

[8] Nejgebauer, V., et al., 1971. Pedološka karta Vojvodine (R 1 : 50.000). Institut za poljoprivredna istraživanja, Novi Sad

[9] IUSS Working Group WRB, 2014: World Reference Base for Soil Resources 2014. International soil classification system for naming soils and creating legends for soil maps. World Soil Resources Reports No. 106. FAO, Rome.

[10] Hoecker, A., et al., 2007. TMVA - Toolkit for Multivariate Data Analysis, PoS ACAT 040, arXiv:physics/070303

НИСКОФОНСКА ЛАБОРАТОРИЈА ИНСТИТУТА ЗА ФИЗИКУ - ПРВИХ ДВАДЕСЕТ ГОДИНА -

Владимир УДОВИЧИЋ, Александар ДРАГИЋ, Радомир БАЊАНАЦ, Дејан ЈОКОВИЋ, Димитрије МАЛЕТИЋ, Никола ВЕСЕЛИНОВИЋ, Михаило САВИЋ, Давид КНЕЖЕВИЋ,

Институт за физику, Београд, Србија, banjanac@ipb.ac.rs

САДРЖАЈ

Представљена је делатност сарадника Нискофонске лабораторије од њене изградње до данас. Почетна мерења концентрације радона, интензитета космичког зрачења и фона гама зрачења временом су, методолошким приступом, прерасла у континуирани мониторинг. Статистички значајни резулатати добијени након дуготрајних мерења, допуњени поузданим симулацијама и анализирани напредним мултиваријантним техникама јасно идентификују Нискофонску лабораторију у свим њеним областима истраживања.

1. УВОД

Природа овог рада је ревијална и представља ретроспективу најважнијих резултата сарадника Лабораторије током последње две деценије.

Почетак научне каријере прва три потписана коаутора практично коинцидира са изградњом подземне лабораторије и конституисањем Нискофонске лабораторије за нуклеарну физику, Института за физику. Иницијална замисао др Радована Антанасијевића и професора др Ивана Аничина о постојању референтне лабораторије за мерење малих активности и проучавање ретких нуклеарних процеса, реализована је 1997. године у оквиру Института за физику. Непроцењиву подршку двојице учитеља додатно је обогатила сарадња колеге Александра Драгића са академиком Звонком Марићем, његовим ментором на теоријским радовима, који је такође веома био заинтересован за Плазма фокус експеримент. У мерењима на тој фузијоној машини, значајна је била техничка подршка Бошка Антанасијевића, Бате Панића и др Драгутина Шевића, као и теоријски прорачуни колеге Јовице Станојевића, па је 2000. године одбрањена прва дисертација на Плазма фокус експерименту, колеге Душана Јоксимовића. После дуже паузе изазване дотрајалошћу опреме, пре неколико година покушана је ревитализација овог експеримента, ентузијазмом колега др Драгана Лукића и Мирослава Максимовића, али је процењено да она захтева значајније инвестирање.

Знања стечена на Плазма фокус експерименту употребом чврстих детектора трагова примењивана су и у првим мерењима концентрације радона у подземној лабораторији. У области детектора трагова, поред великог ауторитета др Радована Антанасијевића, оснивача и првог руководиоца Лабораторије, који је знање преносио на млађе сараднике вредно је поменути и корисне инструкције колегинице др Бојане Грабеж као и искуство професора др Јована Вуковића. То је све заједно допринело да 2006. године у Лабораторији буде одбрањена нова докторска дисертација, колеге Владимира Удовичића поново на тему Плазма фокус експеримента. Убрзо, током 2007. године придружио му се колега

Александар Драгић, одбраном дисертације са теоријским радом о позитронијуму у сарадњи са академиком Звонком Марићем.
Сарадња са професором др Иштваном Бикитом, испред новосадске лабораторије за нуклеарну физику, ПМФ-а у Новом Саду, била је драгоцена већ на почетку током емпиријске селекције радијационо чистих грађевинских материјала за градњу Лабораторије. Први резултати мерења концентрације радона током градње подземне лабораторије публиковани су већ 1999. године [1]. И током наредног периода, проблематика радона била је присутна, периодичном провером у надземној и подземној лабораторији (НЛ/ПЛ), детекторима трагова и канистрима са активним угљем. Упоредо са постепеним опремањем Лабораторије потребном инструментацијом, предност су добијале две примарне области. Најпре је 2001. године иницијативом професора др Ивана Аничина, уз подршку његових асистената др Јована Пузовића и др Горана Шкоре, и виспреним саветима професора др Ђуре Крмпотића у Институту за физику покренута проблематика физике космичког зрачења. Тих година Лабораторија је остала без неколицине сарадника, а непроцењив је био губитак великог Радета, др Радована Антанасијевића нашег драгог шефа, и Лабораторија од те 2003. године носи његово име. Лабораторију су у кратком периоду напустили Драгутин Шевић, Бошко Антанасијевић, Надежда Антанасијевић, Зорка Продановић и Јовица Станојевић, али је стигло и прво појачање. Колега Дејан Јоковић се од самог почетка укључио у покретање проблематике космичког зрачења на којој је магистрирао, а 2011. године и докторирао.
Основна намена надземних или плитко укопаних нискофонских лабораторија је мерење малих активности, било узорака из природе или вештачки обогаћених (НОРМ и ТЕНОРМ), пошто је низак фон обрнуто пропорционалан осетљивости мерења или минималној детектабилној активности мереног узорка. Фон је најчешће синоним за фон гама зрачења којим се, пошто је моноенергетско, јасно идентификује одређени радио изотоп. За мерење гама зрачења најчешће су у употреби германијумски детектори, са ултимативним захтевима за радијационо чистим криостатом, што веће активне запремине (ефикасности), и смештене у одговарајућој пасивној заштити (најчешће олову). Високо осетљива мерења фона, којима се фундаментално истражују ретки процеси (двоструки бета распади и тамна материја) спроводе се у дубоким подземним лабораторијама у којима је минимизован утицај космичког зрачења. Ипак, и плитко укопане лабораторије могу послужити у анализи оних компоненти фона које генерише космичко зрачење (због боље статистике), а које су релевантне у високо осетљивим мерењима у дубоким лабораторијама, као и у селекцији радијационо чистих материјала који се уграђују у инструментацију тих високо осетљивих истраживања. Главни циљ, анулирање нуклеонске компоненте космичког зрачења, присутне на површини и све до око 15 метара воденог еквивалента (м.в.е), постигнуто је укопавањем земунске лабораторије у десну обалу Дунава. Добијено је 12 метара заштитног слоја земље, леса (еквивалентног са 25 метара воде) па је и најпродорнија компонента космичког зрачења, наелектрисани миони, редукована интегрално скоро 4 пута.
Први резултат релативног смањења флукса миона, подземне у односу на надземни простор (око 4 пута), добијен је двема техникама, пластичним сцинтилатором NE102 и преносним германијумским детектором (рел. ефикасности 20%). На жалост, овај први Ge детектор, позајмљен из Винче, није био од користи за нискофонска мерења због његове радијационе запрљаности услед рада на мониторингу

реакторских неутрона. У прво време, Лабораторија је располагала и планарним Ge(Li) детектором, добијеним од колега из Новог Сада, којим се могао детектовати тек нискоенергетски део фона амбијенталног гама зрачења, до око 200keV. Поред доминантних Pb-X пикова, од оловног оклопа, јасно се издвајала линија од урана 238 (тачније његовог првог потомка Th-234) на 63.3keV, што је послужило за први чланак о анализи узорака са ураном [2]. Током годину дана и непосредно пре набавке првог и још увек јединог германијумског детектора у Лабораторији, у подземној лабораторији је био у употреби још један позајмљени Ge детектор, из Лабораторије за заштиту од зрачења из Винче, а у циљу компаративних мерења истих узорака.

2. ПРОБЛЕМАТИКА КОСМИЧКОГ ЗРАЧЕЊА

Прегледни рад, из 2011. године, [3], садржи и детаље конструкције саме подземне лабораторије и описа њеног радног режима, па ће се надаље прича фокусирати на три доминантне области истраживања у Лабораторији. Хронолошки, прва област којом смо се бавили од 2001. године је космичко зрачење, и још увек је област која је предмет интересовања највећег броја сарадника.

Континуирани мониторинг интензитета космичког зрачења у НЛ/ПЛ, траје непрекидно од 2002. године до данас, у почетку са два једнака пластична сцинтилатора мале површине. Мали пластици, како их називамо, стигли су у Србију из Дубне, 1994. године, ентузијазмом професора Аничина и Миодрага Крмара. Детектори су комплетирани у нашој Лабораторији, спајањем сцинтилатора са светловодом и по једним фотомултипликатором. И данас су у функцији са још увек беспрекорном дискриминацијом мионског ΔE пика од нискоенергетског космичког и гама зрачења. Први резултати редом су представљани на светским, Јапан, 2003, Индија, 2005. и европским конференцијама о космичком зрачењу, Италија, 2004. и Португалија 2006. године [4]. На послетку, прецизно одређен флукс космичких миона, први пут на нашим географским ширинама и дужинама, публикован је у [5]. Крајем 2005. године, сналажљивошћу колеге Драгића, у склопу набавке германијумског детектора, успели смо значајно да подигнемо квалитет мерења космичког зрачења, набавком два идентична, 8 пута по површини већа сцинтилатора. Боља статистика мерења значила је и упуштање у временску спектоскопију космичког зрачења, посебно након набавке првог дигиталног анализатора (CAEN), 2008. године, иако су и до тада анализиране временске серије и периодограми космичких података, [6].

Од прошле године у новој просторној конфигурацији расположивих пластичних сцинтилатора (званог ASYMUT, што је асиметрични мион телескоп), отвара се могућност енергетски диференцираног праћења процеса соларне модулације космичког зрачења, слика 1.

Много значајније за потенцијал Лабораторије од скромног опремања хардвером, јесте трансфер поново из Винче, овог пута колеге Димитрија Малетића, препоруком нашег професора Ивана. Његово велико знање стечено на CMS експерименту у CERN-у, на коме је и докторирао 2009. године, посебно софтверских алата, оснажило је способности групе да се применом ново развијених софтвера, на адекватан начин анализира све богатија база космичких података.

У Лабораторији је реализовано десетак дипломских радова, али се од млађих тек колега Никола Веселиновић, радећи најпре дипломски на теми плазма фокуса са

колегом Удовичићем, касније „усудио“ да анализира поменуту базу космичких података те тако управо ове године приводи рад на својој дисертацији. Његовим стопама је, најпре радећи дипломски рад о CAEN дигиталном анализатору, кренуо и колега Михаило Савић, па се ускоро може очекивати још једна дисертација из области космичког зрачења, [7].

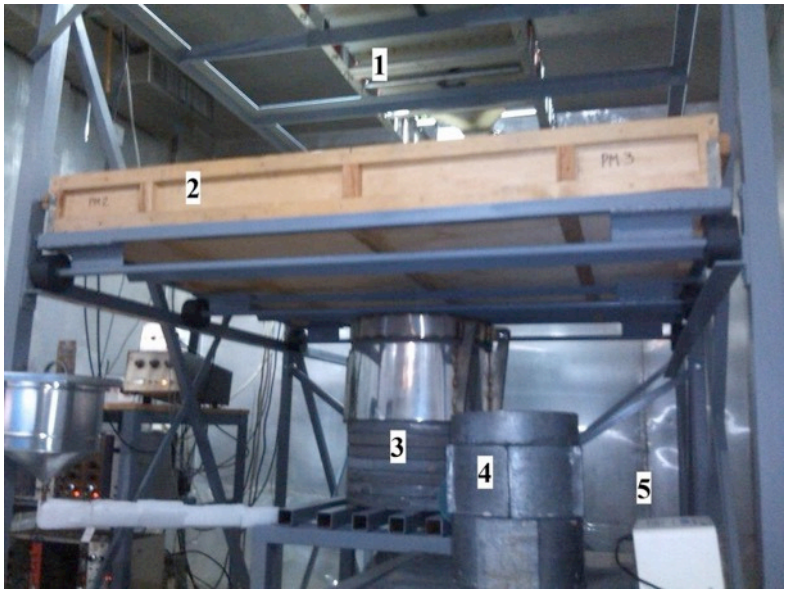

Слика 1. ASYMUT конфигурација у подземној лабораторији, 1-мали пластици, 2-велики пластик, 3-Ge детектор у Pb заштити, и додатно 4-NaI детектор у Pb заштити, 5-радонометар

3. НИСКОФОНСКА ГАМА СПЕКТРОМЕТРИЈА

После 8 година од отварања, у Лабораторију је стигао германијумски детектор, у стандардној вертикалној геометрији криостата који је изабран да буде од нискофонских материјала. Релативне ефикасности од 35% и номиналне енергетске резолуције 1,72 keV, детектор је представљао изврстан инструмент за детаљно упознавање са свим компонентама фона гама зрачења у амбијенту подземне лабораторије. У почетку је пасивна заштита била недовољна, 6cm олова непознате историје (у смислу његовог порекла и старости). Неколико година касније после процене да је оптимална дебљина заштите 12 cm олова, опет уз помоћ колега из Новог Сада, изливени су дискови укупне масе око 900 килограма од довољно старог олова за које је процењен садржај Pb-210 око 25 $Bqkg^{-1}$. Већ је поменута тријажа грађевинских материјала у смислу избора оних са минималном концентрацијом урана, торијума и калујума 40, а за њом је следило зналачко пројектовање вентилационог система који је од највећег значаја за подземне лабораторије. Без њега, спонтана акумулација радона достиже два реда већу концентрацију па би у фонском спектру доминирале бројне пострадонске линије уз њихово интензивно варирање у времену. Непрестаним изменама целокупног ваздуха у подземној лабораторији (запремине око 130 m^3) скоро 4 пута на сат, и филтрацијом ваздуха на улазу у систем у два степена, прво филтером за прашину а потом и великим (око 50 kg) адсорберским филтером са активним угљем, концентрација радона је смање-

на на око 10 Bqm^{-3}. Временом је процењено да је и достигнутих 20 Bqm^{-3} довољно ниско, штедећи на честим заменама великог филтера. Поред филтрације, разликом у брзини упумпавања чистог и испумпавања радоном запрљаног ваздуха, пројектован је и надпритисак од преко 2mbar-a, који спречава дифузију радона кроз евентуалне пукотине из алуминијумом пресвучених зидова и додатно доприноси релативној стабилности концентрације радона.

Још у пројектовању прве конфигурације са великим пластицима ($1m^2$), реализована је вето-активна заштита Ge детектора, са растојањем оловног поклопца до коаксијално постављеног великог пластика од око 60cm. Управо је тежак оловни поклопац и начин приступа самом Ge детектору, захтевао релативно велико растојање што је због широке угаоне расподеле миона ($\cos^2\theta$) значајно умањило учинак вето детектора. Континуирани мониторинг космичког зрачења и упоредо временска спектроскопија пружали су могућност да се у антикоинцидентном режиму смањи фон одбацујући део догађаја детектован у вету, док се у коинцидентном режиму управо анализирао део фонског спектра генерисан од стране космичког зрачења. Први резултати су представљени у [3]. Посебно је занимљива процена флукса неутрона генерисаних од миона у олову, који се детектују преко закаснелих коинциденција њиховом интеракцијом на изотопима германијума, [8]. Поменута ASYMUT конфигурација, слика 1, значајно је побољшала геометрију два детектора па се очекује и значајно нижи интегрални фон и интензитет анихилационе линије у вето режиму. Пре тога, карактеристике фона после дужег мерења представљене су у [9].

Током година континуираног мерења, било је од значаја анализирати утицај варијације радона и космичког зрачења на варијације фона, пошто су варијације фона у спрези са систематском грешком мерења малих активности. Мерења су сукцесивно обављана у обе лабораторије НЛ и ПЛ, и показана је очигледна предност остварених нискофонских услова у подземној лабораторији, [10]. Ово је била и тема дисертације колеге Радомира Бањанца, одбрањене 2011. године.

Нискоенергетски део спектра фона германијумских детектора истраживан је и са аспекта утицаја „skyshine“ радијације у односу на конкурентски допринос космичког зрачења. Миони космичког порекла производе континуирани спектар губитака енергије који има максимум интензитета на високим енергијама, реда неколико десетина MeV, која је најчешће изван области интересовања, али дају допринос и у нискоенергетској области. Свеукупни инструментални фонски спектри одликују се изразитим максимумом, који је у зависности од величине детектора у близини 100keV. Интензитет, природа и порекло фона у овој енергетској области испитивано је апсорпционим мерењима и закључено је да је зрачење континуираног спектра двојаког порекла. Једним делом оно представља расејано и деградирано зрачење електромагнетне компоненте космичког зрачења, док другим делом представља од целокупне околине расејано зрачење терестријалног порекла, често познатог под називом „skyshine radiation“, [11].

Важно је поменути, као што је случај и код проблематике космичког зрачења, да се у анализама фона неизоставно користе симулациони пакети, најчешће черновски GEANT4, [12], и у области космичког зрачења, CORSICA.

4. ДЕТЕКЦИЈА РАДОНА

Радон је свуда присутан јер је по природи гас па дифундује и кроз зидове лабораторија, при томе је и инертан па га је тешко филтрирати и хемијски изоловати. У нискофонској гама спектрометрији увек својим релативно кратким животом, генерише значајну активност потомака који потом својим распадањем продукују мноштво пострадонских гама линија, посебно Pb-214 и Bi-214. Један од начина детекције радона је управо анализом интензитета пострадонских линија након што је сам радон адсорбован у канистрима са активним угљем. Време акумулације је обично 2 дана, а још једна, тзв. пасивна метода је пребројавање трагова од радонових алфа честица у чврстим детекторима (CR-39 и LR-115) после времена експонирања од најмање 3 месеца. Већ је поменуто да радон као сметња у нискофонским мерењима осим што генерише непријатан фон у виду мноштва гама линија и припадајућег Комптоновског континуума, додатно утиче у варијацији, најчешће дневној, истих линија. Начин да се поузданије процени утицај овог варирања јесте активна метода детекције радона која у реалном времену сакупља податке, концентрације радона као и релевантних метеоролошких параметара, температуре и релативне влажности ваздуха. Од 2008. године Лабораторија располаже једним таквим бројачем, радонометром, који је далеко јефтинији од активних спектрометара (Rad7 и Alphaguard), али подједнако прецизан. Дуготрајним мониторингом у амбијенту подземне лабораторије, радонометар је потврдио очекивано дневно варирање али показао и сезонску варијацију радона, [13].

Активни уређај пружио је и могућност примене напредних мултиваријантних техника анализе, које се успешно тренирају на актуелно измереној бази података радона и метео параметара, и потом успешно врше предикцију динамике радона у контролисаним условима подземне лабораторије, [14].

Већ неколико година активан је сајт, http://cosmic.ipb.ac.rs/index.html, наше Лабораторије са линковима на ажуриране податке мерења космичког зрачења, http://147.91.87.156/cgi-bin/bcrs и евалуационе концентрације радона у ПЛ, http://147.91.87.156/nf-cosmic/rad3/Radon_alarm/.

Знањем стеченим применом разноликих техника детекције радона, не само унутар ПЛ/НЛ простора већ систематски и у реалном амбијенту ван лабораторија, [15], уз подршку Агенције за јонизујућа зрачења и нуклеарну сигурност Републике Србије, и реализовану преко IAEA фондова, нови руководилац Лабораторије др Владимир Удовичић успешно је координирао великом кампањом мапирања радона и добијањем прве радонске мапе Србије 2016. године, [16].

5. УМЕСТО ЗАКЉУЧКА

Надајући се да ће се кроз 10 или 20 година поново пружити прилика писању рада сличног садржаја, очекујући напокон боље опремање Лабораторије хардвером и уз задржавање високог нивоа ентузијазма сарадника, сматрамо досадашње ангажовање успешним, а постојање наше Лабораторије оправданим.

Ово је прилика да се присетимо непосреднije сарадње током ових двадесет година и са колегама из Винче, Милојком Ковачевићем, Зором Жунић, Иваном Вуканац, Драганом Тодоровић, Јеленом Крнета Николић, Предрагом Ујићем, и колегама из Новог Сада Миодрагом Крмаром, Софијом Форкапић и Николом Јованчевићем. Управо је наш најмлађи сарадник, Давид Кнежевић, долазећи из јаке новосадске школе нуклеарне физике додатна нада у покретање нових тема.

Наравно, ту је и велики број наших колега из самог Института за физику, заинтересованих за наш рад од којих се од самог формирања Лабораторије у сваком афирмативном смислу истиче др Александар Белић.
Може се ипак закључити да су почетна мерења концентрације радона, интензитета космичког зрачења и фона гама зрачења временом, методолошким приступом, прерасла у континуирани мониторинг. Статистички значајни резулатати добијени након дуготрајних мерења, допуњени поузданим симулацијама и анализирани напредним мултиваријантним техникама јасно идентификују Нискофонску лабораторију у свим њеним областима истраживања.
На крају, као и сваком приликом, радо се сећамо нашег драгог професора Ивана Аничина који је у најтеже време, када је опстанак Лабораторије био угрожен, али и након одласка у пензију, својом харизмом, неограниченим знањем и свеприсутном љубављу међу нама надахњивао истраживачки дух и одржавао јединство свих сарадника Лабораторије.

6. ЛИТЕРАТУРА

[1] R. Antanasijević, I. Aničin, I. Bikit, R. Banjanac, A. Dragić, D. Joksimović, Đ. Krmpotić, V. Udovičić, J.B. Vuković Radon measurements during the building of a low-level laboratory Radiation Measurements 31, (1999) 371

[2] I. Aničin, R. Banjanac, A. Dragić, D. Joković, V. Udovičić, Investigation of the Uranium Solubility and Absorption Physica Scripta T118 (2005) 39-40

[3] Aleksandar Dragić, Vladimir Udovičić, Radomir Banjanac, Dejan Joković, Dimitrije Maletić, Nikola Veselinović, Mihailo Savić, Jovan Puzović, Ivan V. Aničin. The new set-up in the Belgrade low-level and Cosmic-ray laboratory. *Nuclear Technology and Radiation Protection Vol. XXVI, No. 3, 181-192 (2011)*

[4] (а) J. Puzović, A. Dragić, V. Udovičić, D. Joković, R. Banjanac, I. Aničin, Analysis of continuous cosmic ray measurements in Belgrade *Proceedings of 28th International Cosmic Ray Conference 1199-1202, Japan, (2003)*
(б) A. Dragić, R. Banjanac, V. Udovičić, D. Joković, J. Puzović, I. Aničin, Variations of CR-Muon Intensity in the Declining Phase of the 23rd Solar Cycle in Ground and Shallow Underground Data *Proceedings of 29th International Cosmic Ray Conference 101-104, Pune, India, (2005)*
(в) A. Dragić, R. Banjanac, V. Udovičić, D. Joković, I. Aničin, J. Puzović, Comparative Study of Power Spectra of Ground and Shallow Underground Muon Data *Proceedings of 19th European Cosmic Ray Symposium* (Published in International *Journal of Modern Physics A 29 (2005) 6953-6955), Florence, Italy, (2004)*
(г) A. Dragić, R. Banjanac, V. Udovičić, D. Joković, I. Aničin, J. Puzović, Diurnal and seasonal variations of CR-muon intensity in the declining phase of the 23rd solar cycle in ground and 25 m.w.e. underground data at 45oN *Proceedings of 20th European Cosmic Ray Symposium, Lisbon, Portugal, (2006),* http://www.lip.pt/events/2006/ecrs/proc/ecrs06-s2-76.pdf

[5] A. Dragić, D. Joković, R. Banjanac, V. Udovičić, B. Panić, J. Puzović, I. Aničin. Measurement of cosmic ray muon flux in the Belgrade ground level and

underground laboratories *Nuclear Instruments and Methods in Physics Research A 591 (2008) 470-475*

[6] A. Dragić, R. Banjanac, V. Udovičić, D. Joković, J. Puzović, I. Aničin Periodic Variations of CR Muon Intensity in the Period 2002-2004. Proceedings of the 21st European Cosmic Ray Symposium, Košice, Slovakia (2008) 368-373.

[7] (а) N.Veselinović A. Dragić, M. Savić, D. Maletić, D. Joković, R. Banjanac, V. Udovičić. Utilization of a shallow underground laboratory for studies of the energy dependent CR solar modulation. *XXV European Cosmic Ray Symposium, Torino, Sept. 4-9 (2016)*
(б) M. Savic, A. Dragic, N. Veselinovic, V. Udovicic, R. Banjanac, D. Jokovic, D. Maletic. Effect of pressure and temperature corrections on muon flux variability at ground level and underground. *XXV European Cosmic Ray Symposium, Torino, Sept. 4-9 (2016)*

[8] (а) A Dragić, I Aničin, R Banjanac, V Udovičić, D Joković, D Maletić, M Savić, N Veselinović and J Puzović. Neutrons produced by muons at 25 mwe. *Proceedings of the 23rd European Cosmic Ray Symposium (and 32nd Russian Cosmic Ray Conference), Moscow, Russia, July 3 - 7, (2012), J. Phys.: Conf. Ser. 409 012054* doi:10.1088/1742-6596/409/1/012054.
(б) N. Veselinović, D. Maletić, D. Joković, R. Banjanac, V. Udovičić, M. Savić, J. Puzović, I.V. Aničin, A. Dragić. Some peculiarities of digital gamma-ray spectroscopy with germanium detectors. performed in presence of neutrons. *GAMMA-2 Scientific Workshop on Nuclear Fission Dynamics and the Emission of Prompt Neutrons and Gamma Rays, 24 – 26 September 2013, Sremski Karlovci, Serbia. Physics Procedia, 59, pp. 63-70 (2014)*

[9] Radomir Banjanac, Vladimir Udovičić, Dejan Joković, Dimitrije Maletić, Nikola Veselinović, Mihailo Savić, Aleksandar Dragić, Ivan Aničin. Background spectrum characteristics of tfe HPGe detector long-term measurements in the Belgrade low-background laborator.y*Proceedings of Third International Conference on Radiation and Dosimetry in various fields of Research, RAD2015, JUNE 8 – 12, 151-153 (2015)*

[10] R. Banjanac, A. Dragić, V. Udovičić, D. Joković, D. Maletić, N. Veselinović, M. Savić. Variations of Gamma-Ray Background in the Belgrade Shallow Underground Low-Level Laboratory. *Applied Radiation and Isotopes, 87 (2014) 70-72* http://dx.doi.org/10.1016/j.apradiso.2013.11.091

[11] R. Banjanac, D. Maletić, D. Joković, N. Veselinović, A. Dragić, V. Udovičić, I. Aničin. On The Omnipresent Background Gamma Radiation Of The Continuous Spectrum. *Nuclear Instruments and Methods in Physics Research A 745 (2014) pp. 7-11* http://dx.doi.org/10.1016/j.nima.2014.01.065

[12] D. R. Joković, A. Dragić, V. Udovičić, R. Banjanac, J. Puzović, I. Aničin. Monte Carlo simulations of the response of a plastic scintillator and an HPGe spectrometer in coincidence. *Applied Radiation and Isotopes 67 (2009) 719-722*

[13] (а) V. Udovičić, B. Grabež, A. Dragić, R. Banjanac, D. Joković, B. Panić, D. Joksimović, J. Puzović, I. Aničin. Radon problem in an underground low-level laboratory. *Radiation Measurements 44 (2009) 1009-1012*
(б) Udovičić V., Aničin I., Joković D., Dragić A., Banjanac R., Grabež B., Veselinović N. Radon Time-series Analysis in the Underground Low-level Laboratory in Belgrade, Serbia. *Radiation Protection Dosimetry 145 (2-3) (2011):155-158*

(в) V. Udovičić, J. Filipović, A. Dragić, R. Banjanac, D. Joković, D. Maletić, B. Grabež and N. Veselinović. Daily and Seasonal radon variability in the underground low-background laboratory in Belgrade, Serbia. *Radiation Protection Dosimetry 160 (1-3): pp. 62-64 (2014)*

[14] (а) Dimitrije M. MALETIĆ, Vladimir I. UDOVIČIĆ, Radomir M. BANJANAC, Dejan R. JOKOVIĆ, Aleksandar L. DRAGIĆ, Nikola B. VESELINOVIĆ, and Jelena Z. FILIPOVIĆ. Comparison of multivariate classification and regression methods for the indoor radon measurements. *Nuclear Technology and Radiation Protection Vol. XXIX, No. 1, 17-23 (2014)*

(б) D. M. Maletić, V. I. Udovičić, R. M. Banjanac, D. R. Joković, A. L. Dragić, N. B. Veselinović, J. Filipović. Correlative and Multivariate analysis of increased radon concentration in underground laboratory. *Radiation Protection Dosimetry, 162 (1-2): pp. 148-151 (2014) doi:10.1093/rpd/ncu248*

[15] Vladimir Udovicic, Dimitrije Maletic, Jelena Zivanovic, Aleksandar Dragic, Radomir Banjanac, Dejan Jokovic, Sofija Forkapic. Long-term indoor radon measurements in a family house – a case study in Serbia. *In: Book of Abstracts of 8th Conference of Protection against Radon at Home and at Work, 12 - 14 of September 2016, Prague, Czech Republic, Book of Abstracts, pp. 79*

[16] Udovičić V, Maletić D, Eremić Savković M, Pantelić G, Ujić P, Čeliković I, Forkapić S, Nikezić D, Marković V, Arsić V, Ilić J, Nilsson P. Preliminary results of the first national indoor radon survey in Serbia. *In: Book of Abstracts of 8th Conference of Protection against Radon at Home and at Work, September 12-14, 2016; Prague, Czech Republic.*

LOW-BACKGROUND LABORATORY FOR NUCLEAR PHYSICS IN THE INSTITUTE OF PHYSICS -THE FIRST TWENTY YEARS OF EXISTENCE-

Vladimir UDOVIČIĆ, Aleksandar DRAGIĆ, Radomir BANJANAC, Dejan JOKOVIĆ, Dimitrije MALETIĆ, Nikola VESELINOVIĆ, Mihailo SAVIĆ, David KNEŽEVIĆ

Institute of Physics, Belgrade, Serbia, banjanac@ipb.ac.rs

ABSTRACT

The most important scientific activities in the Low-background laboratory are described for the entire period of its existance. Over the period of twenty years, initial measurements of radon concentration, cosmic-rays intensity as well as gamma radiation background through metodological approach evolved into consistent continual monitoring. Statistically significant results obtained by long-term measurements, enriched by reliable simulation and analyzed using advanced analysis tools clearly identify our Lab.

MONTE KARLO SIMULACIJA FONA HPGE DETEKTORA OD RADIONUKLIDA, KOSMIČKOG I SKYSHINE ZRAČENJA

Dimitrije MALETIĆ, Vladimir UDOVIČIĆ, Dejan JOKOVIĆ, Radomir BANJANAC, Aleksandar DRAGIĆ, Mihailo SAVIĆ, Nikola VESELINOVIĆ
Institut za fiziku, Univerzitet u Beogradu

SADRŽAJ
U Niskofonskoj laboratoriji za Nuklearnu fiziku, više godina se izučavaju osobine fona HPGe detektora. Izučavanje fona važno je za eksperimente sa malim brojem interesantnih dogadjaja ili retkih procesa u podzemnim laboratorijama. Izučavanja fona u Niskofonskoj laboratoriji započeta su izučavanjem fona zračenja od radionuklida, kao i fona od kosmičkog zračenja, koincidentnim tehnikama. Nedavno je izučavan i fon od skyshine zračenja. U ovom radu je predstavljena Monte Karlo simulacija fona HPGe detektora koji dolazi od pomenuta tri izvora zračenja. Rezultati simulacija kosmičkog zračenja odlično se slažu sa eksperimentalnim rezultatima, dok se za druge komponente mogu poboljšati. Postoji prednost simulacija koje daju razloženi fon na tri komponente, koja omogućava da se rezultati simulacija tri komponente fona za jednu laboratoriju mogu simulirati za druge podzemne ili nadzemne laboratorije menjanjem parametara u simulacionim programima. Fon se može simulirati za laboratorije koje mogu biti na različitoj geografskoj širini, nadmorskoj visini, sa različitim sastavom radionuklida u zemljištu i geometrijom laboratorije u kojoj se vrše merenja. Predstavljeni su nedostaci simulacija i da se rezultati mogu poboljšati radeći na detaljima u nekoliko faza simulacije.

1. UVOD

U Niskofonskoj laboratoriji za Nuklearnu fiziku u Institutu za fiziku Beograd, vrše se merenja komponenata zračenja prirodnog fona [1]. Prvenstveno se vrše merenja gama zračenja HPGe detektorom sa i bez olovne zaštite, takodje se vrši kontinualno merenje mionske komponente kosmičkog zračenja korišćenjem plastičnih scintilatora površine od po jednog kvadratnog metra, i to i u nadzemnoj i podzemnoj laboratoriji, kao i merenje radona aktivnim i pasivnim metodama, prvenstveno u podzemnoj laboratoriji. Podzemna laboratorija se nalazi 12 metara pod zemljom, što se predstavlja kao da se merenja vrše ispod vodenog absorbera visine od 25 metara, slika 1. Ekvivalencija je dobijena poznavajući sastav zemljišta, odnosno lesa koji je karakterističan za područje Zemuna. Pored merenja, u ovom radu se koriste i Monte Karlo simulacije, koje služe za poredjenje simulacija sa eksperimentalnim rezultatima, ili služe za izučavanje pojedinih komponenata fona. Monte Karlo simulacioni program koji se koristi je programski paket Geant4 [2], razvijen za potrebe simulacije prolaska čestica kroz materiju, odnosno za simulaciju deponovane energije i odziva detektora. Geant4 programski paket je najrašireniji programski paket za Monte Karlo simulacije i razvija se u CERN-u, prvenstveno za potrebe eksperimenata iz Fizike elementarnih čestica. Za simulacije kosmičkog zračenja koristi se programski paket CORSIKA [3] razvijen za potrebe eksperimenata koji izučavaju mionsku i elektromagnetnu komponentu visokoenergetskih kaskada koje se dobijaju upadom visokoenergetskih čestica primarnog kosmičkog zračenja koje interaguje sa atmosferom Zemlje. Ovaj programski paket razvijen je za potrebe Kaskade

експеримента у Технолошком институту Karlsruhe, у Немачкој. За потребе коришћења оба ова програма за намену симулација одговора пластичних сцинтилатора и HPGe детектора, у Niskofonskoj laboratoriji је развијен посебан интерфејс програм који омогућује да се резултати CORSIKA симулација користе у Geant4 симулацијама детектора у Niskofonskoj laboratoriji. Детаљно изучавање природног фона употпуњено је и симулацијама skyshine зрачења. Skyshine гама зрачење до HPGe детектора долази не директном линијом од радионуклида из земљишта и грађевинског материјала, већ одбијањем и расејањем гама зрачења од атоме околног ваздуха, тј. атмосфере. У Niskofonskoj laboratoriji је изучавана мека компонента гама спектра којег добијамо мерењима HPGe детектором, и закључено је да она долази доминантно од skyshine зрачења, а мањи део од космичког зрачења [4]. Симулације skyshine зрачења су веома захтевне у погледу комјутерског времена за симулације, па је пожељно симулације радити на комјутерским кластерима.

Циљ овог рада је представљање експерименталних резултата фона HPGe детекора који долази од радионуклида, космичког зрачења и skyshine зрачења, поредјење са Monte Karlo симулацијама, и представљање начина комбиновања ове три компоненте фона за различита мерна места.

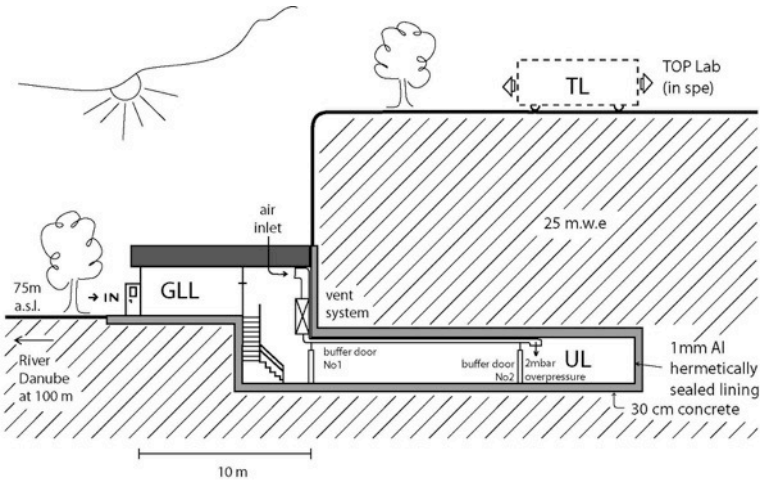

Слика 1. Графички приказ пресека Niskofonske laboratorije za Nuklearnu fiziku

2. ЕКСПЕРИМЕНТАЛНА ПОСТАВКА

Експериментална поставка у подземној и надземној лабораторији је идентична и састоји се од HPGe детектора у оловној заштити, која је отворена на горе, или се као „крov“ стављају танки апсорбери, слика 2. Изнад HPGe детектора налази се пластични сцинтилатор, који користи као veto заштита ако је постављен у anti-koincidentnom modu, или издваја компоненту у HPGe детектору коју добијамо од космичког зрачења, ако је сцинтилатор постављен у koincidentnom modu, што је случај у овом раду. Прикупљање података се врши analogno-digitalnom konverter karticom, који записе сигнала оба детектора шаље на рачунар. Потом се (off-line) врши koincidiranje signala и obradjuju rezultati.

3. MONTE KARLO SIMULACIJE

Симулације почињу programskim paketom CORSIKA, задавањем компонената примарног космичког зрачења које упада на атмосферу Земље од 90% протона и 10%

alfa čestica. Ovo primarno kosmičko zračenje sudara se sa jezgrima atoma vazduha u atmosferi i produkuje sekundarno kosmičko zračenje, koje ima mionsku, elektromagnetnu i hadronsku komponentu koja se sastoji od protona, neutrona i rezultujućih jezgara koji brzo gube energiju u vazduhu. Kao parametri simulacija zadaje se nadmorska visina na kojoj se nalaze detektori u Niskofonskoj laboratoriji, kao i geografska dužina i širina laboratorije. Na ovaj način se za svako merno mesto zadaju različiti parametri i simulacija ima različite spektre za različita merna mesta (laboratorije). Potom se vrši ili simulacija Geant4 programskim paketom i to plastičnog scintilatora i HPGe detektora u olovnoj zaštiti ili simulira prolaz kosmičkog zračenja kroz 12 metara zemlje, pa onda simulira odgovor plastičnog scintilatora i HPGe detektora u podzemnoj laboratoriji.

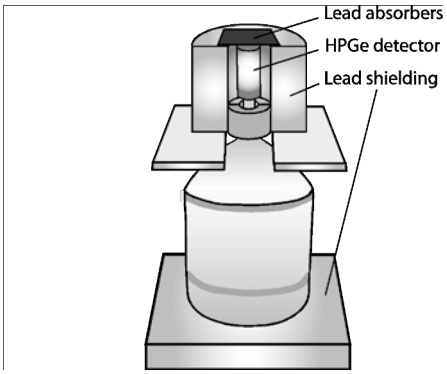

Slika 2. Prikaz postavke HPGe detektora i olovne zaštite otvorene na gore, sa tankim apsorberom na vrhu

Skyshine simulacije se vrše programskim paketom Geant4. Kao ulaz u simulaciju, koristi se pripremljeni set čestica sa pripadajućom energijom koji dolazi iz zemlje i okolnog materijala. Set čestica se priprema tako što se prvo iz snimljenog eksperimentalnog spektra HPGe detektora, uz poznavanje njegove krive efikasnosti, odredjuje odnos intenziteta linija radionuklida iz okoline. Potom ovi podaci služe za odredjivanje frekvencije pojavljivanja čestica zračenja od pojedinih radionuklida, što predstavlja ulaz u Geant4 simulaciju (generator primarnih čestica). Za nastavak simulacije, potrebno je definisati dimenzije i položaj zidova mernog mesta (laboratorije), kako bi se definisala zapremina vazduha i položaj zidova od kojih se zračenje radionuklida rasejava - što je i definicija skyshine zračenja. Simulirani spektar HPGe detektora od radionuklida sa uključenim skyshine zračenjem prikazan je na slici 3.

3. REZULTATI I DISKUSIJA

Monte Karlo simulacioni spektar HPGe detektora u koincidenciji sa scintilacionim veto detektorom u nadzemnoj laboratoriji, koji je predstavljen u ovom radu, dobijen je u dva koraka. Prvi korak se sastoji u simulaciji primarnog kosmičkog zračenja programskim paketom CORSIKA do nadmorske visine laboratorije (sekundarno kosmičko zračenje). Drugi korak je simulacija interakcije sekundarnog kosmičkog zračenja sa HPGe detektorom, a koje ujedno prolazi i kroz veto detektor (koincidentni signal). Drugi korak se simulira korišćenjem Geant4 programskog paketa. Simulacioni spektar HPGe detektora u koincidenciji sa scintilacionim veto detektorom u nadzemnoj laboratoriji prikazan je na slici 3, (crna boja, spektar sa nižim odbrojem), a odlično se slaže sa eksperimental-

nim koincidentnim spektrom. Simulacioni spektar HPGe detektora koji sadrži doprinos od simulacije kosmičkog zračenja i simulacije skyshine zračenja prikazan je na slici 3 (crvena boja, spektar sa višim odbrojem).

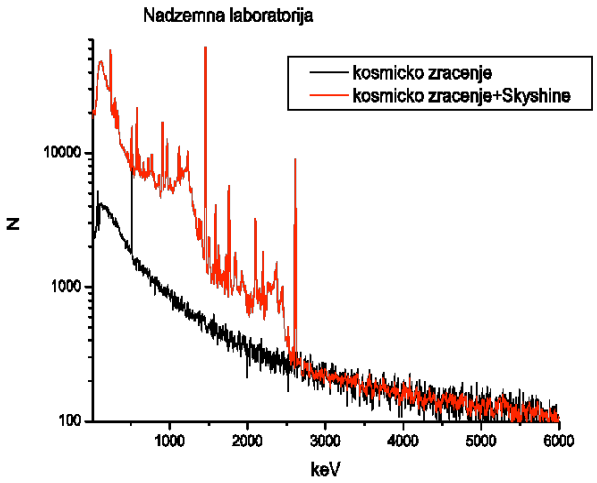

Slika 3. Simulacioni spektar HPGe detektora sa doprinosom kosmičkog zračenja i skyshine i samo doprinosom kosmičkog zračenja – nadzemna laboratorija

Sličnost simulacionog i eksperimentalnog spektra u prikazanim prvim rezultatima nije zanemarljiva. Iako simulacioni spektar u značajnoj meri ne odgovara eksperimentalnom, traba istaći da postoji dosta mesta za unapredjenje i popravku simulacije. Prvi rezultati ohrabruju, i treba nastaviti sa detaljnijim simulacijama da bi se poboljšalo slaganje eksperimenta i simulacije.
Nedostaci prvih rezultata simulacija odgovora HPGe detektora na skyshine simulacije u velikoj meri dolaze od toga što je odnos intenziteta linija određen samo po maksimumu linija a ne integralu linija, potom nedostaci dolaze od toga što je kriva efikasnosti HPGe detektora dobijena simulacijama tačkastih izvora, zanemarujući da zračenje dolazi iz cele polu-sfere iznad detektora, slika 2. Potom nedostaci dolaze od toga što je geometrija laboratorijskih zidova i materijala bila veoma aproksimativna i pojednostavljena, kao i da su u cilju ubrzavanja simulacija, kako bi se dobio prvi rezultat, odabrani pojednostavljeni modeli niskoenergetskih interakcija u Geant4 programskom paketu.

4. ZAKLJUČAK

U ovom radu su prikazani prvi rezultati Monte Karlo simulacija odgovora HPGe detektora na upadno kosmičko zračenje, doprinos od radionuklida iz okoline i doprinos od skyshine zračenja. Rezultati simulacija kosmičkog zračenja dobro se slažu sa eksperimentalnim rezultatima. Prednost simulacija koje daju razloženi fon na tri komponente, omogućavaju da se rezultati simulacija neke od tri komponente fona za jednu laboratoriju mogu koristiti za druge podzemne ili nadzemne laboratorije. Na primer, ako je HPGe detektor sličan i nalazi se u sličnoj zaštiti ali drugoj laboratoriji može da se koristite postojeći rezultati simulacija na doprinos od radionuklida i skyshine zračenja, potom ako su laboratorije na sličnoj geografskoj širini i dužini i nadmorskoj visini može se koristiti ista simulacija doprinosa od kosmičkog zračenja. Delovi simulacija koji ne mogu da se koriste ponovo, simuliraju se koristeći iste simulacione

programime samo sa modifikovanim parametrima (nadmorska visina, geometrija laboratorije i dr.). Tako se fon koji dolazi od kosmičkog zračenja može simulirati za laboratorije koje mogu biti na različitoj geografskoj dužini i širini i nadmorskoj visini menjanjem parametara u simulaciji CORSIKA programskim paketom). Ako laboratorije imaju različit sastav radionuklida u zemljištu i različitu geometriju laboratorije u kojoj se vrše merenja, simulira se modifikovanjem postavki Geant4 programa za simulaciju HPGe detektora. U radu su predstavljeni nedostaci simulacija i načinkako se rezultati mogu poboljšati radeći na detaljima u nekoliko faza simulacije.

5. ZAHVALNICA

Ovaj rad je urađen uz pomoć Ministarstva prosvete, nauke i tehnološkog razvoja Republike Srbije unutar projekta osnovnog istraživanja pod oznakom OI171002.

6. LITERATURA

[1] Dragic Aleksandar, Udovicic Vladimir, Banjanac Radomir, Jokovic Dejan, Maletic Dimitrije, Veselinovic Nikola, Savic Mihailo, Puzovic Jovan, Anicin Ivan V. The New Set-Up in the Belgrade Low-Level and Cosmic-Ray Laboratory. *NTRP*, vol. 26, br. 3, 2011, 181-192.
[2] S. Agostinelli et al. Geant4 - a simulation toolkit. *NIMA*. 506, 2003, 250-303.
[3] D. Heck, J. Knapp, J.N. Capdevielle, G. Schatz, T. Thouw. CORSIKA: A Monte Carlo Code to Simulate Extensive Air Showers, *Forschungszentrum Karlsruhe Report, 6019*, 1998.
[4] Banjanac Radomir, Maletic Dimitrije, Jokovic Dejan, Veselinovic Nikola, Dragic Aleksandar, Udovicic Vladimir, Anicin Ivan. On the omnipresent background gamma radiation of the continuous spectrum*, NIMA*. 745, 2014, 7-11.

MONTE KARLO SIMULATION OF HPGE DETECTOR BACKGROUND COMING FROM RADIONUCLIDS, COSMIC AND SKYSKINE RADIATION

Dimitrije MALETIĆ, Vladimir UDOVIČIĆ, Dejan JOKOVIĆ, Radomir BANJANAC, Aleksandar DRAGIĆ, Mihailo SAVIĆ, Nikola VESELINOVIĆ
Institute of Physics,University of Belgrade

ABSTRACT
In the Low Background Laboratory for Nuclear Physics background radiation of the HPGe detector was researched. This research is important for experiments with small number of interesting events or rare processes studied in underground laboratories. The background radiation research started with research of background from radionuclides and Cosmic rays using coincidence techniques. Recently, the skyshine radiation was researched. In this paper the Monte Carlo simulation of HPGe background is presented. Results for cosmic ray simulations agree very good with the experimental results, and for others can be improved. The simulation for other ground and underground laboratories can be done, by changing longitude, latitude and elevation, composition of radionuclides in soil. The possible improvements of the simulations are discussed.

ДРУШТВО ЗА ЗАШТИТУ ОД ЗРАЧЕЊА
СРБИЈЕ И ЦРНЕ ГОРЕ

ЗБОРНИК РАДОВА

XXX СИМПОЗИЈУМ ДЗЗСЦГ
Дивчибаре
2- 4. октобар 2019. године

Београд
2019. године

DISTRIBUCIJA KONCENTRACIJE RADONA PO SPRATNOSTI STAMBENIH ZGRADA

Vladimir UDOVIĈIĆ[1], Dimitrije MALETIĆ[1], Aleksandar DRAGIĆ[1], Radomir BANJANAC[1], Dejan JOKOVIĆ[1], Nikola VESELINOVIĆ[1], Mihailo SAVIĆ[1], David KNEŢEVIĆ[1] i Maja EREMIĆ-SAVKOVIĆ[2]

1) Institut za fiziku u Beogradu, Institut od nacionalnog značaja za Republiku Srbiju, Beograd, Srbija, udovicic@ipb.ac.rs, maletic@ipb.ac.rs, dragic@ipb.ac.rs, banjanac@ipb.ac.rs, yokovic@ipb.ac.rs, veselinovic@ipb.ac.rs, msavic@ipb.ac.rs, davidk@ipb.ac.rs

2) Direktorat za radijacionu i nuklearnu sigurnost i bezbednost Srbije, Beograd, Srbija, eremic.savkovic@srbatom.gov.rs

SADRŢAJ

Dobro je poznato da je jedan od faktora koji utiče na varijabilnost radona u zatvorenom prostoru spratnost stambenih zgrada. Imajući u vidu činjenicu da glavni izvor radona u zatvorenim prostorijama potiče iz zemljišta, očekuje se smanjenje koncentracije radona na višim spratovima. Na višim spratovima dominantan izvor radona potiče od graĎevinskog materijala, a u nekim slučajevima moţe doći do odstupanja od ove opšte utvrĎene pravilnosti. S druge strane, varijabilnost radona zbog spratnosti, posebno u velikim gradovima, sa mnogo većim brojem visokih zgrada i gustinom naseljenosti u poreĎenju sa ruralnim sredinama, moţe uticati na procenu kolektivne doze koja potiče od radona. U tom smislu, a u svrhu naših istraţivanja, izabrali smo jednu tipičnu porodičnu kuću sa potkrovljem i jedan šesnaestospratni soliter. Merenje koncentracije radona u odabranim stambenim objektima izvršeno je sa dva aktivna ureĎaja. Jedan je bio fiksiran u dnevnoj sobi u prizemlju, a drugi je menjao poziciju po spratovima u stambenim zgradama. Svaki merni ciklus na datom spratu trajao je sedam dana uz vreme uzorkovanja od dva sata. U ovom radu detaljno je uraĎena analiza dobijenih rezultata.

1. Uvod

Izvori radona u stambenim i poslovnim zgradama su, pre svega iz zemljišta, graĎevinskog materijala i vode. S obzirom na prirodu nastanka i svih pomenutih izvora, koncentracija radona je veša u prizemnim prostorijama u odnosu na stanove na višim spratovima stambenih objekata. U literaturi se moţe pronaši dosta radova koji se bave uticajem raznih faktora na nivo i varijabilnost radona u zatvorenim prostorijama, pa izmeĎu ostalih i uticajem spratnosti [1-4]. U sluţaju velikih stambenih objekata sa većim brojem spratova, moţe se uoţiti odstupanje od opšte pravilnosti, jer je na višim spratovima dominantan izvor radona graĎevinski materijal, te se mogu uoţiti povešane koncentracije radona u odnosu na situaciju na niţim spratovima. U tom smislu, uraĎena su merenja radona u dva tipiţna stambena objekta. Izbor zgrada je baziran na rezultatatima iz monografije „Nacionalna tipologija stambenih zgrada Srbije―grupe autora sa Arhitektonskog fakulteta [5]. S obzirom na specifiţnosti gradnje u Srbiji, broj

tipova zgrada je tako sveden na šest kategorija, dve za porodiţno stanovanje i ţetiri kategorije za kolektivno stanovanje; porodiţno stanovanje: 1. slobodnostoješa kuša, 2. kuša u nizu i kolektivno stanovanje: 3. slobodnostoješa zgrada, 4. zgrada u nizu, 5. zgrada u nizu tipa lamele (ponavlja se više zgrada raŤenih po istom projektu, zgrada sa više ulaza...) i 6. soliter (slobodnostoješa zgrada velike spratnosti). Pokazuje se da više od 97% svih stambenih zgrada ţine samostoješe porodiţne kuše. TakoŤe, za sve definisane tipove zgrada broj spratova se kreše od jednog do osam, pri ţemu su samostoješe porodiţne kuše uglavnom prizemne (37%) ili prizemne sa potkrovljem (26%), dok je veoma niska zastupljenost kuša koje imaju više od dva sprata (5%), sa proseţnom visinom porodiţnih zgrada od 1,4 [5].

2. Eksperimentalna postavka

Izabrana su dva stambena objekta, jedan iz grupe za porodično stanovanje i jedan soliter iz grupe za kolektivno stanovanje. Porodična kuća (slika 1) ima karakterističan stil gradnje u kome se kuća gradi više godina uz konstantno dograđivanje i nadogradnju, što potencijalno može biti izvor ulaska radona u takve kuće. Kuća ima podrum i izgrađena je od standardnih materijala (cigla-blok, beton, malter). Na kraju je urađena i izolacija korišćenjem stiropora debljine 5 cm. U kući su već vršena višegodišnja merenja koncentracije radona različitim metodama, o čemu je do sada publikovano nekoliko naučnih radova [6-8].

Slika 1. Tipična porodična kuća u Beogradu.

Iz grupe stambenih zgrada za kolektivno stanovanje izabran je soliter na Novom Beogradu (slika 2). IzgraŤen je šezdesetih godina prošlog veka, blokovskog tipa. Soliter ima podrum, dok se u prizemlju nalaze lokali i poslovne prostorije. Stanovi se nalaze od prvog sprata pa naviše. Soliter ima 16. spratova.

Slika 2. Soliter na Novom Beogradu.

Vremenske serije merenih koncentracija radona u ispitivanim stambenim objektima dobijene su pomošu dva aktivna ureĎaja SN1029 i SN1030 (proizvoĎača Sun Nuclear Corporation). To su merni ureĎaji jednostavne konstrukcije i primene u praksi. U suštini, radi se o brojaču sa dodatkom senzora za merenje meteoroloških parametara. Nedostatak ureĎaja je nemogušnost merenja koncentracije radona u zemljištu i vodi. Operater može podesiti vremenske sekvence od 0,5 do 24 sati. Jedan ciklus merenja može trajati 1000 sati ili ukupno 720 vremenskih sekvenci (broj sukcesivnih merenja, odnosno tačaka u vremenskoj seriji). UreĎaji su bili podešeni da rade u vremenskoj sekvenci od 2 sata. Jedan je bio fiksiran u dnevnoj sobi u prizemlju, a drugi je menjao poziciju po spratovima u stambenim zgradama. Svaki merni ciklus na datom spratu trajao je sedam dana.

3. Rezultati i diskusija

Na slikama 3 i 4 su prikazani dobijeni rezultati merenja, kako vremenske serije tako i usrednjene koncentracije radona u ispitivanim stambenim objektima za zadati ciklus merenja od sedam dana.
S obzirom da je detektor koji je sve vreme stajao u prizemlju solitera pokazao neobično niske vrednosti za koncentraciju radona, uradili smo uporedno merenje sa drugim detektorom u susednom, kao i u stanu u kome se nalazio fiksirani detektor. Dobijeni rezultati pokazuju izvesnu razliku, ali s obzirom da se radi o domenu izrazito niskih nivoa radona, pretpostavka je da su i merne nesigurnosti velike.

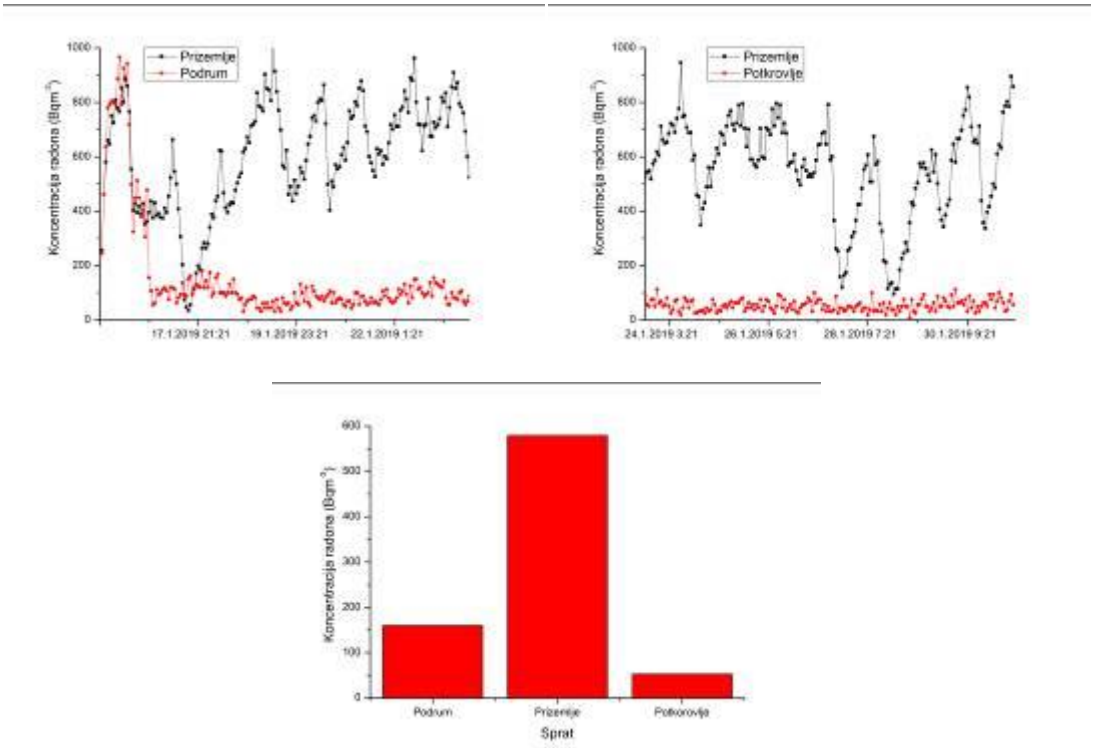

Slika 3. Vremenske serije i srednja koncentracija radona po spratovima u porodičnoj kući.

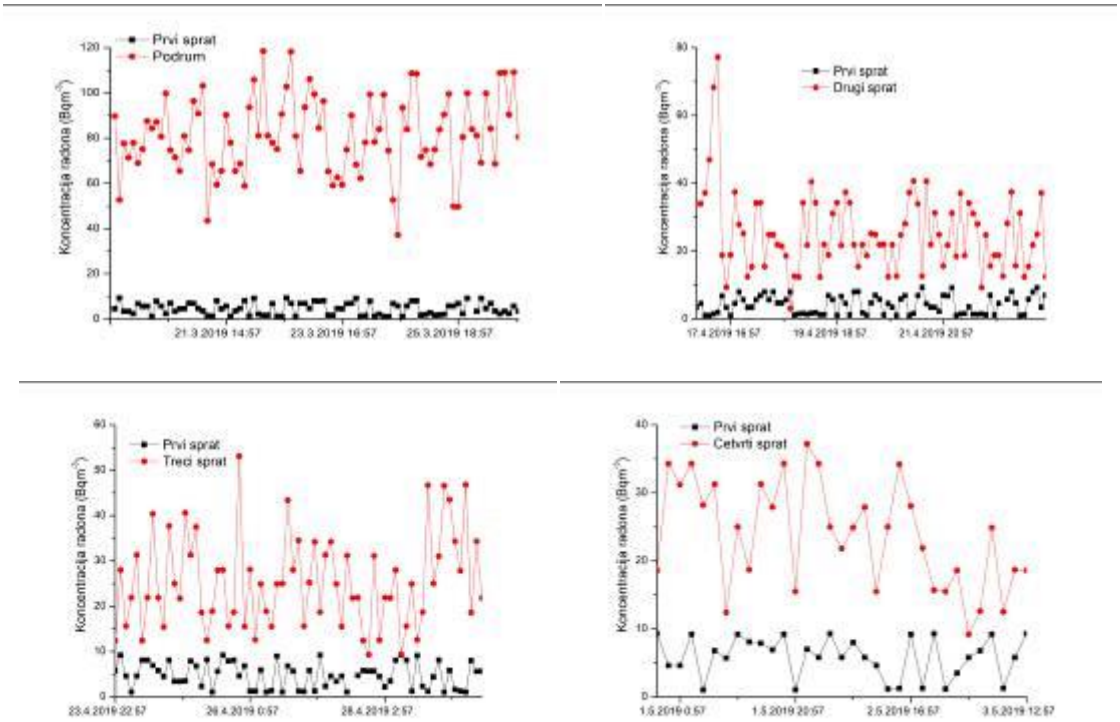

Slika 4. Vremenske serije i srednja koncentracija radona po spratovima u soliteru.

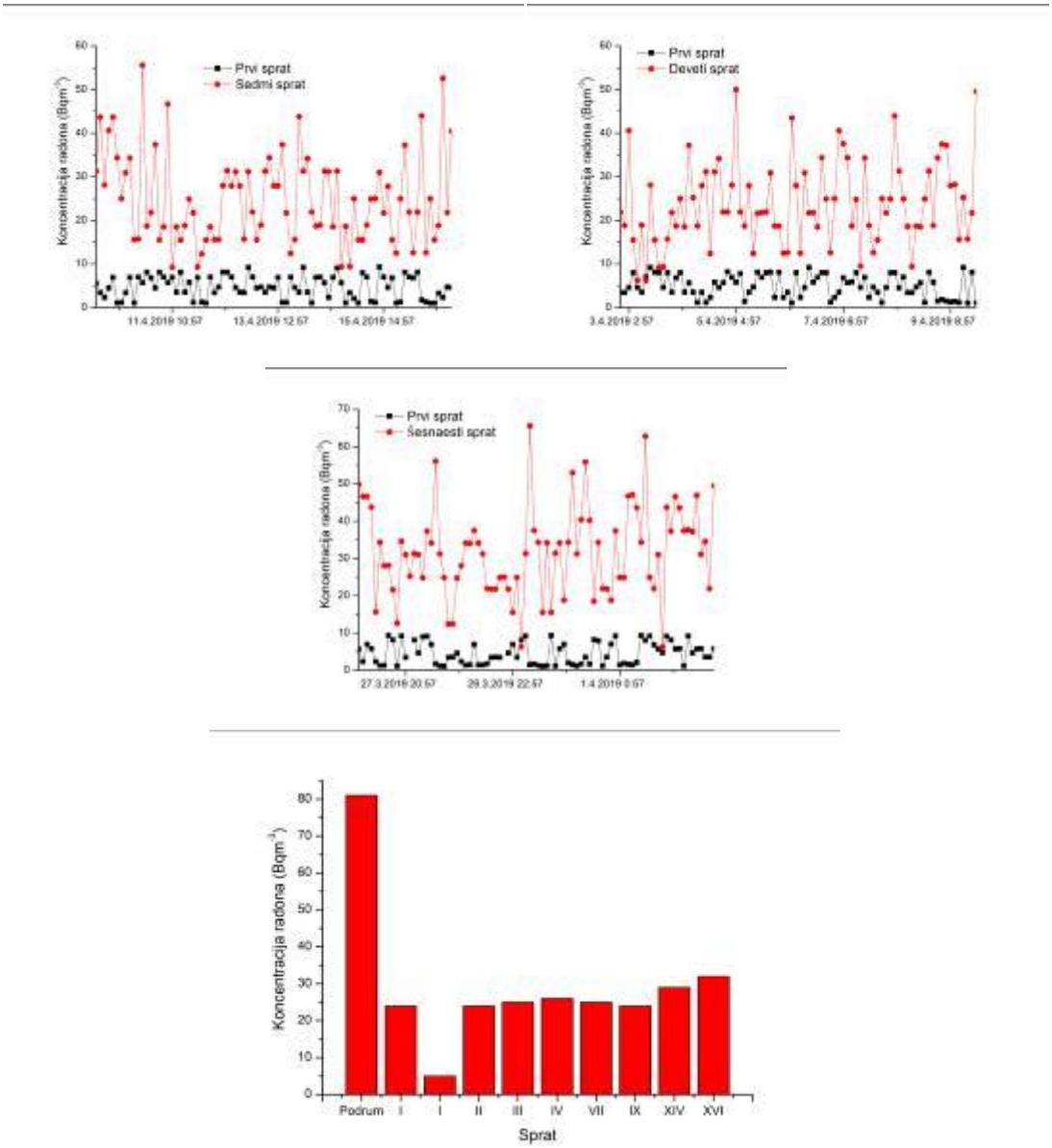

Slika 4. Nastavak.

4. Zaključak

Dobijeni rezultati pokazuju da je ponašanje radona u dva različita stambena objekta dijametralno suprotno. U porodičnoj kući je moguće uočiti izrazite varijacije koncentracije radona uz jednodnevnu periodiku. Takođe, interesantan je odnos koncentracije radona u prizemlju, u odnosu na podrum kuće, koji je suprotan od uobičajene situacije kod kuća sa podrumom. Ovo inverzno ponašanje može se protumačiti činjenicom da podrum ne prekriva celo prizemlje već njegov manji deo. Ostali deo prizemlja je pokriven betonskom pločom kao podlogom, ali sa pukotinama i lošim spojem sa zidovima predstavlja potencijalni izvor povišenog radona. Kod solitera je situacija suprotna i može se smatrati da već od prvog sprata dominantan izvor radona je građevinski materijal. Čak se može uočiti blagi rast srednje koncentracije radona na

višim spratovima. No, dobijeni rezultati u soliteru se mogu predvideti, a na osnovu rada grupe autora koji su odredili interno izlaganje iz graЂevinskog materijala, koji se koristi u Srbiji, a koje potiţe od eshalacije radona i torona [9].

5. Zahvalnica

Ovaj rad je realizovan uz podršku Ministarstva prosvete, nauke i tehnološkog razvoja Republike Srbije u okviru projekta pod brojem III43002.

6. Literatura

[1] F. Bochicchio, G. Campos-Venuti, S. Piermattei, C. Nuccetelli, S. Risica, L. Tommasino, G. Torri, M. Magnoni, G. Agnesod, G. Sgorbati, M. Bonomi, L. Minach, F. Trotti, M.R. Malisan, S. Maggiolo, L. Gaidolfi, C. Giannardi, A. Rongoni, M. Lombardi, G. Cherubini, S. D'Ostilio, C. Cristofaro, M. Pugliese, V. Martucci, A. Crispino, P. Cuzzocrea, A. Sansone Santamaria, M. Cappai. Annual average and seasonal variations of residential radon concentration for all the Italian Regions. *Radiat. Meas.* 40, 2005, 686-694.

[2] H. Friedmann. Final Results of the Austrian Radon Project. *Health Phys.* 89(4), 2005, 339-348.

[3] R. Borgoni, D. De Francesco, D. De Bartolo, N. Tzavidis. Hierarchical modeling of indoor radon concentration: how much do geology and building factors matter? *J. Environ. Radioact*. 138, 2014, 227-237.

[4] M. Lorenzo-González, A. Ruano-Ravina, J. Peón, M. Piñeiro, J. Miguel Barros-Dios. Residential radon in Galicia: a cross-sectional study in a radon-prone area. *J. Radiol. Prot*. 37(3), 2017, 728-741.

[5] M. Jovanoviš Popoviš, D. Ignjatoviš, A. Radivojeviš, A. Rajţiš, N. Šukoviš Ignjatoviš, Lj. Đukanoviš, M. Nediš. National Typology of Residential Buildings in Serbia, Faculty of Architecture University of Belgrade, Belgrade, 2013, ISBN 978-86-7924-102-3.

[6] V. Udoviţiš, D. Maletiš, R. Banjanac, D. Jokoviš, A. Dragiš, N. Veselinoviš, J. Ţivanoviš, M. Saviš, S. Forkapiš. Multiyear Indoor Radon Variability in a Family House – a Case Study in Serbia. *Nucl. Tech. Radiat. Protect*. XXXIII (2), 2018, 174-179.

[7] D. Maletiš, V. Udoviţiš, R. Banjanac, D. Jokoviš, A. Dragiš, N. Veselinoviš, J. Filipoviš. Comparison of multivariate classification and regression methods for indoor radon measurements. *Nucl. Tech. Radiat. Protect.* 29, 2014, 17-23.

[8] J. Filipoviš, D. Maletiš, V. Udoviţiš, R. Banjanac, D. Jokoviš, M. Saviš, N. Veselinoviš. The use of multivariate analysis of the radon variability in the underground laboratory and indoor environment. *Nukleonika* 61(3), 2016, 357-360.

[9] P. Ujiš, I. Ţelikoviš, A. Kandiš, I. Vukanac, M. Đuraševiš, D. Dragosavac, Z. S. Ţuniš. Internal exposure from building materials exhaling ^{222}Rn and ^{220}Rn as compared to external exposure due to their natural radioactivity content. *Appl. Radiat. Isot.* 68, 2010, 201–206.

INDOOR RADON DISTRIBUTION DUE TO FLOOR LEVEL IN THE RESIDENTIAL BUILDINGS

Vladimir UDOVICIC[1], Nikola VESELINOVIC[1], Dimitrije MALETIC[1], Radomir BANJANAC[1], Aleksandar DRAGIC[1], Dejan JOKOVIC[1], Mihailo SAVIC[1], David KNEZEVIC[1] and Maja EREMIC-SAVKOVIC[2]

1) Institute of Physics Belgrade, University of Belgrade, Belgrade, Serbia, udovicic@ipb.ac.rs, maletic@ipb.ac.rs, dragic@ipb.ac.rs, banjanac@ipb.ac.rs, yokovic@ipb.ac.rs, veselinovic@ipb.ac.rs, msavic@ipb.ac.rs, davidk@ipb.ac.rs

2) Serbian Radiation and Nuclear Safety and Security Directorate, Belgrade, Serbia, eremic.savkovic@srbatom.gov.rs

ABSTRACT

It is well known that one of the factors influencing indoor radon variability is the floor level of residential buildings. Bearing in mind the fact that the main source of indoor radon is from radon in soil gas, a radon concentration on upper floors is expected to decrease. On the upper floors, the dominant source of radon originates from building materials, and in some cases there may be deviations from this generally established regularity. On the other hand, radon variability due to floor level, especially in large cities, with a much larger number of high buildings and density of population compared to rural areas, can affect the estimation of the collective dose derived from radon. In this sense, and for the purpose of our research, we chose a typical family house with a loft and sixteen high-rise building. Indoor radon measurements in selected residential buildings were done with two active devices. One was fixed in the living room on the ground floor, while the other was changing the position on the floors in residential buildings. Each measuring cycle on the floor lasted for seven days with a sampling time of two hours. In this paper, an analysis of the obtained results has been done in detail.

PROCENA TEMPERATURSKOG PROFILA ATMOSFERE NA OSNOVU DETEKTOVANOG FLUKSA KOSMIČKIH MIONA

Mihailo SAVIĆ, Vladimir UDOVIĈIĆ, Dimitrije MALETIĆ, Aleksandar DRAGIĆ, Radomir BANJANAC, Dejan JOKOVIĆ, Nikola VESELINOVIĆ i David KNEŢEVIĆ
Institut za fiziku u Beogradu, Institut od nacionalnog znaţaja za Republiku Srbiju, Beograd, Srbija, *msavic@ipb.ac.rs*, *udovicic@ipb.ac.rs*, *maletic@ipb.ac.rs*, *dragic@ipb.ac.rs*, *banjanac@ipb.ac.rs*, *yokovic@ipb.ac.rs*, *veselinovic@ipb.ac.rs*, *davidk@ipb.ac.rs*

SADRŢAJ
Uticaj atmosferskih parametara na intenzitet mionske komponente sekundarnog kosmičkog zračenja dobro je poznat. Dominantan doprinos varijaciji fluksa kosmičkih miona usled atmosferskih parametara daju dva meteorološka efekta - barometarski (usled varijacije atmosferskog pritiska) i temperaturski (usled varijacije temperature atmosfere). Postoji više teorijskih i empirijskih modela koji dobro opisuju ove zavisnosti. Obično se na osnovu ovih modela vrši korekcija kako bi se eliminisala varijacija fluksa kosmičkih miona atmosferskog porekla.
Obrnuto, osetljivost mionskih detektora na varijacije atmosferskih parametara moţe se iskoristiti da se na osnovu poznatih parametara modela i poznatog odbroja kosmičkih miona odredi temperatura različitih nivoa atmosfere. U ovom radu ćemo demonstrirati ovaj pristup na osnovu podataka merenih mionskim monitorima Niskofonske laboratorije za nukelarnu fiziku Instituta za fiziku u Beogradu i primenom empirijskog modela meteoroloških efekata, zasnovanog na tehnici dekompozicije na osnovne komponente.

1. Uvod

Intenzitet pljuskova sekundarnog kosmiţkog zraţenja zavisi od atmosferskih meteoroloških parametara. To se naroţito odnosi na mionsku komponentu sekundarnog kosmiţkog zraţenja. Dva efekta dominantno utiţu na fluks sekundarnih miona: barometarski koji opisuje antikorelaciju fluksa kosmiţkih miona sa atmosferskim pritiskom [1] i temperaturski koji se odnosi na uticaj varijacije atmosferske temperature na detektovani intenzitet miona [2].
Osim fundamentalnog, detaljno poznavanje meteoroloških efekata ima znaţaj u proceduri korekcije na date efekte, ţime se povešava osetljivost zemaljskih detektora kosmiţkog zraţenja na varijacije neatmosferskog porekla. Alternativno, dobar model meteoroloških efekata bi u principu omogušio predviĎanje atmosferskih parametara na osnovu merenja fluksa miona. Ovo je potencijalno znaţajno za odreĎivanje temperatura pojedinih slojeva atmosfere u sluţaju da su druge metode nedostupne.
Postoji više predloţenih metoda za predikciju atmosferskih meteoroloških parametara na osnovu merenja intenziteta kosmiţkog zraţenja zemaljskim detektorima. Mogu se

bazirati na merenju različitih komponenti fluksa kosmičkih miona [3, 4], simultanom merenju neutronske i mionske komponente [5] ili upotrebi mionskog teleskopa sposobnim da meri ugaonu distribuciju intenziteta [6]. Sve pomenute metode karakteriše relativna kompleksnost eksperimentalne postavke i analize. Takođe, zajedničko svim pomenutim metodama je da se u proceduri određivanja atmosferskih temperatura oslanjaju na teorijski izračunate koeficijente za opisivanje zavisnosti inenziteta miona od temperaturskog profila atmosfere. Ovaj pristup ima određenih ograničenja usled nužno aproksimativnog karaktera i neprilagođenosti konkretnom detektorskom sistemu.
U ovom radu, mi šemo demonstrirati upotrebljivost jednostavnije eksperimentalne postavke i primenu empirijskog modela meteoroloških efekata na određivanje temperaturskog profila atmosfere.

2. Eksperimentalni podaci i obrada

U Niskofonskoj laboratoriji za nuklearnu fiziku Instituta za fiziku u Beogradu mionski fluks se meri kontinualno od 2009. godine, na nivou zemlje i na dubini od 25 m.w.e. Eksperimentalna postavka se sastoji od scintilacionog detektora i sistema za akviziciju. Detektor je plastični scintilator dimenzija 100cm×100cm×5cm sa četiri fotomultiplikatora postavljena na šoškove. U srcu sistema za akviziciju nalazi se brzi analogno-digitalni konverter sposoban da u realnom vremenu precizno određuje vreme detekcije i amplitudu signala [7]. U ovoj analizi korišćeni su podaci snimljeni detektorom na nivou zemlje u periodu od 01.06.2010. do 31.05.2011. godine.
Za opisivanje meteoroloških efekata na kosmičke mione, u okviru Niskofonske laboratorije razvijen je empirijski model baziran na tehnici dekompozicije na osnovne komponente (Principal Component Analisys - PCA) [8]. Metod se zasniva na ideji da se u analizi meteoroloških efekata sa skupa visoko korelisanih meteoroloških parametara prelaze na skup linearno nezavisnih promenljivih, kao i potencijalno smanji dimenzionalnost problema zadržavanjem samo statistički značajnih osnovnih komponenti u analizi. Koeficijenti zavisnosti detektovanog odbroja miona od tako određenih osnovnih komponenti su pouzdaniji, jer su manje podložni statističkim fluktuacijama. Ovde šemo primeniti ovaj model kako bismo na osnovu odbroja miona merenog u nadzemnoj laboratoriji odredili temperature različitih nivoa atmosfere.
Neka je C_X matrica tipa $n\times m$ koja predstavlja m merenja n različitih meteoroloških parametara. Dekompozicijom na osnovne komponente se sa skupa n meteoroloških varijabli prelazi na skup n osnovnih komponenti, čije vrednosti su reprezentovane matricom C_Y, takođe tipa $n\times m$. Ova relacije se može prestaviti jednačinom:

$$C_Y = PC_X, \tag{1}$$

gde je P matrica transformacije čiji redovi predstavljaju kompoziciju osnovnih komponenti.
Na slici 1 prikazana je kompozicija prvih 9 osnovnih komponenti. Na x-osi su meteorološke promenljive: pritisak, temperature 24 izobarna nivoa (10, 20, 30, 50, 70, 100, 150, 200, 250, 300, 350, 400, 450, 500, 550, 600, 650, 700, 750, 800, 850, 900, 925 i 975 *mb*) i temperatura na nivou tla. Na y-osi su prikazane vrednosti kosinusa uglova rotacije pri prelasku sa skupa meteoroloških varijabli na skup osnovnih komponenti.

Na osnovu stitistiţke i korelacione analize zaključeno je da su za meteorološke efekte od značaja samo pet osnovnih komponenti, i to komponente 1, 3, 4, 5 i 6 [8].
Zavisnost varijacije detektovanog odbroja miona od ovih komponenti, usled meteoroloških efekata, data je jednaţinom:

$$\delta N|_{PC} = \sum_i k_i PC_i, \quad i = 1,3,4,5,6 \tag{2}$$

gde su PC_i osnovne komponente a k_i odgovarajuši koeficijenti.
Pomošu ove relacije u principu je moguše proceniti vrednosti osnovnih komponenti na osnovu poznatog odbroja.
Dalje, transformišuši jednaţinu 1 kao:

$$C_X = P^{-1} C_Y = P^T C_Y \tag{3}$$

na osnovu procenjenih vrednosti osnovnih komponenti sada je moguše odrediti procenjene vrednosti meteoroloških parametara.

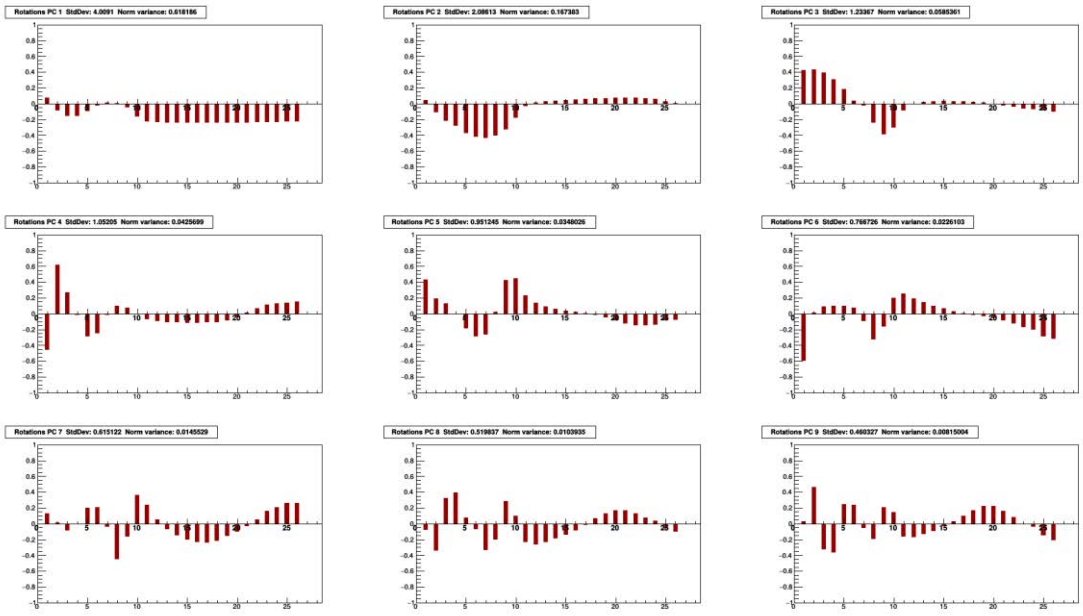

Slika 1. Kompozicija prvih devet osnovnih komponenti. Na x-osi su meteorološke promenljive: pritisak, temperature 24 izobarna nivoa (10, 20, 30, 50, 70, 100, 150, 200, 250, 300, 350, 400, 450, 500, 550, 600, 650, 700, 750, 800, 850, 900, 925 i 975 *mb*) i temperatura na nivou tla. Na y-osi su prikazane vrednosti uglova rotacije.

3. Rezultati i diskusija

Za pomenuti referentni period odreŤeni su koeficijenti u jednaţini 2, uzimajuši u obzir samo geomagnetno mirne dane [8]. Pomošu ovako odreŤenih koeficijenata i merenog odbroja odreŤene su procenjene vrednosti za pet signifikantnih osnovnih komponenti za ceo referentni period. Zatim su na osnovu jednaţine 3 odreŤene procenjene vrednosti meteoroloških parametara. Na slici 2 prikazane su vremenske serije merenih i procenjenih vrednosti meteoroloških parametara za izabrane izobarne nivoe.

Zbog preglednosti, prikazani su grafici za ţetiri razliţita nivoa. Kao referentni izabrani su nivoi od 30 mb (stratosfera), 150 mb (tropopauza/gornja troposfera), 350 mb (troposfera) i 975 mb (u blizini zemlje). Na plotovima crvenom linijom prikazane su merene vrednosti a svetlo zelenom vrednosti procenjene na osnovu merenog odbroja miona. TakoŤe, kako bi se dala jasnija slika i smanjio efekat fluktuacija merenog odbroja, vremenska serija predvidjenih vrednosti je smutovana (*smoothing*) i prikazana na graficima tamno zelenom bojom.

Na slici 3 prikazana je raspodela razlika merenih i procenjenih vrednosti meteoroloških parametara.

Osim analize vremenskih serija, još jedan kriterijum za odreŤivanje efikasnosti predviŤanja temperature pojedinih nivoa mogao bi biti na osnovu širine prikazanih raspodela. MeŤutim, varijacija temperatura razliţitih nivoa nije ista tako da ovo moţe dati nepotpunu sliku. Stoga su u tabeli 1 prikazane vrednosti standardnih devijacija ovih raspodela, standardnih devijacija merenih vrednosti, kao i relativan odnos ove dve veliţine koji daje bolji uvid u efikasnost predikcije temperatura pojedinih nivoa atmosfere.

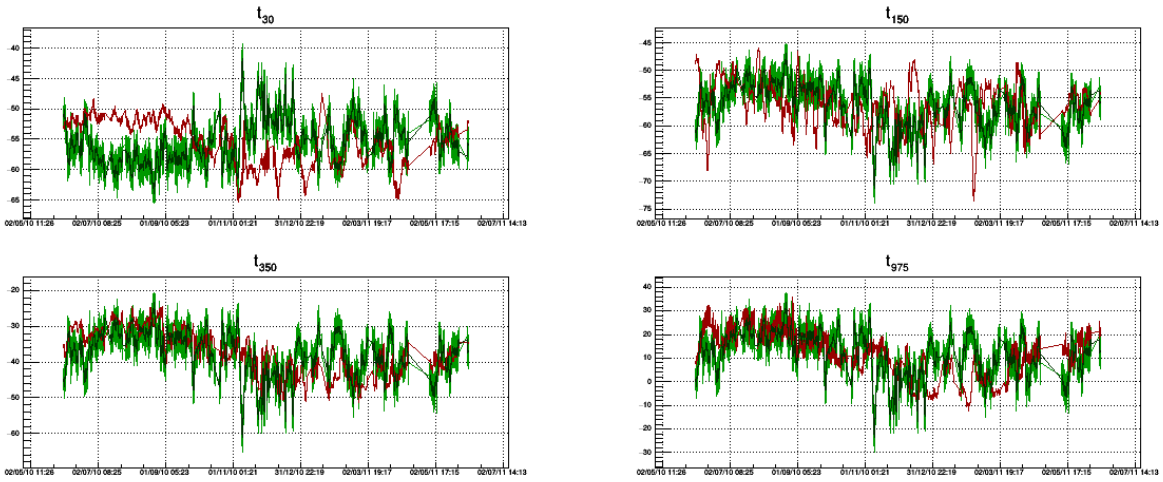

Slika 2. Vremenske serije merenih i procenjenih vrednosti meteoroloških parametara za izobrne nivoe od 30, 150, 350 i 975 mb. Merene vrednosti - crvena linija, procenjene - svetlo zelena linija i smutovane procenjene - tamno zelena linija.

Na osnovu predstavljenih grafika i tabela moţemo videti da se najbolje slaganje dobija za sloj atmosfere od 300 do 600 *mb*. Nešto slabije slaganje dobija se za nivoe u blizini tla, što je u skladu sa kompleksnijom dinamikom temperatura u ovih slojevima, kao i za slojeve od 100 do 200 mb, u kojima dominantno dolazi do produkcije miona. Ovaj drugi podatak je moguša posledica ţinjenice da je za mione detektovane na površini zemlje znaţajniji negativni temperaturski efekat, asociran sa jonizacionim gubicima i verovatnošom raspada miona u niţim slojevima atmosfere, dok pozitivni temperaturski efekat u vezi sa verovatnošom nastanka miona u sloju izmeŤu 100 i 200 mb ima manji doprinos. Najslabije slaganje dobija se za neke od nivoa u stratosferi i tropopauzi, što se moţe videti na primeru temperature nivoa od 30 mb koji je u znaţajnom delu godine antikorelisan sa procenjenom temperaturom. Ovo je moţda uslovljeno manjim varijacijama temperature na ovim nivoima kao i ţinjenicom da postoji znaţajna

varijacija temperature ovih nivoa koja nije korelisana sa intenzitetom kosmiţkih miona, sadrţana u osnovnoj komponenti 2 (slika 1).

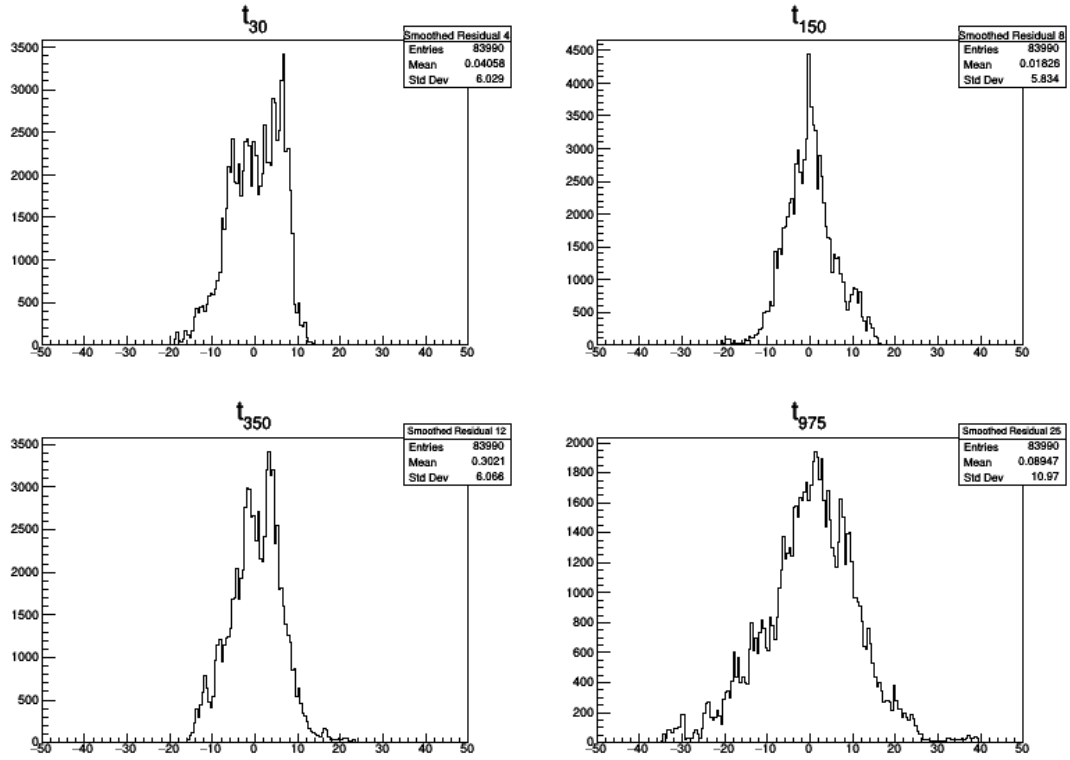

Slika 3. Raspodela razlika merenih i procenjenih vrednosti meteoroloških parametara za izobarne nivoe od 30, 150, 350 i 975 mb.

Tabela 1. Standardna devijacija raspodela razlika merenih i procenjenih vrednosti (σ_r), raspodele vrednosti merenih temperatura (σ_t) i relativan odnos ove dve vrednosti (σ_r/σ_t).

	t_{10}	t_{20}	t_{30}	t_{50}	t_{70}	t_{100}	t_{150}	t_{200}	t_{250}	t_{300}	t_{350}	t_{400}
σ_r	9,314	5,246	6,029	3,645	3,940	4,032	5,834	7,455	5,761	5,679	6,066	6,297
σ_t	7,154	4,844	3,669	3,320	2,862	3,055	4,012	5,754	5,111	5,658	6,237	6,460
σ_r/σ_t	1,302	1,083	1,643	1,098	1,377	1,320	1,454	1,296	1,127	1,004	0,973	0,975

t_{450}	t_{500}	t_{550}	t_{600}	t_{650}	t_{700}	t_{750}	t_{800}	t_{850}	t_{900}	t_{925}	t_{975}	t_{ground}
6,386	6,415	6,389	6,387	6,504	6,863	7,340	8,085	8,985	9,956	10,40	10,97	11,20
6,518	6,510	6,466	6,415	6,428	6,616	6,841	7,253	7,793	8,456	8,810	9,444	9,523
0,980	0,985	0,988	0,996	1,012	1,037	1,073	1,115	1,153	1,177	1,181	1,161	1,176

4. Zaključak

Preliminarna analiza je pokazala da postoji dosta dobro slaganje merenih i procenjenih atmosferskih temperatura za veši broj nivoa. Procenjene temperature imaju uglavnom konzistentne vremenske serije i dobro opisuju godišnju varijaciju. Najbolje slaganje sa merenim vrednostima dobija se u višim slojevima troposfere. Stoga, prikazani rezultati predstavljaju dobru polaznu osnovu za dalju analizu.

5. Zahvalnica

Ovaj rad je realizovan uz podršku Ministarstva prosvete, nauke i tehnološkog razvoja Republike Srbije u okviru projekta pod brojem OI 171002.

6. Literatura

[1] L. Myssowsky, L. Tuwim. Unregelmäßige Intensitätsschwankungen der Höhenstrahlung in geringer Seehöhe. *Zeitschrift für Physik* 39, 1926, 2-3.

[2] A Duperier. The Temperature Effect on Cosmic-Ray Intensity and the Height of Meson Formation. *Proc. Phys. Soc.* 61, 1948, 34-40.

[3] Y. Miyazaki. M. Wada. Simulation of cosmic ray variation due to temperature effect. *Acta phys. Acad. Sci. hung*. 29, 1970, 591-595.

[4] T. Kohno, K. Imai, A. Inue, M. Kodama, M. Wada. Estimation of the Vertical Profile of Atmospheric Temperature from Cosmic-Ray Components. *Proceedings of the 17th International Cosmic Ray Conference, held in Paris, France*. Volume 10., p.289.

[5] L.I. Dorman. *Cosmic Rays in the Earth's Atmosphere and Underground*, Springer 2004.

[6] V.V. Borog, O.V. Belonosova, A.S. Davydov, G.M. Kruchenitskii, S.P. Perov, V.G.Yanke. Study of Atmospheric Temperature at Different Altitudes using Muon Angular Distribution at Sea Level. *29th International Cosmic Ray Conference* Pune, 2005, 381-384.

[7] A. Dragic, V. Udovicic, R. Banjanac, D. Jokovic, D. Maletic, N. Veselinovic, M. Savic, J. Puzovic. The New Setup in the Belgrade Low-Level and Cosmic-Ray Laboratory. *Nucl. Tech. Radiat. Protect.* 26, 2011, 181-192.

[8] M. Saviš, A. Dragiš, D. Maletiš, N. Veselinoviš, R. Banjanac, D. Jokoviš, V. Udoviţiš. A novel method for atmospheric correction of cosmic-ray data based on principal component analysis. *Astropart. Phys.* 109, 2019, 1-11.

ATMOSPHERIC TEMPERATURE PROFILE ESTIMATION BASED ON MEASURED COSMIC RAY MUON FLUX

Mihailo SAVIĆ, Vladimir UDOVIĈIĆ, Dimitrije MALETIĆ, Aleksandar DRAGIĆ, Radomir BANJANAC, Dejan JOKOVIĆ, Nikola VESELINOVIĆ and David KNEŢEVIĆ

Institute of Physics Belgrade, University of Belgrade, Belgrade, Serbia,
msavic@ipb.ac.rs, udovicic@ipb.ac.rs, maletic@ipb.ac.rs, dragic@ipb.ac.rs, banjanac@ipb.ac.rs, yokovic@ipb.ac.rs, veselinovic@ipb.ac.rs, davidk@ipb.ac.rs

ABSTRACT

The effect of atmosphetic parameters in secondary cosmic ray muon component is well known. This is mainly through two dominant meteorological effects - barometric (due to atmospheric pressure variation) and temperature (due to atmospheric temperature variation). There are several theoretical and empirical models that describe these effects well. Usually this knowledge is used to correct for secondary cosmic ray variations due to atmospheric effects.

Alternatively, once model parameters are established, sensitivity of cosmic ray muon detectors to variations od atmospheric origin can be used to estimate temperatures for different layers of the atmosphere. In this work we will demonstrate this procedure using cosmic ray data measured in Low Background Laboratory for Nuclear Physics at Institute of Physics Belgrade, combined with parameters of empirical model for meteorological effects based on principal component analysis.

ЗБОРНИК РАДОВА

XXXI Симпозијум
Друштва за заштиту од зрачења
Србије и Црне Горе

06-08. октобар 2021.
Београд, Србија

SIMULACIJA PRODUKCIJE NEUTRONA MIONIMA IZ KOSMIČKOG ZRAČENJA U OLOVNOJ ZAŠTITI GERMANIJUMSKOG DETEKTORA

Dejan JOKOVIĆ, Dimitrije MALETIĆ, Vladimir UDOVIČIĆ, Radomir BANJANAC, Aleksandar DRAGIĆ, Mihailo SAVIĆ, Nikola VESELINOVIĆ i David KNEŽEVIĆ

Institut za fiziku u Beogradu, Univerzitet u Beogradu, Beograd, Srbija,
yokovic@ipb.ac.rs, maletic@ipb.ac.rs, udovicic@ipb.ac.rs, banjanac@ipb.ac.rs, dragic@ipb.ac.rs, msavic@ipb.ac.rs, veselinovic@ipb.ac.rs, davidk@ipb.ac.rs

SADRŽAJ

Zbog svojih osobina, olovo se uobičajeno koristi kao materijal za zaštitu germanijumskih detektora. Mioni iz kosmičkog zračenja u interakcijama sa olovom proizvode sekundarno zračenje, koje doprinosi ukupnom fonu detektora. Značajan deo ove komponente fona čine neutroni proizvedeni u interakcijama miona u olovnoj zaštiti. Neutroni mogu biti poseban problem u eksperimentima u dubokim podzemnim laboratorijama. U podzemnoj laboratoriji u Institutu za fiziku u Beogradu, germanijumski detektor, koji se nalazi u olovnoj zaštiti, može raditi u koincidenciji sa mionskim detektorom. U ovom režimu rada mogu se proučavati različiti efekti u germanijumskom detektoru izazvani mionima, posebno efekti koji potiču od neutrona proizvedenih mionima. Ovde su predstavljeni rezultati Geant4 simulacija produkcije neutrona u olovu mionima iz kosmičkog zračenja. Rezultat ovih simulacija je procena prinosa neutrona – broja proizvedenih neutrona u olovu po jedinici dužine puta – u interakcijama miona. Pored toga, određena je raspodela multipliciteta neutrona, kao broja proizvedenih neutrona u jednoj interakciji.

1. Uvod

U eksperimentima u kojima se traže retki događaji glavni problem je redukcija fonskog zračenja. Zato se ovi eksperimenti vrše u podzemnim laboratorijama, gde je fon u odnosu na površinu Zemlje znatno niži. Međutim, mioni iz kosmičkog zračenja su veoma prodorne čestice, prisutne i u dubokim podzemnim laboratorijama, i zato čine važan izvor fonskog zračenja u ovakvim osetljivim eksperimentima. Poseban problem je mionima indukovano sekundarno zračenje u detektorima i njihovoj okolini (detektorskoj zaštiti, zidovima, itd). Značajan doprinos fonu potiče od neutrona proizvedenih u interakcijama miona sa materijalom u okolini detektora [1].

U Niskofonskoj laboratoriji Instituta za fiziku u Beogradu intenzitet kosmičkog zračenja kontinuirano se meri od 2002. godine [2,3]. Geografski položaj laboratorije je takav da se kosmičko zračenje koje se detektuje u osnovi sastoji od mionske tvrde komponente, uz izvestan procenat meke elektromagnetne komponente. Laboratorija se sastoji od nadzemnog i plitko ukopanog podzemnog dela na dubini od 12 m ispod površine. Zemljište (les) iznad podzemne laboratorije ima gustinu približno 2,0 g/cm^3 – efektivni apsorpcioni sloj iznosi približno 25 hg/cm^3 (25 m.w.e.). Na toj dubini prisutna je praktično samo mionska komponenta kosmičkog zračenja. Zbog svojih niskofonskih karakteristika, laboratorija je osposobljena za izučavanja različitih pojava generisanih kosmičkim zračenjem, pre svega događaja indukovanih mionima iz kosmičkog zračenja u germanijumskim detektorima, kao i u pasivnoj zaštiti detektora.

U podzemnoj laboratoriji nalazi se HPGe detektor deklarisane aktivne zapremine 149 cm^3 i relativne efikasnosti 35 %. Podzemna pozicija detektora, zajedno sa olovnom

заштитом дебљне 12 cm, даје значајно смањење фонског зрачења. Поред пасивне заштите, за активну вето заштиту германијумског детектора могу се користити постојећи сцинтилациони детектори космичког зрачења. Пластични сцинтилациони детектор налази се неposредно изнад олovне заштите; димензије детектора су 100 cm × 100 cm × 5 cm. Оба детектора – HPGe и сцинтилациони – везани су за аналогно-дигитални конвертор, који омогућава снимање и чување свих детектованих догађаја. Сви догађаји анализирају се *off-line*. Уз одговарајуће селекционе критеријуме могу се издвојити сви коинцидентни и/или антикоинцидентни догађаји у сцинтилационом и HPGe детектору [4,5].

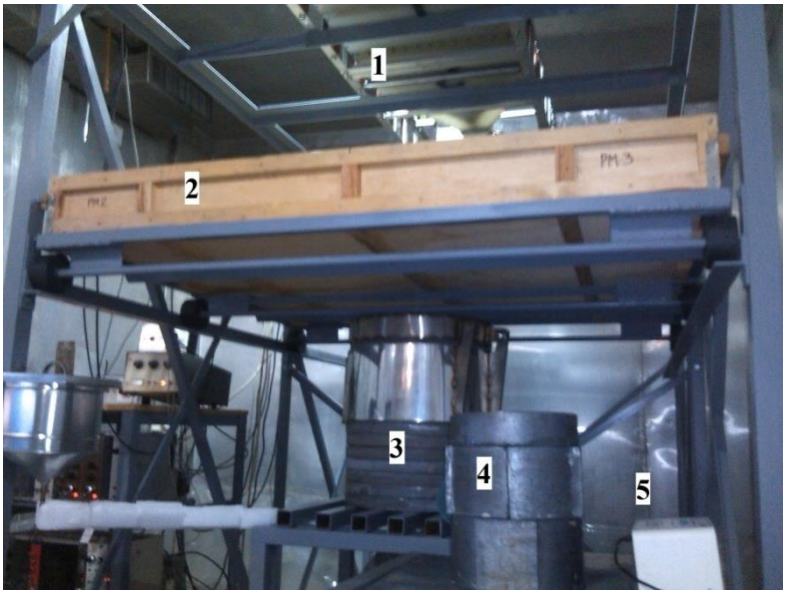

Слика 1. Екперименталнa конфигурација у подземној лабораторији: сцинтилациони детектори (1,2) и германијумски детектор у олovној заштити (3).

Први резултати мерења продукције неутрона мионима из космичког зрачења у олovној заштити HPGe детектора објављени су 2013. године. Подаци су снимани током више од 400 дана мерења, у коинцидентном режиму рада сцинтилатор-HPGe детектор. Анализом ових података добијен је резултат за флукс неутрона произведених мионима, на дубини наше подземне лабораторије [6]. Мерења су континуирано настављена, са већом статистиком снимљених догађаја; анализа ових података је у току. Поред експерименталних мерења, упоредо су урађене Monte Carlo симулације продукције неутрона у олovној заштити, базиране на Geant4 *framework*-у. Овде су представљени први резултати симулација: процена принoса неутрона (број неутрона по јединици дужине) у интеракцијама миона, као и расподела мултиплицитета произведених неутрона.

2. Метод

Geant4 је софтверски пакет за Monte Carlo симулације транспорта и интеракција честица са материјом [7]. Он садржи комплетан алат за моделовање геометрије детектора, физичких процеса, примарних и секундарних догађаја, као и одзива детектора. На основи Geant4 платформе развијена је посебна апликација за симулације одзива германијумског и сцинтилационих детектора у лабораторији. Апликација је флексибилна и омогућује симулације појединачних и коинцидентних режима рада детектора. Претходно је коришћена у различитим

случајевима који су захтевали прецизне симулације сцинтилационих и германијумских детектора [2,4,8,9].
Олovна заштита је геометрије шупљег цилиндра, унутар којег се налази германијумски детектор. Висина цилиндра је 51 cm, пречник основе 41 cm, а дебљина олovног зида је 12 cm. Детектор је конструисан према спецификацији произвођача. Скица детектора и олovног цилиндра приказана је на слици 2.

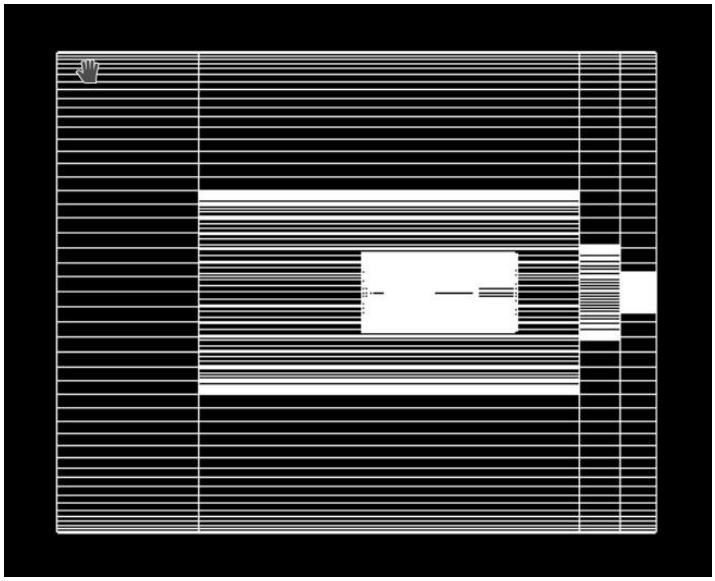

Слика 2. Скица олovне заштите германијумског детектора.

Примарни догађаји генерисани су дефинисањем инцидентне честице, њене позиције, правца кретања и енергије. Инцидентне честице су позитивни и негативни мioни; однос броја позитивних и броја негативних миона је 1,3. Почетне позиције миона на површини олovног цилиндра одређене су на следећи начин: прво се одабере горња хоризонтална страна или вертикална страна цилиндра, према вероватноћи да космички мion погоди хоризонталну или вертикалну страну, а затим се одабере позиција на датој површини из униформне расподеле. Правац кретања миона семплиран је из расподеле миона по правцима, у функцији од зенитног угла θ, која је пропорционална $\cos^{1,55}\theta$. Енергија миона одређена је из енергијске расподеле миона на површини Земље, при чему се узимају они мioни који успеју да прођу кроз 12 m земљишта. Детаљнија процедура генерисања примарних догађаја и изvођење расподеле миона по правцима и енергијама може се видети у [4].
Физички процеси у којима учествују мioни – електромагнетни и нуклеарни – укључени су у симулацију кроз предефинисану Geant4 класу QGSP_BERT_HP; ова класа омогућава симулације интеракција честица са великом прецизношћу.

3. Резултати и дискусија

Први циљ симулације био је да се одреди број произведених неутрона у интеракцијама миона са језгрима олова, по јединици дужине пута, при њиховом пролasku кроз олovну заштиту германијумског детектора. Генерисаних примарних догађаја било је 10^8; овај број може бити повезан са временом експерименталних мерења, узимајући у обзир флукс миона у подземној лабораторији.
Укупан број произведених неутрона био је 934 000. Одавде је одређен принос неутрона, као однос броја неутрона и производа густине олова и средње дужине пута миона кроз

olovo. Srednja dužina puta miona je 26,6 cm, a proizvod gustine olova i srednje dužine puta iznosi 302 g/cm^3. Dobijena vrednost za prinos neutrona je 3,1 × 10^{-5} *neut.*/(gcm^{-2}). Pored prinosa neutrona, određena je raspodela multipliciteta neutrona – broja neutrona proizvedenih u interakciji jednog miona sa olovom. Mion može proizvesti više od jednog neutrona na svom putu kroz olovo, što za rezultat ima više neutronskih fonskih događaja u detektoru koji potiču od jednog miona. Događaji su vremenski razdvojeni, odnosno detektuju se sa vremenskim razmakom, u zavisnosti od trenutka i mesta produkcije neutrona. Ovi događaji registruju se u detektoru kao signali sa vremenskim kašnjenjem, unutar definisanog vremenskog prozora mionskog događaja. To može poslužiti za selekciju fonskih događaja koji potiču od neutrona indukovanih mionima. Raspodela multipliciteta neutrona prikazana je na slici 3. Najveći broj miona proizvede manje od 10 neutrona u kaskadi, dok srednji multiplicitet neutrona iznosi 11,5. Dobijena raspodela slaže se sa rezultatima ranijih sličnih simulacija [10].

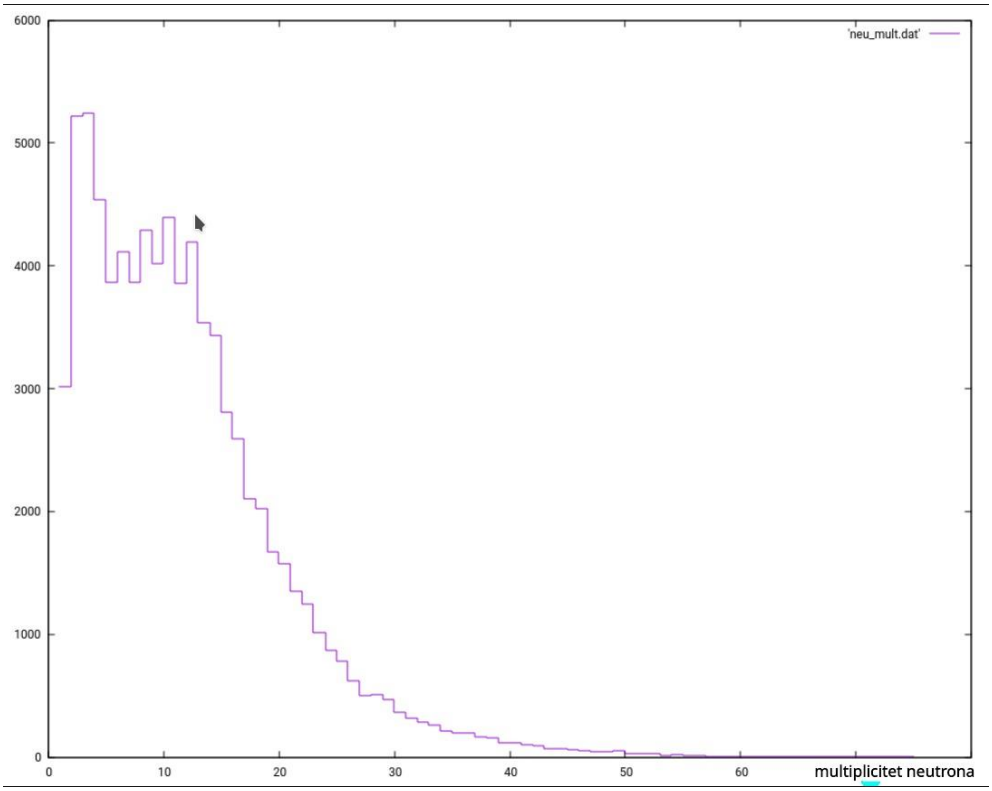

Slika 3. Raspodela multipliciteta neutrona proizvedenih mionima iz kosmičkog zračenja u olovnoj zaštiti HPGE detektora.

Rezultati simulacije pokazali su da ovaj metod može biti koristan za procenu produkcije neutrona mionima iz kosmičkog zračenja. On može dati detaljniji uvid u mehanizam produkcije neutrona. Osim toga, rezultati simulacije mogu pomoći u analizi podataka eksperimentalnih merenja, njihovom boljem razumevanju i evaluaciji.

4. Zahvalnica

Ovaj rad finansiran je od Instituta za fiziku u Beogradu kroz projekat Ministarstva prosvete, nauke i tehnološkog razvoja Republike Srbije.

5. Literatura

[1] D. Mei, A. Hime. Muon-induced background study for underground laboratories. *Phys. Rev. D* 73, 2006*,* 053004.

[2] A. Dragić, D. Joković, R. Banjanac, V. Udovičić, B. Panić, J. Puzović, I. Aničin. Measurement of cosmic ray muon flux in the Belgrade ground level and underground laboratories. *Nucl. Instr. Meth. A* 591, 2008, 470-475.

[3] M. Savić, A. Dragić, D. Maletić, N. Veselinović, R. Banjanac, D. Joković, V. Udovičić. A novel method for atmospheric correction of cosmic-ray data based on principal component analysis. *Astropart. Phys.* 109, 2019, 1-11.

[4] D. Joković, A. Dragić, V. Udovičić, R. Banjanac, J. Puzović, I. Aničin. Monte Carlo simulations of the response of a plastic scintillator and an HPGe spectrometer in coincidence. *Appl. Radiat. Isot.* 67, 2009, 719-722.

[5] A. Dragić, V. Udovičić, R. Banjanac, D. Joković, D. Maletić, N. Veselinović, M. Savić, J. Puzović, I. Aničin. The new set-up in the Belgrade low-level and cosmic-ray laboratory. *Nucl. Techn. Radiat. Prot.* 26, 2011, 181-192.

[6] A. Dragić, I. Aničin, R. Banjanac, V. Udovičić, D. Joković, D. Maletić, M. Savić, N. Veselinović, J. Puzović. Neutrons produced by muons at 25 mwe. *J. Phys.: Conf. Ser.* 409, 2013 012054.

[7] S. Agostinelli et al. Geant4 – a simulation toolkit. *Nucl. Instr. Meth. A* 506, 2003, 250-303.

[8] M. Krmar, J. Hansman, N. Jovančević, N. Lalović, J. Slivka, D. Joković, D. Maletić. A method to estimate a contribution of Ge(n,n') reaction to the low-energy part of gamma spectra of HPGe detectors. *Nucl. Instr. Meth. A* 709, 2013, 8-11.

[9] J. Nikolić, T. Vidmar, D. Joković, M. Rajačić, D. Todorović. Calculation of HPGe efficiency for environmental samples: comparison of EFFTRAN and GEANT4. *Nucl. Instr. Meth. A* 763, 2014, 347-353.

[10] L. Reichhart et al. Measurement and simulation of the muon-induced neutron yield in lead. *Astropart. Phys.* 47, 2017, 67-76.

MONTE CARLO SIMULATION OF THE COSMIC RAY MUON INDUCED NEUTRON PRODUCTION IN THE LEAD SHIELD OF THE GERMANIUM DETECTOR

Dejan JOKOVIĆ, Dimitrije MALETIĆ, Vladimir UDOVIČIĆ, Radomir BANJANAC, Aleksandar DRAGIĆ, Mihailo SAVIĆ, Nikola VESELINOVIĆ and David KNEŽEVIĆ

Institute of Physics Belgrade, University of Belgrade, Belgrade, Serbia,
yokovic@ipb.ac.rs, maletic@ipb.ac.rs, udovicic@ipb.ac.rs, banjanac@ipb.ac.rs, dragic@ipb.ac.rs, msavic@ipb.ac.rs, veselinovic@ipb.ac.rs, davidk@ipb.ac.rs

ABSTRACT

Lead is usually used as a common shielding material for germanium detectors. Cosmic ray muons produce secondary particles in their interactions with lead nuclei, which contribute to overall background radiation detected by germanium detectors. Neutrons produced in muon interactions in lead shield make a significant part of this background component. Cosmi ray induced neutrons are a particular problem in experiments carried out in deep underground laboratories.

In the low-level underground laboratory at Institute of Physics Belgrade, a germanium detector and a muon detector operate in conicidence. This provides studying of different effects in the germanium detector induced by cosmic rays, especially effects originated from the cosmic ray induced neutrons.

Here, the results of Geant4 simulations of the cosmic ray muon induced neutron production in the lead shield of the germanium detector are presented. Estimate of the neutron yield – number of neutrons produced per unit path length – in muon interactions is obtained. The result is 3.1×10^{-5} neutrons/(gcm^{-2}). Also, the neutron multiplicity distribution is determined, as a distribution of number of neutrons produced per muon interaction. The average multiplicity is 11.5.